VALORIZATION OF WHITE GRAPE POMACE: INTEGRATED STRATEGIES FOR ADVANCED APPLICATIONS

PhD Dissertation presented by

JULEN DIAZ RAMIREZ

Under the supervision of

Dr. NAGORE GABILONDO LÓPEZ

Dr. ALOÑA RETEGI MINER

Donostia–San Sebastián, December 2023

Seguimos recogiendo tanto como sembraste

Para Loli Ramírez Domínguez

Acknowledgments

Una de las partes más complicadas de la tesis doctoral es la de escribir los agradecimientos. Se atraganta un poco porque es difícil condensar cuatro años de trabajo y emociones en un par páginas. En mi caso, aunque voy a ser breve, tengo la sensación de que podría escribir una tesis entera solamente con agradecimientos.

En primer lugar, quiero agradecer al Gobierno Vasco y en concreto al programa de becas Ikertalent (00020-PIT2019-22) la asistencia económica necesaria para realizar este proyecto. Del mismo modo, me gustaría agradecer a las doctoras Aloña Retegi y Nagore Gabilondo su ayuda y confianza al darme la oportunidad de realizar la tesis doctoral bajo su supervisión.

Por otra parte, quisiera agradecer al Departamento de Ingeniería Química y del Medioambiente de la UPV/EHU y su grupo 'Materials + Technologies' por facilitarme las instalaciones y equipos necesarios para llevar a cabo el proyecto. También tengo que agradecer a los Servicios Generales (SGIker) de la UPV/EHU el apoyo técnico en los numerosos trabajos de caracterización realizados durante los últimos cuatro años. En concreto, me gustaría agradecer a la técnico Loli Martin toda su ayuda y sobre todo, saber encajar siempre bien todas mis bromitas.

Likewise, I would like to acknowledge Dr. Lydie Ploux and Dr. Corinne Nardin for allowing me to engage in a stay at the University of Strasbourg. Despite the results did not align with initial expectations, the experience on both a professional and personal level was highly beneficial and stimulating. Of course, I also remember the laboratory technicians (Sofi and Christine) and the students (Nour and Elora) who accompanied and brightened my work every

day. Gracias también a Ernesto por hacerle creer a una piedra como yo que se podría convertir en un campeón de bailar salsa.

En cuanto a las personas que me han acompañado durante todo este aquelarre científico, voy a empezar por la columna vertebral del grupo GMT. Muchas gracias a Tamara, Izaskun y Kizkitza por hacerme sentir más especial que Brad Pitt, Gerard Piqué e Iñigo Martinez juntos todos los días. Gracias a Raquel por la ayuda en el laboratorio y todas las risas de los pintxopotes fuera de él. Sois, sin ninguna duda, la mejor generación que ha conocido Hogwarts. Muchas gracias a toda la gente que forma o ha formado parte del grupo GMT, particularmente a las viejas glorias como Senda, Julen, Ane o Gabriel y a la savia nueva como Nerea o Ander. El laboratorio se queda en buenas manos. Estoy muy agradecido también a Irati y a Nagore, junto con la gente de abajo, por aguantarme cuando más pesado estaba en el sexto piso.

Asimismo, me gustaría agradecer a las personas que han pasado a ser parte de mi vida gracias a la tesis. Al signore Stefano, gracias por demostrar que se puede ser compañero de trabajo, compañero de piso y amigo, tanta generosidad como rizos. Muchas gracias a Leire y Olatz, las científicas más guapas y trabajadoras del mundo, por acogerme al principio y cuidarme tantísimo. En el laboratorio o en el barro, la mitad de esta tesis es vuestra.

Una de las implicaciones de la tesis suele ser tener que reciclarte y moverte a nuevos puertos. En paralelo al proyecto científico, a mí la tesis me trajo la suerte de vivir en Donosti, desde Berio hasta Easo. Todas las carcajadas de sobremesa y la familia que se ha formado han echado raíces aquí, y ya han empezado a dar sus frutos en forma de segunda generación. A Lluís, Juan, Andrea, Juanjo, Jandri, Ainhoa, Ana, la cuadrilla, los panitas... es imposible mencionar a todos, pero muchísimas gracias. No es casualidad que mi futuro

hoy siga pasando por tomar el aire los domingos en el Paseo nuevo. No me quiero olvidar tampoco de Isa, mi principal apoyo cuando todo estaba atascado por la pandemia. Como tampoco me puedo olvidar de toda la gente de genética de Leioa que me abrió las puertas de la ciencia y la farándula (JonLa, Gartze, JonVa, Adrian…), científicos y soñadores a partes iguales.

Por último, volviendo a mis orígenes, gracias a mi cuadrilla de Lezama por mantener su esencia en todas mis escapadas y ser el mejor zoológico, hardcore.

Pero, sobre todo, gracias a mi padre y mi hermano. Mi ejemplo y mis piedras angulares, gracias por darme equilibrio en los momentos que el suelo se vuelve resbaladizo, incluso cuando lo hacéis sin daros cuenta. Cuando se apagó la luz de nuestro faro más importante, aprendimos a guiarnos con la luz de las estrellas.

Muchas gracias a todos de corazón, habéis hecho que disfrute cada día en el laboratorio.

Summary

The sustainable management of agricultural waste is a critical challenge in modern society, given the increasing demands for food production. Agricultural waste, such as grape pomace (GP) from Txakoli wine production, poses environmental problems like pollution, ecosystem disruption, and greenhouse gas emissions. To address these issues, the circular economy is emerging as a solution, aiming to minimize waste and maximize resource use.

GP, composed of grape skins, seeds, and stalks, is a significant agricultural residue in the Basque Country. Despite being considered waste, GP holds nutritional value with high fiber, phenolic compounds, and nutrients. From a biotechnological perspective, GP can be a sustainable source for high-value products.

Bacterial cellulose (BC), which can be biosynthesized from GP, is a biodegradable biopolymer with exceptional properties. BC's 3D network structure and high water-holding capacity make it versatile for various applications. Furthermore, GP, rich in polyphenolic compounds concentrated in grape skins and seeds, has bioactive properties valuable to industries such as pharmaceuticals, cosmetics, and food.

This thesis explores GP valorization strategies, focusing on BC in membrane, nanofiber, and nanocrystal forms, along with its combination with polyphenolic extracts from GP. These innovative systems have potential applications in agriculture, biomedicine, food, pharmaceuticals, and cosmetics, contributing to a circular economy approach.

INDEX

CHAPTER 1

1. Introduction 1

1.1 Motivation 3

1.2 Grape Pomace 5

1.2.1 GP production and concerns 5

1.2.2 GP composition 6

1.2.2.1 *GP phenolic compounds* 8

1.2.3 GP applications 10

1.2.3.1 *Direct applications* 10

1.2.3.2 *Indirect applications* 12

1.3 Bacterial cellulose 14

1.3.1 Cellulose structure and origin 14

1.3.2 BC biosynthesis 16

1.3.3 BC properties 19

1.3.4 Culture medium design 20

1.3.5 Culture conditions 22

1.3.6 BC applications 24

1.4 Circular economy approach 27

1.5 General objectives 28

1.6 References 30

CHAPTER 2

2. Materials and characterization techniques 49

2.1 Materials and reagents 51

2.2 Characterization techniques 53

2.2.1 Physicochemical characterization 53

2.2.1.1 *Chromatographic techniques* 53

2.2.1.2 *X-ray diffraction* 55

2.2.1.3 *Fourier transform infrared spectroscopy* 56

2.2.1.4 *Ultraviolet-visible spectrophotometry* 57

2.2.1.5 *Dynamic light scattering* 58

2.2.1.6 *Fluorescence spectroscopy* 59

2.2.2 Thermal characterization 60

2.2.2.1 *Differential scanning calorimetry* 60

2.2.2.2 *Thermogravimetric analysis* 61

2.2.3 Hydrophilicity 61

2.2.3.1 *Water holding capacity* 61

2.2.3.2 *Water contact angle* 61

2.2.4 Morphological characterization 62

2.2.4.1 *Atomic force microscopy* 62

2.2.4.2 *Scanning electron microscopy* 63

2.2.4.3 *Optical microscopy* 63

2.2.5 Rheological characterization 64

2.2.6 Antioxidant activity characterization 65

2.2.6.1 *DPPH radical scavenging activity* 65

2.2.6.2 *ABTS radical scavenging activity* 66

2.2.6.3 *Total phenolic content* 66

2.2.7 Biocompatibility 67

2.2.7.1 *Cytotoxicity assay* 67
2.2.8 Antimicrobial activity 68
2.2.8.1 *Agar diffusion assay* 68
2.2.9 Statistical analysis 69
2.3 References 69

CHAPTER 3

3. From agriculture to agriculture 71
3.1 Introduction 73
3.2 Experimental section 75
3.2.1 GP and bacterial strain origin 75
3.2.2 BC biosynthesis 76
3.2.3 BC yield 78
3.2.4 Urea release study 78
3.3 Results and discussion 80
3.3.1 Characterization of culture media 80
3.3.1.1 *Biosynthesis optimization and BC yield* 80
3.3.1.2 *GP culture medium sugar composition* 85
3.3.2 Physicochemical characterization of BC 88
3.3.3 Superabsorbent capacity 91
3.3.4 Urea release study 95
3.4 Conclusions 98
3.5 References 98

CHAPTER 4

4. Active Pickering emulsions 107

4.1 Introduction 109

4.2 Experimental section 112

4.2.1 BC hydrolysis 112

4.2.1.1 *Enzymatic hydrolysis* 112

4.2.1.2 *Acid hydrolysis* 113

4.2.2 GPPE extraction and characterization 114

4.2.2.1 *Ultrasound-assisted polyphenol extraction* 114

4.2.3 BCNC-GPPE complex preparation and characterization 115

4.2.3.1 *Antioxidant activity assay* *115*

4.2.4 Pickering emulsions 116

4.2.4.1 *Oxidative stability* 116

4.2.4.2 *Physical stability* 117

4.3 Results and discussion 118

4.3.1 BCNC production and characterization 118

4.3.1.1 *BCNC particle size distribution* 118

4.3.1.2 *BCNC characterization* 120

4.3.2 GPPE characterization 122

4.3.3 BC and GPPE complex characterization 125

4.3.4 Pickering Emulsion characterization 131

4.4 Conclusion 138

4.5 References 139

CHAPTER 5

5. Personalized pharmacology through 3D printing 153

5.1 Introduction 155

5.2 Experimental section 159

5.2.1 Preparation of the starch-based inks 159

5.2.2 BCNF production 160

5.2.3 3D printing procedure 160

5.2.4 In vitro drug release studies 161

5.3 Results and discussion 162

5.3.1 BCNFs for Ibuprofen loaded NM starch tablets 162

5.3.1.1 *BCNC and NM ink setup* 162

5.3.1.2 *3D printing of NM starch-based tablets* 171

5.3.1.3 *Ibuprofen in vitro release* *176*

5.3.2 WM starch tablets for GPPE release 179

5.3.2.1 *WM and GPPE ink setup* 179

5.3.2.2 *3D printing of WM starch-based tablets* 184

5.3.2.3 *GPPE in vitro release* *185*

5.4 Conclusions 187

5.5 References 189

CHAPTER 6

6. Advanced antimicrobial wound dressing 201

6.1 Introduction 203

6.2 Experimental section 206

6.2.1 Synthesis of Cs-SH 206

6.2.2 Fluorescent labelling of Cs-SH 207

6.2.3 FITC-Cs-SH and curcumin loaded Cs-SH nanoparticle formation 208

6.2.4 Loading BC by vacuum filtration 209

6.2.5 In vitro FITC-Cs-SH nanoparticle and curcumin delivery 210

6.2.5.1 *FITC-Cs-SH nanoparticle release* 210

6.2.5.2 *Curcumin release from Cur-Cs-SH nanoparticles* 211

6.2.6 Adhesion force tests 212

6.3 Results and discussion 214

6.3.1 Characterization of Cs-SH nanoparticles 214

6.3.2 Vacuum filtration efficiency 216

6.3.3 In vitro release of FITC-Cs-SH nanoparticles and curcumin 218

6.3.3.1 *Release* of *FITC-Cs-SH nanoparticle* 218

6.3.3.2 *Curcumin release from Cur-Cs-SH nanoparticles* 221

6.3.4 Adhesion force tests 222

6.3.5 Antimicrobial tests 225

6.4 Conclusions 226

6.5 References 228

CHAPTER 7

7. General conclusions, future work and list of publications 239

7.1 General conclusions 241

7.2 Future work 244

7.3 List of publications and communications 246

ANNEXES

List of abbreviations 251

List of Figures 255

List of Schemes 263

List of Tables 263

Supplementary material 265

CHAPTER 1

INTRODUCTION



1.1 Motivation 3
1.2 Grape Pomace 5
1.2.1 GP production and concerns 5
1.2.2 GP composition 6
1.2.3 GP applications 10
1.3 Bacterial cellulose 14
1.3.1 Cellulose structure and origin 14
1.3.2 BC biosynthesis 16
1.3.3 BC properties 19
1.3.4 Culture medium design 20
1.3.5 Culture conditions 22
1.3.6 BC applications 24
1.4 Circular economy approach 27
1.5 General objectives 28
1.6 References 30

Chapter 1: Introduction

1.1 Motivation

The sustainable supply of food and goods for a continuously growing population is one of the main challenges of modern society. Meeting the food demands of an increasingly consumer-oriented society results in the generation of tons of agricultural waste every year. The accumulation of these waste leads to water and soil pollution, disruption of local ecosystems, and greenhouse gas emissions.

In the face of these problems, the application of circular economy emerges as an essential solution. The circular economy is an economic model that seeks to minimize waste generation and maximize resource utilization through reuse, recycling, and valorization. In the agricultural context, the circular economy involves harnessing agricultural residues as resources rather than considering them as waste.

Grape pomace (GP) generated from the production of Txakoli wine is one of the main agricultural residues in the Basque Country. GP refers to the solid matter remaining after pressing grapes in the wine industry and it is composed of seeds, skin and stalks. Despite being one of the largest representatives of agricultural waste globally, GP offers numerous opportunities for valorization from a circular economy perspective. It is indeed a byproduct with high nutritional value due to its high content of dietary fiber, phenolic compounds, and nutrients. These interesting qualities of GP can be exploited in several ways.

From a biotechnological point of view, GP represents a sustainable source of compounds for the development of high-value-added products. On the one hand, the high fermentable sugar and mineral content of GP makes it a low-cost carbon source for the design of bacterial culture media. One of the best examples of this valorization strategy is bacterial cellulose (BC) biosynthesis. BC is a biodegradable and biocompatible biopolymer with excellent physicochemical and mechanical properties. Given its glucan chains assembly and its porous 3D network-like structure of interconnected cellulose ribbons or nanofibers, BC presents exceptional purity and crystallinity and outstanding water holding capacity. Indeed, BC has become one of the major topics of research in the last decade to produce composites with applications in a wide variety of fields.

On the other hand, GP, especially that which is derived from Txakoli production, contains an extraordinary amount of polyphenolic compounds, primarily concentrated in the skins and seeds of grapes. In fact, GP from white wines has greater polyphenol content due to the absence of a maceration process prior to fermentation. Polyphenolic compounds are bioactive molecules with recognized antimicrobial, antioxidant, anti-inflammatory, and anticancer properties, among others. Therefore, the extraction of these compounds is of special interest to the pharmaceutical, cosmetic, and food industries.

This thesis explores different valorization strategies for GP derived from local Txakoli production. The work follows a biorefinery concept of investigation, exploring the promising applications of BC in the form of membranes, nanofibers, and nanocrystals, as well as their combination with polyphenolic extract from GP. In this way, advanced systems have been designed with

applications in the fields of agriculture, biomedicine, food, pharmacy, and cosmetics.

1.2 Grape Pomace

1.2.1 Production and concerns of GP

Grape is one of the largest and most significant fruit crops in the world, with an approximate production of 80 million tons in 2018 [1]. Mediterranean countries in the southern region of Europe, such as Spain, Italy, and France, with a rich winemaking tradition, are the leading grape harvesters globally. To be more precise, it is estimated that European countries contribute to the 38% of total grape harvest, of which more than 70% is used for wine production [2,3].

Wine production is traditionally more concentrated in certain regions than others. For example, only in the Basque Country, around 7500 tons of grapes were cultivated in 2020 for the production of Txakoli [4], a white wine with a certificate of origin in the region. The winemaking process is characterized by the generation of a large volume of waste and by-products, with grape pomace (GP) being the most predominant [5] (Figure 1.1).

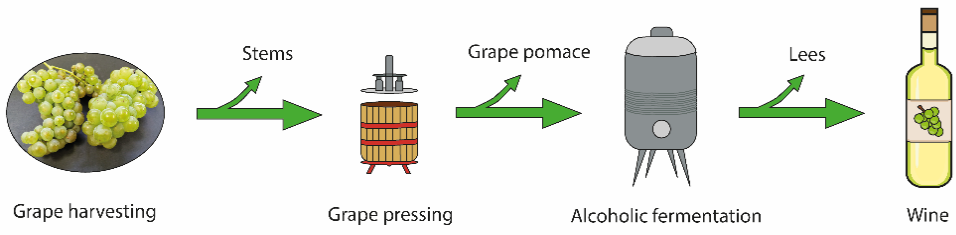

Figure 1.1 *Graphical representation of the white wine production process with the waste generated at each step.*

GP is the residue resulting from grape pressing prior to the fermentation process as it is represented in Figure 1.1. It is estimated that GP accounts for approximately 25% w/w of the total grape production, resulting in tons of this residue accumulating within a short period of time, thereby exacerbating its potential risks [6,7]. In fact, the accumulation of agricultural residues such as GP involves several environmental drawbacks, including water and soil contamination, germination inhibition, oxygen depletion, slow decomposition, odor and the production of greenhouse gases [8–10].

1.2.2 GP composition

GP is composed of 50% grape skins, 25% grape seeds and the remaining 25% are grape stems or stalks as represented in Figure 1.2 [11]. Each component of the GP exhibits numerous high-value compounds, making it an excellent candidate for integrated biorefinery and environmental impact minimization (Figure 1.2) [2,9]. However, the composition of the GP varies depending on geographical location, viticulture, grape variety, maturity, and climatic conditions [12].



Figure 1.2 *Representation of the main compounds that can be found in each component of GP.*

The grape skin is primarily composed of dietary fiber, phenolic compounds and sugars [11]. The amount of dietary fiber and sugars is strongly related to the grape variety, with higher percentages of both found in red grape varieties [13]. Polyphenolic pigments such as anthocyanins can be detected in varying concentrations also depending on grape variety. Similarly, despite lacking such pronounced pigmentation, white grape varieties could have a higher concentration of polyphenols due to the absence of the pre-fermentation maceration process [14]. Proteins, lipids, ash and minerals have also been identified in grape skins [15].

The stalk is the lignocellulosic residue that serves as a connection structure between the grapes to form a bunch. It is primarily composed of lignin, hemicellulose, and cellulose, but it also contains a significant amount of phenolic compounds, predominantly tannins [11,16]. It is worth noting that the contribution of this residue within GP is linked to the destemming technology employed by the winery.

Equally, the seeds are characterized by the presence of unsaturated fatty acids (oleic and linoleic) and numerous phenolic compounds [17,18]. Proteins, lignin and minerals have also been reported to be constituents of GP seeds [15]. Tannins of seeds and stalks are commonly used to modify the sensory properties of wine and provide it with increased astringency when needed [19]. Grape seed extract is considered a valuable byproduct of viticulture, although it has not been extensively exploited, likely due to the difficulty of selective seed separation [2]. In fact, the proportion of total extractable phenolics in GP is approximately 60-70% in seeds, 30-35% in the skin, and nearly 10% or less in the pulp [19].

1.2.2.1 GP phenolic compounds

The current lifestyle with unhealthy habits, lack of sleep or physical exercise, and environmental pollution, contribute to the increasing oxidative stress in society. Oxidative stress leads to disruptions and elevated levels of Reactive Oxygen Species (ROS) that endogenous antioxidants in the human body cannot always counteract. For this reason, oxidative stress has been associated with several physiological alterations, ageing, and various pathologies such as atherosclerosis, carcinogenesis or neurodegenerative disorders [20]. In this context, polyphenols from plants can play a crucial role, whether as dietary supplements, food ingredients, medical formulations, or topical applications [5,19,21]. Existing literature provides evidence of the health-promoting properties of grapes and their byproducts showing their anticholesterolemic, antimicrobial, antiviral, cardioprotective, neuroprotective and anti-cancer activity, among others [22–27]. Accordingly, the market value of phenolic compounds is continuously growing, and it is expected to reach 2 billion US$ by 2025 [28].

Certainly, GP is particularly rich in phytochemicals with reported health benefits, such as polyphenols, which enhance its added value. According to Dwyer et al, around 70% of the grape phenolics persist in the pomace after the winemaking procedure [29]. Polyphenols are secondary metabolites of the plant kingdom that, in addition to contributing to aromas and color, are part of the plant's defense system. Figure 1.3 depicts the main phenolic compounds found in white GP.

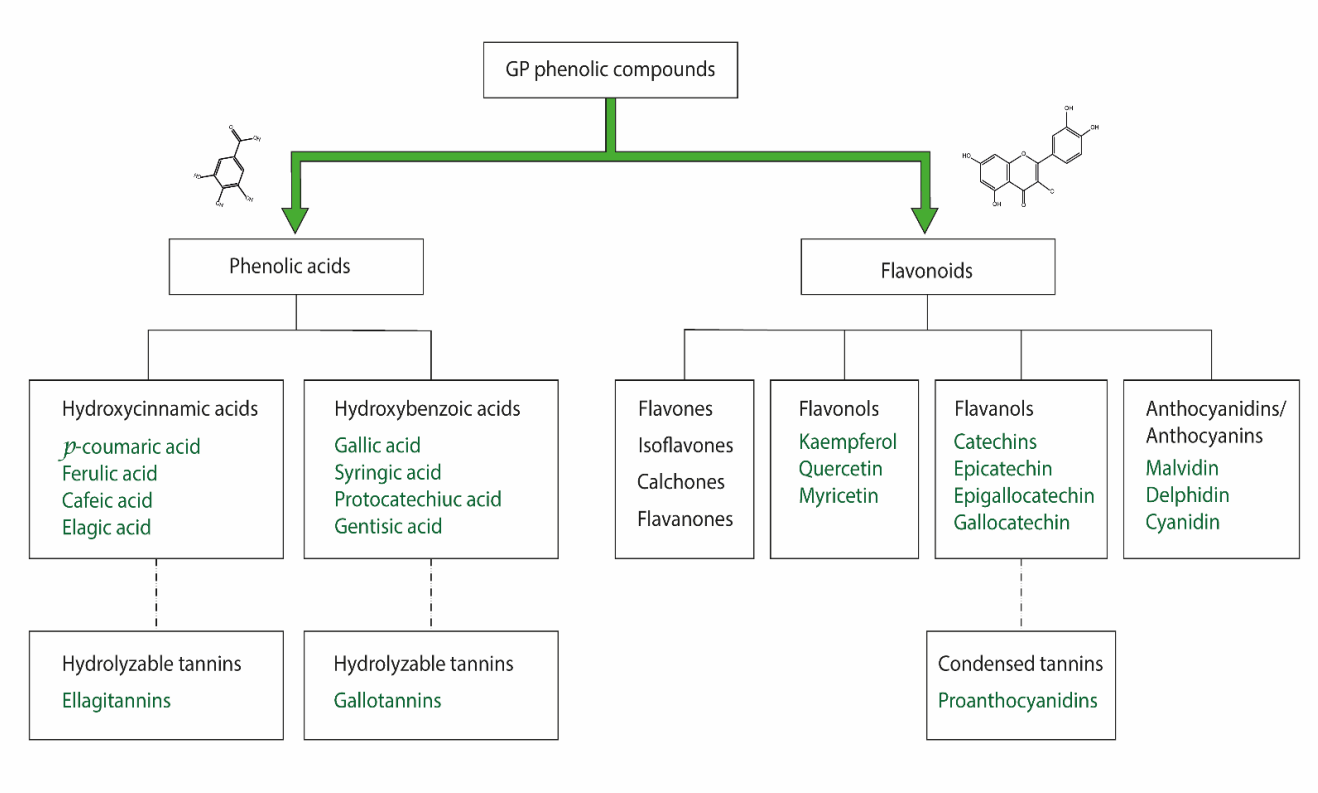

Figure 1.3 *Schematic representation of the main phenolic compounds present in white GP. The dashed lines refer to the condensation process of phenolic acids/polyphenols in the formation of tannins.*

Polyphenols are mainly divided into two families based on their chemical structure: flavonoids and non-flavonoids. Non-flavonoids include phenolic acids that are characterized by one functional carboxylic acid, for example hydroxycinnamic acids and hydroxybenzoic acids (Figure 1.3) [19]. These compounds are distinguished by their antioxidant activity, as they scavenge free radicals and decrease ROS levels. On the other hand, flavonoids can be divided into seven subgroups: flavones, flavanones, flavanols, isoflavones, flavonols, anthocyanidins/anthocyanins and chalcones [30]. Flavanols (catechins) or anthocyanins, are the main polyphenols in grapes, and in addition to influence the sensory properties of wine, they also exhibit diverse antioxidant mechanisms of action. For example, these compounds can avoid peroxidation processes scavenging free radicals and chelating metals [2,15].

1.2.3 GP applications

GP has traditionally been considered a low-value residue with difficult handling due to its low pH [29]. The main applications of GP are reviewed below, starting with traditional direct applications and ending with the most innovative indirect applications, which require further processing of the residue but allow for the exploitation of its bioactive components. Figure 1.4 depicts a graphic representation of the known GP applications.

1.2.3.1 Direct applications

The direct applications are those that do not require any treatment or involve just minimal treatment of GP. For this reason, they have been more commonly used by winegrowers (Figure 1.4).

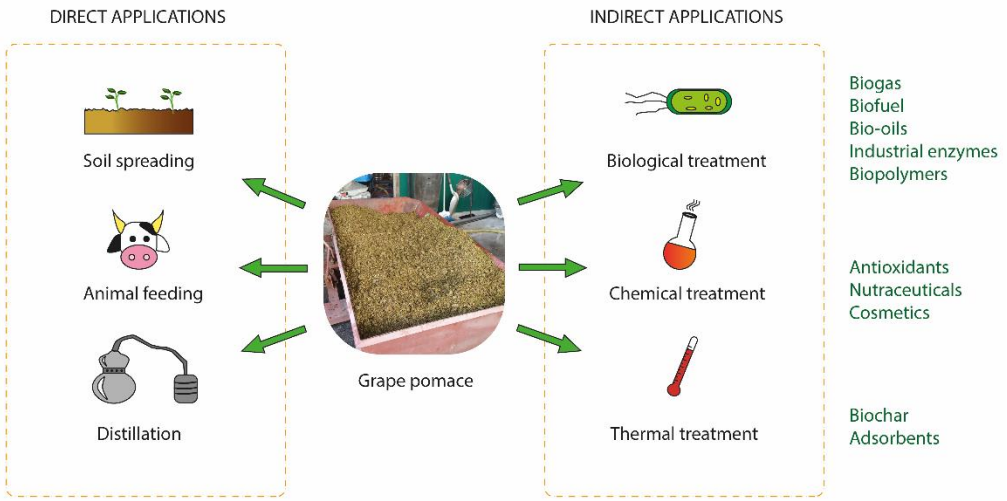

Figure 1.4 *GP applications classified according to the type of treatment required and the main products obtained.*

One typical use of GP is its direct spreading on agricultural soil. However, its chemical composition and certain phytochemicals can be detrimental to the environment [31]. In fact, the high concentration of phenols can have an inhibitory effect on germination [10,32,33]. Additionally, the presence of lignin hinders the degradability of polysaccharides that could be beneficial for the soil [34]. For this reason, in some regions, the spreading dosage is limited, and composting is recommended before using it as a fertilizer [31]. Composting GP, either alone or with other agricultural residues, allows for the production of an effective fertilizer without causing harm to the environment [31,35–37]. However, this is not the most commonly used strategy by winegrowers who tend to rely on more commercially available fertilizers on a more occasional basis.

Another direct alternative would be its use for animal and poultry feed. Depending on the composition of GP, the high concentration of lignin and secondary metabolites such as tannins and anthocyanins hinders digestion and decreases the caloric content [9,38]. In this regard, GP animal feeding in farming has been considered more as an approach to improve the quality of the obtained final milk, eggs or meat through the polyphenol intake [39–41].

Finally, the distillation of GP is the primary application for winegrowers. Indeed, the production of spirits is a prosperous industry in certain regions of Italy, France, or Spain [42,43]. However, it is a process that demands large volumes of GP, entails significant resource consumption and the generation of potentially toxic waste [44].

1.2.3.2 Indirect applications

Indirect applications are those that involve prior treatment of GP to generate high-value-added products. Generally, indirect applications can be divided into those requiring thermal treatment, chemical treatment, or biological treatment (Figure 1.5).

Similar to other organic wastes, pomace has the potential to be utilized in thermal processes such as combustion, gasification, and pyrolysis [2]. For instance, high-energetic potential pellets have been produced through the combustion of GP [45]. By adopting a circular economy approach, pyrolysis is an alternative for producing biochar from GP without compromising the added value of the residue. This type of biochar has demonstrated its adsorption capacity for heavy metal and pesticide removal [46–48]. Considering the high water content of GP, hydrothermal carbonization also appears to be a an

interesting topic of research for this type of agricultural residue, as suggested by some authors [49,50].

Another valorization strategy for GP is the extraction of high-value polyphenols. Selecting the appropriate extraction method to obtain the desired polyphenolic compound or profile is a crucial process to consider [51]. Given the numerous applications of phenolic compounds, various methodologies have been published for their extraction from GP [9,19]. Among these technologies, the use of hydroalcoholic solvents and ultrasound or microwaves stands out for obtaining the product in a sustainable and highly effective manner [19]. In this context, the extraction of phenolic supplements is one of the more interesting applications of GP.

Certainly, given the antioxidant and bioactive nature of GP, the utilization of its extracts is of great interest in the food industry, nutraceuticals, and cosmetics [15,19,52]. Numerous components of GP, particularly those present in the seeds, have demonstrated anti-hypertensive, antimicrobial, anticancer, or anti-aging properties that can be useful in diverse pathologies. Namely, the effectiveness of supplementation with gallic acid, proanthocyanidins, catechins and linoleic acid has previously been demonstrated [5,53,54]. In this regard, the encapsulation of grape polyphenols within different formulations appears to be one of the most promising alternatives to enhance their availability and prevent rapid degradation [55–57].

Finally, the biotechnological treatment of GP is definitely of great interest within the scientific community. The presence of fermentable sugars in GP and the wide variety of microorganisms that can thrive in acidic environments significantly increase the applicability of the residue. Red wine generates

biomass that contains yeast and ethanol for fermenting grape material, whereas white wine has a higher concentration of water-soluble carbohydrates and a lower level of ethanol [19]. In this scenario, the biosynthesis of biofuels (ethanol, acetone and butanol) [11], biogas (methane and succinic acid) [58–60], bio-oils [61], industrial enzymes [62], and biopolymers (bacterial cellulose, gellan gum, polyhydroxybutyrate and polyhydroxyalkanoates) [63–67] has been documented through both aerobic and anaerobic fermentation processes. The utilization of GP for cultivating mushrooms and producing vitamin, low fat, dietary fibre, protein and mineral-rich foods with umami flavor has even been proposed [68].

1.3 Bacterial cellulose

1.3.1 Cellulose structure and origin

Production characteristics, as well as the global volume of grape production, make GP an ideal candidate for obtaining high-value-added products from low-cost culture media. A promising example of valorization is the utilization of GP for biosynthesizing BC, as BC is one of the biopolymers that has attracted significant interest from the scientific community over the past two decades [69].

Cellulose is the most abundant and cost-effective biopolymer in the world, naturally synthesizing approximately 150 billion tons annually [70]. Combined with lignin and hemicellulose, it serves as a structural element in vegetal tissues and is typically extracted from plants and their lignocellulosic residues. Cellulose is composed of chains of D-glucopyranose monomers linked by β(1-4) glucosidic bonds as represented in Figure 1.5. The presence of hydroxyl groups, primary at C_6 and secondary at C_2 and C_3, allows for hydrogen bonding

between the glucan chains, resulting in a highly ordered semicrystalline biopolymer. Indeed, the ordered crystalline regions are normally interspersed with amorphous regions, and the presence of each domain determines the final crystallinity of the material. Additionally, the chemical, enzymatic or mechanical extraction techniques alter the physicochemical properties of plant-derived cellulose [71]. In fact, holocellulose, a mixture of cellulose, hemicellulose, and lignin derived from plants, is primarily used for fractionation into its monomers. These monomers are subsequently bioconverted into valuable chemicals and biofuels, as explained earlier [72].

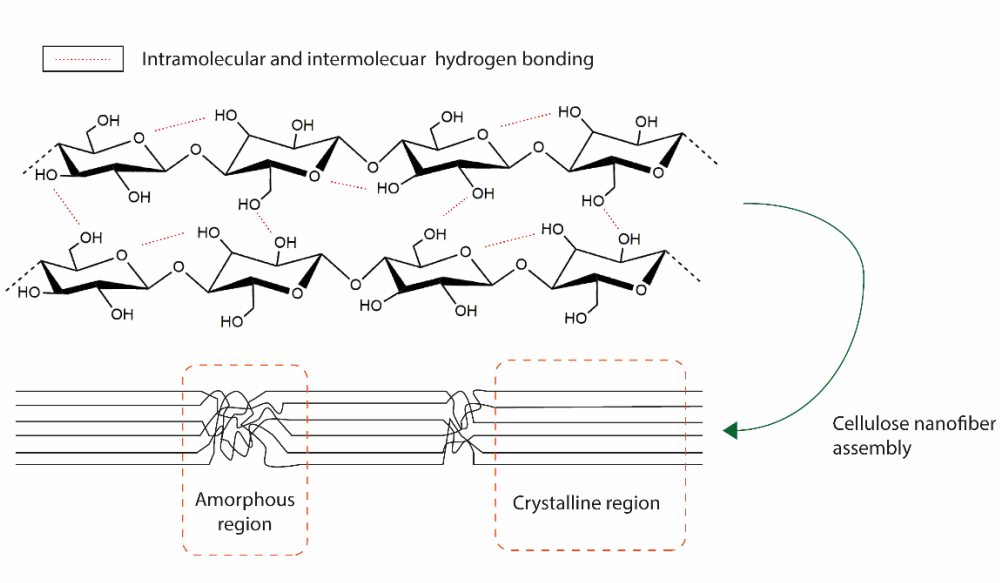

Figure 1.5 *Molecular structure of cellulose and distribution of its crystalline and amorphous regions.*

In this context, cellulose biosynthesized by bacteria emerges as a highly interesting source of biopolymer for the scientific and industrial world [69]. BC exhibits exceptional purity, which provides it with unique nanostructure, water

retention capacity, mechanical strength and crystallinity [73]. Furthermore, it has even been published that in a period of 7 years, plants produce 80 tons of cellulose on 1-hectare land, whereas it only takes 22 days to produce 79.2 tons of BC in a 500,000 L culture [74].

1.3.2 BC biosynthesis

BC is biosynthesized by different species of bacteria commonly found in fruits, vegetables, fermented beverages, or vinegars [75,76]. The bacterial genera capable of producing BC are diverse, including *Komagataeibacter* (formerly known as *Glucanoacetobacter* and *Acetobacter*), *Azotobacter*, *Pseudomonas*, *Salmonella*, *Sacina* and *Agrobacterium* [71]. All of them are strict aerobes and mostly gram-negative. This implies that they have an obligatory requirement for oxygen both for their growth and for BC production. The most exploited bacteria species is *Komagataibacter xylinus*, from the *Acetobacteriaceae* family, known for its demonstrated high BC production rate [77,78]. However, in this thesis, we focused on *K. medellinensis*, a species of the same bacterial genus that is characterized by its high BC production capacity in particularly acidic environments [76,79]. Taking into account the scaling up of BC production, selecting a potent bacterial strain is a key parameter to consider in the experimental design [71].

BC biosynthesis of *Acetobacter xylinum* was first described by Brown in 1886 [80]. BC is produced extracellularly as a pellicle at the in interface of liquid media and air, when cultured in nutrient-rich static media [79]. This provides the bacteria with access to oxygen from the air and nutrients from the medium, while also offering protection against the environment, UV rays, and competing microorganisms [81]. The biosynthesis process of BC is complex and

involves different enzymes that catalyze four main reactions, as depicted in Figure 1.6 [71].

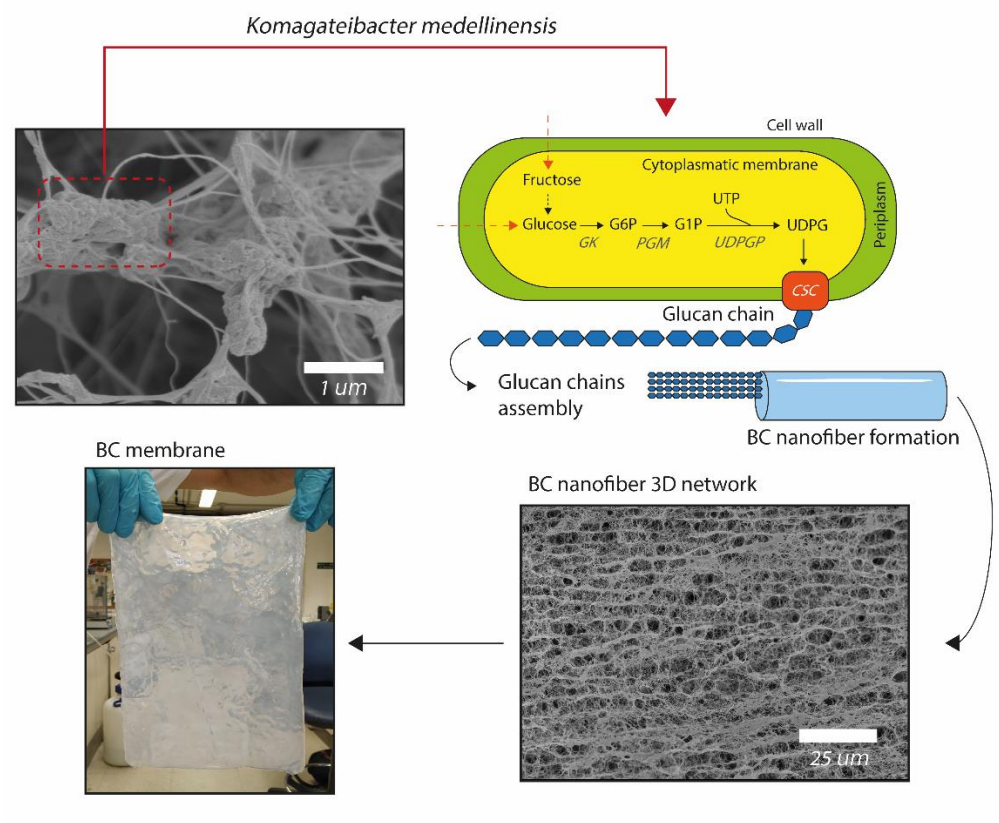

Figure 1.6 *Graphical representation of the biosynthesis process of BC by K. medellinensis. G6P=Glucose-6-phosphate, GK=Glucokinase, G1P=Glucose-1-phosphate UTP=Uridine triphosphate, PGM=Phosphoglucomutase, UDPG=Uridyl di-phosphate glucose, UDPGP= UDPG phosphorylase, CSC=Cellulose synthase complex.*

The first reaction is the phosphorylation of glucose to glucose-6-phosphate (G6P) catalyzed by the enzyme glucokinase (Figure 1.6). G6P is then isomerized to glucose-1-phosphate (G1P) by phosphoglucomutase. Next, the enzyme phosphorylase catalyzes the reaction between G1P and uridine triphosphate

(UTP) to generate uridine diphosphate glucose (UDPG). Finally, UDPG is polymerized into glucan chains by the cellulose synthase complex in the cell membrane and released into the medium through tiny pores on the cell envelope [82]. These chains combine and assemble into primary fibers that subsequently aggregate to form cellulose ribbons (nanofibers) (Figure 1.6). It should be noted that if the initial carbon source is not glucose, it will undergo enzymatic isomerization or hydrolysis reactions in the case of fructose and sucrose, respectively [83].

Similarly, it is important to identify and understand the genetic mechanism that encodes and regulates the biosynthesis of BC. This biochemical process is encoded by four genes of the bsc operon (bscA, bcsB, bcsC, and bcsD) [84]. An operon is a set of contiguous genes on the DNA strand with transcription regulatory capability. The proteins encoded by the bcsA and bcsB genes are associated with the activity of cellulose synthase, while the bcsC and bcsD genes have been linked to the transport and assembling of glucan chains [85,86]. Different types of bcs operons have been published, with type 1 and 2 being the most described ones and encoding the synthesis of different types of cellulose depending on the environment and culture conditions [84,87]. Since the composition of operons can vary among *Komagataeibacter* species, the genetic mechanism behind BC synthesis in *K. medellinensis* has also been described. Hernandez-Arriaga et al. identified four independent *bcs* operons in *K. medellinensis* ID13488 [88]. They found that the *bcs1* and *bcs4* operons were the most highly expressed during BC biosynthesis. Furthermore, in line with the literature, they observed that the *bcs1* operon was directly associated with the synthesis of type I cellulose, the most extended cellulose type in nature. Indeed, the *bcs1* operon was transcribed at pH 3.6, confirming the

strain's functionality under acidic conditions [79,88]. Deciphering the genetics behind BC biosynthesis is crucial as it allows for the maximization of production through the overexpression of specific genes using a synthetic biology approach [89].

1.3.3 BC properties

The properties that usually characterize BC are its high purity and crystallinity compared to plant cellulose [90]. The most common polymorph of BC is type I cellulose, although bacteria can also synthesize type II cellulose [87,91]. Type I cellulose polymorph exhibits a mixture of two types of crystalline structure forms (I_α and I_β), with I_α being more prevalent in BC, while I_β is more commonly found in plant cellulose [73,92].

As explained before, the glucan chains are packed together through intra- and intermolecular hydrogen bonds, forming a highly interconnected 3D nanofiber network. The result is a material with high mechanical strength in both dry and wet conditions [81,93,94]. Due to these hydroxyl groups and the nanofiber content, BC presents numerous opportunities for chemical and physical modifications. The hydroxyl groups present on the glucan chains can be easily functionalized with desired moieties, enabling BC to acquire advanced properties such as adjustable hydrophobicity, antimicrobial capacity, controlled drug release, or improved mechanical properties, among others [95–97]. However, there is often a trend to avoid relying on chemical reactions and instead embrace less impactful methodologies [95], which is why the simple ex situ and in situ modification techniques are widely documented in the literature. Ex situ approaches involve the utilization of purified BC through impregnation techniques to attach, coat, or infiltrate additives within the gaps

between the nanofibers of the BC membrane [98–100]. In situ techniques enable the incorporation of the additive into the developing nanofiber network, as the compound is added to the culture medium and is present during the biosynthesis process of BC [101,102].

On the other hand, BC can also be physically or chemically modified to expand its applicability. Through mechanical disintegration and enzymatic/acid digestion, obtaining BC nanofibers (BCNF) and nanocrystals (BCNC) has gained increasing interest. Both exhibit a rod-like shape with a nanoscale diameter and several microns in length in the case of BCNF and less than 1 μm in the case of BCNCs. Certainly, the increased crystallinity and aspect ratio of the BCNFs and BCNCs make them highly promising as reinforcement in composite materials, drug encapsulation devices or emulsion stabilizers [103–106].

Furthermore, BC is considered biodegradable due to its high water content, which makes it suitable for colonization by bacteria and fungi [107,108]. In fact, due to its hydroxyl groups, BC is highly hydrophilic, with water estimated to comprise over 95% of its mass. The biocompatibility of BC has also been successfully tested in numerous studies involving artificial skin, artificial blood vessels, biosensors, and tissue regeneration [109,110].

1.3.4 Culture medium design

In the production of BC, commercial media specifically designed for bacterial growth are commonly used, with the most widely used one being the Hestrin and Schramm (HS) medium [111]. The composition and conditions of HS medium are tailored to support the growth and cellulose production of specific bacterial strains. HS medium typically contains glucose or another carbon source, yeast extract/peptone (nitrogen sources), and mineral salts under an

adjusted pH. However, the BC production yield and the cost of HS medium involve challenges for industrial scaling as it is not economically competitive. In fact, it is estimated that the culture medium accounts for 30% of the total cost of BC production [112,113]. For this reason, the search for alternative and cost-effective carbon sources is crucial.

The use of agroindustrial residues could be a strategic alternative from a circular economy perspective. As previously explained, these wastes represent a considerable source of nutrients at zero cost. For this reason, the biosynthesis of BC from agrowastes is a strategy of growing interest [73]. Depending on the agricultural residue, different treatments are required to obtain fermentable carbohydrates. Residues with a higher lignocellulosic component, such as oat hulls, corn stalks, rice bark, or wheat straw, often require chemical and enzymatic hydrolysis treatments, which entail higher energy costs and potential environmental risks [78,114–116].

In this regard, fruit waste or food industry by-products can be more sustainable and suitable. Fruit waste, both agricultural and industrial, due to its higher sugar content, only requires simple extraction treatments to prepare an appropriate culture medium. On the other hand, the main drawback they present is their low pH, as is the case with GP [29]. Thus, it is important to choose the correct bacterial strain and identify the required nutrients in the waste to maximize BC production. Additional nitrogen sources or supplements are often used to complement culture media like orange peel, pineapple peel, or apple pomace [79,117–119]. These additives can not only increase BC production but also impart interesting mechanical properties to BC [112]. There have also been cases where two agroindustrial residues have been combined to create a more complete culture medium [79,117].

It should be noted that designing a culture medium from agricultural residues involves a balance between the nutritional requirements of the bacteria, the composition of the waste, and the cultivation conditions. This implies that certain species of *Komagataeibacter* may perform better with certain carbon sources than others [120,121]. Equally, a bacterium with high BC production yield in HS medium may be affected by certain components present in an agricultural residue [122]. In this work, the strain *K. medellinensis* ID13488 was chosen to investigate BC biosynthesis in GP medium due to its good performance with other acidic agricultural residues in previous studies [79,118,121].

1.3.5 Culture conditions

The optimization studies of BC biosynthesis at the laboratory scale are commonly carried out using two types of cultures: static cultures and dynamic or agitated cultures. Static culture for BC production is the most widely used due to its simplicity and ease of comparison. In this type of culture, BC develops as a film on the surface of the culture medium, and the cellulose takes the shape of the flask/container used [123]. Fermentation is conducted at 28-30°C for 5-20 days, depending on the container. Typically, cultures do not extend much beyond 14 days when the bacteria enter the stationary phase. One of the main drawbacks of this technique is the accumulation of inhibitory metabolites such as glycolic acids or formic acids over time [124]. The result of this type of production is usually a robust BC membrane with variable thickness depending on the incubation time [125]. Considering the excellent properties of BC explained previously, BC produced in static culture has numerous membrane-based applications [73,112].

The second most used biosynthesis technique is dynamic or agitated culture, also known in some cases as submerged culture. This technique is adopted as an alternative to increase BC production over time as it allows for constant oxygenation of the medium [112]. The main characteristic of agitated cultures is that BC is produced in the form of spheres, small filaments, or aggregates depending on the culture media, inoculum or agitation speed employed [126,127]. Although it has been reported that some key properties of BC, such as crystallinity, can be affected by agitation, the increased surface area of BC and the possibility of producing it in other forms have expanded the potential applications of the biopolymer [118,128,129]. The main drawback of dynamic production is the formation of non-BC-producing mutant bacteria, induced by shear forces and high bacterial proliferation rates [87,130]. For this reason, the final BC yield compared to static cultures is still under discussion [71,73,112]. Similarly, the process of BC beads formation during biosynthesis and the influence of agitation are still under study [131,132].

From an industrial scaling viewpoint, both static and agitated production techniques have the limitation of requiring a significant amount of time and low yield [71,112]. For this reason, different forms of cultivation or alternative bioreactors have been designed to improve oxygen supply to the bacteria [82,133]. Fed-batch cultivation, for example, is a strategy that involves intermittent feeding of fresh medium to increase the productivity of a static culture. The technique involves adding fresh medium on top of the previous BC film, inducing the formation of a new BC membrane [134,135]. The introduction of a partially submerged rotating plastic composite support has also been studied [136,137]. The disk successfully acts as a platform for bacterial growth and, consequently, BC production. Another alternative is the

air-lift bioreactor designed by Wu et al. [133], where vertically placed plates with air distribution from the bottom were able to biosynthesize BC pellets/aggregates in agitated media. In summary, although optimization studies for BC production are conducted in static and agitated modes to facilitate comparison, the search for bioreactors that enable industrial scaling of BC production is beneficial to fully spread the applications of this biopolymer [112].

1.3.6 BC applications

The combination of the structural and mechanical properties of BC, along with the ease of its functionalization, results in a wide range of promising applications [138]. Its biodegradable and biocompatible nature further facilitates its incorporation into various functionalities related to the human body. Moreover, BC can be easily transformed into BCNFs and BCNCs, expanding its usefulness in additional areas. The following are some of the published applications to date.

BC is an excellent candidate for the treatment of contaminated water. Certainly, modified BC membranes and composites have been developed, capable of absorbing a wide range of organic dyes, oils, pesticides, and toxic metals [139–142]. Additionally, hydrolysis treatments can yield BCNFs or BCNCs aerogels with increased contact surface area, thereby enhancing their oil-water separation capacity [143]. Similarly, when BCNFs and BCNCs are suspended in water, their absorption ability is significantly improved, allowing the formation of stable oil-in-water emulsions and extending their applicability to cosmetics, pharmaceuticals, and food industries [144,145].

Similarly, the hydrophilic nature, biocompatibility, prolonged half-life, and versatility make BC an excellent candidate for tissue engineering [138]. Due to the fibrous structure of BC, the development of composites with collagen, muscle cells, or other biopolymers has been employed to create grafts with advanced mechanical properties tailored to specific target tissues [146,147].

In this sense, one of the most promising applications is its use in wound healing. BC does not cause adverse allergic reactions and provides an immediate comforting sensation when applied to skin wounds/burns [148–151]. Indeed, the ease of functionalization after biosynthesis and the highly porous network make BC an excellent device for drug delivery [152,153]. Additionally, BCNCs can act as nanocarriers within different polymer matrixes, protecting and releasing diverse bioactive compounds [154,155].

Furthermore, BC has been considered Generally Recognized as Safe (GRAS) by the FDA since 1992. BC is regarded as non-carcinogenic, genotoxic, or tumor-promoting, and it does not pose any toxic effects when incorporated into human food [156,157]. In this particular field, the utilization of BCNFs and BCNCs holds great potential as they can act as thickeners and emulsifiers, replacing non-organic particles commonly used in Pickering emulsions [144,158]. Equally, BC and BCNCs can also be utilized as reinforcing materials for other active packaging materials [94,159,160].

Additionally, numerous authors have proposed the use of BC as a biosensor and a precursor for electronic devices [73,138]. Its flexibility, transparency, and thermal stability are highly promising characteristics in this field [161,162]. The combination of BC with conductive elements offers the potential for electrodes and piezoelectric biosensors with great potential in clinical diagnostics and any

application sensitive to strain, respectively [138]. Recently, BC has been proposed for the development of high-potential supercapacitors and batteries [163,164].

One of the emerging applications that is generating substantial interest is the integration of BC into 3D printing technology. With this technology, it is possible to synthesize matrices in the desired 3D geometry, which is a limitation in current BC cultivation methods [73,165,166]. In this context, another extra advantage offered by BCNFs and BCNCs is their ability to customize the mechanical properties of polymeric matrices, both in 3D printing and in the development of new materials [105,167–169].

It is worth noting that BC obtained from agricultural waste has certain limitations that may conflict with the restrictive regulatory standards of sectors such as biomedicine, pharmacy, cosmetics, and the food industry [170,171]. Although there is literature on various applications of BC from agro-wastes, it is necessary to establish quality standards and purification processes for BC to ensure its viability [73].

Finally, all the mentioned applications of BC contribute to the increasing market potential year by year. Actually, it is projected that by 2026, the market value of BC-based products will reach $700 million [71]. The first popularized BC product was nata de coco, which emerged in the 1970s. Nata de coco is a traditional dessert in the Philippines, produced through the fermentation of coconut water by *K. xylinum* [172]. It is a cholesterol-free and healthy food, widely consumed throughout Southeast Asia [173]. In fact, the value of coconut water, an agro-industrial residue, has increased due to the high

demand for this food product. Since then, the number of BC-derived products in the market is increasing constantly.

Currently, thickeners, surfactants, skincare cosmetics, and wound healing products have been commercialized [71]. In a techno-economic approach, Gama et al estimated that industrial fermentation of BC could reach a net profit of $3.3 million per year, provided that a significant initial investment is made [174]. In this regard, all researchers and producers agree that further studies on high-yielding strains, low-cost media, novel applications, and alternative cultivation methods are necessary.

1.4 Circular economy approach

Circular economy is an economic model that aims to maximize resource utilization and minimize waste and environmental degradation. In contrast to the traditional linear model of "take, make, dispose," the circular economy is based on the principles of reduce, reuse, recycle, and regenerate. Within this framework, agricultural residue GP, with its high-value components and large volume produced in specific regions within a short period, represents a strategically significant resource.

Given the GP nutritional content and the variety of applications of BC, biosynthesis of BC from GP is a highly promising alternative that demands further investigation. Furthermore, the literature emphasizes the need for integrated valorization methods for GP, as its utilization can be approached through various pathways [2,9,19]. For this reason, studying the performance of high-value components such as polyphenols and their combination with all the properties of BC is of great socio-economic and scientific interest.

1.5 General objectives

The main objective of this study was the valorization of GP from the Basque Country through biotechnology and sustainable chemical treatments. In this way, value was added to a voluminous local agricultural waste by developing a medium for BC biosynthesis and extracting GP phenolic compounds. Different combinations of BC and GP polyphenolic extract (GPPE) were studied, resulting in materials with advanced applications in the fields of agriculture, food, cosmetics, pharmacy, and biomedicine.

- In Chapter 1, a brief introduction is provided, and in Chapter 2, the reagents and characterization techniques used throughout the work are detailed. The overall objectives of each chapter in this thesis are described as follows:
- In Chapter 3, BC was biosynthesized from GP derived from Txakoli production, in both static and agitated cultures. The superabsorbent condition of BC spheres was successfully characterized, along with their usefulness for fertilizer release in agriculture.
- In Chapter 4, BCNCs and GPPE were synergistically combined to create active Pickering emulsions with applications in the food and cosmetic sectors. Both BCNCs and GPPEs were obtained using sustainable procedures while preserving the intrinsic antioxidant properties of the polyphenols.
- In Chapter 5, the potential utilization of BCNF and GPPE in 3D printing of starch tablets was exploited. The rheological properties of starch inks when interacting with nanofibers and polyphenols were

modulated, followed by the analysis of the influence of BCNF on the shape, structure, and drug release of printed starch tablets.

- In Chapter 6, BC membranes were used as support of thiolated chitosan nanoparticles. The active membranes exhibited enhanced mucoadhesion to human tissues and antimicrobial activity, both of significant interest for wound healing applications.
- Chapter 7 presents the general conclusions of the study and provides an outlook on future work that emerged from BC applications and valorization of GP.

In Figure 1.7, the different integrated approaches studied throughout this work can be observed, in accordance with the objectives described above.

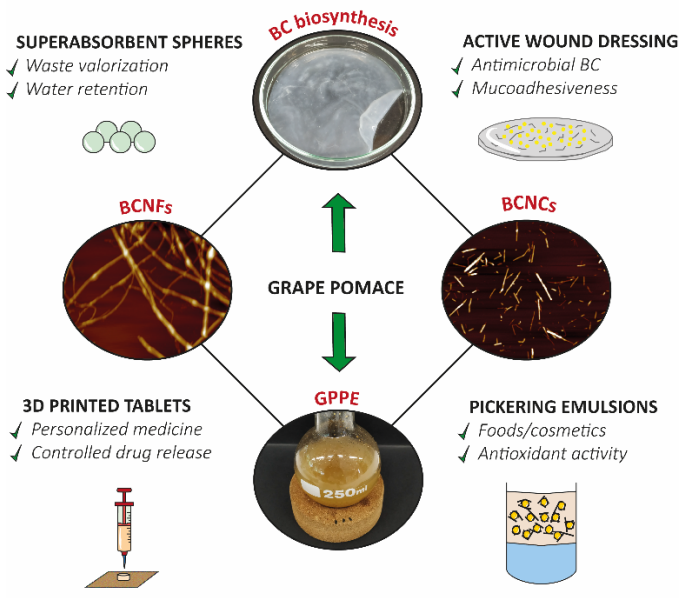

Figure 1.7 *Graphical representation of the different valorization strategies explored in this work.*

1.6 References

1 OIV and International Organisation of Vine and Wine. (2019) 2019 Statistical Report on World Vitiviniculture. 2019 Stat. Rep. World Vitiviniculture 23.

2 Perra, M., Bacchetta, G., Muntoni, A., De Gioannis, G., Castangia, I., Rajha, H. N., Manca, M. L. and Manconi, M. (2022) An outlook on modern and sustainable approaches to the management of grape pomace by integrating green processes, biotechnologies and advanced biomedical approaches. J. Funct. Foods, Elsevier Ltd **98**, 105276.

3 García-Lomillo, J. and González-SanJosé, M. L. (2017) Applications of Wine Pomace in the Food Industry: Approaches and Functions. Compr. Rev. Food Sci. Food Saf. **16**, 3–22.

4 Ardoa Basque Wine Office.

5 Kalli, E., Lappa, I., Bouchagier, P., Tarantilis, P. A. and Skotti, E. (2018) Novel application and industrial exploitation of winery by-products. Bioresour. Bioprocess., Springer Berlin Heidelberg **5**.

6 Spanghero, M., Salem, A. Z. M. and Robinson, P. H. (2009) Chemical composition, including secondary metabolites, and rumen fermentability of seeds and pulp of Californian (USA) and Italian grape pomaces. Anim. Feed Sci. Technol. **152**, 243–255.

7 Favre, G., Hermosín-Gutiérrez, I., Piccardo, D., Gómez-Alonso, S. and González-Neves, G. (2019) Selectivity of pigments extraction from grapes and their partial retention in the pomace during red-winemaking. Food Chem., Elsevier **277**, 391–397.

8 Yaashikaa, P. R., Senthil Kumar, P. and Varjani, S. (2022) Valorization of agro-industrial wastes for biorefinery process and circular bioeconomy: A critical review. Bioresour. Technol., Elsevier Ltd **343**, 126126.

9 Chowdhary, P., Gupta, A., Gnansounou, E., Pandey, A. and Chaturvedi, P. (2021) Current trends and possibilities for exploitation of Grape pomace as a potential source for value addition. Environ. Pollut., Elsevier Ltd **278**, 116796.

10 Negro, C., Tommasi, L. and Miceli, A. (2003) Phenolic compounds and

antioxidant activity from red grape marc extracts **87**, 41–44.

11 Jin, Q., Neilson, A. P., Stewart, A. C., Keefe, S. F. O., Kim, Y., Mcguire, M. and Huang, H. (2018) Integrated Approach for the Valorization of Red Grape Pomace: Production of Oil, Polyphenols, and Acetone − Butanol − Ethanol.

12 Jin, Q., Hair, J. O., Stewart, A. C., Keefe, S. F. O., Neilson, A. P., Kim, Y., Mcguire, M., Lee, A. and Huang, H. (2019) Industrial White and Red Grape Pomaces in Virginia Major Components. Foods **8**, 667.

13 Deng, Q., Penner, M. H. and Zhao, Y. (2011) Chemical composition of dietary fiber and polyphenols of five different varieties of wine grape pomace skins. Food Res. Int., Elsevier Ltd **44**, 2712–2720.

14 Muhlack, R. A., Potumarthi, R. and Jeffery, D. W. (2018) Sustainable wineries through waste valorisation: A review of grape marc utilisation for value-added products. Waste Manag., Elsevier Ltd **72**, 99–118.

15 Beres, C., Costa, G. N. S., Cabezudo, I., da Silva-James, N. K., Teles, A. S. C., Cruz, A. P. G., Mellinger-Silva, C., Tonon, R. V., Cabral, L. M. C. and Freitas, S. P. (2017) Towards integral utilization of grape pomace from winemaking process: A review. Waste Manag., Elsevier Ltd **68**, 581–594.

16 Ping, L., Brosse, N., Sannigrahi, P. and Ragauskas, A. (2011) Evaluation of grape stalks as a bioresource. Ind. Crop. Prod., Elsevier B.V. **33**, 200–204.

17 Guo, Y., Huang, J., Chen, Y., Hou, Q. and Huang, M. (2012) Effect of grape seed extract combined with modi fi ed atmosphere packaging on the quality of roast chicken. Poult. Sci., Elsevier Inc. **99**, 1598–1605.

18 Jin, Q., Keefe, S. F. O., Stewart, A. C., Neilson, A. P., Kim, Y. and Huang, H. (2021) Food and Bioproducts Processing Techno-economic analysis of a grape pomace biorefinery : Production of seed oil , polyphenols , and biochar **7**, 139–151.

19 Sirohi, R., Tarafdar, A., Singh, S., Negi, T., Kumar, V., Gnansounou, E. and Bharathiraja, B. (2020) Bioresource Technology Green processing and biotechnological potential of grape pomace : Current trends and opportunities for sustainable biorefinery. Bioresour. Technol., Elsevier **314**, 123771.

20 Farías, J. G., Herrera, E. A., Carrasco-Pozo, C., Sotomayor-Zárate, R., Cruz, G., Morales, P. and Castillo, R. L. (2016) Pharmacological models and approaches for pathophysiological conditions associated with hypoxia and oxidative stress. Pharmacol. Ther., Elsevier Inc. **158**, 1–23.

21 Bacchetti, T., Turco, I., Urbano, A., Morresi, C. and Ferretti, G. (2019) Relationship of fruit and vegetable intake to dietary antioxidant capacity and markers of oxidative stress: A sex-related study. Nutrition, Elsevier Inc. **61**, 164–172.

22 Barbalho, S. M., Bueno Ottoboni, A. M. M., Fiorini, A. M. R., Guiguer, É. L., Nicolau, C. C. T., Goulart, R. de A. and Flato, U. A. P. (2020) Grape juice or wine: which is the best option? Crit. Rev. Food Sci. Nutr., Taylor & Francis **60**, 3876–3889.

23 Yang, J. and Xiao, Y. Y. (2013) Grape Phytochemicals and Associated Health Benefits. Crit. Rev. Food Sci. Nutr. **53**, 1202–1225.

24 Dohadwala, M. M. and Vita, J. A. (2009) Grapes and cardiovascular disease. J. Nutr. **139**.

25 Singh, C. K., Mintie, C. A., Ndiaye, M. A., Chhabra, G., Dakup, P. P., Ye, T., Yu, M. and Ahmad, N. (2019) Chemoprotective Effects of Dietary Grape Powder on UVB Radiation-Mediated Skin Carcinogenesis in SKH-1 Hairless Mice. J. Invest. Dermatol., The Authors **139**, 552–561.

26 Svezia, B., Cabiati, M., Matteucci, M., Passino, C., Pè, M. E., Lionetti, V. and Del Ry, S. (2020) Tuscany Sangiovese grape juice imparts cardioprotection by regulating gene expression of cardioprotective C-type natriuretic peptide. Eur. J. Nutr. **59**, 2953–2968.

27 Nash, V., Ranadheera, C. S., Georgousopoulou, E. N., Mellor, D. D., Panagiotakos, D. B., McKune, A. J., Kellett, J. and Naumovski, N. (2018) The effects of grape and red wine polyphenols on gut microbiota – A systematic review. Food Res. Int., Elsevier **113**, 277–287.

28 Leite, P., Belo, I. and Salgado, J. M. (2021) Co-management of agro-industrial wastes by solid-state fermentation for the production of bioactive compounds. Ind. Crops Prod. **172**.

29 Dwyer, K., Hosseinian, F. and Rod, M. (2014) The Market Potential of Grape Waste Alternatives. J. Food Res. **3**, 91.

30 Dai, J. and Mumper, R. J. (2010) Plant phenolics: Extraction, analysis and their antioxidant and anticancer properties. Molecules **15**, 7313–7352.

31 Cortés, A., Moreira, M. T., Domínguez, J., Lores, M. and Feijoo, G. (2020) Unraveling the environmental impacts of bioactive compounds and organic amendment from grape marc. J. Environ. Manage. **272**.

32 Olszewska, M. A., Gędas, A. and Simões, M. (2020) Antimicrobial polyphenol-rich extracts: Applications and limitations in the food industry. Food Res. Int., Elsevier **134**, 109214.

33 Ahmad, B., Yadav, V., Yadav, A., Rahman, M. U., Yuan, W. Z., Li, Z. and Wang, X. (2020) Integrated biorefinery approach to valorize winery waste: A review from waste to energy perspectives. Sci. Total Environ., Elsevier B.V. **719**, 137315.

34 Troncozo, M. I., Ljević, M., Beškoski, V. P., Anđelković, B., Balatti, P. A. and Saparrat, M. C. N. (2019) Fungal transformation and reduction of phytotoxicity of grape pomace waste. Chemosphere **237**, 1–8.

35 Eleonora, N., Alina, D., Erzsebet, K. and Valeria, C. (2014) Grape pomace as fertilizer. For. Biotechnol. **18**, 141–145.

36 Martínez Salgado, M. M., Ortega Blu, R., Janssens, M. and Fincheira, P. (2019) Grape pomace compost as a source of organic matter: Evolution of quality parameters to evaluate maturity and stability. J. Clean. Prod., Elsevier Ltd **216**, 56–63.

37 Hungría, J., Gutiérrez, M. C., Siles, J. A. and Martín, M. A. (2017) Advantages and drawbacks of OFMSW and winery waste co-composting at pilot scale. J. Clean. Prod. **164**, 1050–1057.

38 Rouches, E., Herpoël-Gimbert, I., Steyer, J. P. and Carrere, H. (2016) Improvement of anaerobic degradation by white-rot fungi pretreatment of lignocellulosic biomass: A review. Renew. Sustain. Energy Rev., Elsevier **59**, 179–198.

39 Guerra-Rivas, C., Gallardo, B., Mantecón, Á. R., del Álamo-Sanza, M. and Manso, T. (2017) Evaluation of grape pomace from red wine by-product as feed for sheep. J. Sci. Food Agric. **97**, 1885–1893.

40 Flores, D. R. M., Fonseca, P. A. da and Nornberg, J. L. (2019) Effect of

Grape Pomace Inclusion on the Production and Quality of Sheep Meat. Trends Appl. Sci. Res. **14**, 226–232.

41 Kara, K., Kocaoɨlu Güçlü, B., Baytok, E. and Şentürk, M. (2016) Effects of grape pomace supplementation to laying hen diet on performance, egg quality, egg lipid peroxidation and some biochemical parameters. J. Appl. Anim. Res., Taylor & Francis **44**, 303–310.

42 Cisneros-Yupanqui, M., Rizzi, C., Mihaylova, D. and Lante, A. (2022) Effect of the distillation process on polyphenols content of grape pomace. Eur. Food Res. Technol., Springer Berlin Heidelberg **248**, 929–935.

43 Botelho, G., Anjos, O., Estevinho, L. M. and Caldeira, I. (2020) Methanol in grape derived, fruit and honey spirits: A critical review on source, quality control, and legal limits. Processes **8**, 1–21.

44 Strong, P. J. and Burgess, J. E. (2008) Treatment methods for wine-related and distillery wastewaters: A review. Bioremediat. J. **12**, 70–87.

45 Benetto, E., Jury, C., Kneip, G., Vázquez-Rowe, I., Huck, V. and Minette, F. (2015) Life cycle assessment of heat production from grape marc pellets. J. Clean. Prod. **87**, 149–158.

46 Almeida, P. V., Rodrigues, R. P., Slezak, R. and Quina, M. J. (2022) Effect of phenolic compound recovery from agro-industrial residues on the performance of pyrolysis process. Biomass Convers. Biorefinery, Springer Berlin Heidelberg **12**, 4257–4269.

47 Yoon, J. Y., Kim, J. E., Song, H. J., Oh, K. Bin, Jo, J. W., Yang, Y. H., Lee, S. H., Kang, G., Kim, H. J. and Choi, Y. K. (2021) Assessment of adsorptive behaviors and properties of grape pomace-derived biochar as adsorbent for removal of cymoxanil pesticide. Environ. Technol. Innov., Elsevier B.V. **21**, 101242.

48 Jin, Q., Wang, Z., Feng, Y., Kim, Y. T., Stewart, A. C., O'Keefe, S. F., Neilson, A. P., He, Z. and Huang, H. (2020) Grape pomace and its secondary waste management: Biochar production for a broad range of lead (Pb) removal from water. Environ. Res., Elsevier Inc. **186**, 109442.

49 Garrido, R. A., Lagos, C., Luna, C., Sánchez, J. and Díaz, G. (2021) Study of the potential uses of hydrochar from grape pomace and walnut

shells generated from hydrothermal carbonization as an alternative for the revalorization of agri-waste in Chile. Sustain. **13**.

50 Salaudeen, S. A., Acharya, B. and Dutta, A. (2021) Steam gasification of hydrochar derived from hydrothermal carbonization of fruit wastes. Renew. Energy, Elsevier Ltd **171**, 582–591.

51 Soquetta, M. B., Terra, L. de M. and Bastos, C. P. (2018) Green technologies for the extraction of bioactive compounds in fruits and vegetables. CYTA - J. Food, Taylor & Francis **16**, 400–412.

52 Lavelli, V., Kerr, W. L., García-lomillo, J. and González-sanjosé, M. L. (2017) Compounds in Food Products. Handb. Grape Process. By-Products, Elsevier Inc.

53 De Groote, D., Van Belleghem, K., Devire, J., Van Brussel, W., Mukaneza, A. and Amininejad, L. (2012) Effect of the intake of resveratrol, resveratrol phosphate, and catechin-rich grape seed extract on markers of oxidative stress and gene expression in adult obese subjects. Ann. Nutr. Metab. **61**, 15–24.

54 Antonacci D, B. M. (2014) Anticancer Effects of Grape Seed Extract on Human Cancers: A Review. J. Carcinog. Mutagen. **s8**.

55 Carra, J. B., Matos, R. L. N. de, Novelli, A. P., Couto, R. O. do, Yamashita, F., Ribeiro, M. A. dos S., Meurer, E. C., Verri, W. A., Casagrande, R., Georgetti, S. R., et al. (2022) Spray-drying of casein/pectin bioconjugate microcapsules containing grape (Vitis labrusca) by-product extract. Food Chem. **368**.

56 Giovanna Simonetti, C. P. (2019) Anti- Candida biofilm activity of pterostilbene or crude extract from non-fermented Grape pomace. Molecules **24**, 1–14.

57 Gaber Ahmed, G. H., Fernández-González, A. and Díaz García, M. E. (2020) Nano-encapsulation of grape and apple pomace phenolic extract in chitosan and soy protein via nanoemulsification. Food Hydrocoll. **108**.

58 El Achkar, J. H., Lendormi, T., Hobaika, Z., Salameh, D., Louka, N., Maroun, R. G. and Lanoisellé, J. L. (2016) Anaerobic digestion of grape pomace: Biochemical characterization of the fractions and methane production in batch and continuous digesters. Waste Manag., Elsevier

Ltd **50**, 275–282.

59 Zheng, Y., Lee, C., Yu, C., Cheng, Y. S., Simmons, C. W., Zhang, R., Jenkins, B. M. and Vandergheynst, J. S. (2012) Ensilage and bioconversion of grape pomace into fuel ethanol. J. Agric. Food Chem. **60**, 11128–11134.

60 Filippi, K., Georgaka, N., Alexandri, M., Papapostolou, H. and Koutinas, A. (2021) Valorisation of grape stalks and pomace for the production of bio-based succinic acid by Actinobacillus succinogenes. Ind. Crops Prod., Elsevier B.V. **168**, 113578.

61 Khiari, B. and Jeguirim, M. (2018) Pyrolysis of grape marc from Tunisian wine industry: Feedstock characterization, thermal degradation and kinetic analysis. Energies **11**.

62 Papadaki, E., Kontogiannopoulos, K. N., Assimopoulou, A. N. and Mantzouridou, F. T. (2020) Feasibility of multi-hydrolytic enzymes production from optimized grape pomace residues and wheat bran mixture using Aspergillus niger in an integrated citric acid-enzymes production process. Bioresour. Technol., Elsevier **309**, 123317.

63 Altan Kamer, D. D., Gumus, T., Palabiyik, I., Demirci, A. S. and Oksuz, O. (2021) Grape pomace as a promising source for gellan gum production. Food Hydrocoll., Elsevier Ltd **114**, 106584.

64 Martinez, G. A., Domingos, J. B., Rebecchi, S., Fava, F., Bologna, U., Porto, C. Da, Natolino, A., Decorti, D. and Udine, U. (2014) An agro-industrial waste valorization : biopolymer production from dephenolized and fermented grape pomace 1–6.

65 Follonier, S., Goyder, M. S., Silvestri, A. C., Crelier, S., Kalman, F., Riesen, R. and Zinn, M. (2014) Fruit pomace and waste frying oil as sustainable resources for the bioproduction of medium-chain-length polyhydroxyalkanoates. Int. J. Biol. Macromol., Elsevier B.V. **71**, 42–52.

66 Cerrutti, P., Roldán, P., García, R. M., Galvagno, M. A., Vázquez, A. and Foresti, M. L. (2016) Production of bacterial nanocellulose from wine industry residues: Importance of fermentation time on pellicle characteristics. J. Appl. Polym. Sci. **133**, 1–9.

67 Carreira, P., Mendes, J. A. S., Trovatti, E., Serafim, L. S., Freire, C. S. R.,

Silvestre, A. J. D. and Neto, C. P. (2011) Utilization of residues from agro-forest industries in the production of high value bacterial cellulose. Bioresour. Technol.

68 Atila, F. (2019) A Useful Way to Dispose of Phenolic-rich Agro-industrial Wastes: Mushroom Cultivation. Turkey) EJENS **3**, 32–41.

69 Andriani, D., Apriyana, A. Y. and Karina, M. (2020) The optimization of bacterial cellulose production and its applications: a review. Cellulose, Springer Netherlands **27**, 6747–6766.

70 Hon, D. N. S. (1994) Cellulose: a random walk along its historical path. Cellulose **1**, 1–25.

71 Singhania, R. R., Patel, A. K., Tseng, Y. S., Kumar, V., Chen, C. W., Haldar, D., Saini, J. K. and Dong, C. Di. (2022) Developments in bioprocess for bacterial cellulose production. Bioresour. Technol., Elsevier Ltd **344**, 126343.

72 Singhania, R. R., Ruiz, H. A., Awasthi, M. K., Dong, C. Di, Chen, C. W. and Patel, A. K. (2021) Challenges in cellulase bioprocess for biofuel applications. Renew. Sustain. Energy Rev. **151**.

73 Urbina, L., Corcuera, M. Á., Gabilondo, N., Eceiza, A. and Retegi, A. (2021) A review of bacterial cellulose: sustainable production from agricultural waste and applications in various fields. Cellulose **28**, 8229–8253.

74 Jozala, A. F., de Lencastre-Novaes, L. C., Lopes, A. M., de Carvalho Santos-Ebinuma, V., Mazzola, P. G., Pessoa-Jr, A., Grotto, D., Gerenutti, M. and Chaud, M. V. (2016) Bacterial nanocellulose production and application: a 10-year overview. Appl. Microbiol. Biotechnol. **100**, 2063–2072.

75 Numata, Y., Kono, H., Mori, A., Kishimoto, R. and Tajima, K. (2019) Structural and rheological characterization of bacterial cellulose gels obtained from Gluconacetobacter genus. Food Hydrocoll., Elsevier Ltd **92**, 233–239.

76 Castro, C., Zuluaga, R., Álvarez, C., Putaux, J. L., Caro, G., Rojas, O. J., Mondragon, I. and Gañán, P. (2012) Bacterial cellulose produced by a new acid-resistant strain of Gluconacetobacter genus. Carbohydr.

Polym. **89**, 1033–1037.

77 Hong, F., Guo, X., Zhang, S., Han, S. fen, Yang, G. and Jönsson, L. J. (2012) Bacterial cellulose production from cotton-based waste textiles: Enzymatic saccharification enhanced by ionic liquid pretreatment. Bioresour. Technol., Elsevier Ltd **104**, 503–508.

78 Chen, L., Hong, F., Yang, X. xia and Han, S. fen. (2013) Biotransformation of wheat straw to bacterial cellulose and its mechanism. Bioresour. Technol., Elsevier Ltd **135**, 464–468.

79 Urbina, L., Hernández-Arriaga, A. M., Eceiza, A., Gabilondo, N., Corcuera, M. A., Prieto, M. A. and Retegi, A. (2017) By-products of the cider production: an alternative source of nutrients to produce bacterial cellulose. Cellulose **24**, 2071–2082.

80 Brown, J. (1886) XLIII-on an acetic ferment which forms cellulose. J. Chem. Soc. Trans. 432–439.

81 Retegi, A., Gabilondo, N., Peña, C., Zuluaga, R., Castro, C., Gañan, P., de la Caba, K. and Mondragon, I. (2010) Bacterial cellulose films with controlled microstructure-mechanical property relationships. Cellulose **17**, 661–669.

82 Lee, K. Y., Buldum, G., Mantalaris, A. and Bismarck, A. (2014) More than meets the eye in bacterial cellulose: Biosynthesis, bioprocessing, and applications in advanced fiber composites. Macromol. Biosci. **14**, 10–32.

83 Singhsa, P., Narain, R. and Manuspiya, H. (2018) Physical structure variations of bacterial cellulose produced by different Komagataeibacter xylinus strains and carbon sources in static and agitated conditions. Cellulose, Springer Netherlands **25**, 1571–1581.

84 Singhania, R. R., Patel, A. K., Tsai, M., Chen, C., Rani, R., Patel, A. K., Tsai, M. and Chen, C. (2021) Genetic modification for enhancing bacterial cellulose production and its applications. Bioengineered, Taylor & Francis **12**, 6793–6807.

85 Mehta, K. and Pfeffer, S. (2015) Characterization of an acsD disruption mutant provides additional evidence for the hierarchical cell-directed self-assembly of cellulose in Gluconacetobacter xylinus 119–137.

86 Omadjela, O., Narahari, A., Strumillo, J., Mélida, H., Mazur, O. and Bulone, V. (2013) BcsA and BcsB form the catalytically active core of bacterial cellulose synthase suf fi cient for in vitro cellulose synthesis **110**, 1–6.

87 Matsutani, M., Ito, K., Azuma, Y. and Ogino, H. (2015) Adaptive mutation related to cellulose producibility in Komagataeibacter medellinensis (Gluconacetobacter xylinus) NBRC 3288 7229–7240.

88 Cerro, C., Urbina, L. and Eceiza, A. (2019) Genome sequence and characterization of the bcs clusters for the production of nanocellulose from the low pH resistant strain Komagataeibacter medellinensis.

89 Florea, M., Hagemann, H., Santosa, G., Abbott, J. and Micklem, C. N. (2016) Engineering control of bacterial cellulose production using a genetic toolkit and a new cellulose- producing strain 3431–3440.

90 Shaghaleh, H., Xu, X. and Wang, S. (2018) Current progress in production of biopolymeric materials based on cellulose, cellulose nanofibers, and cellulose derivatives. RSC Adv. **8**, 825–842.

91 van Zyl, E. M. and Coburn, J. M. (2019) Hierarchical structure of bacterial-derived cellulose and its impact on biomedical applications. Curr. Opin. Chem. Eng., Elsevier Ltd **24**, 122–130.

92 Castro, C., Zuluaga, R., Putaux, J. L., Caro, G., Mondragon, I. and Gañán, P. (2011) Structural characterization of bacterial cellulose produced by Gluconacetobacter swingsii sp. from Colombian agroindustrial wastes. Carbohydr. Polym. **84**, 96–102.

93 Wang, S., Jiang, F., Xu, X., Kuang, Y., Fu, K., Hitz, E. and Hu, L. (2017) Super-Strong, Super-Stiff Macrofibers with Aligned, Long Bacterial Cellulose Nanofibers. Adv. Mater. **29**, 1–8.

94 Urbina, L., Corcuera, M. Á., Eceiza, A. and Retegi, A. (2019) Stiff all-bacterial cellulose nanopaper with enhanced mechanical and barrier properties. Mater. Lett., Elsevier B.V. **246**, 67–70.

95 Gao, M., Li, J., Bao, Z., Hu, M., Nian, R., Feng, D., An, D., Li, X., Xian, M. and Zhang, H. (2019) A natural in situ fabrication method of functional bacterial cellulose using a microorganism. Nat. Commun., Springer US **10**, 1–10.

96 Shao, W., Wu, J., Liu, H., Ye, S., Jiang, L. and Liu, X. (2017) Novel bioactive surface functionalization of bacterial cellulose membrane. Carbohydr. Polym., Elsevier **178**, 270–276.

97 Lee, K. Y., Quero, F., Blaker, J. J., Hill, C. A. S., Eichhorn, S. J. and Bismarck, A. (2011) Surface only modification of bacterial cellulose nanofibres with organic acids. Cellulose **18**, 595–605.

98 Stumpf, T. R., Yang, X., Zhang, J. and Cao, X. (2018) In situ and ex situ modifications of bacterial cellulose for applications in tissue engineering. Mater. Sci. Eng. C, Elsevier B.V. **82**, 372–383.

99 Faisul Aris, F. A., Mohd Fauzi, F. N. A., Tong, W. Y. and Syed Abdullah, S. S. (2019) Interaction of silver sulfadiazine wıth bacterial cellulose via ex-situ modification method as an alternative diabetic wound healing. Biocatal. Agric. Biotechnol., Elsevier Ltd **21**, 101332.

100 Adepu, S. and Khandelwal, M. (2020) Ex-situ modification of bacterial cellulose for immediate and sustained drug release with insights into release mechanism. Carbohydr. Polym., Elsevier **249**, 116816.

101 Urbina, L., Guaresti, O., Requies, J., Gabilondo, N., Eceiza, A., Corcuera, M. A. and Retegi, A. (2018) Design of reusable novel membranes based on bacterial cellulose and chitosan for the filtration of copper in wastewaters. Carbohydr. Polym., Elsevier **193**, 362–372.

102 Khandelwal, M., Windle, A. H. and Hessler, N. (2016) In situ tunability of bacteria produced cellulose by additives in the culture media. J. Mater. Sci., Springer US **51**, 4839–4844.

103 Surendran, G. and Sherje, A. P. (2022) Cellulose nanofibers and composites: An insight into basics and biomedical applications. J. Drug Deliv. Sci. Technol., Elsevier B.V. **75**, 103601.

104 Mali, P. and Sherje, A. P. (2022) Cellulose nanocrystals: Fundamentals and biomedical applications. Carbohydr. Polym., Elsevier Ltd **275**, 118668.

105 Anusiya, G. and Jaiganesh, R. (2022) A review on fabrication methods of nanofibers and a special focus on application of cellulose nanofibers. Carbohydr. Polym. Technol. Appl., Elsevier Ltd **4**, 100262.

106 Bangar, S. P., Harussani, M. M., Ilyas, R. A., Ashogbon, A. O., Singh, A., Trif, M. and Jafari, S. M. (2022) Surface modifications of cellulose nanocrystals: Processes, properties, and applications. Food Hydrocoll., Elsevier Ltd **130**, 107689.

107 Torgbo, S. and Sukyai, P. (2020) Biodegradation and thermal stability of bacterial cellulose as biomaterial: The relevance in biomedical applications. Polym. Degrad. Stab., Elsevier Ltd **179**, 109232.

108 Urbina, L., Algar, I., García-Astrain, C., Gabilondo, N., González, A., Corcuera, M., Eceiza, A. and Retegi, A. (2016) Biodegradable composites with improved barrier properties and transparency from the impregnation of PLA to bacterial cellulose membranes. J. Appl. Polym. Sci. **133**, 1–10.

109 Lima, F. de M. T. de, Pinto, F. C. M., Andrade-da-Costa, B. L. da S., Silva, J. G. M. da, Campos Júnior, O. and Aguiar, J. L. de A. (2017) Biocompatible bacterial cellulose membrane in dural defect repair of rat. J. Mater. Sci. Mater. Med., Springer US **28**.

110 Urbina, L., Alonso-Varona, A., Saralegi, A., Palomares, T., Eceiza, A., Corcuera, M. Á. and Retegi, A. (2019) Hybrid and biocompatible cellulose/polyurethane nanocomposites with water-activated shape memory properties. Carbohydr. Polym., Elsevier **216**, 86–96.

111 HESTRIN, S. and SCHRAMM, M. (1954) Synthesis of cellulose by Acetobacter xylinum. II. Preparation of freeze-dried cells capable of polymerizing glucose to cellulose. Biochem. J. **58**, 345–352.

112 Blanco Parte, F. G., Santoso, S. P., Chou, C. C., Verma, V., Wang, H. T., Ismadji, S. and Cheng, K. C. (2020) Current progress on the production, modification, and applications of bacterial cellulose. Crit. Rev. Biotechnol., Taylor & Francis **40**, 397–414.

113 Rivas, B., Moldes, A. B., Domínguez, J. M. and Parajó, J. C. (2004) Development of culture media containing spent yeast cells of Debaryomyces hansenii and corn steep liquor for lactic acid production with Lactobacillus rhamnosus. Int. J. Food Microbiol. **97**, 93–98.

114 Skiba, E. A., Budaeva, V. V, Ovchinnikova, E. V, Gladysheva, E. K., Kashcheyeva, E. I., Pavlov, I. N. and Sakovich, G. V. (2020) A technology for pilot production of bacterial cellulose from oat hulls. Chem. Eng. J.,

Elsevier **383**, 123128.

115 Goelzer, F. D. E., Faria-Tischer, P. C. S., Vitorino, J. C., Sierakowski, M. R. and Tischer, C. A. (2009) Production and characterization of nanospheres of bacterial cellulose from Acetobacter xylinum from processed rice bark. Mater. Sci. Eng. C, Elsevier B.V. **29**, 546–551.

116 Cheng, Z., Yang, R., Liu, X., Liu, X. and Chen, H. (2017) Green synthesis of bacterial cellulose via acetic acid pre-hydrolysis liquor of agricultural corn stalk used as carbon source. Bioresour. Technol., Elsevier Ltd **234**, 8–14.

117 Jozala, A. F., Pértile, R. A. N., dos Santos, C. A., de Carvalho Santos-Ebinuma, V., Seckler, M. M., Gama, F. M. and Pessoa, A. (2015) Bacterial cellulose production by Gluconacetobacter xylinus by employing alternative culture media. Appl. Microbiol. Biotechnol. **99**, 1181–1190.

118 Algar, I., Fernandes, S. C. M., Mondragon, G., Castro, C., Garcia-Astrain, C., Gabilondo, N., Retegi, A. and Eceiza, A. (2014) Pineapple agroindustrial residues for the production of high value bacterial cellulose with different morphologies. J. Appl. Polym. Sci. **132**, 1–8.

119 Kuo, C. H., Huang, C. Y., Shieh, C. J., Wang, H. M. D. and Tseng, C. Y. (2019) Hydrolysis of Orange Peel with Cellulase and Pectinase to Produce Bacterial Cellulose using Gluconacetobacter xylinus. Waste and Biomass Valorization, Springer Netherlands **10**, 85–93.

120 Mohite, B. V. and Patil, S. V. (2014) Physical, structural, mechanical and thermal characterization of bacterial cellulose by G. hansenii NCIM 2529. Carbohydr. Polym., Elsevier Ltd. **106**, 132–141.

121 Molina-Ramírez, C., Castro, M., Osorio, M., Torres-Taborda, M., Gómez, B., Zuluaga, R., Gómez, C., Gañán, P., Rojas, O. J. and Castro, C. (2017) Effect of different carbon sources on bacterial nanocellulose production and structure using the low pH resistant strain Komagataeibacter medellinensis. Materials (Basel). **10**.

122 Pastorkova, E., Zakova, T., Landa, P., Novakova, J., Vadlejch, J. and Kokoska, L. (2013) Growth inhibitory effect of grape phenolics against wine spoilage yeasts and acetic acid bacteria. Int. J. Food Microbiol., Elsevier B.V. **161**, 209–213.

123 Gao, H., Sun, Q., Han, Z., Li, J., Liao, B., Hu, L., Huang, J., Zou, C., Jia, C., Huang, J., et al. (2020) Comparison of bacterial nanocellulose produced by different strains under static and agitated culture conditions. Carbohydr. Polym., Elsevier **227**, 115323.

124 Erbas Kiziltas, E., Kiziltas, A. and Gardner, D. J. (2015) Synthesis of bacterial cellulose using hot water extracted wood sugars. Carbohydr. Polym., Elsevier Ltd. **124**, 131–138.

125 Sheykhnazari, S., Tabarsa, T., Ashori, A., Shakeri, A. and Golalipour, M. (2011) Bacterial synthesized cellulose nanofibers; Effects of growth times and culture mediums on the structural characteristics. Carbohydr. Polym., Elsevier Ltd. **86**, 1187–1191.

126 Hu, Y., Catchmark, J. M. and Vogler, E. A. (2013) Factors impacting the formation of sphere-like bacterial cellulose particles and their biocompatibility for human osteoblast growth. Biomacromolecules **14**, 3444–3452.

127 Czaja, W., Romanovicz, D. and Brown, R. malcolm. (2004) Structural investigations of microbial cellulose produced in stationary and agitated culture. Cellulose **11**, 403–411.

128 Urbina, L., Eceiza, A., Gabilondo, N., Corcuera, M. Á. and Retegi, A. (2020) Tailoring the in situ conformation of bacterial cellulose-graphene oxide spherical nanocarriers. Int. J. Biol. Macromol., Elsevier B.V. **163**, 1249–1260.

129 Hoshi, T., Yamazaki, K., Sato, Y., Shida, T. and Aoyagi, T. (2018) Production of hollow-type spherical bacterial cellulose as a controlled release device by newly designed floating cultivation. Heliyon, Elsevier Ltd **4**, e00873.

130 Liu, M., Zhong, C., Wu, X. Y., Wei, Y. Q., Bo, T., Han, P. P. and Jia, S. R. (2015) Metabolomic profiling coupled with metabolic network reveals differences in Gluconacetobacter xylinus from static and agitated cultures. Biochem. Eng. J., Elsevier B.V. **101**, 85–98.

131 Caro-Astorga, J., Walker, K. T., Herrera, N., Lee, K. Y. and Ellis, T. (2021) Bacterial cellulose spheroids as building blocks for 3D and patterned living materials and for regeneration. Nat. Commun., Springer US **12**, 1–9.

132 Esa, F., Tasirin, S. M. and Rahman, N. A. (2014) Overview of Bacterial Cellulose Production and Application. Agric. Agric. Sci. Procedia, Elsevier Srl **2**, 113–119.

133 Wu, S. C. and Li, M. H. (2015) Production of bacterial cellulose membranes in a modified airlift bioreactor by Gluconacetobacter xylinus. J. Biosci. Bioeng., Elsevier Ltd **120**, 444–449.

134 Bae, S. and Shoda, M. (2004) Bacterial Cellulose Production by Fed-Batch Fermentation in Molasses Medium 1366–1371.

135 Hsieh, J. T., Wang, M. J., Lai, J. T. and Liu, H. S. (2016) A novel static cultivation of bacterial cellulose production by intermittent feeding strategy. J. Taiwan Inst. Chem. Eng., Elsevier B.V. **63**, 46–51.

136 Cheng, K. C., Catchmark, J. M. and Demirci, A. (2009) Enhanced production of bacterial cellulose by using a biofilm reactor and its material property analysis. J. Biol. Eng. **3**, 1–10.

137 Lin, S. P., Hsieh, S. C., Chen, K. I., Demirci, A. and Cheng, K. C. (2014) Semi-continuous bacterial cellulose production in a rotating disk bioreactor and its materials properties analysis. Cellulose **21**, 835–844.

138 Navya, P. V., Gayathri, V., Samanta, D. and Sampath, S. (2022) Bacterial cellulose: A promising biopolymer with interesting properties and applications. Int. J. Biol. Macromol., Elsevier B.V. **220**, 435–461.

139 Tyagi, N., Thangadurai, P. and Suresh, S. (2020) Application of bacterial cellulose–silver nanoprism composite for detoxification of endosulfan and inactivation of Escherichia coli cells. Int. J. Environ. Sci. Technol., Springer Berlin Heidelberg **17**, 1713–1726.

140 Hou, Y., Duan, C., Zhu, G., Luo, H., Liang, S., Jin, Y., Zhao, N. and Xu, J. (2019) Functional bacterial cellulose membranes with 3D porous architectures: Conventional drying, tunable wettability and water/oil separation. J. Memb. Sci., Elsevier B.V. **591**, 117312.

141 Gholami Derami, H., Jiang, Q., Ghim, D., Cao, S., Chandar, Y. J., Morrissey, J. J., Jun, Y. S. and Singamaneni, S. (2019) A Robust and Scalable Polydopamine/Bacterial Nanocellulose Hybrid Membrane for Efficient Wastewater Treatment. ACS Appl. Nano Mater. **2**, 1092–1101.

142 Urbina, L., Guaresti, O., Requies, J., Gabilondo, N., Eceiza, A., Corcuera, M. A. and Retegi, A. (2018) Design of reusable novel membranes based on bacterial cellulose and chitosan for the filtration of copper in wastewaters. Carbohydr. Polym., Elsevier **193**, 362–372.

143 Sai, H., Fu, R., Xing, L., Xiang, J., Li, Z., Li, F. and Zhang, T. (2015) Surface modification of bacterial cellulose aerogels' web-like skeleton for oil/water separation. ACS Appl. Mater. Interfaces **7**, 7373–7381.

144 Dai, H., Wu, J., Zhang, H., Chen, Y., Ma, L., Huang, H., Huang, Y. and Zhang, Y. (2020) Recent advances on cellulose nanocrystals for Pickering emulsions: Development and challenge. Trends Food Sci. Technol., Elsevier **102**, 16–29.

145 Yan, H., Chen, X., Song, H., Li, J., Feng, Y., Shi, Z., Wang, X. and Lin, Q. (2017) Synthesis of bacterial cellulose and bacterial cellulose nanocrystals for their applications in the stabilization of olive oil pickering emulsion. Food Hydrocoll., Elsevier Ltd **72**, 127–135.

146 Zahedmanesh, H., MacKle, J. N., Sellborn, A., Drotz, K., Bodin, A., Gatenholm, P. and Lally, C. (2011) Bacterial cellulose as a potential vascular graft: Mechanical characterization and constitutive model development. J. Biomed. Mater. Res. - Part B Appl. Biomater. **97 B**, 105–113.

147 Lv, X., Yang, J., Feng, C., Li, Z., Chen, S., Xie, M., Huang, J., Li, H., Wang, H. and Xu, Y. (2016) Bacterial Cellulose-Based Biomimetic Nanofibrous Scaffold with Muscle Cells for Hollow Organ Tissue Engineering. ACS Biomater. Sci. Eng. **2**, 19–29.

148 Portela, R., Leal, C. R., Almeida, P. L. and Sobral, R. G. (2019) Bacterial cellulose: a versatile biopolymer for wound dressing applications. Microb. Biotechnol. **12**, 586–610.

149 Zhao, Q., Wang, S., Xie, Y., Zheng, W., Wang, Z., Xiao, L., Zhang, W. and Jiang, X. (2012) A rapid screening method for wound dressing by cell-on-a-chip device. Adv. Healthc. Mater. **1**, 560–566.

150 Gupta, A., Briffa, S. M., Swingler, S., Gibson, H., Kannappan, V., Adamus, G., Kowalczuk, M., Martin, C. and Radecka, I. (2020) Synthesis of Silver Nanoparticles Using Curcumin-Cyclodextrins Loaded into Bacterial Cellulose-Based Hydrogels for Wound Dressing Applications.

Biomacromolecules **21**, 1802–1811.

151 Savitskaya, I. S., Kistaubayeva, A. S., Digel, I. E. and Shokatayeva, D. H. (2017) Physicochemical and antibacterial properties of composite films based on bacterial cellulose and chitosan for wound dressing materials. Eurasian Chem. J. **19**, 255–264.

152 Abeer, M. M., Mohd Amin, M. C. I. and Martin, C. (2014) A review of bacterial cellulose-based drug delivery systems: Their biochemistry, current approaches and future prospects. J. Pharm. Pharmacol. **66**, 1047–1061.

153 Pandey, M., Mohamad, N. and Amin, M. C. I. M. (2014) Bacterial cellulose/acrylamide pH-sensitive smart hydrogel: Development, characterization, and toxicity studies in ICR mice model. Mol. Pharm. **11**, 3596–3608.

154 Yuan, Y., Zhang, S., Ma, M., Wang, D. and Xu, Y. (2022) Encapsulation and delivery of curcumin in cellulose nanocrystals nanoparticles using pH-driven method. Lwt, Elsevier Ltd **155**, 112863.

155 Singhsa, P., Narain, R. and Manuspiya, H. (2018) Bacterial Cellulose Nanocrystals (BCNC) Preparation and Characterization from Three Bacterial Cellulose Sources and Development of Functionalized BCNCs as Nucleic Acid Delivery Systems. ACS Appl. Nano Mater. **1**, 209–221.

156 Dourado, F., Gama, M. and Rodrigues, A. C. (2017) A Review on the toxicology and dietetic role of bacterial cellulose. Toxicol. Reports, Elsevier **4**, 543–553.

157 Shi, Z., Zhang, Y., Phillips, G. O. and Yang, G. (2014) Utilization of bacterial cellulose in food. Food Hydrocoll., Elsevier Ltd **35**, 539–545.

158 Zhai, X., Lin, D., Liu, D. and Yang, X. (2018) Emulsions stabilized by nanofibers from bacterial cellulose: New potential food-grade Pickering emulsions. Food Res. Int., Elsevier **103**, 12–20.

159 Campano, C., Merayo, N., Negro, C. and Blanco, Á. (2018) Low-fibrillated bacterial cellulose nanofibers as a sustainable additive to enhance recycled paper quality. Int. J. Biol. Macromol. **114**, 1077–1083.

160 Cabañas-Romero, L. V., Valls, C., Valenzuela, S. V., Roncero, M. B.,

Pastor, F. I. J., Diaz, P. and Martínez, J. (2020) Bacterial Cellulose-Chitosan Paper with Antimicrobial and Antioxidant Activities. Biomacromolecules **21**, 1568–1577.

161 Moradi, M., Tajik, H., Almasi, H., Forough, M. and Ezati, P. (2019) A novel pH-sensing indicator based on bacterial cellulose nanofibers and black carrot anthocyanins for monitoring fish freshness. Carbohydr. Polym., Elsevier **222**, 115030.

162 Pirsa, S. and Chavoshizadeh, S. (2018) Design of an optical sensor for ethylene based on nanofiber bacterial cellulose film and its application for determination of banana storage time. Polym. Adv. Technol. **29**, 1385–1393.

163 Chen, L. F., Huang, Z. H., Liang, H. W., Gao, H. L. and Yu, S. H. (2014) Three-dimensional heteroatom-doped carbon nanofiber networks derived from bacterial cellulose for supercapacitors. Adv. Funct. Mater. **24**, 5104–5111.

164 Zhao, N., Wu, F., Xing, Y., Qu, W., Chen, N., Shang, Y., Yan, M., Li, Y., Li, L. and Chen, R. (2019) Flexible Hydrogel Electrolyte with Superior Mechanical Properties Based on Poly(vinyl alcohol) and Bacterial Cellulose for the Solid-State Zinc-Air Batteries. ACS Appl. Mater. Interfaces **11**, 15537–15542.

165 Schaffner, M., Rühs, P. A., Coulter, F., Kilcher, S. and Studart, A. R. (2017) 3D printing of bacteria into functional complex materials. Sci. Adv. **3**.

166 Shin, S., Kwak, H., Shin, D. and Hyun, J. (2019) Solid matrix-assisted printing for three-dimensional structuring of a viscoelastic medium surface. Nat. Commun., Springer US **10**.

167 Olmos-Juste, R., Alonso-Lerma, B., Pérez-Jiménez, R., Gabilondo, N. and Eceiza, A. (2021) 3D printed alginate-cellulose nanofibers based patches for local curcumin administration. Carbohydr. Polym. **264**.

168 Larraza, I., Vadillo, J., Calvo-Correas, T., Tejado, A., Martin, L., Arbelaiz, A. and Eceiza, A. (2022) Effect of Cellulose Nanofibers' Structure and Incorporation Route in Waterborne Polyurethane–Urea Based Nanocomposite Inks. Polymers (Basel). **14**.

169 Vadillo, J., Larraza, I., Calvo-Correas, T., Gabilondo, N., Derail, C. and Eceiza, A. (2022) Bioactive inks suitable for 3D printing based on waterborne polyurethane urea, cellulose nanocrystals and Salvia extract. React. Funct. Polym., Elsevier B.V. **175**, 105286.

170 Velásquez-Riaño, M. and Bojacá, V. (2017) Production of bacterial cellulose from alternative low-cost substrates. Cellulose **24**, 2677–2698.

171 Menzel, C., González-Martínez, C., Chiralt, A. and Vilaplana, F. (2019) Antioxidant starch films containing sunflower hull extracts. Carbohydr. Polym. **214**, 142–151.

172 Ul-Islam, M., Ullah, M. W., Khan, T. and Park, J. K. (2021) Bacterial cellulose: Trends in synthesis, characterization, and applications. Handb. Hydrocoll. 3rd ed., Elsevier Ltd.

173 Vergara, B. S., Idowu, P. M. H. and Sumangil, J. H. (1999) Nata de Coco: A Filipino Delicacy.

174 Gama, M., Dourado, F. and Bielecki, S. (2016) Bacterial Nanocellulose, Elsevier.

CHAPTER 2

MATERIALS AND CHARACTERIZATION TECHNIQUES



2.1 Materials and reagents 51
2.2 Characterization techniques 53
2.2.1 Physicochemical characterization 53
2.2.2 Thermal characterization 60
2.2.3 Hydrophilicity 61
2.2.4 Morphological characterization 62
2.2.5 Rheological characterization 64
2.2.6 Antioxidant activity characterization 65
2.2.7 Biocompatibility 67
2.2.8 Antimicrobial activity 68
2.2.9 Statistical analysis 69
2.3 References 69

Chapter 2: Materials and characterization techniques

2.1 Materials and reagents

The following reagents were required for the preparation of the HS culture medium and BC purification in Chapter 3: D-Glucose ($C_6H_{12}O_6$ ≥ 99.0%), yeast extract (≥89.0%), disodium hydrogen phosphate (Na_2HPO_4 ≥ 99.0%) and citric acid ($C_6H_8O_7$ ≥ 99.5%) were purchased from Sigma Aldrich (USA). Peptone (≥85%) and potassium hydroxide (KOH) were obtained from Panreac Applychem (Spain). Urea detection studies were carried out using acetonitrile from Scharlab (Spain), 4-(dimethylamino) benzaldehyde 99% (DMAB) from Sigma Aldrich (USA) and hydrochloric acid (HCl 37%) Panreac Applychem (Spain).

Regarding Chapter 4, cellulase from *Trichoderma sp*. 6,9 U/mg for BC enzymatic digestion was obtained from Sigma Aldrich (USA) and sodium citrate buffer from Panreac Applychem (Spain). Sulfuric acid (H_2SO_4 ≥ 95%) was acquired from Panreac Applychem (Spain) in the acid hydrolysis of the BC. For the polyphenol extraction experiments ascorbic acid (≥89.0%) from Sigma Aldrich (USA), acetic acid (HAc ≥ 99.5%) from Panreac Applychem (Spain) and methanol (99%) from Scharlau (Spain) were utilized.

Antioxidant activity assays in Chapter 4 were carried out with 6-hydroxy-2,5,7,8-tetramethylchroman-2-carboxylic acid (Trolox), 2,2-diphenyl-1-picrylhydrazyl (DPPH), potassium persulfate ($K_2S_2O_8$), Folin–Ciocalteu, sodium carbonate (Na_2CO_3), gallic acid (GA) and 2,2'-azinobis(3-ethylbenzothiazoline-6-sulfonic acid) diammonium salt (ABTS) were from Sigma Aldrich (USA).

For the formation of Pickering emulsions, hexadecane from Merck (99%), and commercial olive oil and polysorbate 20 (Tween 20) from Qerlan were used (Chapter 4).

The 3D printing bioinks in Chapter 5 were prepared using normal maize (NM) and waxy maize (WM) starches, and the form Sigma Aldrich (USA). The ibuprofen for the drug release studies was also obtained from Sigma Aldrich (USA). Panreac Applychem (Spain) supplied the phosphate buffered saline (PBS) tablets used for the drug delivery tests.

Nanoparticles were synthetized with chitosan (Cs) of low molecular weight (M_w = 67000 Da, estimated by viscosimetry in 0.3 M acetic acid/0.2 M sodium acetate trihydrate from Sigma Aldrich (USA) at 25 ºC) (Chapter 6). Deacetylation degree of Cs, DD = 80 %, was calculated by nuclear magnetic resonance. N-hydroxysuccinimide (NHS, 98 %), N-(3-dimethylaminopropyl)-Ni-ethylcarbodiimide hydrochloride (EDC, 98 %), sodium tripolyphosphate pentabasic (TPP, 98 %), thiolactic acid (TLA, 95 %), curcumin (a mixture of curcumin, demethoxycurcumin and bisdemethoxycurcumin; CUR, 98 %), fluorescein-5-isothiocyanate (FITC), mucin (type II, from porcine stomach), and deuterium oxide (D_2O, 99.96 %) were acquired from Sigma-Aldrich (USA). Glacial acetic acid, hydrochloric acid (HCl, 37 %), acetone (99 %) and sodium hydroxide (NaOH, 1M) were purchased from Panreac Applychem (Spain). Ethanol (99.8%) was acquired in Honeywell (USA).

Regarding the cytotoxicity assay in Chapter 4, 3-(4,5-dimethylthiazol-2-yl)-2,5-diphenyltetrazolium bromide (MTT) was acquired from Sigma Aldrich (USA) and dimethyl sulfoxide (DMSO, purity 99 %) was purchased from Fisher Scientific (USA). All reagents for cell culture: cell medium (DMEM (Dulbecco's

Modified Eagle's Medium)), PBS 1X, Penicillin/Streptomycin 100X (P/S), trypsin-EDTA and Fetal Bovine Serum (FBS) were purchased from Dominique Dutscher (France).

2.2 Characterization techniques

The characterization techniques used throughout this thesis are described in the following pages. The experiments and characterization methods that are focused on specific applications are detailed in their corresponding Chapters.

2.2.1 Physicochemical characterization

2.2.1.1 Chromatographic techniques

High-Performance Anion-exchange Chromatography

To appreciate the in-depth behavior of the bacteria in the culture medium, detailed sugar analysis was conducted during the incubation process (Chapter 3). For that, the evolution of glucose, sucrose, fructose, xylose, arabinose, galactose and mannose content was analyzed by Ion Chromatography in GP culture medium over cultivation time, registering the sugar consumption during biosynthesis. Samples were filtered through 0.2 µm syringe filters and stored at -20°C until analysis. The determination was made with a Dionex ICS-5000 + Ion Chromatograph using the High Performance Anion-Exchange Chromatography with Pulsed Amperometric Detection technique (HPAEC-PAD). The analytic column was Dionex CarboPac PA210-4 µm, 2x150 mm and the protective column was Dionex CarboPac PA210 G-4 µm, 2x30 mm. The injection volume was of 2.5 µL and the flow rate 0.2 mL min^{-1}. The eluent gradient was isocratic, KOH 14 mM, Dionex EGC 500 KOH eluent generator was used with a Dionex CR-ATC 500 Anion Trap column continuously regenerated.

Ultra-High-Performance Liquid Chromatography – Mass Spectrometry

The identification of the polyphenolic profile was performed by Ultra High Performance Liquid Chromatography (UHPLC) from the supernatant of the centrifuged GPPE (Chapter 4). The UHPLC, with an ACQUITY UPLCTM system from Waters (Milford, MA, USA), equipped with a binary solvent delivery pump, an autosampler, a column compartment and a PDA detector. A reverse phase column (Acquity UPLC BEH C18 2.1x100 mm, 1.7 µm) and a precolumn (Acquity UPLC BEH C18 1.7 µm VanGuardTM) from Waters (Milford, MA, USA) were used at 40 °C for the separation. The flow rate was 35 µL/min and the injection volume was 2.0 µL. Mobile phases consisted of 0.1 % acetic acid in water (A) and 0.1 % acetic acid in acetonitrile (B). The gradient conditions for the separation were as follows: 0–1.6 min, 2% B isocratic; 1.6–2.11 min, linear gradient from 2% to 8% B; 2.11–8.80 min, 8% B isocratic; 8.80–9.80 min, linear gradient from 8% to 10% B; 9.80–17.00 min, 10 % B isocratic; 17.00–22.00 min, linear gradient from 10 to 20% B; 22.00–23.40 min, linear gradient from 20% to 23% B; 23.40–54.20 min, linear gradient from 23% to 60% B; 54.20–55.20 min, linear gradient from 60% to 100% B, finally followed by washing and conditioning of the column. The temperature of the samples was maintained at 4 °C during the analysis. The wavelength range of the PDA detector was 210–500 nm (20 Hz, 1.2 nm resolution). Hydroxybenzoic acids were monitored at 254 nm, flavanols at 280 nm, hydroxycinnamic acids at 320 nm and flavonols and dihydroflavonols at 370 nm. Once the chromatographic peaks corresponding to polyphenols were assigned, their identity was studied by mass spectrometry [1].

Mass Spectrometry (MS) data acquisitions were performed on a SYNAPT G2 HDMS with a quadrupole time-of-flight (QTOF) configuration (Waters, Milford,

MA, USA) equipped with an electro-spray ionization (ESI) source operating in positive and negative modes. The capillary voltage was set to 1.0 kV for both ESI+ and ESI-. Nitrogen was used as the desolvation and cone gas at flow rates of 1000 L/h and 10 L/h, respectively. The source temperature was 120 °C, and the desolvation temperature was 400 °C. The two acquisition modes used were MS^E and MS/MS. Data acquisition took place across the 50–1200 *m/z* mass range in resolution mode (FWHM ≈ 20.000), and the scan time was 0.1 s. The collision energy for MS^E was 4 V in the trap cell and 4 V in the transfer cell for Function 1, and a collision ramp of 10 to 40 V in the trap cell and 4 V in the transfer cell for Function 2. The collision energy for MS/MS was a collision ramp of 10 to 40 V in the trap cell and 4 V in the transfer cell.

2.2.1.2 X-ray diffraction

X-ray diffraction (XRD) diffraction patterns of BC and BCNC samples were obtained using PHILIPS X'Pert Pro diffractometer, in θ - θ configuration secondary monochromator with CuKα (λ = 0.154 nm) and a solid state pixel detector, operating at 40 kV with a filament of 40 mA. The diffraction data were collected from 2θ values 5° to 40°, where θ is the angle of incidence of the X-ray been on the sample. The crystallinity index (CI) of produced BC was determined by the following equation [2]:

$$CI\ (\%) = \frac{I_{200} - I_{am}}{I_{200}} \cdot 100 \qquad \text{(Equation 2.1)}$$

where I_{200} is the maximum intensity of the (200) lattice diffraction at 2θ = 22.7° and I_{am} is the intensity scattered by the amorphous part of the sample (the location of the amorphous material signal considered was at 2θ = 18°).

Additionally, texture evaluation of an starch tablet reinforced with BCNF was measured using a Bruker D8 Discover diffractometer (USA) equipped with a Cr Twist tube, V filter (λ = 2.2910 Å), PolyCap™ (1μ single crystal cylinders) system for parallel been generation (divergence of 0.25°), and a 1-D LynxEye detector (active length in 2θ 2.6°). The sample was mounted on an Eulerian Cradle with automatic controlled X-Y-Z stage. Data were collected for the mean reflection at 33.5º in 2Theta, using a fixed mode and time per orientation of 20s. The data collection in thinned mode with 5° of δ was measured for full circle 0-360 incr. 5° in Phi (φ) and 0-70 incr. 5° in Psi (ψ) range giving 693 total orientations.

Texture analysis using X-ray Diffraction has typically been performed via the use of pole figure measurement. Such measurements were performed by measuring exact 2θ maxima and rocking the sample through Psi ψ (tilt) angles and Phi φ (spindle) rotations via a texture Cradle attachment. The measured intensities are then plotted as an intensity map where the hemisphere-like distribution of scattered intensity is projected on a 2D "pole figure" showing the variation of intensity with sample orientation.

The pole density for a given point is determined by the intensity of a X-ray beam diffracted for this orientation. Measured data were evaluated using Multex 3 software, no texture component simulations was able, due to the high dispesionof the signals in the pole figures. These results indicated that the crystal orientations are more or less isotropic.

2.2.1.3 Fourier transform infrared spectroscopy

Fourier transform infrared spectroscopy (FTIR) was used to identify functional groups of BC, BCNCs, WM and GPPE. This technique relies on irradiating the sample with an infrared light source, causing the absorbed light to be reflected

in the spectrum at various wavenumbers. A Nicolet Nexus spectrophotometer provided with MKII Golden gate accessory (Specac) with diamond crystal at a nominal incidence angle of 45° and ZnSe lens was used. Spectra were recorded between 4000 and 650 cm^{-1} averaging 32 scans with a resolution of 4 cm^{-1}. The areas of absorbance bands around 710 cm^{-1} and 750 cm^{-1} were used to estimate the percentage of cellulose I_β according to Equation 2.2 [3].

$$I_\beta = \frac{A_{710}}{A_{710} - A_{750}} \qquad \text{(Equation 2.2)}$$

where A_{710} is the integrated area of absorbance band at 710 cm^{-1} and A_{750} is the integrated area of the absorbance band at 750 cm^{-1}.

2.2.1.4 Ultraviolet-visible spectrophotometry

D-glucose and D-fructose detection kit

The amount of D-glucose and D-fructose in GP treated and untreated mixtures was analysed by spectrophotometry (Chapter 3). Measurements were carried out before nitrogen supplementation, using a commercial kit from Byosystems (Spain). The content of these reducing sugars was followed measuring the absorbance change of the reduction of NADPH at 340 nm in the presence of phosphoglucose isomerase by a Shimadzu UV-Vis-Nir 3600 spectrophotometer (Japan).

Ninhydrin assay for thiol–functionalized Cs

The quantitative determination of amine substitution in the thiol-functionalized chitosan sample was carried out using UV-vis spectroscopy (Shimadzu UV-Vis-Nir 3600 spectrophotometer, Japan) (Chapter 6). This analysis was an adaptation of previous works found in literature [4,5]. To

quantify the degree of thiolation, ninhydrin reagent was reacted with the primary free amino groups of chitosan, resulting in the formation of a colored reaction product that exhibited an absorbance signal at 570 nm. Solutions with varying concentrations (ranging from 0.1 to 0.03 mg/mL) were prepared from initial chitosan and thiol-functionalized chitosan solutions, both at a concentration of 0.15% (w/v), in a mixture of 2% (v/v) acetic acid, 1% (w/v) acetic acid/acetate buffer (pH 5.5), and a 2% solution of ninhydrin reagent from Sigma-Aldrich (Spain). These solutions were incubated at 100 °C for 20 minutes and then cooled in an ice bath before measuring the absorbance. The degree of substitution (DS) was determined using Equation 2.3, considering the slope (m) of the absorption-concentration curves, which was empirically found to be proportional to the percentage of free amino groups.

$$DS_{CsSH}(\%) = \left(1 - \frac{m_{CsSH}}{m_{Cs}}\right) \cdot 100 \qquad \text{(Equation 2.3)}$$

where m_{CsSH} is the slope-value of the thiolated polymer curve and m_{Cs} is the slope-value of the neat polymer curve.

2.2.1.5 Dynamic light scattering

The stability of both the BCNCs and BCNC-GPPE dispersions was analyzed by Dynamic light scattering (DLS) measuring the Z potential using a ZetaSizer Nano Series ZEN3600 (Malvern Instruments, UK) connected to MPT-3 autotitrator at an angle of 173° (Chapter 4). The Z potential is a parameter that reveals the distribution of surface charge at the interface between a solid particle and water. When a solid surface is immersed in a polar liquid medium, an electric charge can be induced at the solid-liquid interface. By subjecting a dispersion to laser diffraction while manipulating the applied electric field, the

resulting diffracted light can be correlated with the applied field. Through measurement of the frequency change in the diffracted light, a Z potential analyzer can determine the surface charge of nanoparticles, which directly influences their dispersion stability. Surface charge was measured at different pHs and values were taken in triplicate in specific cells from Malvern Instruments (DTS1070). Samples were prepared diluting the dispersions with ultrapure water.

Additionally, DLS measurements were conducted with Cs and functionalized Cs nanoparticle dispersions. DLS technique is often used to measure the size of ultra-small particles in the submicron range that exhibit Brownian motion in suspension. When light is scattered by these particles, interference phenomena occur. This interference changes over time, resulting in variations in the intensity of the scattered light. Therefore, the time dependence of the scattered light intensity reflects the speed of particle motion, which in turn is related to the particle size. Autocorrelation analysis is commonly employed to analyze this relationship. The measurements were made in polystyrene UV disposable cells in triplicate. Z potential and particle size (Z average) were calculated in a pH range from 3 to 8.

2.2.1.6 Fluorescence spectroscopy

Fluorescence spectroscopy allows for the determination of the concentration of fluorescent particles in a sample. The absorption of light by the sample (excitation spectrum) and the emission of light from the sample (emission spectrum) can be measured and quantified. In this case, it was used to detect and monitor the amount of thiolated Cs nanoparticles covalently linked to the fluorescent marker FITC (Chapter 6). Fluorescence of the nanoparticle release

media was measured with the spectrofluorimeter (Microbeam 2396-MP1 Brytebox 2.2 115-230VAC, Spain). Previously, a calibration curve was performed with FITC concentrations ranging from 0.5 to 500 µg/mL in aqueous medium (R^2=0.9967). Therefore, the detection limit was set at 0.5 µg/mL. The measurements in the spectrofluorimeter were carried out according to the fluorescence excitation and emission wavelengths of FITC, 486 nm and 515 nm, respectively [6,7].

2.2.2 Thermal characterization

2.2.2.1 Differential scanning calorimetry

Thermal behavior of urea loaded BC spheres was analyzed through Differential Scanning Calorimetry (DSC) measurements in Chapter 3. This technique involves applying heat to both a sample and a reference material in order to maintain a constant temperature. As the sample undergoes thermal transitions, the heat required by the sample will differ from that of the reference, resulting in distinguishable variations in the thermograms. For this study, a Mettler Toledo (USA) 822e instrument equipped with a robotic arm and an electric intracooler as the refrigeration unit was utilized. The sample, weighing between 5-10 mg, was placed in an aluminum pan and subjected to a heating cycle from 25 to 170 °C at a scanning rate of 10 °C/min under a nitrogen atmosphere. The melting temperature (T_m) of urea was used to determine the presence of the fertilizer in BC. At this temperature, an endothermic peak is observed in the DSC as the urea undergoes a solid-to-liquid transition.

2.2.2.2 Thermogravimetric analysis

In the Thermogravimetric analysis (TGA), the degradation process of BCNCs samples was monitored by measuring its mass using a microbalance during a heating scan (Chapter 4). This allowed for quantification of the change in mass relative to the initial mass of the sample. The measurements were conducted using a TGA/SDTA 851 instrument from Mettler Toledo (USA). The tests were performed by heating the sample from 25 to 750 °C at a rate of 10 °C/min. To prevent thermoxidative degradation, the tests were carried out under a nitrogen atmosphere.

2.2.3 Hydrophilicity

2.2.3.1 Water holding capacity

Water holding capacity (WHC) assays are very useful to assess the hydrophilicity and superabsorbent nature of polymeric systems. Freeze-dried BC membranes and spheres were used for WHC assays in Chapter 3. The weighted freeze-dried samples (W_{dry}) were immersed in deionized water until constant weight (W_{wet}) [3]. The WHC was calculated following Equation 2.4:

$$WHC\ (\%) = \frac{W_{wet} - W_{dry}}{W_{dry}} \cdot 100 \qquad \text{(Equation 2.4)}$$

where W_{wet} is the weight of the swollen BC and W_{dry} is that of the freeze-dried BC.

2.2.3.2 Water contact angle

The surface hydrophobicity of the BC/GPPE membranes was evaluated using static water contact angle (WCA) measurements (Chapter 4). This method

involves placing a drop of deionized water onto the membrane surface to determine the equilibrium contact angle between the air, water, and membrane interface. The method was adapted from the work published previously by Hu et al and Li et al [8,9]. The contact angle value reflects the chemical interactions occurring at the surface. The BC membranes were loaded with solutions of increasing concentrations of GPPE and subsequently dried in a vacuum dryer. The samples were named BC 0.5GPPE, BC 2.5GPPE, BC 5GPPE, and BC 10GPPE about the w/w percentage of GPPE of the loading solution. The measurements were performed at room temperature using an OCA20 instrument (Dataphysics, Germany). At least six contact angle values were obtained by depositing 5 µl of deionized water onto the membrane surface and averaged for analysis.

2.2.4 Morphological characterization

2.2.4.1 Atomic force microscopy

Atomic force microscopy (AFM) is a scanning probe technique that relies on the interactions between the tip and the sample surface. By measuring the attractive and repulsive forces between the tip and sample, a deflection in the tip is produced, and images are generated by mapping these deflections at each point of the sample. AFM images of BC, BCNF, BCNC and Cs-nanoparticle samples were obtained in tapping mode using a Dimension ICON scanning probe microscope with Nanoscope VI Controller (Bruker, Germany) with an integrated force generated by cantilever/silicon probes, applying a resonance frequency of about 180 kHz. Cantilevers with tips of 5–10 nm in radius and 125 µm long were used.

For BCNF/BCNC samples, a BCNF/BCNC water suspension drop was applied on mica and spin-coated at 2000 rpm for 120 s (Spincoater SCC-200 K.L.M. Micromaterials GmbH, Germany). Prior to imaging the sample in a vacuum chamber for 24 h at room temperature, water was removed. In the case of Cs nanoparticles, a drop of acidic solution (HAc, 2% v/v) of the nanoparticles (0.05 mg/mL) was settled on a mica disk and was dried at room temperature for 24 hours before measuring. ImageJ (NIH, USA) and AFM softwares were utilized to obtain diameter and length measurements of the samples from height images.

2.2.4.2 Scanning electron microscopy

Scanning electron microscopy (SEM) is a technique that involves directing a high-energy electron beam onto the surface of a sample to analyze the various signals produced by electron-sample interactions. SEM was employed to capture images of the surfaces and cross-sections of BC membranes, BC spheres, Cs-nanoparticle loaded BC membranes and 3D printed NM and WM tablets. Prior to SEM analysis, the samples were freeze-fractured using liquid nitrogen to expose their cross-sectional structure. A JEOL JSM-6400 scanning electron microscope equipped with a tungsten filament was utilized, operating at an accelerated voltage of 20 kV and a working distance of 5-10 mm. The samples were coated with approximately 20 nm of chromium using a Quorum Q150 TES metallizer.

2.2.4.3 Optical microscopy

Optical Microscopy (OM) was used to observe and measure the hexadecane-in-water Pickering emulsions stabilized by BCNC-GPPE complexes. Droplet volume mean diameter was calculated as detailed in Chapter 4 with a Nicon Eclipse E600 instrument (Japan). Additionally, the appearance, size and

morphology of the NM and WM starch granules were evaluated by OM in transmission mode with the same optical microscope (Chapter 5). The size of the starch granules and emulsion droplets was calculated with ImageJ software (NIH, USA).

2.2.5 Rheological characterization

A rheometer is a specialized instrument used to measure the rheological behavior of materials. It applies controlled stress or strain to the sample and monitors its response, allowing for the characterization of its flow and deformation behavior. Rheometers offer a range of functions and capabilities to evaluate different rheological parameters which are directly related to structural integrity of the samples. For this reason, rheological characterization of hexadecane-in-water Pickering emulsions stabilized by the BCNC and BCNC-GPPE complex (Chapter 4), and all the different NM and WM starch inks for 3D printing was carried out (Chapter 5).

The rheological measurements were performed using an ARES G2 rheometer (TA instruments, USA) equipped with a Peltier temperature controller system and a solvent trap. In the case of hexadecane-in-water Pickering emulsions, dynamic oscillatory strain sweep and frequency sweep tests as well as flow tests were performed at 23 °C using cone-plate geometry (50 mm diameter). The linear viscoelastic region (LVR) was determined by monitoring both the storage modulus (G') and loss modulus (G'') in a strain sweep test at 1 Hz. After that, G' and G'' were analyzed versus frequency from 0.1 to 100 Hz at a fixed strain within the LVR region. Flow test measurements were performed, in which the evolution of the viscosity was measured by varying the shear rate from 0.01 to 1000 s^{-1}.

Rheological characterization of starch inks was conducted using a cone-plate geometry (25 mm) at a temperature of 37 °C. The ink samples, consisting of gelatinized starches at a concentration of 30 % w/w and with different quantities of BCNFs and GPPE, underwent flow tests, oscillatory stress sweep tests, and recovery tests. In the flow tests, viscosity was studied with shear rates varying from 0.01 to 1000 s^{-1}, while the oscillatory shear stress sweep tests were performed measuring G' and G'' with stress values ranging from 1 to 1000 Pa at a frequency of 1 Hz. The experimental results obtained from the viscosity test were fitted to a power-law model [10], which can be described by the following equation:

$$\eta = K\,\dot{\gamma}^{n-1} \qquad \text{(Equation 2.5)}$$

where η is the viscosity of the ink measured in Pa·s, K is the consistency coefficient, $\dot{\gamma}$ is the shear rate measured in s^{-1} and n is the power-law index.

Recovery tests involved measuring viscosity in a shear stress test conducted in three consecutive stages: 1) at 0.2 s^{-1} for 180 s, 2) at 100 s^{-1} for 180 s, and 3) at 0.2 s^{-1} for 180 s. Recovery percentages were calculated taking values after 100 s at zero shear rate [11]. All rheological measurements were performed at least in triplicate.

2.2.6 Antioxidant activity characterization

2.2.6.1 DPPH radical scavenging activity

The DPPH free radical method was carried out following the procedure described by Ventura-Aguilar et al., with some modifications (Chapter 4) [12]. Trolox was utilized for the calibration curve. The DPPH method was used in the

free radical DPPH absorbance reduction when mixed with a substance with antioxidant activity, with the formation of DPPH-H and free radical of the antioxidant species. 250 mL of either GPPE 2.5 % *w/v* solution or BCNC-GPPE dispersion were added to 2 mL of DPPH solution (6.25×10^{-5} M) in methanol, and left to stand in the dark for 30 min at room temperature. After this period, the absorbance was measured at 517 nm in 1 mL quartz cuvettes using UV-vis equipment. Measurements were conducted in triplicate, and the results were expressed in mg Trolox equivalent (TE) per g of dry extract (mg TE/g dry GP).

2.2.6.2 ABTS radical scavenging activity

The ABTS radical cation, which is a blue chromophore, was generated through the reaction of ABTS with a 0.6 mM potassium persulfate solution (1:1) in the dark for 16 h at room temperature [13]. Trolox was employed as a standard in the assay, and a calibration curve was established in the concentration range of 10–50 mg Trolox/l. A mixture of 250 mL of GPPE or standard diluted with methanol and 2 mL of the $ABTS^{\cdot+}$ solution was prepared, and the absorbance of the samples was measured at 734 nm using a UV-vis spectrophotometer after 40 min. The experiment was conducted in triplicate, and the results were reported as mg Trolox equivalent per gram of dry GP (mg TE/g dry GP).

2.2.6.3 Total phenolic content

The total phenolic content (TPC) method was modified from the procedure developed by Diñeiro et al [14]. GA was utilized as a standard in the assay, and the calibration curve was created in a concentration range of 5–400 mg GA/l. A mixture of 0.1 mL of GPPE or standard diluted with methanol, 2 mL of a 20% Na_2CO_3 solution, 5 mL of H_2O and 0.5 mL of Folin–Ciocalteu reagent was prepared in a test tube. The absorbance was measured in triplicate at 765 nm

using a UV-vis spectrophotometer after 30 min at 40 °C, and the results were determined using the calibration curve. The findings were reported as mg of GA equivalent per g of dry GP (mg GA/g dry GP).

2.2.7 Biocompatibility

2.2.7.1 Cytotoxicity assay

Cytotoxicity assessment was carried out in to evaluate the potential adverse effects of BC and BC/GPPE on living cells based on ISO 10993-5 guidelines (Chapter 4). This experiment was conducted during the international stay carried out at the University of Strasbourg with the Biomaterials-Bioengineering group of CRBS (INSERM U1121). In this case, the cell viability of murine NIH 3T3 fibroblasts was analyzed in extractive media that had been in contact with BC loaded with different concentrations of GPPE. Previously, GPPE incorporation into the BC punches of 12mm diameter was carried out by immersion for at least 2 h in 24-well plates at 140 rpms. Then, sterilized BC punches loaded with GPPE solutions of 25, 50, and 75 mg/mL were immersed in DMEM medium supplemented with 10 % FBS and 1 % P/S for 24 hours at 37 ºC. 200 of µL this active media were used to incubate seeded NIH 3T3 cells in a 96-well plate and at density of 10000 cells per well (24 hours at 37°C and 5% CO_2). Positive control containing DMSO and negative control at the same cell density of the inoculum were used in the study. Subsequently, the medium was collected, and the cells were washed twice with PBS and incubated with 100 µL of an MTT solution (0.5 mg/mL in cell medium). The plates were incubated for 3 hours at 37°C and 5% CO_2, after which the MTT solution was removed, and 100 µL of DMSO were added to each well to dissolve the crystals while subjected to orbital shaking. The absorbance was measured at 570 nm

using a microplate reader (Xenius XC spectrophotometer, SAFAS, Monaco). The cytotoxicity was expressed as a percentage of cell viability compared to the control cells that were not exposed to GPPE (negative control). Each condition was tested in at least three independent experiments.

2.2.8 Antimicrobial activity

2.2.8.1 Agar diffusion assay

Antimicrobial activity test was performed using agar diffusion assay method. This technique involves depositing, on the surface of a pre-inoculated Petri dish, the study material impregnated with different antibiotics or biocidal agents. In this case, BC membranes loaded with thiolated Cs nanoparticles encapsulating curcumin (30BCnp) were tested against *Staphylococcus aureus* CECT 239 and *Escherichia coli* CECT 405. As soon as the biopolymer encounters the moist agar surface, the antimicrobial agent diffuses into the surrounding agar, creating a concentration gradient. As the microorganisms encounter the antimicrobial substance, their growth is inhibited, leading to the formation of clear zones, known as inhibition zones, around the material. The size of these zones is measured and serves as an indicator of the material's antimicrobial activity. After depositing the samples with the active ingredients onto the plate inoculated with the test microorganism, the plates are incubated at 37 °C for 24 hours. Measurements were done in triplicate to ensure the reproducibility of the results.

2.2.9 Statistical analysis

In this thesis, R version 4.1.2 (R Core Team, 2021) was used to perform statistical analyses, including a two-sample t-test to compare means between

groups. All experiments were conducted at least in triplicate and differences were considered to be statistically significant when $p < 0.05$.

2.3 References

1 Abad-García, B., Berrueta, L. A., Garmón-Lobato, S., Gallo, B. and Vicente, F. (2009) A general analytical strategy for the characterization of phenolic compounds in fruit juices by high-performance liquid chromatography with diode array detection coupled to electrospray ionization and triple quadrupole mass spectrometry. J. Chromatogr. A **1216**, 5398–5415.

2 Segal, L., Creely, J. J., Martin, A. E. and Conrad, C. M. (1959) An Empirical Method for Estimating the Degree of Crystallinity of Native Cellulose Using the X-Ray Diffractometer. Text. Res. J. **29**, 786–794.

3 Urbina, L., Hernández-Arriaga, A. M., Eceiza, A., Gabilondo, N., Corcuera, M. A., Prieto, M. A. and Retegi, A. (2017) By-products of the cider production: an alternative source of nutrients to produce bacterial cellulose. Cellulose **24**, 2071–2082.

4 Shitrit, Y. and Bianco-Peled, H. (2017) Acrylated chitosan for mucoadhesive drug delivery systems. Int. J. Pharm., Elsevier B.V. **517**, 247–255.

5 Mahmood, A., Lanthaler, M., Laffleur, F., Huck, C. W. and Bernkop-Schnürch, A. (2017) Thiolated chitosan micelles: Highly mucoadhesive drug carriers. Carbohydr. Polym. **167**, 250–258.

6 Amini, Y., Amel Jamehdar, S., Sadri, K., Zare, S., Musavi, D. and Tafaghodi, M. (2017) Different methods to determine the encapsulation efficiency of protein in PLGA nanoparticles. Biomed. Mater. Eng. **28**, 613–620.

7 Li, M. G., Lu, W. L., Wang, J. C., Zhang, X., Wang, X. Q., Zheng, A. P. and Zhang, Q. (2007) Distribution, transition, adhesion and release of insulin

loaded nanoparticles in the gut of rats. Int. J. Pharm. **329**, 182–191.

8 Hu, Z., Berry, R. M., Pelton, R. and Cranston, E. D. (2017) One-Pot Water-Based Hydrophobic Surface Modification of Cellulose Nanocrystals Using Plant Polyphenols. ACS Sustain. Chem. Eng. **5**, 5018–5026.

9 Li, X., Li, J., Gong, J., Kuang, Y., Mo, L. and Song, T. (2018) Cellulose nanocrystals (CNCs) with different crystalline allomorph for oil in water Pickering emulsions. Carbohydr. Polym., Elsevier **183**, 303–310.

10 Chen, H., Xie, F., Chen, L. and Zheng, B. (2019) Effect of rheological properties of potato, rice and corn starches on their hot-extrusion 3D printing behaviors. J. Food Eng., Elsevier **244**, 150–158.

11 Olmos-Juste, R., Guaresti, O., Calvo-Correas, T., Gabilondo, N. and Eceiza, A. (2021) Design of drug-loaded 3D printing biomaterial inks and tailor-made pharmaceutical forms for controlled release. Int. J. Pharm., Elsevier B.V. **609**, 121124.

12 Ventura-Aguilar, R. I., Bautista-Baños, S., Flores-García, G. and Zavaleta-Avejar, L. (2018) Impact of chitosan based edible coatings functionalized with natural compounds on Colletotrichum fragariae development and the quality of strawberries. Food Chem.

13 Wang, X., Li, C., Liang, D., Zou, Y., Li, P. and Ma, F. (2015) Phenolic compounds and antioxidant activity in red-fleshed apples. J. Funct. Foods, Elsevier Ltd **18**, 1086–1094.

14 Diñeiro García, Y., Valles, B. S. and Picinelli Lobo, A. (2009) Phenolic and antioxidant composition of by-products from the cider industry: Apple pomace. Food Chem., Elsevier Ltd **117**, 731–738.

CHAPTER 3

FROM AGRICULTURE TO AGRICULTURE



3.1 Introduction 73
3.2 Experimental section 75
3.2.1 GP and bacterial strain origin 75
3.2.2 BC biosynthesis 76
3.2.3 BC yield 78
3.2.4 Urea release study 78
3.3 Results and discussion 80
3.3.1 Characterization of culture media 80
3.3.2 Physicochemical characterization of BC 88
3.3.3 Superabsorbent capacity 91
3.3.4 Urea release study 95
3.4 Conclusions 98
3.5 References 98

Chapter 3: From agriculture to agriculture

3.1 Introduction

As detailed in Chapter 1, white GP is an agricultural residue of large volume, and its accumulation can be harmful to the environment at a global level. Therefore, the development of new strategies for the revalorization and exploitation of GP is a sustainable solution of great socioeconomic interest. Equally, in addition to residue accumulation, other challenging agricultural concerns are the over usage of agrochemicals for crop growth or protection and the fresh water exploitation [1, 2].

The development of controlled release systems and superabsorbent hydrogels is an alternative to these threats [3, 4]. In this way, it is intended to prevent the excessive application of harmful pesticides from contaminating food or water bodies. More recent research works promote the use of biodegradable polymers such as alginate, cyclodextrins, chitosan or cellulose and their derivatives, that have the ability to attenuate or control the release of agrochemicals, so that it continues to reach the target [5–7]. The common characteristic of natural polymer-based hydrogels is their ability to retain water, given their three-dimensional macromolecular structure, which is also beneficial for agriculture when crops are subjected to abiotic stress conditions such as water shortage [6]. Thus, cellulose-derived superabsorbent polymers have been proposed since they offer similar performance in water optimization to common acrylate-based superabsorbent polymers, and are environmentally friendly [8].

This chapter focuses on the production and characterization of BC from GP agricultural residue. Given the pH of GP, *Komagateibacter medellinensis* bacterial strain ID13488 was chosen since it can produce high yields of BC from low cost carbon sources and acidic culture media, as it has been previously reported with other acidic agricultural residues [9].Thus, *K. medellinensis* could prevent previous pH neutralization and polysaccharide hydrolyzing steps of the GP to adequate the residue for bacterial development. In this way, the aim was to provide insight into the biosynthesis process of BC through static and agitated conditions.

As explained in Chapter 1, physicochemical characteristics of BC depend on the production mechanism, thus causing the potential application of the biopolymer to change when cultured in agitated conditions. The characteristic microstructure of BC obtained in agitated cultures along with the higher surface area due to the spherical shape extend the potential applications of the BC as carrier of enzymes or adsorbent of heavy metals, oils and organic solvents, among others [10]. Nevertheless, little is known about the morphology and properties of BC synthetized from agricultural residues under agitated conditions and their possible effects on the nucleation processes in BC. Hence, there is a strong need for studies that exploit the great advantages of BC spheres in many advanced fields, by exploring the main factors that control their formation.

As a result, the development of BC membranes and sphere-shaped BCs biosynthesized from GP culture media was optimized. Additionally, to expand the applicability of BC, the superabsorbent nature of the sphere-shaped BCs and their urea retention capacity were assessed.

Certainly, nitrogen is a crucial macronutrient for the growth of diverse crops, and urea is considered to be the predominant nitrogen-containing fertilizer [10]. However, only a small fraction of applied urea is effectively utilized by plants due to its high solubility in water. Indeed, the development of efficient fertilizers is of growing importance as a significant portion (approximately 40-70%) of nitrogen applied to plants through conventional fertilizers is lost to the environment [11]. As a consequence, a substantial quantity of urea needs to be applied, leading to elevated costs and environmental pollution through surface and groundwater contamination [12]. This loss renders these nutrients unavailable to plants, resulting in economic and environmental burdens. In this context, the use of superabsorbent polymers for controlled release of fertilizers has gained recent scientific interest [13–16]. Thereby, the applicability of BC was explored in three of the main threats to agriculture: waste accumulation, drought, and controlled release of fertilizers.

3.2 Experimental section

3.2.1 GP and bacterial strain origin

GP culture medium was prepared with Hondarrabi zuri white grape variety pomace, which was kindly provided by Bodega Butroi, a local winery (Biscay, Spain).

Following the criteria of the oenologist, the grapes were harvested at their optimum point of ripeness, according to the potential alcohol level after the winemaking process and the acidity index of the grapes. GP was collected the same day of grape harvest, after destemming and pressing the grapes under identical conditions. Finally, GP consisting on some stems, sheds and skins, was stored at −80 °C until its analysis.

Komagataeibacter medellinensis bacteria strain ID13488 was isolated from vinegar broth fermentation and kindly supplied by New Materials Research Group, Pontificia Bolivariana University of Medellín, Colombia [17].

3.2.2 BC biosynthesis

BC membranes and sphere-shaped BCs were biosynthesized by *K. medellinensis* in white GP culture media, both under static and agitated growth conditions.

For the preparation of the GP culture medium, first GP was crushed with a blender and different residue/water mixtures with GP percentages ranging from 2.5% (w/v) to 20% (w/v) were prepared. GP mixtures were passed through a cloth strainer and the filtrated was subjected to two types of treatments, ultrasonication and hot water hydrolysis, either individually or in combination. These treatments were used to facilitate the accessibility and diffusion of nutrients through the medium, the extraction of fermentable sugars and to reduce the number of suspended solids. The ultrasonication was conducted for 30 min at room temperature (JP Selecta 3,000,683 50/60 Hz), whereas the hot water treatment was carried out at 80 °C for 1 h. Subsequently, the mixtures were centrifuged at 4500 rpm for 45 min (Hettich Zentrifugen D-78532). The pH of the solutions was then adjusted to 3.5 with citric acid if necessary and autoclaved separately at 120 °C for 15 min before inoculating the bacteria. The pH of the culture media was determined by employing a pH meter (GLP22, Crison Instruments). The inoculum of a commercial HS medium in the exponential growth phase was stablished as 1% (v/v) for static cultures and 1.5% (v/v) for agitated cultures. 150 mL and 100 mL volumes of culture medium were used in 250 mL Erlenmeyer flasks for static

and agitated growing conditions respectively. The inoculum and culture volume were decided taking into account previous work conducted by our research group and the studies carried out by Hu et al in agitated cultures [18–20].

GP juice was mixed with commercial peptone or yeast extract to analyze the effect of each supplement on the culture medium. (Culture media with additional nitrogen sources were labelled with *pp* and *ex* in reference to peptone and yeast extract, respectively.) Additionally, a low-cost yeast extract was prepared by adapting the method described by Zarei et al for its study as a source of amino acids, vitamins, and minerals [21]. The yeast extract was obtained from the lees of white wine production from the same winery that supplied the GP. Briefly, 500 g of lees were crushed and mixed with 2 L of distilled water. Subsequently, this mixture was autoclaved for 10 min and the resulting solution was rapidly cooled in a water bath. Next, the solution was centrifuged for 10 min at 4500 rpm to remove cell debris, and the supernatant was freeze-dried to obtain a yeast extract powder.

All culture media, both under static and agitated conditions, were incubated at 28 °C for 7 days. The agitated cultures were subjected to rotatory speeds of 120 rpm, 130 rpm and 150 rpm in an IKA KS 4000i Control (Germany). Lastly, obtained BC samples were washed with KOH at 2% (w/v) for 24 h to remove all non-cellulosic components and afterwards, they were subjected to several washes with deionized water until total neutralization. Finally, BC samples were dried on Teflon plates in the oven at 50 °C until constant weight or freeze-dried (Telstar LyoQuest HT40) for their subsequent characterization. In Figure 3.1, a graphical representation of static and agitated GP cultures can be observed.

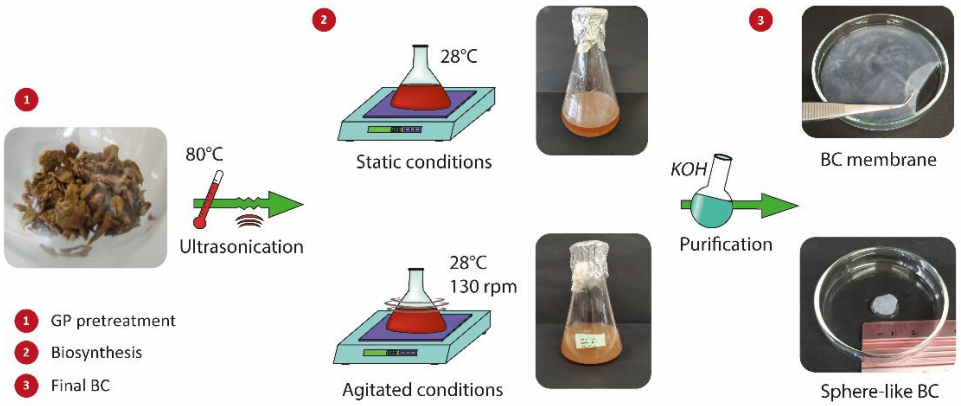

Figure 3.1 *Graphic representation of the biosynthesis processes of BC from GP under static and agitated growth conditions.*

3.2.3 BC yield

In both growing conditions, BC production was calculated after 7 days of incubation to better compare the yields following Eq. (3.1). Values were taken in triplicate.

$$Yield\ \left(\frac{g}{L}\right) = \frac{m_d}{V} \qquad \text{(Equation 3.1)}$$

where m_d is the dried BC mass in grams and V is the total volume of the culture media in liters.

3.2.4 Urea release study

Freeze-dried sphere-shaped BCs were immersed in 1 M aqueous urea solution for 48 h. Then, samples were freeze-dried again, and urea loading (UL) was measured in triplicate using the following equation:

$$Urea\ loading\ (\%) = \frac{W_L - W_{dry}}{W_{dry}} \qquad \text{(Equation 3.2)}$$

where W_L is the weight of loaded and freeze-dried BC and W_{dry} is that of the freeze-dried BC before urea loading [15].

The urea release measurements were carried out placing the loaded and dried sphere-shaped BCs in aqueous medium at neutral pH without stirring. Two different drying methods were applied to the urea loaded BC samples, freeze-drying and oven drying at 50°C until constant weight, with the objective of studying the effect of the drying method on the release profile. At different time points, samples were taken from the release medium and the amount of urea was measured by spectrophotometry (UV-Vis-Nir Shimadzu 3600) after the reaction with 4-dimethylamino benzaldehyde (DMAB) and HCl as reagent [22]. The interaction between DMAB and urea begins with the protonation of the dimethylamino group, causing a partial positive charge on the carbonyl group and making it susceptible to a nucleophilic attack by the urea, with the subsequent formation of the chromogen, as depicted in Figure 3.2, i.e., an imine or Schiff base that exhibits absorption at 420 nm in the UV-Vis spectrum.

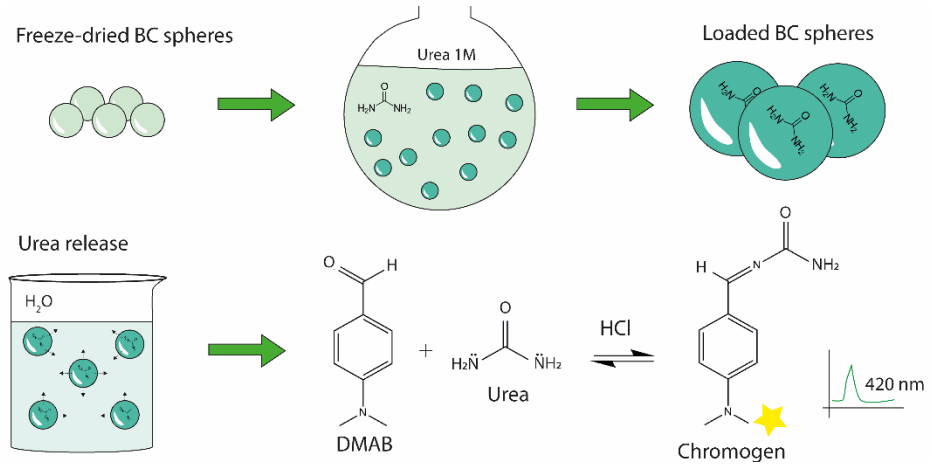

Figure 3.2 *Graphical representation of the urea loading process onto BC spheres for UL calculation, followed by its subsequent release and spectrophotometric detection.*

The concentration of urea in the release medium was determined using a calibration curve with constructed urea concentrations from 0.5 mM to 50 mM. Acetonitrile was used as solvent for the reaction as published by Giraldo and Rivas and each assay was carried out in triplicate [23].

The cumulative urea release (CUR) was calculated from the following equation:

$$Cumulative\ urea\ release\ (\%) = \frac{W_t}{W_U} \cdot 100 \qquad \text{(Equation 3.3)}$$

where W_t is the amount of urea released from the sphere-shaped BC at time t and W_U is the total amount of urea loaded into the sample.

3.3 Results and discussion

3.3.1 Characterization of culture media

3.3.1.1 Biosynthesis optimization and BC yield

Several GP/water solutions were prepared with the purpose of stablishing the correct nutrient balance for bacterial development in GP medium. Table 3.1 depicts the obtained results for BC production in static cultures within the studied conditions.

As observed in Table 3.1, GP based culture medium was suitable to produce BC from concentrations exceeding 5% (w/v). GP concentrations above 20% (w/v) were also tested, although this cultures did not produce BC. In this regard, Hu et al. reported that initial glucose concentrations in the medium above 20 g/L could have an inhibitory effect on cellulose yield [20]. Additionally, it should be noted that further increase of GP into the medium above 5% (w/v) resulted in a progressive reduction of BC production, despite the higher glucose and

fructose content. Indeed, it has been published that increased viscosity and concentration of polyphenolic compounds could also hinder BC biosynthesis [24].

Table 3.1 *GP concentration, supplementation with nitrogen sources, BC production and glucose + fructose content of the different culture media tested under static conditions. Culture media with additional nitrogen source was labelled with pp in reference to peptone.*

Growth conditions	**Culture**	**GP % (w/v)**	**Nitrogen source**		**Glucose + fructose (g/L)**	**BC yield (g/L)**
			Peptone % (w/v)	Yeast extract % (w/v)		
Static	*HS*	-	0.5	0.5	20.0	0.75 ± 0.12
	GP2.5	2.5	-	-	2.1 ± 0.1	-
	GP2.5-pp	2.5	0.5	-		0.53 ± 0.02
	GP5	5	-	-	4.4 ± 0.7	-
	GP5-pp	5	0.5	-		0.73 ± 0.03
	GP10	10	-	-	9.2 ± 0.2	0.26 ± 0.07
	GP10-pp	10	0.5	-		0.35 ± 0.02
	GP20	20	-	-	20.6 ± 0.5	0.10 ± 0.04
	GP20-pp	20	0.5	-		0.31 ± 0.00

As expected, the measured glucose and fructose concentrations in the medium increased with the GP content, being similar to the HS culture in the case of the GP 20% (w/v) culture. According to Table 3.1, GP concentrations with sugar content lower than 5 g/l did not produce BC. However, upon supplementation of these media with peptone, higher BC production was observed in all samples, reaching similar values of BC production to those of the HS culture medium, especially in the case of a 5% (w/v) GP concentration. Actually, according to literature, agricultural waste media supplementation with additional nitrogen, mineral or carbon sources is a widely extended practice to increase BC production [18, 25–28].

Additionally, yeast extract was prepared from winery lees with the aim of testing them as an alternative nitrogen source derived from winemaking wastes. In this case, the BC production from a 5% (w/v) GP culture supplemented with lees extract was 0.36 ± 0.10 g/l. Attending to Table 3.1, despite the interesting conditions of the lees to be used as a source of yeast extract [29], BC yield was lower than that of its homologous one supplemented with peptone. In fact, depending on the type of winery and weather conditions, lees may contain pesticides, sulfites, or phenolic compounds that could hinder bacterial growth. Nevertheless, this result demonstrated that despite the lower production, BC could be biosynthesized and, therefore, lees extract could also act as an additional nitrogen source for the medium.

Next, BC yields obtained in static cultures were used as reference for the design of the agitated cultures. Thus, *GP5-pp* culture was selected as control for BC characterization and as starter medium for agitated cultures. It is worth mentioning that when agricultural residues are used into culture media under agitated conditions, additional factors must be considered for the production of BC. Indeed, the suspended solid amount was a key element for the uniform BC production in agitated cultures, and, therefore, different treatments of GP were studied in order to reduce turbidity and increase solubility and availability of fermentable sugars. Given that acid or enzymatic treatments are expensive, environmentally unsustainable, require further neutralizing steps and enhance bacterial growth inhibitory compounds formation [30], hot water treatment was chosen as the most suitable method for non-cellulosic monosaccharide extraction [26, 27]. Furthermore, it has been reported that ultrasound assisted extractions of vegetal raw materials increases the efficiency of sugar recovery [31], since ultrasounds weaken cell walls and

promotes mass transfer, increasing the permeability of vegetal tissues to solvents [32]. Therefore, ultrasound and/or hot water treatments were carried out to improve the nutritive profile of the GP medium.

On the other hand, peptone was discarded for the preparation of agitated cultures, since preliminary experiments showed that it formed aggregates in combination with the GP. Hence, commercial yeast extract was used as nitrogen extra source in dynamic conditions. Namely, four agitated GP based culture media were prepared at 5% (w/v) GP concentration: non-treated (*GP5-ex*), ultrasound treated (*GP5-exUs*), hot water treated (*GP5-exH*) and that with combined treatments (*GP5-exUs+H*). Table 3.2 shows the obtained BC production yields in agitated cultures.

Table 3.2 *GP concentration, supplementation with nitrogen sources, BC production and glucose + fructose content of the different culture media tested under agitated conditions. Us, H and Us + H refer to the application of ultrasound treatment, hot water treatment and the combination of both treatments, respectively. Culture media with yeast extract were labelled with ex.*

Growth conditions	**Culture**	**GP % (w/v)**	**Nitrogen source**		**Glucose + fructose (g/l)**	**BC yield (g/l)**
			Peptone % (w/v)	Yeast extract % (w/v)		
Agitated	*HS*	-	0.5	0.5	20.0	0.18 ± 0.02
	GP5-ex	5	-	0.5	4.4 ± 0.7	0.58 ± 0.08
	GP5-exUs	5	-	0.5	4.6 ± 0.1	0.60 ± 0.09
	GP5-exH	5	-	0.5	5.5 ± 0.2	0.73 ± 0.02
	GP5-exUs+H	5	-	0.5	5.8 ± 0.1	1.17 ± 0.21

As observed in Table 3.2, ultrasonic and hot water treatments favored the glucose and fructose extraction from GP. However, higher monosaccharide concentration was obtained for the hot water extracted media compared to the ultrasound treated media, as it has been reported before [26]. According

to the results obtained, treatment with ultrasound alone did not have a significant effect on sugar extraction. The combination of both treatments in *GP5-exUs+H* sample was the most effective procedure with statistically significant differences compared to non-treated samples, increasing up to 31% the content of fermentable sugar with respect to *GP5-ex* samples. Accordingly, the increase of glucose and fructose concentration led to improvement of BC production. These results suggest that ultrasounds and hot water treatments could be interesting alternatives to acid or enzymatic treatments when an increase of fermentable sugars for bacterial growth is desired.

Ultrasonic and hot water treatments where also applied to a static *GP5-ex* culture medium in order to corroborate the positive effect observed in agitated cultures. The BC yield results of the static *GP5-exUS+H* culture increased to 0.91 ± 0.06 g/l compared to the 0.73 ± 0.03 g/l of *GP-pp* observed in Table 3.1. Therefore, these results also indicated that the selected treatments were effective to improve the suitability of the medium for both growing conditions. Regardless of the culture conditions and with low-cost treatments, both from economic and ecological points of view, the results demonstrated that BC can be produced from small amounts of grape residue in a competitive way.

Furthermore, when comparing BC yields of *GP5-exUs+H*, the production of BC in agitated cultures (1.17 ± 0.21 g/l) was slightly higher than that in static cultures (0.91 ± 0.06 g/l). It should be noted that there is some controversy regarding which culture conditions are more favorable for biosynthesizing a higher amount of BC [33–35]. It has been published that the agitation process generates mutant bacteria that are not capable of synthesizing cellulose, which leads to lower BC production [36]. The formation of gluconic acids is another

reason why cellulose production generally diminishes [37], and it has been stated that the concentration of these secondary metabolites increases in agitated cultures [38].

Nevertheless, according to the results a high quantity of BC can be produced under agitated conditions in less time than under static conditions. Certainly, previous researches revealed that the production of BC was notably higher under gentle agitation conditions (100 rpm) when compared to that with static cultures [38, 39]. Indeed, Revin et al published high BC purity and yield values from acidic agricultural residues [40]. It has also been reported that agitated growing conditions are the most suitable for profitable production [20, 33].

An additional factor to consider is that there are *Komagateibacter* strains that perform better under agitated conditions than others as they suffer less genetic instability [39, 41]. For example, Algar et al produced higher amounts of BC from pineapple residues in static cultures than in agitated cultures with the same *K. medellinensis* strain [18]. Hence, our BC yields suggested that the same bacterial strain could behave differently under static or agitated growth conditions depending on the culture medium. This circumstance may be due to the fact that BC production is strongly influenced by the relationship between the bacterial strain and the carbon sources used [9, 39, 42]. This is one of the reasons why the interaction between different culture media, growth conditions and bacterial strain should be carefully studied when BC production is desired on an industrial scale.

3.3.1.2 GP culture medium sugar composition

The initial amount of and consumption rate of different sugars was monitored in the *GP5-exUs+H* culture. As detailed in Chapter 2, numerous

monosaccharides and disaccharides of *GP5-exUs+H* sample were analyzed by UHPLC, though only glucose, fructose and arabinose were detected with concentrations of 2.22 g/L, 2.48 g/L and 0.01 g/L, respectively.

Some previously reported studies offered higher total sugar concentrations and diversity, up to 20% (w/w) in the case of white GP [27, 43]. However, these values refer to higher GP concentrations used and obtained with only skins, whereas in our research seeds and stalks were also used in the cultures. Moreover, excessive extracted fermentable sugar concentration could not be ideal since BC could be successfully produced with small amounts of GP and, as demonstrated in Tables 3.1 and 3.2, higher sugar concentrations were not always related to higher BC production. Figure 3.3 shows the evolution of the of glucose and fructose concentration over time in static and agitated cultures.

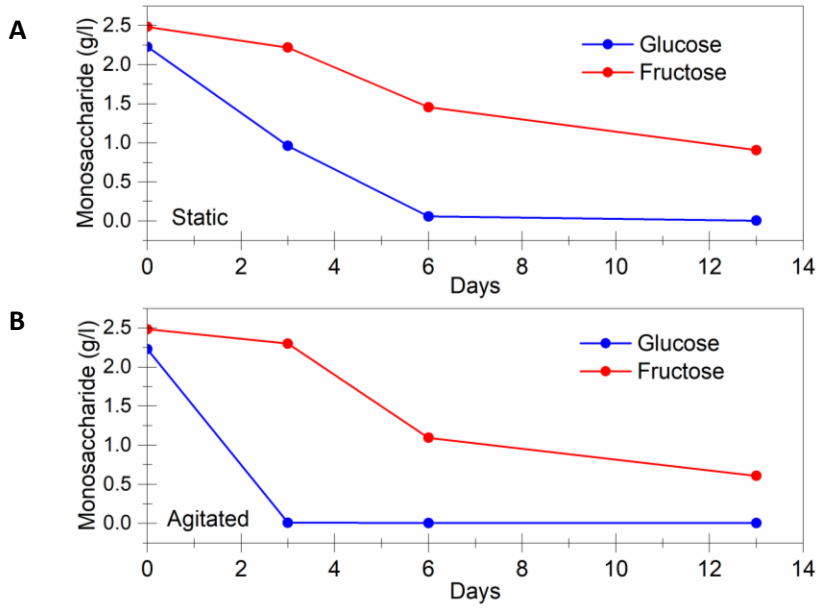

Figure 3.3 *Variation of glucose and fructose contents in static (**A**) and agitated (**B**) GP culture media at 5% (w/v).*

As observed in Figure 3.3, the consumption of the two monosaccharides in the case of agitated cultures is clearly faster than in static cultures. Indeed, in agitated cultures, glucose depletion occurs on the third day, whereas it took six days in the case of static cultures. In the case of dynamic cultures, it has been published that the BC spheres achieve their final size in nearly 60 hours, so that the total culture time tend to be around three to seven days [19, 40, 44]. The results in Figure 3.3 do not coincide with previously reported studies with *K. medellinensis* strain ID13488, in which glucose depletion took much longer [9, 25]. However, it is also true that similar consumption rates were found for *G.sucrofermentans* B-11267 using agitated cultures, from acidic agroindustrial residues [40]. Likewise, it is known that the acidic pH favors the growth of *K. medellinensis* as well as increases the consumption of glucose in *K. xylinus* agitated cultures [25, 38]. In any case, this disparity in sugar consumption rate could be caused by the lower amount of initial sugar of GP, monosaccharide availability, and the different composition of the culture medium.

The relationship between the bacterial strain and the culture medium composition is closely linked to the production and properties of the cellulose. In fact, within the same genus, the different cellulose-producing bacterial species show metabolic preferences for certain carbon sources and its concentrations [17, 39, 45]. In a comparative study between glucose, fructose and sucrose as unique carbon sources in each culture medium of *K. medellinensis*, a considerable higher production of BC was observed in glucose-based culture media [9]. Thus, it seems that better yields are obtained in *Komagateibacter* genus when glucose is the main carbon source maybe due to the fact that it can be used both as energy source and directly as precursor of cellulose polymerization [9].

Similarly, as it is represented in Figure 3.3, after glucose depletion, the rate of fructose consumption increased markedly in both culture conditions, indicating a variation of the main carbon source. These results reinforced the above mentioned statement that the bacterium *K. medellinensis* has priority over glucose. The additional energy requirement of the enzymatic isomerization of fructose for the subsequent polymerization to BC may explain this preference for glucose [46]. Furthermore, the stationary phase observed for fructose consumption could be due to the negative effect on fructokinase of using an inoculum grown in a medium where the only carbon source was glucose [47].

3.3.2 Physicochemical characterization of BC

The biosynthesized BC in different culture media was characterized by FTIR and XRD in order to evaluate its quality and purity. The experimental conditions are detailed in Chapter 2. FTIR spectra of the different BC samples produced under static and agitated conditions are shown in Figure 3.4.

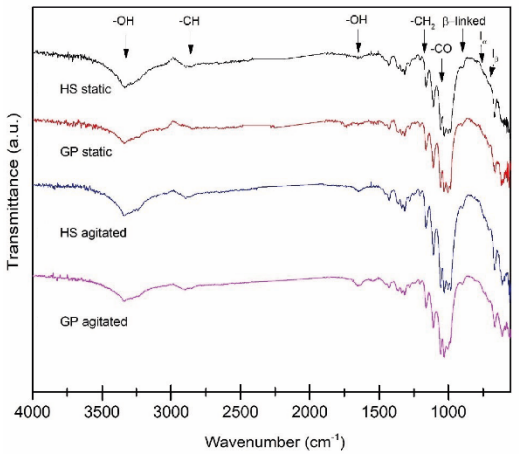

Figure 3.4 *FTIR spectra of BC samples biosynthesized in static and agitated conditions from HS and GP culture media.*

The characteristic type I cellulose allomorph was identified in all analyzed samples through the absorption bands at 1427, 1280 and 897 cm^{-1} [48]. The bands located at around 3300 cm^{-1} were assigned to the stretching vibration of the O-H linkage. The absorption bands between 2900–2880 cm^{-1} and 1460–1250 cm^{-1} corresponded to the stretching and bending vibrations of CH and CH_2, respectively. Likewise, vibrations of the C-O-C bond of the glycosidic bridges were detected by the bands at 1170–1050 cm^{-1}, whereas the broad band at 897 cm^{-1} is characteristic of β-linked glucose-based polymers. Finally, the band at around 1650 cm^{-1} was associated to adsorbed water. In view of the infrared spectra, it was concluded that regardless of the use of GP media and agitated conditions, all BC obtained shared the same chemical structure as well as the characteristic high purity.

As it is well known, cellulose I occurs in metastable cellulose I_α allomorph (triclinic structure) and stable cellulose I_β allomorph (monoclinic structure). The bands at 710 cm^{-1} and 750 cm^{-1}, which correspond to I_β and I_α respectively, were integrated to estimate the cellulose I_β percentage as represented in Table 3.3 [49].

Table 3.3 *I_β percentage (FTIR) and CI values (XRD) of the different culture media in static and agitated conditions.*

Culture	**Growth conditions**	**I_β (%)$_{FTIR}$**	**CI (%)$_{XRD}$**
HS	Static	37.2 ± 0.3	87.3 ± 0.9
GP5-exUs+H	Static	41.5 ± 1.0	75.2 ± 7.1
HS	Agitated	41.1 ± 0.6	85.1 ± 2.3
GP5-exUs+H	Agitated	41.6 ± 1.2	76.2 ± 2.8

As expected for BC and in contrast to vegetal cellulose, I_α was the dominant polymorph with I_β values between 37-41% [28]. It is worthy to note that the

used agitation conditions did not remarkably alter the crystallization of nanofibers and similar percentages of the stable I_β allomorph were obtained [45].

Further characterization of the crystallinity of BC samples was conducted by XRD. In Figure 3.5 the X-ray diffraction patterns of the BC produced in HS and GP media under static and agitated conditions are shown. The patterns presented the typical crystalline structure of type I cellulose with three main peaks located at 2θ = 14.5°, 16.8° and 22.7° that correspond to (100), (010) and (110) crystallographic planes, respectively, which agrees with that observed in the FTIR spectra [50, 51].

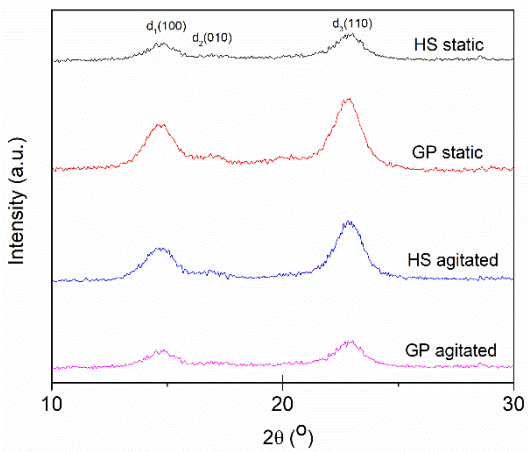

Figure 3.5 *X-ray diffraction patterns of BC biosynthesized in static and agitated conditions from HS and GP culture media.*

The CI was calculated using the Segal equation (Equation 2.1) and it is given in Table 3.3. As it can be seen, the CI of the samples obtained from GP was slightly lower than that of the samples from HS culture medium, probably related to the lower homogeneity of the culture medium that could affect the

crystallization process. Besides, CI values for BCs from agitated samples in this work were similar to those of the static samples. These findings were in agreement with the hypothesis that under agitated conditions below 150 rpm the interference of the agitation is not sufficient to affect crystallization and, the CI of celluloses from agitated media are similar to that of celluloses from static media [38]. Furthermore, these CI values were comparable to the ones previously reported by our group [18], and higher than those of other studies of BC obtained from agitated media, where values between 45 and 70% were obtained [39, 52, 53].

3.3.3 Superabsorbent capacity

The final shape of cellulose in agitated cultures depends on numerous factors such as bacterial concentration, culture time, rotation speed, bacterial strain, turbidity or pH of the medium which lead to a layered structure, porous character and high surface area [20, 52]. However, the exact mechanism by which the spheres are produced remains unknown and requires further study.

In this work, particular attention was given to the amount of suspended solids and the rotational speed during the preparation of agitated cultures. In fact, it was found that the production of sphere-shaped BCs was not possible in high turbidity levels. Thus, as described in the experimental section, GP/water mixtures were thoroughly strained and centrifuged for the culture media preparation. The rotation speed was found to be a key variable to obtain well defined cellulose spheres. For instance, rotation speed values of 150 rpm or higher, triggered BC in the form of 2-3 mm filaments (Figure 3.6C), while reducing it to 120 rpm or less, led to the formation of large aggregates of cellulose and impurities (Figure 3.6A). Finally, at 130 rpm, sphere shaped

cellulose with diameters of 6-8 mm were successfully obtained (Figure 3.3B). Therefore, 130 rpm was chosen as the optimal rotation speed for the synthesis of the desired sphere-shaped BC beads. These results are in agreement with those reported by Hu and Catchmark where sphere shaped BC was obtained with diameters of 8 mm in the range of 120-150 rpm rotation speeds [44].

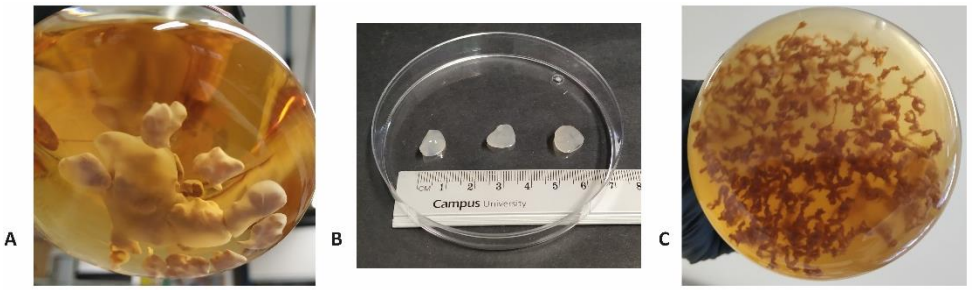

Figure 3.6 *BC samples produced in agitated GP cultures at rotation speeds of (**A**) 120 rpm, (**B**) 130 rpm and (**C**) 150 rpm.*

The surface morphology of BC membranes and spheres as well as the dimensions of the nanofibers were analyzed by AFM. Figure 3.7A and B show the AFM images obtained of the cellulose surfaces from GP media both in agitated and static conditions, respectively. The BC height and phase images were utilized to analyze the morphology and structure of the samples.

As observed, in all cases, the characteristic 3D network-like structure of interconnected nanofibers was appreciated. However, the nanofibers obtained in static GP cultures presented a slightly larger diameter (77.8 ± 15.6 nm) than those from agitated GP cultures (63.8 ± 8.2 nm). Further, it could be noted that agitated cultures caused more irregular network, thus leading to a more porous BC structure. The nanofibers synthesized from the GP culture media

were slightly thicker than those published by other authors for agitated cultures from different agricultural wastes [18, 45].

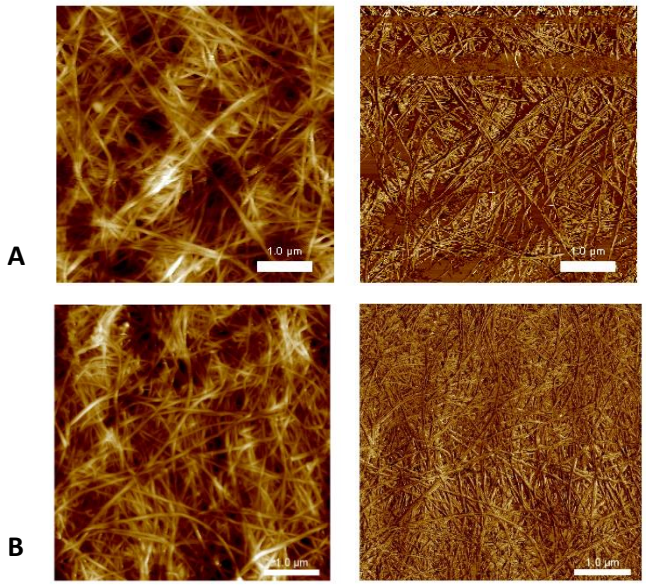

Figure 3.7 *Height (left) and phase (right) AFM images of BC samples biosynthesized from agitated GP and static GP culture media are represented in (**A**) and (**B**), respectively.*

Additionally, the surface morphological variations between static and agitated cultures were analyzed by SEM. As observed in Figure 3.8, the 3D network formed in agitated media presented a more porous cellulosic structure comparing to that of the BC membranes from static media. This porosity and increased free space of the BC spheres confirmed AFM results in Figure 3.7 and agreed with the findings reported in the literature [18, 54, 55]. The agitation of the cultures prevented the orderly alignment of the fibers, thus creating more spaces and empty cavities.

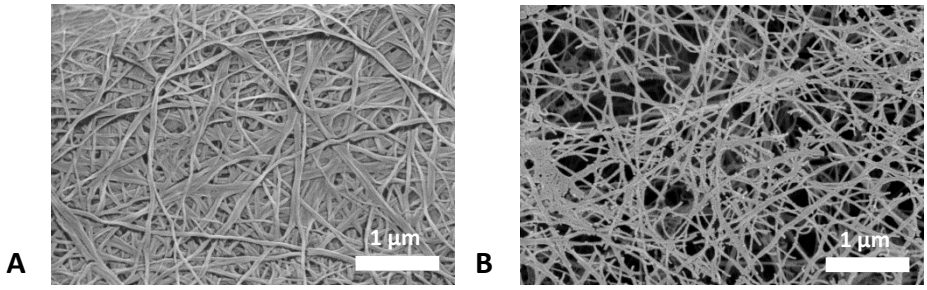

Figure 3.8 *SEM images of BC surfaces produced in static (**A**) and agitated (**B**) GP cultures.*

These morphological characteristics are relevant for the performance of the BC as a superabsorbent material, since the WHC of the samples could be affected. Table 3.4 shows the WHC results obtained for the BC membranes and sphere-shaped BCs from GP culture media after a swelling period of 48 hours (Equation 2.4 in Chapter 2).

Table 3.4 *Nanofiber diameter and WHC of BC from GP cultures in static and agitated conditions.*

Culture	Growth conditions	Nanofiber diameter (nm)	WHC (%)
GP5-exUs+H	Static	77.6 ± 13.7	4870 ± 350
GP5-exUs+H	Agitated	63.8 ± 8.2	7860 ± 35

Attending to the results in Table 3.4, regardless of the culture conditions both BC samples showed high WHC, though higher values were obtained for the agitated medium since the surface area per mass unit increased. Indeed, WHC values were 60% higher for BCs from GP medium biosynthesized under agitation. The particular biosynthesis into 3D networks of separated nano- and microfibrils enhances the surface area in comparison with vegetal cellulose. It is worthy to note that this feature is boosted in agitated culture conditions as it was clearly reflected in AFM and SEM images. Hence, BC could retain larger amounts of water without losing its structural coherence due to the numerous

hydrogen bonding interactions between water and the hydroxyl groups present on the nanofibers. Of course this capacity also depends on the interstitial spaces of the inner area in the never dried matrix [56]. In this sense, the drying method influences porosity since freeze-drying prevents pore shrinkage of the BC better than hot air drying [57].

In the same way, the fiber diameter decreased slightly with agitation, suggesting that finer and longer nanofibers could positively influence the WHC, as it has been demonstrated in previous studies [25, 58]. Consequently, the values of WHC were similar [25, 56, 59], and in most cases higher compared to other BC water absorption studies [18, 60], especially when using the same WHC measurement method. Furthermore, it is worth mentioning that the utilization of agricultural residues in the medium formulation may present a limitation in obtaining high WHC values. However, this limitation was not observed in this study.

3.3.4 Urea release study

The high WHC value of BC is an interesting feature that has already been successfully exploited mainly for the food and biomedical sectors [61, 62]. Thereby, the versatility and high WHC contribute to a more effective GP valorization. In fact, the added superabsorbent capacity of the sphere-shaped BCs expanded the applications of these systems, and it enhanced the usefulness of agitated growing conditions.

Therefore, given the properties of the sphere-shaped BC, its applicability as fertilizer release agent in agriculture was proposed, considering the lack of knowledge about the potential of BC in this field. Therefore, the ability of BC biosynthesized from GP to absorb and release urea was evaluated. Urea was

chosen due to its condition of organic fertilizer. The fertilizer was loaded into the freeze-dried and sphere-shaped BC from GP cultures by immersion. Subsequently, the urea-loaded BC spheres were freeze-dried, or oven dried again for the UL measurement and release studies.

The UL capacity of the sphere-shaped BC from GP culture was calculated to be higher than 375% for freeze-dried spheres, and 130% for oven-dried samples (Equation 3.2). This high loading capacity would be related to both the spherical shape and high porosity of the samples, that resulted in great WHC as explained before. Moreover, the loading efficiency was further enhanced by the hydrophilicity of urea and the hydrogen bonding interactions between its –NH_2 groups and the –OH groups of cellulose. This ability of the sphere-shaped BCs to retain the urea was confirmed by DSC, as shown in Figure 3.9.

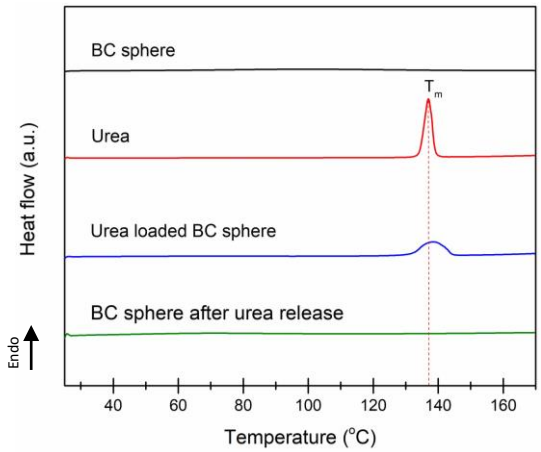

Figure 3.9 *DSC curves of urea, urea-loaded BC sphere, and BC sphere after the release study.*

As DSC curves evidenced, the presence of urea in the loaded BC samples was confirmed, displaying a peak at the fertilizer's T_m (133°C) in contrast to unloaded BC spheres. Subsequently, urea release from BC spheres in an

aqueous medium was monitored after its reaction with DMAB at 30 min and 60 min.

The results indicated that irrespective of the drying method, the release of urea occurred immediately and reached 100% in 30 minutes. Accordingly, DSC curve of BC spheres after the release studies also confirmed the complete liberation of the fertilizer (Figure 3.9). Certainly, the hydrophilicity of urea facilitated its rapid release from the nanofiber network. This behavior is common for highly water-soluble compounds, and the release process is strongly correlated with swelling [63].

Furthermore, it was observed that the release showed no difference between the two drying methods. Though the drying process may affect the porous structure and result in a lower fertilizer loading, it did not influence the final release. In fact, the drying process can be used as a tool for controlling drug loading and release, although it may not have been observed in this study due to the high solubility of urea in water [63]. In this sense, the addition of regulators for the controlled release of urea is an interesting research topic where the use of BCNCs could have great potential.

3.4 Conclusions

In this Chapter, sphere shaped BCs were successfully biosynthesized from GP based culture media contributing to the revaluation of this agro-industrial residue. The growth of *K. medellinensis* was analyzed and optimized under both static and agitated culture conditions. In this regard, it was found that gentle agitation conditions at 130 rpm were effective in producing spherical-shaped BC and in promoting a high rate of BC biosynthesis. Furthermore, the

use of ultrasound and hot water pretreatments in the GP improved the availability of nutrients in the culture, and consequently, larger BC production yields were obtained. As a result, sphere shaped BCs of great purity and high crystallinity were obtained, as it was proved in their physicochemical characterization. To assess the applicability of BC spheres in agriculture, their superabsorbent nature and their ability to retain and release a fertilizer were favorably evidenced. Thus, they could be considered as dual systems, able to help in soil water retention as well as release urea in the presence of water until their degradation. Further studies are needed to determine the behavior of the system in agricultural soil, where the biodegradability of the biopolymer may also be a key factor for fertilizer release. In fact, this biodegradable nature of BC further enhances the attractiveness of the system as it reduces the reliance on synthetic polymers.

3.5 References

1 Tilman, D., Cassman, K. G., Matson, P. A., Naylor, R. and Polasky, S. (2002) 2 Tilman. *Nature* **418**, 671–677

2 FAO. (2011) The state of the world's land and water resources for food and agriculture

3 Demitri, C., Scalera, F., Madaghiele, M., Sannino, A. and Maffezzoli, A. (2013) Potential of cellulose-based superabsorbent hydrogels as water reservoir in agriculture. *Int. J. Polym. Sci.* **2013** https://doi.org/10.1155/2013/435073

4 Romanazzi, G., Mancini, V., Feliziani, E., Servili, A., Endeshaw, S. and Neri, D. (2016) Impact of alternative fungicides on grape downy mildew control and vine growth and development. *Plant Dis.* **100**, 739–748 https://doi.org/10.1094/PDIS-05-15-0564-RE

5 Roy, A., Singh, S. K., Bajpai, J. and Bajpai, A. K. (2014) Controlled pesticide release from biodegradable polymers. *Cent. Eur. J. Chem.* **12**,

453–469 https://doi.org/10.2478/s11532-013-0405-2

6 Behera, S. and Mahanwar, P. A. (2020) Superabsorbent polymers in agriculture and other applications: a review. *Polym. Technol. Mater.*, Taylor & Francis **59**, 341–356 https://doi.org/10.1080/25740881.2019.1647239

7 Neri-Badang, M. C. and Chakraborty, S. (2019) Carbohydrate polymers as controlled release devices for pesticides. *J. Carbohydr. Chem.*, Taylor & Francis **38**, 67–85 https://doi.org/10.1080/07328303.2019.1568449

8 Montesano, F. F., Parente, A., Santamaria, P., Sannino, A. and Serio, F. (2015) Biodegradable Superabsorbent Hydrogel IncreasesWater Retention Properties of Growing Media and Plant Growth. *Agric. Agric. Sci. Procedia*, The Authors **4**, 451–458 https://doi.org/10.1016/j.aaspro.2015.03.052

9 Molina-Ramírez, C., Castro, M., Osorio, M., Torres-Taborda, M., Gómez, B., Zuluaga, R., et al. (2017) Effect of different carbon sources on bacterial nanocellulose production and structure using the low pH resistant strain Komagataeibacter medellinensis. *Materials (Basel).* **10** https://doi.org/10.3390/ma10060639

10 Li, J., Zhu, Y., Liu, M., Liu, Z., Zhou, T., Liu, Y., et al. (2023) Network interpenetrating slow-release nitrogen fertilizer based on carrageenan and urea: A new low-cost water and fertilizer regulation carrier. *Int. J. Biol. Macromol.*, Elsevier B.V. **242**, 124858 https://doi.org/10.1016/j.ijbiomac.2023.124858

11 Giroto, A. S., Guimarães, G. G. F., Foschini, M. and Ribeiro, C. (2017) Role of Slow-Release Nanocomposite Fertilizers on Nitrogen and Phosphate Availability in Soil. *Sci. Rep.*, Nature Publishing Group **7** https://doi.org/10.1038/srep46032

12 Ni, B., Liu, M. and Lü, S. (2009) Multifunctional slow-release urea fertilizer from ethylcellulose and superabsorbent coated formulations. *Chem. Eng. J.* **155**, 892–898 https://doi.org/10.1016/j.cej.2009.08.025

13 Li, X., Li, Q., Xu, X., Su, Y., Yue, Q. and Gao, B. (2016) Characterization, swelling and slow-release properties of a new controlled release fertilizer based on wheat straw cellulose hydrogel. *J. Taiwan Inst. Chem. Eng.*, Elsevier B.V. **60**, 564–572

https://doi.org/10.1016/j.jtice.2015.10.027

14 Sarmah, D. and Karak, N. (2020) Biodegradable superabsorbent hydrogel for water holding in soil and controlled-release fertilizer. *J. Appl. Polym. Sci.* **137**, 1–12 https://doi.org/10.1002/app.48495

15 Ibrahim, S., Nawwar, G. A. M. and Sultan, M. (2016) Development of bio-based polymeric hydrogel: Green, sustainable and low cost plant fertilizer packaging material. *J. Environ. Chem. Eng.*, Elsevier B.V. **4**, 203–210 https://doi.org/10.1016/j.jece.2015.10.028

16 Suprabawati, A., Aisyah, L. S. and Firzatullah, M. R. (2020) Crosslinked CMC-urea hydrogel made from natural carboxymethyl cellulose (CMC) as slow-release fertilizer coating. *AIP Conf. Proc.* **2243** https://doi.org/10.1063/5.0002056

17 Castro, C., Cleenwerck, I., Trček, J., Zuluaga, R., de Vos, P., Caro, G., et al. (2013) Gluconacetobacter medellinensis sp. nov., cellulose- and non-cellulose-producing acetic acid bacteria isolated from vinegar. *Int. J. Syst. Evol. Microbiol.* **63**, 1119–1125 https://doi.org/10.1099/ijs.0.043414-0

18 Algar, I., Fernandes, S. C. M., Mondragon, G., Castro, C., Garcia-Astrain, C., Gabilondo, N., et al. (2014) Pineapple agroindustrial residues for the production of high value bacterial cellulose with different morphologies. *J. Appl. Polym. Sci.* **132**, 1–8 https://doi.org/10.1002/app.41237

19 Urbina, L., Eceiza, A., Gabilondo, N., Corcuera, M. Á. and Retegi, A. (2020) Tailoring the in situ conformation of bacterial cellulose-graphene oxide spherical nanocarriers. *Int. J. Biol. Macromol.*, Elsevier B.V. **163**, 1249–1260 https://doi.org/10.1016/j.ijbiomac.2020.07.077

20 Hu, Y., Catchmark, J. M. and Vogler, E. A. (2013) Factors impacting the formation of sphere-like bacterial cellulose particles and their biocompatibility for human osteoblast growth. *Biomacromolecules* **14**, 3444–3452 https://doi.org/10.1021/bm400744a

21 Zarei, O., Dastmalchi, S. and Hamzeh-Mivehroud, M. (2016) A simple and rapid protocol for producing yeast extract from Saccharomyces cerevisiae suitable for preparing bacterial culture media. *Iran. J. Pharm. Res.* **15**, 907–913

22 Dutta, G. K. and Karak, N. (2018) One-Pot Synthesis of Bio-Based Waterborne Polyester as UV-Resistant Biodegradable Sustainable Material with Controlled Release Attributes. *ACS Omega* **3**, 16812–16822 https://doi.org/10.1021/acsomega.8b02790

23 Giraldo, J. D. and Rivas, B. L. (2017) Determination of urea using p-N,N-dimethylaminobenzaldehyde: Solvent effect and interference of chitosan. *J. Chil. Chem. Soc.* **62**, 3538–3542 https://doi.org/10.4067/S0717-97072017000200023

24 Pastorkova, E., Zakova, T., Landa, P., Novakova, J., Vadlejch, J. and Kokoska, L. (2013) Growth inhibitory effect of grape phenolics against wine spoilage yeasts and acetic acid bacteria. *Int. J. Food Microbiol.*, Elsevier B.V. **161**, 209–213 https://doi.org/10.1016/j.ijfoodmicro.2012.12.018

25 Urbina, L., Hernández-Arriaga, A. M., Eceiza, A., Gabilondo, N., Corcuera, M. A., Prieto, M. A., et al. (2017) By-products of the cider production: an alternative source of nutrients to produce bacterial cellulose. *Cellulose* **24**, 2071–2082 https://doi.org/10.1007/s10570-017-1263-4

26 Carreira, P., Mendes, J. A. S., Trovatti, E., Serafim, L. S., Freire, C. S. R., Silvestre, A. J. D., et al. (2011) Utilization of residues from agro-forest industries in the production of high value bacterial cellulose. *Bioresour. Technol.* https://doi.org/10.1016/j.biortech.2011.04.081

27 Bayrak, E. and Büyükkileci, A. O. (2018) Utilization of White Grape Pomace for Lactic Acid Production. *Gida / J. Food* **43**, 129–138 https://doi.org/10.15237/gida.gd17088

28 Cerrutti, P., Roldán, P., García, R. M., Galvagno, M. A., Vázquez, A. and Foresti, M. L. (2016) Production of bacterial nanocellulose from wine industry residues: Importance of fermentation time on pellicle characteristics. *J. Appl. Polym. Sci.* **133**, 1–9 https://doi.org/10.1002/app.43109

29 Pérez-Bibbins, B., Torrado-Agrasar, A., Salgado, J. M., Oliveira, R. P. de S. and Domínguez, J. M. (2015) Potential of lees from wine, beer and cider manufacturing as a source of economic nutrients: An overview. *Waste Manag.* **40**, 72–81

https://doi.org/10.1016/j.wasman.2015.03.009

30 Mosier, N., Wyman, C., Dale, B., Elander, R., Lee, Y. Y., Holtzapple, M., et al. (2005) Features of promising technologies for pretreatment of lignocellulosic biomass. *Bioresour. Technol.* **96**, 673–686 https://doi.org/10.1016/j.biortech.2004.06.025

31 Vilkhu, K., Mawson, R., Simons, L. and Bates, D. (2008) Applications and opportunities for ultrasound assisted extraction in the food industry - A review. *Innov. Food Sci. Emerg. Technol.* **9**, 161–169 https://doi.org/10.1016/j.ifset.2007.04.014

32 Mason, T. J., Paniwnyk, L. and Lorimer, J. P. (1996) The uses of ultrasound in food technology. *Ultrason. Sonochem.* **3** https://doi.org/10.1016/S1350-4177(96)00034-X

33 Blanco Parte, F. G., Santoso, S. P., Chou, C. C., Verma, V., Wang, H. T., Ismadji, S., et al. (2020) Current progress on the production, modification, and applications of bacterial cellulose. *Crit. Rev. Biotechnol.*, Taylor & Francis **40**, 397–414 https://doi.org/10.1080/07388551.2020.1713721

34 Singhania, R. R., Patel, A. K., Tseng, Y. S., Kumar, V., Chen, C. W., Haldar, D., et al. (2022) Developments in bioprocess for bacterial cellulose production. *Bioresour. Technol.*, Elsevier Ltd **344**, 126343 https://doi.org/10.1016/j.biortech.2021.126343

35 Urbina, L., Corcuera, M. Á., Gabilondo, N., Eceiza, A. and Retegi, A. (2021) A review of bacterial cellulose: sustainable production from agricultural waste and applications in various fields. *Cellulose* **28**, 8229–8253 https://doi.org/10.1007/s10570-021-04020-4

36 Huang, Y., Zhu, C., Yang, J., Nie, Y., Chen, C. and Sun, D. (2014) Recent advances in bacterial cellulose. *Cellulose* **21**, 1–30 https://doi.org/10.1007/s10570-013-0088-z

37 Lee, K. Y., Buldum, G., Mantalaris, A. and Bismarck, A. (2014) More than meets the eye in bacterial cellulose: Biosynthesis, bioprocessing, and applications in advanced fiber composites. *Macromol. Biosci.* **14**, 10–32 https://doi.org/10.1002/mabi.201300298

38 Chen, G., Wu, G., Chen, L., Wang, W., Hong, F. F. and Jönsson, L. J.

(2019) Performance of nanocellulose-producing bacterial strains in static and agitated cultures with different starting pH. *Carbohydr. Polym.*, Elsevier **215**, 280–288 https://doi.org/10.1016/j.carbpol.2019.03.080

39 Singhsa, P., Narain, R. and Manuspiya, H. (2018) Physical structure variations of bacterial cellulose produced by different Komagataeibacter xylinus strains and carbon sources in static and agitated conditions. *Cellulose*, Springer Netherlands **25**, 1571–1581 https://doi.org/10.1007/s10570-018-1699-1

40 Revin, V., Liyaskina, E., Nazarkina, M., Bogatyreva, A. and Shchankin, M. (2018) Cost-effective production of bacterial cellulose using acidic food industry by-products. *Brazilian J. Microbiol.*, Sociedade Brasileira de Microbiologia **49**, 151–159 https://doi.org/10.1016/j.bjm.2017.12.012

41 Czaja, W., Romanovicz, D. and Brown, R. malcolm. (2004) Structural investigations of microbial cellulose produced in stationary and agitated culture. *Cellulose* **11**, 403–411 https://doi.org/10.1023/b:cell.0000046412.11983.61

42 Mohite, B. V. and Patil, S. V. (2014) Physical, structural, mechanical and thermal characterization of bacterial cellulose by G. hansenii NCIM 2529. *Carbohydr. Polym.*, Elsevier Ltd. **106**, 132–141 https://doi.org/10.1016/j.carbpol.2014.02.012

43 Corbin, K. R., Hsieh, Y. S. Y., Betts, N. S., Byrt, C. S., Henderson, M., Stork, J., et al. (2015) Bioresource Technology Grape marc as a source of carbohydrates for bioethanol : Chemical composition , pre-treatment and saccharification, Elsevier Ltd **193**, 76–83 https://doi.org/10.1016/j.biortech.2015.06.030

44 Hu, Y. and Catchmark, J. M. (2010) Formation and characterization of spherelike bacterial cellulose particles produced by acetobacter xylinum JCM 9730 strain. *Biomacromolecules* **11**, 1727–1734 https://doi.org/10.1021/bm100060v

45 Ruka, D. R., Simon, G. P. and Dean, K. M. (2012) Altering the growth conditions of Gluconacetobacter xylinus to maximize the yield of bacterial cellulose. *Carbohydr. Polym.*, Elsevier Ltd. **89**, 613–622 https://doi.org/10.1016/j.carbpol.2012.03.059

46 Römling, U. (2002) Molecular biology of cellulose production in bacteria. *Res. Microbiol.* **153**, 205–212 https://doi.org/10.1016/S0923-2508(02)01316-5

47 Benziman, M. and Rivetz, B. (1972) Factors affecting hexose phosphorylation in Acetobacter xylinum. *J. Bacteriol.* **111**, 325–333 https://doi.org/10.1128/jb.111.2.325-333.1972

48 Castro, C., Zuluaga, R., Putaux, J. L., Caro, G., Mondragon, I. and Gañán, P. (2011) Structural characterization of bacterial cellulose produced by Gluconacetobacter swingsii sp. from Colombian agroindustrial wastes. *Carbohydr. Polym.* **84**, 96–102 https://doi.org/10.1016/j.carbpol.2010.10.072

49 Szymańska-Chargot, M., Cybulska, J. and Zdunek, A. (2011) Sensing the structural differences in cellulose from apple and bacterial cell wall materials by Raman and FT-IR Spectroscopy. *Sensors* **11**, 5543–5560 https://doi.org/10.3390/s110605543

50 Xu, X., Liu, F., Jiang, L., Zhu, J. Y., Haagenson, D. and Wiesenborn, D. P. (2013) Cellulose nanocrystals vs. Cellulose nanofibrils: A comparative study on their microstructures and effects as polymer reinforcing agents. *ACS Appl. Mater. Interfaces* **5**, 2999–3009 https://doi.org/10.1021/am302624t

51 Sullivan, E. M., Moon, R. J. and Kalaitzidou, K. (2015) Processing and characterization of cellulose nanocrystals/polylactic acid nanocomposite films. *Materials (Basel).* **8**, 8106–8116 https://doi.org/10.3390/ma8125447

52 Watanabe, K., Tabuchi, M., Morinaga, Y. and Yoshinaga, F. (1998) Structural features and properties of bacterial cellulose produced in agitated culture. *Cellulose* **5**, 187–200 https://doi.org/10.1023/A:1009272904582

53 Lu, H. and Jiang, X. (2014) Structure and properties of bacterial cellulose produced using a trickling bed reactor. *Appl. Biochem. Biotechnol.* **172**, 3844–3861 https://doi.org/10.1007/s12010-014-0795-4

54 Zhu, H., Jia, S., Yang, H., Jia, Y., Yan, L. and Li, J. (2011) Preparation and application of bacterial cellulose sphere: A novel biomaterial. *Biotechnol. Biotechnol. Equip.* **25**, 2233–2236

https://doi.org/10.5504/bbeq.2011.0010

55 Zhu, H., Jia, S., Wan, T., Jia, Y., Yang, H., Li, J., et al. (2011) Biosynthesis of spherical Fe3O4/bacterial cellulose nanocomposites as adsorbents for heavy metal ions. *Carbohydr. Polym.*, Elsevier Ltd. **86**, 1558–1564 https://doi.org/10.1016/j.carbpol.2011.06.061

56 Ul-Islam, M., Khan, T. and Park, J. K. (2012) Water holding and release properties of bacterial cellulose obtained by in situ and ex situ modification. *Carbohydr. Polym.*, Elsevier Ltd. **88**, 596–603 https://doi.org/10.1016/j.carbpol.2012.01.006

57 Tang, W., Jia, S., Jia, Y. and Yang, H. (2010) The influence of fermentation conditions and post-treatment methods on porosity of bacterial cellulose membrane. *World J. Microbiol. Biotechnol.* **26**, 125–131 https://doi.org/10.1007/s11274-009-0151-y

58 Ougiya, H., Watanabe, K., Matsumura, T. and Yoshinaga, F. (1998) Relationship between suspension properties and fibril structure of disintegrated bacterial cellulose. *Biosci. Biotechnol. Biochem.* **62**, 1714–1719 https://doi.org/10.1271/bbb.62.1714

59 Tsouko, E., Kourmentza, C., Ladakis, D., Kopsahelis, N., Mandala, I., Papanikolaou, S., et al. (2015) Bacterial cellulose production from industrial waste and by-product streams. *Int. J. Mol. Sci.* **16**, 14832–14849 https://doi.org/10.3390/ijms160714832

60 Jung, H. Il, Lee, O. M., Jeong, J. H., Jeon, Y. D., Park, K. H., Kim, H. S., et al. (2010) Production and characterization of cellulose by acetobacter sp. V6 using a cost-effective molasses-corn steep liquor medium. *Appl. Biochem. Biotechnol.* **162**, 486–497 https://doi.org/10.1007/s12010-009-8759-9

61 Shi, Z., Zhang, Y., Phillips, G. O. and Yang, G. (2014) Utilization of bacterial cellulose in food. *Food Hydrocoll.*, Elsevier Ltd **35**, 539–545 https://doi.org/10.1016/j.foodhyd.2013.07.012

62 Picheth, G. F., Pirich, C. L., Sierakowski, M. R., Woehl, M. A., Sakakibara, C. N., de Souza, C. F., et al. (2017) Bacterial cellulose in biomedical applications: A review. *Int. J. Biol. Macromol.*, Elsevier B.V. **104**, 97–106 https://doi.org/10.1016/j.ijbiomac.2017.05.171

63 Adepu, S. and Khandelwal, M. (2020) Ex-situ modification of bacterial cellulose for immediate and sustained drug release with insights into release mechanism. *Carbohydr. Polym.*, Elsevier **249**, 116816 https://doi.org/10.1016/j.carbpol.2020.116816

CHAPTER 4

ACTIVE PICKERING EMULSIONS



1.1 Introduction 109
1.2 Experimental section 112
1.2.1 BC hydrolysis 112
1.2.2 GPPE extraction and characterization 114
1.2.3 BCNC-GPPE complex preparation and characterization 115
1.2.4 Pickering emulsions 116
1.3 Results and discussion 118
1.3.1 BCNC production and characterization 118
1.3.2 GPPE characterization 122
1.3.3 BC and GPPE complex characterization 125
1.3.4 Pickering emulsion characterization 131
1.4 Conclusion 138
1.5 References 139

Chapter 4: Active Pickering emulsions

4.1 Introduction

An emulsion is a heterogeneous mixture of two or more normally immiscible liquids, referred to as oil-in-water (O/W) or water-in-oil (W/O) in the case of binary ones. Nowadays, the use of emulsions is fully widespread, mainly in the food and cosmetic industries, and, therefore, their stability is a critical issue that must be carefully controlled [1]. Indeed, the undesirable phenomena of phase inversion, flocculation and coalescence affect the physicochemical and organoleptic properties, and surfactants or stabilizing particles are necessary [2].

In this context, Pickering emulsions, in which surfactants are replaced by solid particles, have recently gained interest, since they reduce coalescence risks, add adjustable permeability and lead to unique rheological behavior [3,4]. These solid (inorganic or organic) particles include graphene sheets, clay particles, silica based particles, starch, cellulose or proteins among others [5–7]. The current trend in the preparation of Pickering emulsions lies in the use of greener stabilizing particles that are biodegradable and biocompatible, thus suitable for human intake or use [8].

As explained in Chapter 1, when BC is subjected to controlled enzymatic hydrolysis (EH) or acid hydrolysis (AH) treatments, rod-shaped BCNCs are obtained [9,10]. In this regard, although AH most traditional methods have advantages in terms of yield, it is mandatory to look for greener and economically sustainable alternatives, such as EH [11]. BCNCs are distinguished by their high crystallinity, green condition, and particularly high length-to-

diameter aspect ratio. Therefore, BCNCs have great applicability in various fields, including the stabilization of Pickering emulsions [12–14]. The morphology and amphiphilic nature of BCNCs allow the stabilization of the oil–water interface of O/W emulsions at lower concentrations than other inorganic spherical particles used for Pickering emulsions [15]. Furthermore, as BCNCs are easily hydrated and well dispersed in aqueous media, they are capable of emulsifying a wide range of oils [14,16].

Besides, cellulose nanocrystals (CNCs) can not only stabilize the prepared O/W emulsion, but they could also create synergistic complexes with other components of the emulsion to further improve colloidal stability and/or provide additional bioactivity to the emulsion [4]. In particular, the interactions between cellulose and certain polyphenolic compounds have been assessed to increase the physical and oxidative stability of lipids in O/W emulsions (Figure 4.1) [17–20].

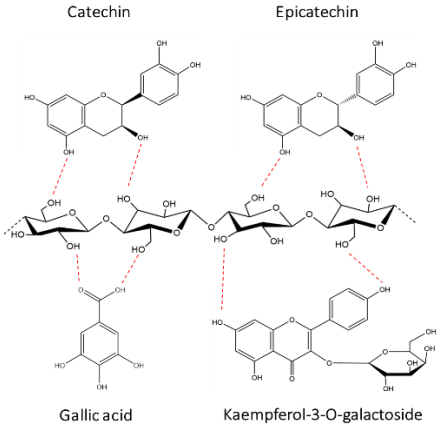

Figure 4.1 *Graphical representation of the interactions between BC and phenolic compounds characteristic of GP through hydrogen bonding (red dashed lines).*

As represented in Figure 4.1, these polyphenol–cellulose-based complexes are mostly formed through hydrogen bonding, hydrophobic and ionic interactions [21,22]. These interactions have been exploited elsewhere for the encapsulation of curcumin or raspberry phenols to protect thus extending their bioactive properties [23,24]. Furthermore, phenolic acids such as tannic acid have shown to be effective in adjusting the hydrophobicity of CNCs in their Pickering emulsions [4,18]. However, the literature related to the combination of cellulose and polyphenols in the creation of Pickering emulsions is still scarce.

In parallel, polyphenolic extracts from plants have been proposed for colloidal aggregates intended for the food, pharma and cosmetic industries, mainly due to their antioxidant activity [25,26]. The antioxidant capacity of stabilizers aimed for emulsions is particularly important in the food or cosmetic industries, where the quality and nutritional value of lipids could be lost during storage. In fact, anthocyanins from black rice or epigallocatechin gallate from green tea have already proved to be useful in inhibiting lipid oxidation in emulsions [20,26].

In this chapter, the contribution of polyphenolic compounds from GP to BCNCs in the stabilization of active Pickering emulsions was assessed. Continuing with the integral harnessing concept of GP, the residue was used as a raw material for the biosynthesis of BC and, at the same time, as a source of polyphenolic extract after ultrasound-assisted hydroalcoholic treatment. Enzymatically hydrolyzed BCNCs were evaluated as emulsifiers in terms of colloidal stability and antioxidant capacity, and their competitiveness with AH was assessed in different concentrations. The synergistic performance of the BCNC–GPPE

complex was analyzed by monitoring the oxidative stability of olive oil-in-water and the physical stability of hexadecane-in-water Pickering emulsions.

4.2 Experimental section

4.2.1 Hydrolysis of BC

4.2.1.1 Enzymatic hydrolysis

For the EH, the procedures detailed by George et al were conducted with some modifications, those represented in Figure 4.2 [27]. BC membranes, biosynthesized from GP as described in Chapter 3, were cut into pieces, surface water was removed, and they were mechanically disintegrated with a blender at maximum speed to yield a final uniform paste. The paste was then subjected to a high-shear homogenization (Ultraturrax IKA T25, Staufen, Germany) for 10 min at 15000 rpm. Then, 20 g of this BC paste were mixed with 200 mL of 0.1 M sodium acetate buffer (pH 5.2 ± 0.1). The mixture was kept overnight at 55 °C under gentle agitation; hence, the buffer completely infiltrated the BC network in order to facilitate the subsequent enzymolysis [28]. Indeed, BC membranes enable working in wet state, thus increasing the surface area and facilitating the enzyme activity. Then, 10 mg of cellulase (*Trichoderma reesei* 6.9 U/mg) was added, and the reaction was maintained at 55 °C and 300 rpm magnetic stirring for 4 days. The final cloudy solution was placed in a cold-water bath to slow down the reaction. The resulting solution was centrifuged three times at 4500 rpm for 15 min. The precipitate was then thoroughly washed with cold distilled water to remove the buffer and residual enzyme, freeze-dried and stored in a desiccator until use. The BCNCs obtained from EH are referred to as BCNC EH in this work.

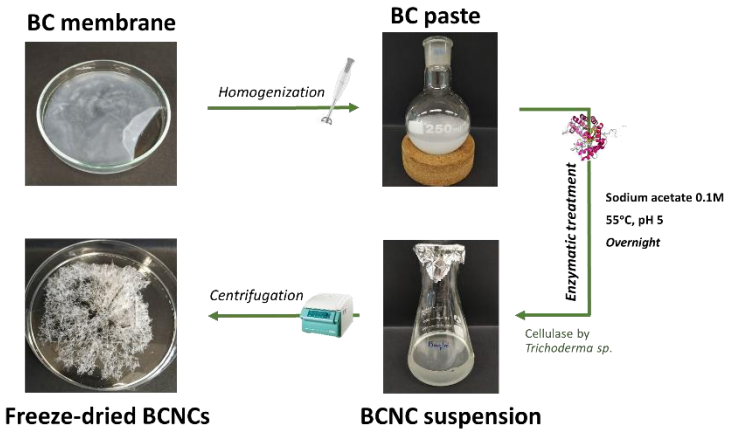

Figure 4.2 *Schematic representation of the used enzymatic hydrolysis procedure.*

4.2.1.2 Acid hydrolysis

Similarly, the used AH method was adapted from that published by Yan et al 2017 and George et al 2012, as represented in Figure 4.3 [14,27]. First, 20 g of BC paste were mixed with 120 mL of 50% (*v/v*) sulfuric acid. The hydrolysis was carried out for 4 h at 80 °C at 300 rpm magnetic stirring. Cold distilled water was added to stop the hydrolysis at a 1:5 (*v/v*) ratio with respect to the reaction volume. The resulting solution was subjected to three 15 min centrifugation cycles at 4500 rpm. The precipitate was suspended in cold distilled water after each centrifugation cycle, and it was ultrasonicated for five minutes. Finally, the obtained suspension was dialyzed against distilled water (Medicell Membranes Ltd., 3.5 KDa, London, United Kingdom) to a neutral pH. The BCNC suspension was freeze-dried and maintained in a desiccator until use. The BCNCs obtained from the AH method are referred to as BCNC AH in this work.

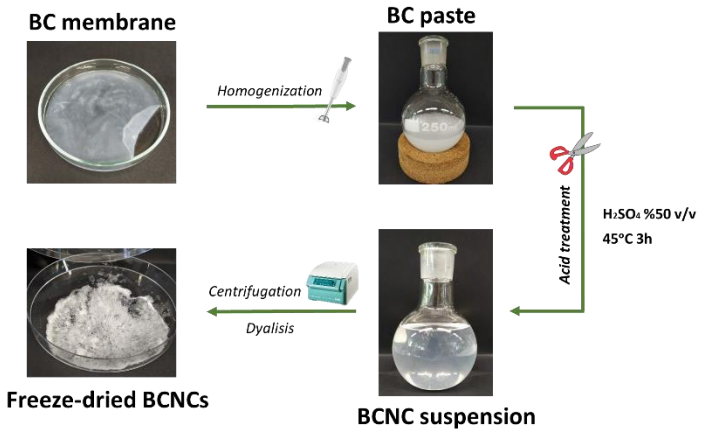

Figure 4.3 *Schematic representation of the acid hydrolysis process used.*

The EH and AH yields were calculated gravimetrically related to freeze-dried untreated BC weight following Equation 4.1:

$$Hydrolysis\ yield\ (\%) = \frac{W_{BCNC}}{W_{BCp}} \cdot 100 \qquad \text{(Equation 4.1)}$$

where W_{BCNC} is the weight of the freeze-dried BCNCs and W_{BCp} is the estimated freeze-dried weight of the BC paste used in each hydrolysis reaction.

4.2.2 GPPE extraction and characterization

4.2.2.1 Ultrasound-assisted polyphenol extraction

Following the procedure published by Abad-Garcia et al, polyphenolic extract was obtained through ultrasound-assisted extraction from 122 mg of previously freeze-dried and ground GP with 3 mL of MeOH:H_2O:HAc (30:69:1, *v/v/v*) solvent mixture and ascorbic acid (2 g/L) as antioxidant [29]. The mixture was first stirred in a vortex for 1 min and the extraction was performed in an ultrasonic bath for 15 min. Then, the hydroalcoholic solution

was centrifuged for 4 min at 4000 rpm and 10 °C and the supernatant was dried in a rotational evaporator (Heidolph Hei-Vap Core, Schwabach, Germany) at 100 mmHg and 50 °C. Finally, the extract was freeze-dried to remove residual water and stored in a desiccator in the dark until use.

The extraction of polyphenols for the oxidative and physical stability measurements followed a similar procedure, but, in this case, ascorbic acid was not added in order to not interfere with the intrinsic antioxidant activity of the GPPE, and the ultrasound treatment was extended to 20 min at 50 °C [30].

4.2.3 BCNC-GPPE complex preparation and characterization

Firstly, a homogenous dispersion of BCNCs was prepared through ultrasonic treatment at 750 W, 20 kHz and 30% amplitude of the ultrasonic device (Vibracell 75041, Bioblock scientific, Illkirch-Graffenstaden, France). Then, once BCNCs were rehydrated and well dispersed, GPPE aqueous solution was gradually added to the BCNC dispersion. The mixture was kept under gentle agitation overnight, and the final dispersions gave BCNC:GPPE weight ratios of 1:1, 2.5:1 and 5:1 for a fixed GPPE concentration of 0.25 mg/mL.

4.2.3.1 Antioxidant activity assay

The oxidative stability of the free GPPE and BCNC-GPPE complex dispersions was measured over time according to the DPPH free radical method. In particular, the loss of antioxidant capacity of the samples exposed to light, in the dark and in the dark at 4 °C was monitored for 40 days, selecting 1, 9, 20 and 40 days as time points. In order to observe the effect of BCNCs on the antioxidant capacity of the GPPE, BCNC-GPPE weight ratios of 1:1, 2.5:1 and 5:1 were studied.

With the purpose of comparing the degradation of the BCNC-GPPE complex and free GPPE, a first-order reaction kinetic model was used. Degradation rate constants (λ) and half-lives ($t_{1/2}$) were calculated according to Equations 4.2 and 4.3, respectively:

$$\ln\frac{C}{C_0} = -\lambda\, t \qquad \text{(Equation 4.2)}$$

$$t_{1/2} = \frac{\ln 2}{\lambda} \qquad \text{(Equation 4.3)}$$

where C_0 is the initial mg TE/g GPPE and C_t is the mg TE/g GPPE at time t.

4.2.4 Pickering emulsions

4.2.4.1 Oxidative stability

The oxidative stability of two 10 mL emulsions prepared with 10% *w/w* olive oil and stabilized by the BCNC (2.5 mg/mL) and BCNC-GPPE complexes (2.5:1 weight ratio) was assessed by measuring the increase in primary oxidation products of a polyunsaturated acid [31]. Additionally, a third emulsion was prepared with the commercial emulsifier Tween 20 (TW20) as a control. The emulsions were prepared through tip sonication using a 3 mm diameter titanium probe at 750 W, 20 kHz and 30% amplitude. Each sample was then subjected to 3 s ultrasound and 3 s standby cycles of 20 s. The formation of conjugated dienes (CD) was monitored for 4 days by analyzing their absorbance at 233 nm (Shimadzu UV–Vis-NIR 3600). The emulsions were subjected to the Schaal oven test and kept in the dark at 60 °C in an adaptation of the methodology published by Listete-Torres et al [32]. All samples were vortexed for 1 min every 24 h to maintain the emulsion's physical integrity. At different time points, 100 µL of each sample was diluted in 10 mL ethanol and

analyzed in the UV spectrophotometer. The oxidative experiments were carried out in triplicate.

4.2.4.2 Physical stability

Hexadecane-in-water Pickering emulsions were prepared in a 30:70 ratio with the same ultrasonic device, to study the physical stability of the emulsions [33]. The aqueous phase was prepared with concentrations of 1, 2.5 and 5 mg/mL of previously dispersed BCNCs and BCNC-GPPE complexes. The stability of the emulsion was tested by subjecting the samples to 4000 *g* for 5 min [13]. The result was a milky white Pickering emulsion with a creamy phase of emulsified hexadecane close to the surface. After 24 h, the creamy phase started to condense on the surface, and its height was measured. Simultaneously, a transparent aqueous phase emerged at the bottom of the emulsions. Figure 4.4 shows an example of a Pickering emulsion stabilized by BCNCs.

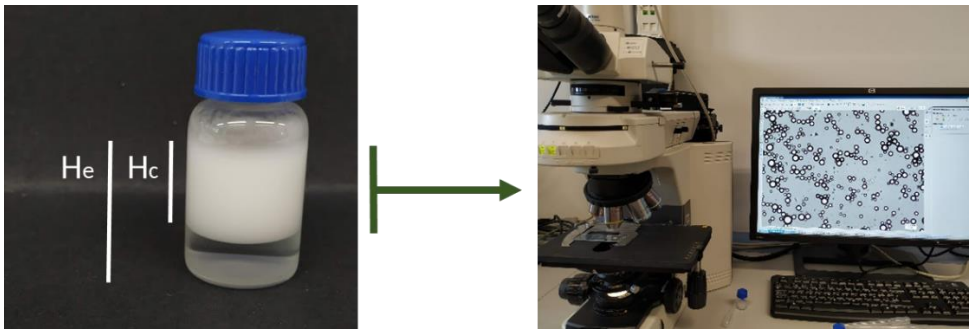

Figure 4.4 *Digital images of a BCNC-stabilized Pickering emulsion (left) and the study of the creamy phase under an optical microscope (right).*

The emulsion ratio (ER) was calculated with the following equation [34]:

$$ER\ (\%) = \frac{H_c}{H_e} \cdot 100 \qquad \text{(Equation 4.4)}$$

where H_c is the height of the creamy phase and H_e the total height of the emulsion (Figure 4.4).

In order to observe the possible coalescence of the different phases over time, 50 µL of the emulsion was dissolved in 1 mL of water after 7 days. A drop of this solution was then deposited onto a glass slide and observed in an optical microscope (Nikon Eclipse 80i) at a magnification of 10× (Figure 4.4). Subsequently, Image J software was used to analyze the emulsion droplet size of the optical micrographs. Finally, the diameter was calculated as the volume mean diameter D [4,3], employing the following equation:

$$D[4,3] = \frac{\sum n_i d^4}{\sum n_i d^3} \qquad \text{(Equation 4.5)}$$

where $n_i d$ is the diameter of the oil drops in the Pickering emulsion.

4.3 Results and discussion

4.3.1 BCNC production and characterization

4.3.1.1 BCNC particle size distribution

The morphology (size and shape) of nanoparticles is a key factor in the formation of any Pickering emulsion [34,35]. In this work, rod-like BCNCs were successfully obtained through both EH and AH, as can be observed in the AFM images in Figure 4.5A and B, respectively. According to the images, their sizes varied up to 1.5 µm in length and between 5 and 30 nm in width, confirming

their high aspect ratio. As seen, the obtained BCNCs showed large polydispersity in size, which was slightly higher in the case of EH, likely due to enzyme type diversity. Thus, smaller nanocrystals together with some nanofibers exceeding 1 µm could be found. However, this broad size distribution not only was considered a disadvantage, but it could favor the final applicability of the BCNCs, since, unlike the inorganic spherical particles commonly used for Pickering emulsions, the combination of large aspect ratio rod-shaped particles and nanofibers could form bridging structures that contribute to stabilizing the emulsion by creating entangled networks [13,35].

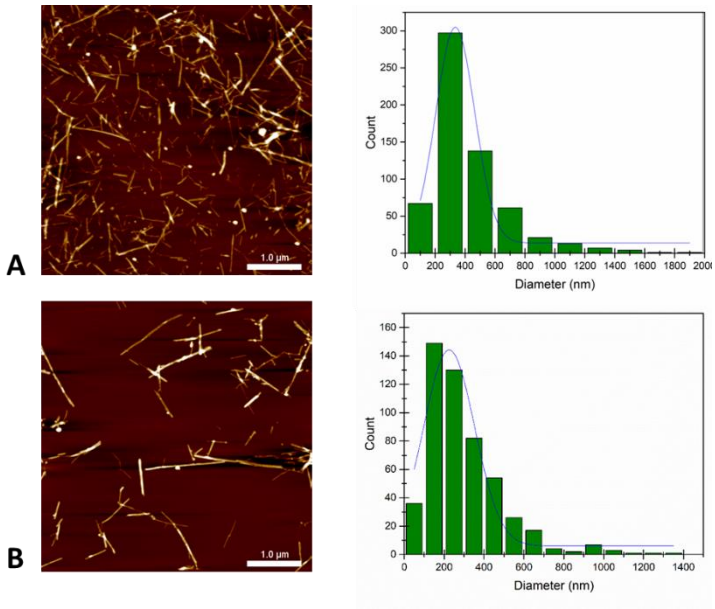

Figure 4.5 *AFM images and size distribution of BCNC EH (**A**) and BCNC AH (**B**), respectively.*

Regarding the hydrolysis, the calculated BCNC yield of the EH procedure relative to the initial dry BC was close to 35%. This value was in line with those reported in the literature for EH [28,36], indicating that despite being lower than those of the traditional AH process [14,37,38], the highly selective and

sustainable EH method was successfully carried out. However, increasing the usually low EH yield value is one of the topics of great interest in order to completely substitute the less sustainable AH process.

4.3.1.2 BCNC characterization

The crystalline structure of BCNCs was analyzed using XRD as shown in Figure 4.6A. As expected, all patterns corresponded to the typical cellulose I allomorph, as detailed in Chapter 3.

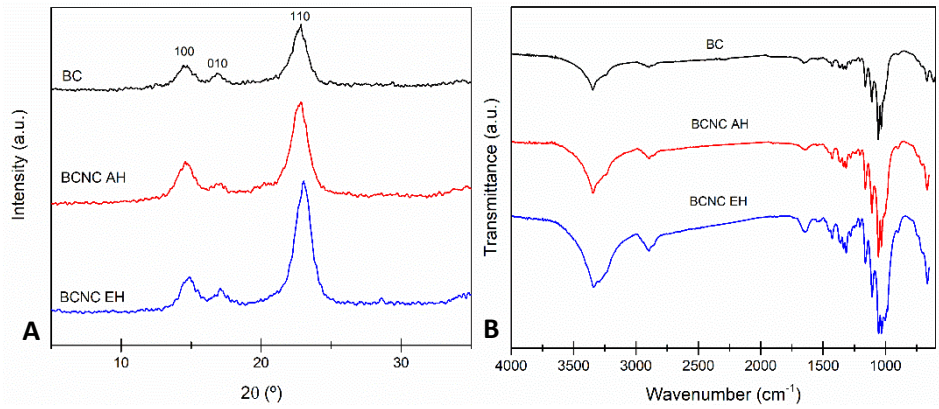

Figure 4.6 *X-ray diffractograms (**A**) and FTIR spectra (**B**) of BC, BCNC EH and BCNC AH samples.*

According to the spectra, the calculated CIs were (Equation 2.1, Chapter 2) 77% for the BC membrane, 87% for BCNC EH and 86% for BCNC AH, in close agreement with the CI values found in literature [14,39]. These results demonstrated that EH effectively removed amorphous regions of the original BC, and high crystalline nanocrystals could be obtained. It is worth noting that even though the wet state of the BC contributed to milder acidic conditions [33], the risk of the commonly reported allomorphic transformation from cellulose I to cellulose II of AH [40] further recommends the EH alternative.

Furthermore, some authors have suggested that the cellulose I allomorph, which is more hydrophobic, would be preferable to cellulose II for stabilizing Pickering emulsions and reinforcing polymers [41,42].

Next, the obtained FTIR spectra of the BC membrane and different BCNCs are shown in Figure 4.6B. Accordingly, the cellulose I allomorph was identified in all samples through the characteristic absorption bands detailed in Chapter 3. In agreement with the XRD results, the increase in crystallinity in BCNC samples could be verified by the sharpening of the broad band between 3400 and 3000 cm^{-1} corresponding to hydrogen-bonded hydroxyl groups [43].

The thermal stability of BC and BCNCs was analyzed using TGA under a nitrogen atmosphere. The obtained thermograms and the corresponding derivative curves (dTG) are displayed in Figure 4.7A and 4.7B.

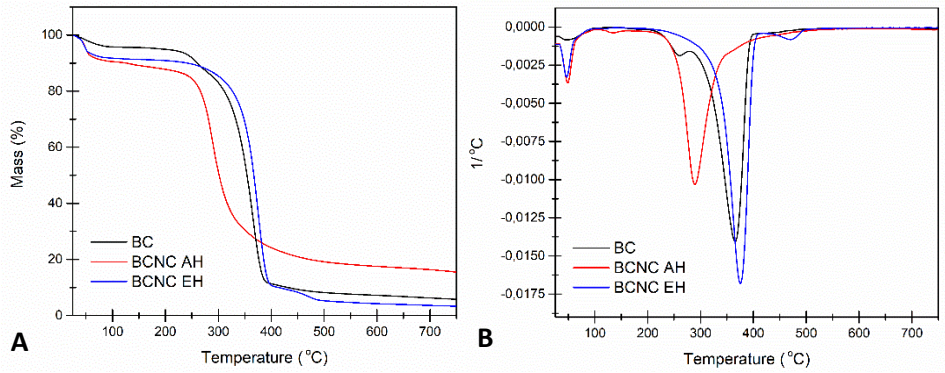

Figure 4.7 *TGA (**A**) and dTG (**B**) curves of BC, BCNC EH and BCNC AH.*

Attending to the results in Figure 4.7A, the curves followed the expected cellulose decomposition profile, in which three major events were distinguished. The first event, near 100 °C, corresponded to the evaporation of surface adsorbed humidity and low-molecular weight compounds. Then,

cellulose depolymerization, dehydration and the decomposition of glycosidic bonds took place in a second event between 250 and 450 °C. In the case of the BC membrane, a small decrease and a peak at 250 °C can be observed in TGA and dTG curves in Figure 4.7A and B, respectively. This drop was associated with possible residual organic debris from the biosynthesis process. As can be noted, BCNCs obtained via the enzymatic route showed higher thermal stability than those arising from the acidic route, and the degradation was moderately later than that of native BC. The esterification of cellulosic hydroxyl groups and subsequent sulfate group formation of the AH might decrease thermal degradation activation energy of cellulose and, thus, accelerate the thermal decomposition of BCNCs [44]. Finally, the ash percentage calculated at 750 °C was lower in the BC and BCNC EH samples, also likely related to sulfate groups that acted as dehydration catalysts [43]. Therefore, it was concluded that the EH favored thermal stability of the BCNCs in contrast to AH, as it has been reported before [14,27].

4.3.2 GPPE characterization

First, in order to characterize GPPE, its functional groups were identified by FTIR in Figure 4.8. Attending to the GPPE spectrum, the broad band between 3500 cm^{-1} and 3200 cm^{-1} was associated to the O-H wagging of phenolic compounds [45,46]. The presence of phenolic acids could be inferred from the shoulder at 1723 cm^{-1}, attributed to their carboxyl groups [47]. The broad peak at 1675 cm^{-1}, 1626 cm^{-1}, and 1601 cm^{-1} have been assigned to aromatic ring deformations, C=C conjugations, and C=O conjugations, respectively, confirming the presence of polyphenols and flavonoids [46,48,49]. The presence of $-CH_2$, $-CH_3$ and aromatic rings was indicated by the band at 1451 cm^{-1} [50,51]. Besides, the peaks between 1308-1212 cm^{-1} have been associated

to proanthocyanidins [52], common condensed tannins of white GP seeds as explained in Chapter 1. To conclude, the peaks at wavenumbers below 919 cm^{-1} were ascribed to C-H bonds in aromatic complexes [53]. In summary, the spectra in Figure 4.8 confirmed the presence of functional groups of polyphenolic compounds associated with grape extracts.

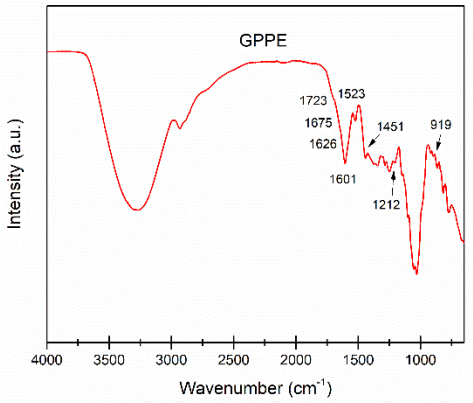

Figure 4.8 *FTIR spectrum of GPPE.*

Further identification of the different polyphenolic compounds in the GPPE was performed using UHPLC coupled to MS. These types of polyphenolic extracts stand out for having a wide variety of complex phenolic molecules [54]. According to the UHPLC-MS results (Supplementary material of Annexes), the obtained extract presented polyphenols belonging mainly to flavanols, flavonols and hydroxycinnamic and hydroxybenzoic acids. The most numerous group corresponded to that of the flavanols, where procyanidin and procyanidin trimer were identified. In addition, signals attributed to catechin, epicatechin and procyanidin gallate could be also detected. Among the flavonols, different glycosides of quercetin, kaempferol and isorhamnetin were mainly identified. Hydroxycinnamic acids such as as *p*-coumaroyl hexose were

also found, likely coming from grape skin. Finally, gallic acid and galloyl derivatives were detected within the group of hydroxybenzoic acids. These results are in agreement with those published in the literature for similar white GPs [55,56].

Subsequently, taking into account the variety of mechanisms of action of polyphenols, DPPH, ABTS, and TPC assay methods were used with the purpose of evaluating the antioxidant capacity of GPPE [56]. The antioxidant activity values exhibited by GPPE were 174.4 ± 15.5 (mg TE/g dry GP), 281.4 ± 86.1 (mg TE/g dry GP) and 195.5 ± 56.2 (mg GA/g dry GP), respectively. These findings are consistent with the profile of the FTIR spectra, and the wide variety of polyphenolic compounds observed in the UHPLC-MS analysis. The antioxidant activity results per dry matter obtained are in the same order of magnitude and even slightly higher than those found in the literature for residues from the wine industry, thus demonstrating the excellent antioxidant properties of white GP from Txakoli production [26,32,33].

As explained, ultrasound and hydroalcoholic solvents were used for the extraction of GPPE, which have separately proven to be effective even at low temperatures [30,57,58]. Indeed, higher temperatures help to improve the extraction yield, but it has been demonstrated that temperatures above 60 ºC can irreversibly degrade the polyphenols [59,60]. Likewise, shock waves of ultrasound can damage the plant cell wall, facilitating the extraction of desired compounds into the extraction solvent. Nevertheless, despite the advantages of using ultrasound-assisted extractions, it has rarely been used for the extraction of polyphenols from grapes, and, in fact, a standardized protocol for this type of extraction does not yet exist [61]. In view of the antioxidant activity results and in accordance with GP literature, the combination of

ultrasound and hydroalcoholic solvents at mild temperatures appears to be a promising strategy that preserves the intrinsic bioactivity of polyphenols [8,31,57,60].

4.3.3 BC and GPPE complex characterization

The effective formation of the BC-GPPE complex was firstly assessed through WCA measurements. In general, contact angles below 40° are typically associated to highly hydrophilic surfaces, whereas contact angles ranging from 70° to 90° indicate the presence of hydrophobic surfaces. Figure 4.9 shows images of different bare or loaded BC membranes as well as their respective WCAs.

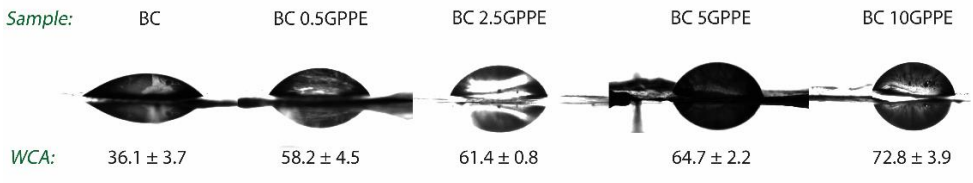

Figure 4.9 *WCA values of the different BC films immersed in solutions with increasing concentrations of GPPE (0-10 mg/mL).*

According to the obtained values, the addition of the polyphenolic extract progressively increased the WCA values up to 72.8° for BC membranes loaded with solutions of 10% GPPE w/w. These results indicated an increase in the hydrophobic character of the BC surface. The observed increase in WCA could be attributed to the interactions between both hydroxyl and acidic groups of polyphenols and the free hydroxyl groups on the cellulosic surface that hindered the interaction with water [62]. This behavior is in agreement with literature, where polyphenolic extracts tend to increase the WCA of their respective polymeric systems [63–65].

In order to corroborate these interactions between GPPE and BC also in colloidal systems, BCNC-GPPE complexes were prepared in dispersion, and their Z potentials were measured at different pHs. Thus, BCNCs obtained both from the EH and AH treatments were combined with the GPPE for the preparation of BCNC-GPPE 2.5:1 (w/w) aqueous dispersions. The Z potential values were measured as indicators of the surface charge and the colloidal stability of dispersions of bare BCNCs and the BCNC-GPPE complex, and thus suitability of the complexes to stabilize Pickering emulsions. Figure 4.10A and B show the Z potential of BCNC EH and BCNC AH dispersions at different pHs, respectively.

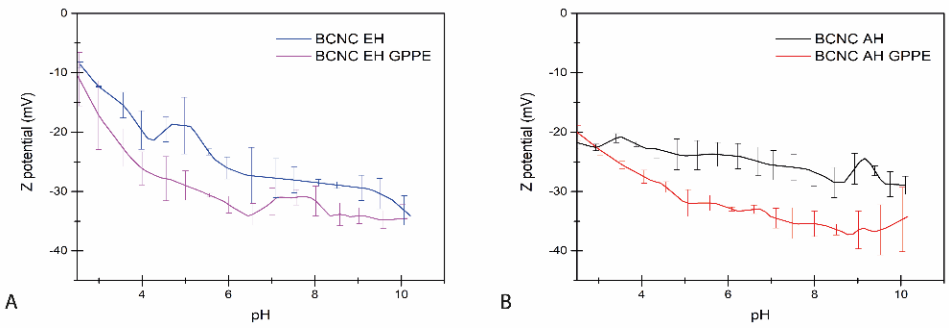

Figure 4.10 *Z potential value evolution of BCNC EH and BCNC EH-GPPE (**A**) and BCNC AH and BCNC AH-GPPE (**B**) dispersions.*

As observed in Figure 4.10, BCNCs showed negative Z potentials in all cases that gradually increased with the pH in agreement with previous reports [16,42]. However, BCNC AH showed slightly more negative Z potential values than BCNC EH at acidic pHs. This decrease in surface charge could be attributed to the sulfate groups formed during the AH [67]. The decreasing Z potential with the pH revealed that above pH 6, BCNCs had sufficient negative

surface charge so that repulsive forces produced stable colloids (<-25 mV) [14,67–69].

However, the Z potential of the BCNC-GPPE complex dispersion was lower in both cases, indicating more negative surface charge and higher colloidal stability in the complexes, even at pH 4. Polyphenolic extracts are rich in both hydroxyl and carboxylic acid groups and, consequently, the incorporation of GPPE contributed to increase the negative charge once deprotonated, thus improving colloidal properties [70].

In accordance with WCA results, it was proven that the combination of GPPE and BCNC adjusted the surface properties of the nanocrystals and increased repulsive forces, which resulted of particular interest for BNCN EH at lower pH [4,71]. In this way, the complexes promoted an easier, more economical and environmentally friendly approach of tuning the hydrophobicity and interfacial tension without the necessity of additional chemical reactions for the surface functionalization of the nanocrystals [72].

Moreover, given the applicability of Pickering emulsions in the food, cosmetic and biomedical sectors, the cytotoxicity of GPPE once incorporated into BC matrix was evaluated. More in detail, cell viability of GPPE was studied by measuring the cytotoxicity of activated media on murine NIH 3T3 fibroblasts as explained in Chapter 2. Sterilized BC membrane punches loaded with GPPE solutions of 25, 50, and 75 mg/mL were immersed in cell culture media at 37 ºC. The cytotoxicity of the different extraction media after 24 hours of incubation is shown in Figure 4.11.

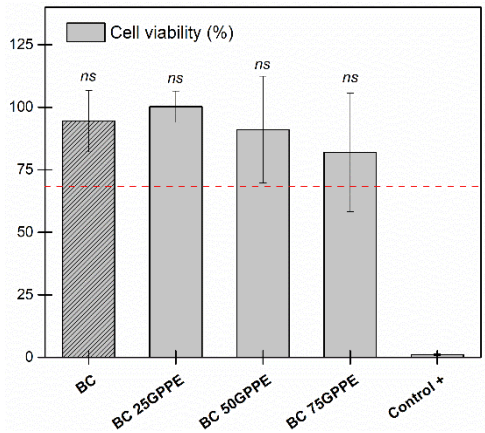

Figure 4.11 *Viability of 3T3 cells exposed to different GPPE concentration media for 24 hours. BC refers to media without GPPE, ns indicates a statistically non-significant difference with the negative control.*

As observed in Figure 4.11, media in contact with unloaded BC did not show any cytotoxic effects, as expected. In addition, in the range of GPPE concentration used, none of the media was harmful to the cell line and did not show a statistically significant difference from the negative control. A dose-dependent decreasing tendency in cell viability was observed, but it did not exceed the 70% biocompatibility threshold. Some cytotoxic effects of bare polyphenolic compounds from GP extracts have been reported previously [73]. Nevertheless, it should be noted that the cytotoxic behavior of a particular polyphenolic compound and that of a polyphenolic mixture can vary significantly.

Consistent with the results in Figure 4.11, the different biocompatibility results of GP extract encapsulated in diverse matrices in literature have been positive [74–79]. In fact, the FDA confers to GP extract the GRAS status as mentioned in Chapter 1. As a result, these findings demonstrated the non-toxic nature of

both BC and GPPE, even at GPPE concentrations much higher than those at which the extract exhibited antioxidant capacity.

To conclude with the characterization of the complexes, the stability of the antioxidant activity of both the GPPE and BCNC-GPPE complex at different concentrations was measured using the DPPH method. For this purpose, samples were subjected to different temperature and visible light conditions for 40 days. Table 4.1 shows the half-life ($t_{1/2}$) of the antioxidant activity loss for each sample, calculated according to Equations 4.2 and 4.3.

In this regard, with respect to the effect of storage conditions, the data showed that light exposure and ambient temperature accelerated the degradation of the polyphenols with the subsequent antioxidant activity decrease. As observed, the formation of BCNC-GPPE complexes notably delayed the degradation and the loss of antioxidant activity of GPPE at higher BCNC:GPPE ratios, demonstrating the usefulness of polyphenol encapsulation [60,80]. The higher the used BCNC:GPPE ratio, the longer the antioxidant capacity lasted over time, with the best obtained ratios of 5:1, enhancing the protective activity even in the more aggressive storage conditions. Interestingly, it is worth mentioning that BCNC AH presented a longer protective effect than BCNC EH, likely due to their slightly better colloidal stability, which might protect the most-exposed polyphenolic hydroxyl groups [81].

These findings demonstrated that GPPE can form stable and active complexes with BCNCs with prolonged antioxidant capacity over time suitable to be used as a potential active stabilizer for the cosmetics, food and pharmaceutical industries.

Table 4.1 *The half-life of DPPH assay was measured for bare GPPE and the BCNC AH-GPPE and BCBN EH-GPPE complexes under various light and temperature conditions.*

BCNC:GPPE	Storage	$t_{1/2}$ (Days)	r^2
0:1	light	43.5	0.96
	dark	64.8	0.97
	dark + 4 °C	97.9	0.97
1:1	AH light	46.8	0.99
	AH dark	45.9	0.98
	AH dark + 4 °C	121.6	0.80
	EH light	43.6	0.99
	EH dark	55.5	0.99
	EH dark + 4 °C	96.3	0.96
2.5:1	AH light	46.2	0.97
	AH dark	68.0	0.92
	AH dark + 4 °C	150.7	0.80
	EH light	42.3	0.95
	EH dark	67.3	0.80
	EH dark + 4 °C	106.6	0.86
5:1	AH light	41.0	0.90
	AH dark	111.8	0.93
	AH dark + 4 °C	256.7	0.90
	EH light	37.3	0.92
	EH dark	68.6	0.78
	EH dark + 4 °C	130.8	0.78

Finally, although some authors had previously reported encapsulation of plant-derived polyphenols by cellulose or its derivatives [24,82,83], in this work, extended polyphenol degradation protection was achieved through an integral agricultural waste valorization strategy. It should be noted that DPPH was chosen as the analytical method for the degradation study, and the antioxidant capacity of some of the previously mentioned polyphenols may not have been fully represented.

4.3.4 Pickering emulsion characterization

The oxidative stability of lipids is a key parameter to validate the stability of an O/W emulsion intended for food or cosmetic industries, since they are responsible for off-flavors as well as of the loss of nutritional attributes [20,84,85]. In order to assess the active protection capacity of the prepared BCNC and the BCNC-GPPE complex in Pickering emulsions, three olive oil-in-water emulsions were prepared using TW20 (control), BCNC and the BCNC-GPPE complex as emulsifiers, respectively. Their oxidative stability was studied by monitoring the evolution of the UV absorbance at 233 nm, associated with the formation of primary lipid oxidation products such as CD, as depicted in Figure 4.12A. Figure 4.12B depicts an illustration of the emulsion stabilization process using the BCNC-GPPE complex.

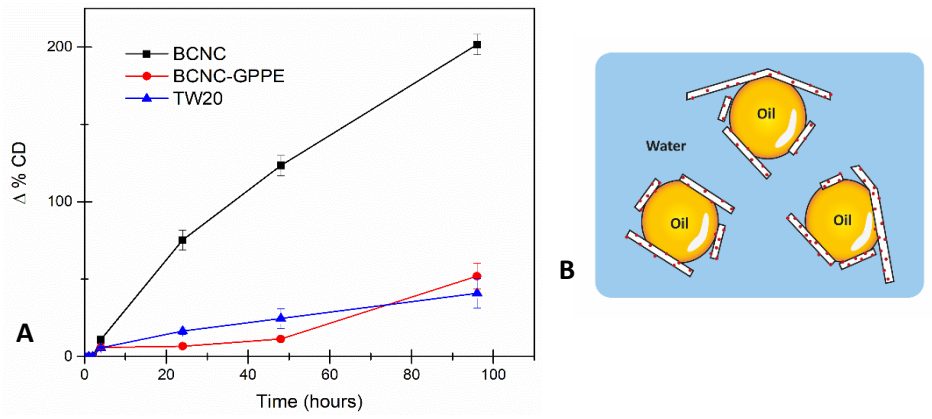

Figure 4.12 *BCNC, BCNC-GPPE complex- and TW20-stabilized olive oil-in-water emulsion's oxidative stability measured through CD increase (**A**). Illustration of the stabilization of an oil-in-water emulsion with the BCNC-GPPE complex (**B**).*

Attending to the results in Figure 4.12 and considering the low percentage of CD formation in the TW20-stabilized control emulsion, in absence of an

additional antioxidant agent, the complete coverage of the oil–water interface by the surfactant could be concluded. In case of Pickering emulsions, effective bridging structures and the tight packing of solid particles at the interface may also prevent direct contact with oxygen or free radicals and, thus, improve oxidative stability. Indeed, recently Li et al. attributed to BC nanofibers this protective capacity in their curcumin-loaded Pickering emulsions [23]. As observed in Figure 4.12, the BCNC-stabilized olive oil Pickering emulsion showed substantially higher CD formation than that of the control. This finding indicated that the bare BCNCs did not achieve the required degree of interface coverage to effectively protect against the oxidation of the olive oil. In contrast, the protective activity of the BCNC-GPPE complex was successfully assessed, demonstrating that it contributed to inhibit the oxidative reactions of the olive oil lipids, even after four days of the Schaal oven test. The BCNC-GPPE Pickering emulsion presented similar protective activity against oxidation to that of the control, without statistically significant differences were observed at the end of the test. Furthermore, in the first 48 h, the active protection of the BCNC-GPPE complex seemed to be higher than that of the control. These results are consistent with those published by Pazos et al., with flavanol oligomers extracted from grapes that showed a potent antioxidant activity for oil-in-water emulsions [86]. Similarly, Yi et al. observed that the addition of anthocyanins improved the physical stability and prevented lipid oxidation of whey protein-stabilized emulsions [26]. Certainly, the unique structure of polyphenols allowed them to scavenge free radicals by donating the phenolic hydroxyl proton [87,88]. In this context, GPPE could play a dual role, both scavenging radicals and contributing to the complete coverage of the oil–water interface of the emulsion [31,32,89,90].

Finally, once the oxidative stability was evaluated, the capacity of the BCNC and BCNC-GPPE complexes to form stable Pickering emulsions was studied by preparing hexadecane-in-water emulsions with different concentrations of neat BCNC EH and BCNC AH. Different GPPE concentrations were also tested independently to evaluate its emulsification capacity, but in those cases, the emulsification could not be achieved, indicating that the GPPE did not present emulsification capacity by itself. The emulsion stability was analyzed by calculating both the ER and the D [4,3] values of BCNC EH- and BCNC AH-stabilized emulsions (Equations 4.4 and 4.5), as displayed in Figure 4.13A and B, respectively.

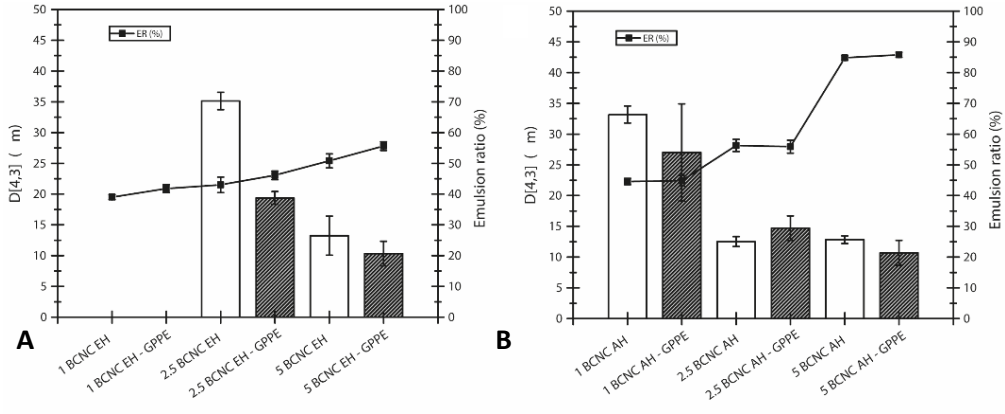

Figure 4.13 *ER and emulsion drop D [4,3] of hexadecane-in-water Pickering emulsions stabilized by neat BCNC AH and BCNC AH-GPPE complex (**A**), and neat BCNC EH and BCNC EH-GPPE complex (**B**).*

In general, an emulsion is considered stable when both particle size and particle size distribution remain constant over an extended period. Physical disturbances such as centrifugation, filtration or agitation could accelerate the coalescence and phase separation of the emulsion. In this case, centrifugation was used to induce emulsion packing and accelerate the creaming

phenomenon [14,33]. The higher the ER value, the better the emulsion stability and the resistance against centrifugation.

According to Figure 4.13, the calculated ER value increased progressively with the concentration of BCNCs, and uniform white emulsions were obtained above 2.5 mg/mL [12,14,91]. The statistical analysis revealed that the differences were significant at each increase in BCNC concentration compared to the previous one. Nevertheless, in the case of 1 mg/mL BCNC, with lower emulsification capacity, hexadecane droplets began to coalesce and rise to the surface after centrifugation, forming a thin hexadecane layer.

Accordingly, optical images of the obtained Pickering emulsions are shown in Figure 4.14. As observed, the emulsified phase of these samples was characterized by a small number of huge droplets in suspension. This behavior usually occurs when the amount of stabilizing particles is not sufficient to emulsify the entire discontinuous phase [33,92].

Likewise, the droplet size values were consistent with those of ER, and each increase in BCNC concentration showed statistically significant differences in the reduction in D [4,3] in all samples (Figures 4.13 and 4.14). In other words, the higher the BCNC concentration, the higher the number of droplets and the smaller the droplet diameter, as can be confirmed in the images displayed in Figure 4.14 [14,92,93]. Thus, it seemed that the decrease in the drop size as well as their spherical shape were favored by BCNCs, being effectively placed at the oil–water interface and preventing the droplets from coalescence.

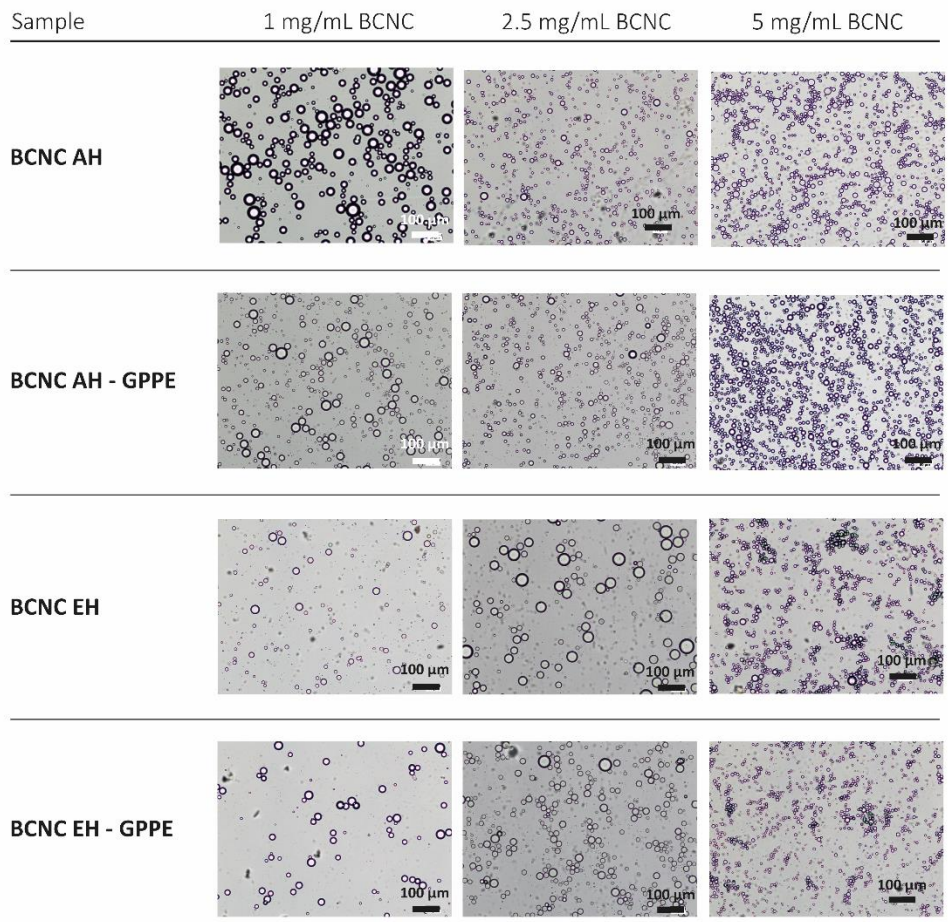

Figure 4.14 *Optical microscope images of hexadecane-in-water Pickering emulsions stabilized by different concentrations of BCNC AH, BCNC AH-GPPE complex, BCNC EH and BCNC EH-GPPE complex dispersions. GPPE concentration remained constant against increasing concentrations of BCNCs.*

Regarding the used hydrolysis procedure, the ER values obtained for BCNC AH were higher than those of BCNC EH. Considering the slightly acidic pH of the prepared emulsions, near 4.5, the better performance of BCNC AH could be related to their better colloidal stability. This difference was reduced at higher concentrations of BCNC, where steric hindrance and electrostatic repulsion are more dominant between BCNC-coated droplets [69]. However, the formation

of the BCNC-GPPE complex had a positive influence on the ER values and droplet size in all BCNC EH emulsions, while this effect was not appreciable in the case of BCNC AH. In fact, this decreasing trend for D [4,3] showed statistically significant differences in the case of the 2.5BCNC EH-GPPE sample (Figure 4.13A).

Certainly, polyphenolic extracts possess excellent amphiphilic properties due to their abundance in hydrophobic aromatic nuclei and hydrophilic groups that might contribute to the physical stability [19,20,89,94]. This feature of polyphenols was exploited by Hu et al. by chemically functionalizing CNCs to improve their colloidal properties [18].

Nevertheless, the results in the present research suggested a synergistic effect arising from the formation of the BCNC EH-GPPE complex, which led to improved emulsion stability without additional chemical treatments of BCNCs. This improvement coincided with the decrease in Z potential and the delay in the appearance of the undesirable CD in the O/W emulsions in the case of the BCNC-GPPE complex. Moreover, physical stability enhancement may also positively influence the oxidative stability, as was demonstrated with BCNC-GPPE [95]. The results demonstrated that Pickering emulsions with prolonged antioxidant properties can be obtained through a green and fully sustainable valorization strategy of an agricultural residue such as GP.

Finally, in order to further confirm the improvement in the physical stability, the rheological behavior of hexadecane-in-water Pickering emulsions stabilized by BCNC and the BCNC-GPPE complex was studied. Flow test results are represented in Figure 4.15. Equally, dynamic oscillatory strain and frequency sweep test results are displayed in Figure 4.16A and 4.16B, respectively.

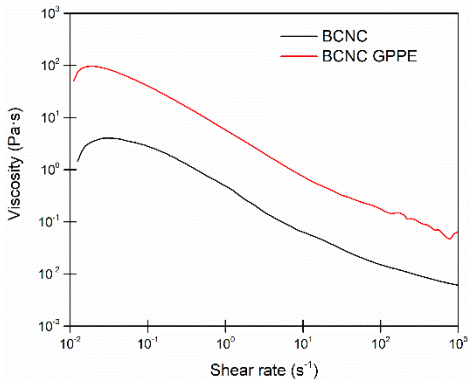

Figure 4.15 *Flow test measurements of hexadecane-in-water BCNC and BCNC-GPPE Pickering emulsions.*

As depicted in Figure 4.15, both the BCNC and BCNC-GPPE emulsions presented a pseudoplastic character and showed the classic shear thinning behavior, in which a decrease in their viscosities with the increasing shear rate was observed [95,96]. The emulsions stabilized by the BCNC-GPPE complex presented higher apparent viscosity in the whole range, thus suggesting that the addition of GPPE contributed to creating a stronger structural network.

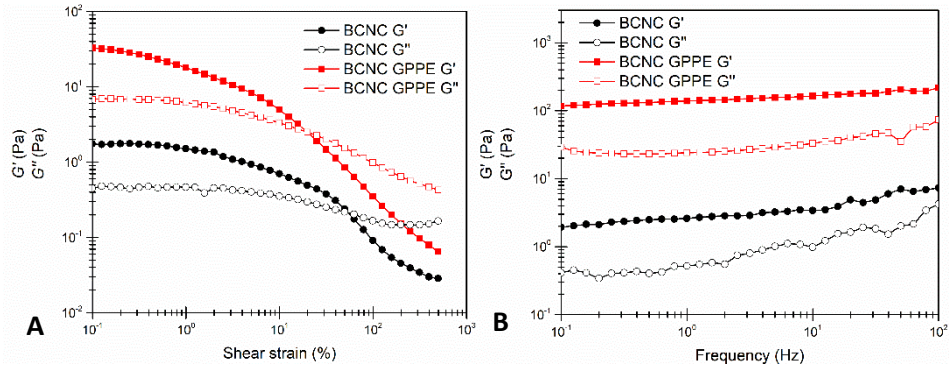

Figure 4.16 *Dynamic oscillatory strain test (**A**) and frequency sweep tests (**B**) of hexadecane-in-water BCNC and BCNC-GPPE Pickering emulsions. Storage modulus (filled symbols) and loss modulus (empty symbols).*

Attending to the results in Figure 4.16, both the BCNC- and BCNC-GPPE complex-stabilized emulsions presented gel-like rheological behavior, with G' above *G*''. However, emulsions stabilized with the BCNC-GPPE complex showed higher moduli values, indicating stronger network structure formation in this case. At the same time, emulsions presented gel-like behavior in the linear viscoelastic region (LVR), where both moduli remained constant in the whole frequency range. Again, the BCNC-GPPE emulsion obtained higher values in the studied range and, moreover, the gap between the two moduli remained even at the highest frequency values, whereas in the case of BCNC-stabilized emulsions, the gel-like network character weakening was noticed since the G'' value approached to the G'. Thus, it could be deduced that GPPE improved the structural strength as well as the physical stability of the emulsion [23].

4.4 Conclusions

The results of this Chapter demonstrated a promising approach towards the comprehensive valorization of GP agro-industrial waste. On the one hand, its nutrients were utilized for the biosynthesis of BC, which, in turn, could be enzymatically treated to obtain high-purity BCNCs. On the other hand, the wide variety of polyphenols in GP were effectively extracted by a combination of ultrasound and a hydroalcoholic solvent. Thus, the typical polyphenolic compounds of white GP were identified, and their bioactive properties were confirmed through different antioxidant capacity assays. The formation of the BCNC-GPPE complex demonstrated protective effect on the polyphenolic compounds, prolonging the half-life of their antioxidant capacity. Additionally, the polyphenols acted as modulators of the surface charge of the BCNCs,

increasing their hydrophobicity and improving their colloidal stability. As a result, the complex showed an increased ability to stabilize Pickering emulsions with antioxidant activity.

Furthermore, the biocompatibility of GPPE and the use of more sustainable methodologies increased the added value of the product and expanded its applicability to the cosmetic, nutraceutical, and pharmaceutical sectors. Similarly, the synergistic effect observed between BCNCs and GPPE could be further studied. In addition to food-grade Pickering emulsion formation, the enhanced lipophilic affinity opens up a range of promising applications for cellulose–polyphenolic extract complexes, such as the recovery of contaminating oils, modulation of lipid digestion or the development of antimicrobial biopolymers.

4.5 References

1 Dickinson, E. (2017) Biopolymer-based particles as stabilizing agents for emulsions and foams. Food Hydrocoll., Elsevier Ltd **68**, 219–231.

2 McClements, D. J. (2004) Food emulsions: Principles, practices, and techniques: Second edition. Food Emuls. Princ. Pract. Tech. Second Ed.

3 Wu, Y., Zhang, X., Qiu, D., Pei, Y., Li, Y., Li, B. and Liu, S. (2021) Effect of surface charge density of bacterial cellulose nanofibrils on the rheology property of O/W Pickering emulsions. Food Hydrocoll., Elsevier Ltd **120**, 106944.

4 Dai, H., Wu, J., Zhang, H., Chen, Y., Ma, L., Huang, H., Huang, Y. and Zhang, Y. (2020) Recent advances on cellulose nanocrystals for Pickering emulsions: Development and challenge. Trends Food Sci. Technol., Elsevier **102**, 16–29.

5 Chevalier, Y. and Bolzinger, M. A. (2013) Emulsions stabilized with solid

nanoparticles: Pickering emulsions. Colloids Surfaces A Physicochem. Eng. Asp., Elsevier B.V. **439**, 23–34.

6 Nonomura, Y. and Kobayashi, N. (2009) Phase inversion of the Pickering emulsions stabilized by plate-shaped clay particles. J. Colloid Interface Sci., Elsevier Inc. **330**, 463–466.

7 Xiao, J., Li, Y. and Huang, Q. (2016) Recent advances on food-grade particles stabilized Pickering emulsions: Fabrication, characterization and research trends. Trends Food Sci. Technol., Elsevier Ltd **55**, 48–60.

8 Nie, C., Bu, X., Ma, S., Zhang, J., Ma, Q., Li, W., Zhang, X., Wu, H., Hu, S., Fan, G., et al. (2022) Pickering emulsions synergistically stabilized by cellulose nanocrystals and peanut protein isolate. Lwt, Elsevier Ltd **167**, 113884.

9 Rovera, C., Fiori, F., Trabattoni, S., Romano, D. and Farris, S. (2020) Enzymatic hydrolysis of bacterial cellulose for the production of nanocrystals for the food packaging industry. Nanomaterials **10**, 1–11.

10 Trache, D., Hussin, M. H., Haafiz, M. K. M. and Thakur, V. K. (2017) Recent progress in cellulose nanocrystals: Sources and production. Nanoscale **9**, 1763–1786.

11 Karim, Z., Afrin, S., Husain, Q. and Danish, R. (2017) Necessity of enzymatic hydrolysis for production and functionalization of nanocelluloses. Crit. Rev. Biotechnol. **37**, 355–370.

12 Bai, L., Greca, L. G., Xiang, W., Lehtonen, J., Huan, S., Nugroho, R. W. N., Tardy, B. L. and Rojas, O. J. (2019) Adsorption and Assembly of Cellulosic and Lignin Colloids at Oil/Water Interfaces. Langmuir **35**, 571–588.

13 Kalashnikova, I., Bizot, H., Bertoncini, P., Cathala, B. and Capron, I. (2013) Cellulosic nanorods of various aspect ratios for oil in water Pickering emulsions. Soft Matter **9**, 952–959.

14 Yan, H., Chen, X., Song, H., Li, J., Feng, Y., Shi, Z., Wang, X. and Lin, Q.

(2017) Synthesis of bacterial cellulose and bacterial cellulose nanocrystals for their applications in the stabilization of olive oil pickering emulsion. Food Hydrocoll., Elsevier Ltd **72**, 127–135.

15 Parajuli, S. and Ureña-Benavides, E. E. (2022) Fundamental aspects of nanocellulose stabilized Pickering emulsions and foams. Adv. Colloid Interface Sci. **299**.

16 Paximada, P., Koutinas, A. A., Scholten, E. and Mandala, I. G. (2016) Effect of bacterial cellulose addition on physical properties of WPI emulsions. Comparison with common thickeners. Food Hydrocoll., Elsevier Ltd **54**, 245–254.

17 Shaghaleh, H., Xu, X. and Wang, S. (2018) Current progress in production of biopolymeric materials based on cellulose, cellulose nanofibers, and cellulose derivatives. RSC Adv. **8**, 825–842.

18 Hu, Z., Berry, R. M., Pelton, R. and Cranston, E. D. (2017) One-Pot Water-Based Hydrophobic Surface Modification of Cellulose Nanocrystals Using Plant Polyphenols. ACS Sustain. Chem. Eng. **5**, 5018–5026.

19 Dai, T., Li, T., Li, R., Zhou, H., Liu, C., Chen, J. and McClements, D. J. (2020) Utilization of plant-based protein-polyphenol complexes to form and stabilize emulsions: Pea proteins and grape seed proanthocyanidins. Food Chem. **329**.

20 Tong, Q., Yi, Z., Ran, Y., Chen, X., Chen, G. and Li, X. (2021) Green Tea Polyphenol-Stabilized Gel-Like High Internal Phase Pickering Emulsions. ACS Sustain. Chem. Eng. **9**, 4076–4090.

21 Fernandes, I. de A. A., Maciel, G. M., Ribeiro, V. R., Rossetto, R., Pedro, A. C. and Haminiuk, C. W. I. (2021) The role of bacterial cellulose loaded with plant phenolics in prevention of UV-induced skin damage. Carbohydr. Polym. Technol. Appl. **2**, 100122.

22 Jakobek, L. (2015) Interactions of polyphenols with carbohydrates,

lipids and proteins. Food Chem., Elsevier Ltd **175**, 556–567.

23 Li, Z., Hu, W., Dong, J., Azi, F., Xu, X., Tu, C., Tang, S. and Dong, M. (2023) Food Science and Human Wellness The use of bacterial cellulose from kombucha to produce curcumin loaded Pickering emulsion with improved stability and antioxidant properties. Food Sci. Hum. Wellness, Elsevier B.V. **12**, 669–679.

24 Vukoja, J., Buljeta, I., Pichler, A., Šimunović, J. and Kopjar, M. (2021) Formulation and stability of cellulose-based delivery systems of raspberry phenolics. Processes **9**, 1–12.

25 Asante, B., Sirviö, J. A., Li, P., Lavola, A., Julkunen-Tiitto, R., Haapala, A. and Liimatainen, H. (2020) Adsorption of bark derived polyphenols onto functionalized nanocellulose: Equilibrium modeling and kinetics. AIChE J. **66**, 1–10.

26 Yi, J., Qiu, M., Liu, N., Tian, L., Zhu, X., Decker, E. A. and McClements, D. J. (2020) Inhibition of Lipid and Protein Oxidation in Whey-Protein-Stabilized Emulsions Using a Natural Antioxidant: Black Rice Anthocyanins. J. Agric. Food Chem. **68**, 10149–10156.

27 George, J., Ramana, K. V., Bawa, A. S. and Siddaramaiah. (2011) Bacterial cellulose nanocrystals exhibiting high thermal stability and their polymer nanocomposites. Int. J. Biol. Macromol., Elsevier B.V. **48**, 50–57.

28 Rovera, C., Ghaani, M., Santo, N., Trabattoni, S., Olsson, R. T., Romano, D. and Farris, S. (2018) Enzymatic Hydrolysis in the Green Production of Bacterial Cellulose Nanocrystals. ACS Sustain. Chem. Eng. **6**, 7725–7734.

29 Abad-García, B., Berrueta, L. A., Garmón-Lobato, S., Gallo, B. and Vicente, F. (2009) A general analytical strategy for the characterization of phenolic compounds in fruit juices by high-performance liquid chromatography with diode array detection coupled to electrospray ionization and triple quadrupole mass spectrometry. J. Chromatogr. A **1216**, 5398–5415.

30 Natolino, A. and Da Porto, C. (2020) Kinetic models for conventional and ultrasound assistant extraction of polyphenols from defatted fresh and distilled grape marc and its main components skins and seeds. Chem. Eng. Res. Des., Institution of Chemical Engineers **156**, 1–12.

31 Costa, M., Freiría-Gándara, J., Losada-Barreiro, S., Paiva-Martins, F. and Bravo-Díaz, C. (2020) Effects of droplet size on the interfacial concentrations of antioxidants in fish and olive oil-in-water emulsions and nanoemulsions and on their oxidative stability. J. Colloid Interface Sci., Elsevier Inc. **562**, 352–362.

32 Lisete-Torres, P., Losada-Barreiro, S., Albuquerque, H., Sánchez-Paz, V., Paiva-Martins, F. and Bravo-Díaz, C. (2012) Distribution of hydroxytyrosol and hydroxytyrosol acetate in olive oil emulsions and their antioxidant efficiency. J. Agric. Food Chem. **60**, 7318–7325.

33 Kalashnikova, I., Bizot, H., Cathala, B. and Capron, I. (2011) New pickering emulsions stabilized by bacterial cellulose nanocrystals. Langmuir **27**, 7471–7479.

34 Jia, Y., Zhai, X., Fu, W., Liu, Y., Li, F. and Zhong, C. (2016) Surfactant-free emulsions stabilized by tempo-oxidized bacterial cellulose. Carbohydr. Polym., Elsevier Ltd. **151**, 907–915.

35 Wu, J. and Ma, G. H. (2016) Recent Studies of Pickering Emulsions: Particles Make the Difference. Small **12**, 4633–4648.

36 Brandes, R., De Souza, L., Carminatti, C. and Recouvreux, D. (2020) Production with a High Yield of Bacterial Cellulose Nanocrystals by Enzymatic Hydrolysis. Int. J. Nanosci. **19**, 1–8.

37 Wen, C., Yuan, Q., Liang, H. and Vriesekoop, F. (2014) Preparation and stabilization of d -limonene Pickering emulsions by cellulose nanocrystals. Carbohydr. Polym., Elsevier Ltd. **112**, 695–700.

38 Revol, J., Bradford, H., Giasson, J., Marchessault, R. H. and Gray, D. G. (1992) Helicoidal self-ordering of cellulose microfibrils in aqueous

suspension 1–3.

39 Urbina, L., Corcuera, M. Á., Eceiza, A. and Retegi, A. (2019) Stiff all-bacterial cellulose nanopaper with enhanced mechanical and barrier properties. Mater. Lett., Elsevier B.V. **246**, 67–70.

40 Martelli-tosi, M., Torricillas, S., Martins, M. A., Benedito, O., Assis, G. De and Tapia-blácido, D. R. (2016) Using Commercial Enzymes to Produce Cellulose Nanofibers from Soybean Straw **2016**.

41 Li, X., Li, J., Gong, J., Kuang, Y., Mo, L. and Song, T. (2018) Cellulose nanocrystals (CNCs) with different crystalline allomorph for oil in water Pickering emulsions. Carbohydr. Polym., Elsevier **183**, 303–310.

42 Zhou, Y., Sun, S., Bei, W., Zahi, M. R., Yuan, Q. and Liang, H. (2018) International Journal of Biological Macromolecules Preparation and antimicrobial activity of oregano essential oil Pickering emulsion stabilized by cellulose nanocrystals. Int. J. Biol. Macromol., Elsevier B.V. **112**, 7–13.

43 Martínez-sanz, M., Lopez-rubio, A. and Lagaron, J. M. (2011) Optimization of the nanofabrication by acid hydrolysis of bacterial cellulose nanowhiskers **85**, 228–236.

44 Roman, M. and Winter, W. T. (2004) Effect of Sulfate Groups from Sulfuric Acid Hydrolysis on the Thermal Degradation Behavior of Bacterial Cellulose 1671–1677.

45 Alara, O. R., Abdurahman, N. H., Ukaegbu, C. I. and Azhari, N. H. (2018) Vernonia cinerea leaves as the source of phenolic compounds, antioxidants, and anti-diabetic activity using microwave-assisted extraction technique. Ind. Crops Prod., Elsevier **122**, 533–544.

46 Park, H. R., Rho, S. J. and Kim, Y. R. (2019) Solubility, stability, and bioaccessibility improvement of curcumin encapsulated using 4-α-glucanotransferase-modified rice starch with reversible pH-induced aggregation property. Food Hydrocoll., Elsevier Ltd **95**, 19–32.

47 Lu, P. and Hsieh, Y. Lo. (2012) Cellulose isolation and core-shell nanostructures of cellulose nanocrystals from chardonnay grape skins. Carbohydr. Polym., Elsevier Ltd. **87**, 2546–2553.

48 Li, J., Shin, G. H., Lee, I. W., Chen, X. and Park, H. J. (2016) Soluble starch formulated nanocomposite increases water solubility and stability of curcumin. Food Hydrocoll., Elsevier Ltd **56**, 41–49.

49 Zhao, X., Zhu, H., Zhang, G. and Tang, W. (2015) Effect of superfine grinding on the physicochemical properties and antioxidant activity of red grape pomace powders. Powder Technol., Elsevier B.V. **286**, 838–844.

50 Li, Y., Yang, Y., Zhu, S., Liu, B., Zhong, F. and Huang, D. (2023) Tea polyphenols-OSA starch interaction and its impact on interface properties and oxidative stability of O/W emulsion. Food Hydrocoll., Elsevier Ltd **135**, 108187.

51 Zhang, L., Yang, X., Li, S. and Gao, W. (2011) Preparation, physicochemical characterization and in vitro digestibility on solid complex of maize starches with quercetin. Lwt, Elsevier Ltd **44**, 787–792.

52 De Souza, V. B., Thomazini, M., Balieiro, J. C. D. C. and Fávaro-Trindade, C. S. (2015) Effect of spray drying on the physicochemical properties and color stability of the powdered pigment obtained from vinification byproducts of the Bordo grape (Vitis labrusca). Food Bioprod. Process., Institution of Chemical Engineers **93**, 39–50.

53 Sardella, F., Gimenez, M., Navas, C., Morandi, C., Deiana, C. and Sapag, K. (2015) Conversion of viticultural industry wastes into activated carbons for removal of lead and cadmium. J. Environ. Chem. Eng., Elsevier B.V. **3**, 253–260.

54 Elejalde, E., Lopez-de-armentia, I., Ram, D., Murillo, R. and Mar, R. (2022) Study of Unpicked Grapes Valorization : A Natural Source of Polyphenolic Compounds and Evaluation of Their Antioxidant Capacity.

55 Aizpurua-olaizola, O., Ormazabal, M., Vallejo, A., Olivares, M., Navarro, P. and Etxebarria, N. (2015) Optimization of Supercritical Fluid Consecutive Extractions of Fatty Acids and Polyphenols from Vitis Vinifera Grape Wastes.

56 González-Centeno, M. R., Jourdes, M., Femenia, A., Simal, S., Rosselló, C. and Teissedre, P. L. (2013) Characterization of polyphenols and antioxidant potential of white grape pomace byproducts (Vitis vinifera L.). J. Agric. Food Chem. **61**, 11579–11587.

57 Panzella, L., Moccia, F., Nasti, R., Marzorati, S., Verotta, L. and Napolitano, A. (2020) Bioactive Phenolic Compounds From Agri-Food Wastes: An Update on Green and Sustainable Extraction Methodologies. Front. Nutr. **7**, 1–27.

58 Rusjan, D. and Koro, Z. (2007) A Comparison of Extraction Methods for Selected Phenolic Compounds from Grape Berry Skins Using Liquid Chromatography and Spectrophotometry 114–118.

59 Ferri, M., Vannini, M., Ehrnell, M., Eliasson, L., Xanthakis, E., Monari, S., Sisti, L., Marchese, P., Celli, A. and Tassoni, A. (2020) From winery waste to bioactive compounds and new polymeric biocomposites: A contribution to the circular economy concept. J. Adv. Res., THE AUTHORS **24**, 1–11.

60 Brezoiu, A. M., Matei, C., Deaconu, M., Stanciuc, A. M., Trifan, A., Gaspar-Pintiliescu, A. and Berger, D. (2019) Polyphenols extract from grape pomace. Characterization and valorisation through encapsulation into mesoporous silica-type matrices. Food Chem. Toxicol., Elsevier **133**, 110787.

61 Maleti, E. (2019) Extraction Methods of Polyphenol From Grapes : Extractions of Grape Polyphenols.

62 Feng, M., Yu, L., Zhu, P., Zhou, X., Liu, H., Yang, Y., Zhou, J., Gao, C., Bao, X. and Chen, P. (2018) Development and preparation of active starch films carrying tea polyphenol. Carbohydr. Polym., Elsevier **196**, 162–

167.

63 Zhu, F. (2021) Polysaccharide based films and coatings for food packaging: Effect of added polyphenols. Food Chem., Elsevier Ltd **359**, 129871.

64 Liu, X., Xu, Y., Liao, W., Guo, C., Gan, M. and Wang, Q. (2023) Preparation and characterization of chitosan/bacterial cellulose composite biodegradable films combined with curcumin and its application on preservation of strawberries. Food Packag. Shelf Life, Elsevier Ltd **35**, 101006.

65 Zhou, X., Liu, X., Wang, Q., Lin, G., Yang, H., Yu, D., Cui, S. W. and Xia, W. (2022) Antimicrobial and antioxidant films formed by bacterial cellulose, chitosan and tea polyphenol – Shelf life extension of grass carp. Food Packag. Shelf Life, Elsevier Ltd **33**, 100866.

66 Xia, G., Ji, X., Xu, Z. and Ji, X. (2022) Transparent cellulose-based bio-hybrid films with enhanced anti-ultraviolet, antioxidant and antibacterial performance. Carbohydr. Polym., Elsevier Ltd **298**, 120118.

67 Vasconcelos, N. F., Feitosa, J. P. A., da Gama, F. M. P., Morais, J. P. S., Andrade, F. K., de Souza Filho, M. de S. M. and Rosa, M. de F. (2017) Bacterial cellulose nanocrystals produced under different hydrolysis conditions: Properties and morphological features. Carbohydr. Polym., Elsevier Ltd. **155**, 425–431.

68 Salas, C., Nypelö, T., Rodriguez-Abreu, C., Carrillo, C. and Rojas, O. J. (2014) Nanocellulose properties and applications in colloids and interfaces. Curr. Opin. Colloid Interface Sci., Elsevier Ltd **19**, 383–396.

69 Meirelles, A. A. D., Costa, A. L. R. and Cunha, R. L. (2020) Cellulose nanocrystals from ultrasound process stabilizing O/W Pickering emulsion. Int. J. Biol. Macromol., Elsevier B.V. **158**, 75–84.

70 Chenglin, Y., Yiqun, Y., Ye, Z., Na, L., Xiaoya, L., Jing, L. and Ming, J. (2012) Self-Assembly and Emulsification of Poly{[styrene- alt -maleic

acid]- co -[styrene- alt -(N -3,4-dihydroxyphenylethyl-maleamic acid)]}. Langmuir **28**, 9211–9222.

71 Phan, A. D. T., Netzel, G., Wang, D., Flanagan, B. M., D'Arcy, B. R. and Gidley, M. J. (2015) Binding of dietary polyphenols to cellulose: Structural and nutritional aspects. Food Chem., Elsevier Ltd **171**, 388–396.

72 Hu, Z., Patten, T., Pelton, R. and Cranston, E. D. (2015) Synergistic Stabilization of Emulsions and Emulsion Gels with Water-Soluble Polymers and Cellulose Nanocrystals. ACS Sustain. Chem. Eng. **3**, 1023–1031.

73 Memar, M. Y., Adibkia, K., Farajnia, S., Kafil, H. S., Yekani, M., Alizadeh, N. and Ghotaslou, R. (2019) The grape seed extract: A natural antimicrobial agent against different pathogens. Rev. Res. Med. Microbiol. **30**, 173–182.

74 Costa, J. R., Xavier, M., Amado, I. R., Gonçalves, C., Castro, P. M., Tonon, R. V., Cabral, L. M. C., Pastrana, L. and Pintado, M. E. (2021) Polymeric nanoparticles as oral delivery systems for a grape pomace extract towards the improvement of biological activities. Mater. Sci. Eng. C, Elsevier **119**, 111551.

75 Manconi, M., Marongiu, F., Castangia, I., Manca, M. L., Caddeo, C., Tuberoso, C. I. G., D'hallewin, G., Bacchetta, G. and Fadda, A. M. (2016) Polymer-associated liposomes for the oral delivery of grape pomace extract. Colloids Surfaces B Biointerfaces, Elsevier B.V. **146**, 910–917.

76 Perra, M., Lozano-Sánchez, J., Leyva-Jiménez, F. J., Segura-Carretero, A., Pedraz, J. L., Bacchetta, G., Muntoni, A., De Gioannis, G., Manca, M. L. and Manconi, M. (2021) Extraction of the antioxidant phytocomplex from wine-making by-products and sustainable loading in phospholipid vesicles specifically tailored for skin protection. Biomed. Pharmacother. **142**.

77 Ugartondo, V., Mitjans, M., Lozano, C., Torres, J. L. and Vinardell, M. P.

(2006) Comparative study of the cytotoxicity induced by antioxidant epicatechin conjugates obtained from grape. J. Agric. Food Chem. **54**, 6945–6950.

78 Peixoto, C. M., Dias, M. I., Alves, M. J., Calhelha, R. C., Barros, L., Pinho, S. P. and Ferreira, I. C. F. R. (2018) Grape pomace as a source of phenolic compounds and diverse bioactive properties. Food Chem., Elsevier **253**, 132–138.

79 Milinčić, D. D., Stanisavljević, N. S., Kostić, A., Soković Bajić, S., Kojić, M. O., Gašić, U. M., Barać, M. B., Stanojević, S. P., Lj Tešić, Ž. and Pešić, M. B. (2021) Phenolic compounds and biopotential of grape pomace extracts from Prokupac red grape variety. Lwt **138**.

80 Aizpurua-Olaizola, O., Navarro, P., Vallejo, A., Olivares, M., Etxebarria, N. and Usobiaga, A. (2016) Microencapsulation and storage stability of polyphenols from Vitis vinifera grape wastes. Food Chem., Elsevier Ltd **190**, 614–621.

81 Sun, B., Zhang, M. and Ni, Y. (2018) Use of sulfated cellulose nanocrystals towards stability enhancement of gelatin-encapsulated tea polyphenols. Cellulose, Springer Netherlands **25**, 5157–5173.

82 Yuan, Y., Zhang, S., Ma, M., Wang, D. and Xu, Y. (2022) Encapsulation and delivery of curcumin in cellulose nanocrystals nanoparticles using pH-driven method. Lwt, Elsevier Ltd **155**, 112863.

83 Zheng, L., Ding, Z., Zhang, M. and Sun, J. (2011) Microencapsulation of bayberry polyphenols by ethyl cellulose: Preparation and characterization. J. Food Eng., Elsevier Ltd **104**, 89–95.

84 Wang, J., Wang, A., Zang, X., Tan, L., Ge, Y., Lin, X., Xu, B., Jin, Z. and Ma, W. (2018) Food Hydrocolloids Physical and oxidative stability of functional avocado oil high internal phase emulsions collaborative formulated using citrus nano fi bers and tannic acid **82**, 248–257.

85 Mao, X., Gu, C., Chen, D., Yu, B. and He, J. (2017) Oxidative stress-

induced diseases and tea polyphenols **8**, 81649–81661.

86 Gallardo, M., Lluı, J., Medina, I. and Pazos, M. (2005) Food Chemistry Activity of grape polyphenols as inhibitors of the oxidation of fish lipids and frozen fish muscle **92**, 547–557.

87 Noon, J., Mills, T. B. and Norton, I. T. (2020) The use of natural antioxidants to combat lipid oxidation in O / W emulsions. J. Food Eng., Elsevier Ltd **281**, 110006.

88 Ean, M. A. R. M. A. C. L., Ardner, P. E. G., Uthie, G. A. G. D., Okota, T. A. Y. and Rozier, A. L. A. N. C. (2002) Ellagitannins , Flavonoids , and Other Phenolics in Red Raspberries and Their Contribution to Antioxidant Capacity and Vasorelaxation Properties 0–5.

89 Di Mattia, C. D., Sacchetti, G., Mastrocola, D. and Pittia, P. (2009) Effect of phenolic antioxidants on the dispersion state and chemical stability of olive oil O/W emulsions. Food Res. Int., Elsevier Ltd **42**, 1163–1170.

90 Abdelazim, A. A. and Mahmoud, A. (2013) Oxidative stability of vegetable oils as affected by sesame extracts during accelerated oxidative storage **50**, 868–878.

91 Zhang, H., Chen, Y., Wang, S., Ma, L., Yu, Y., Dai, H. and Zhang, Y. (2020) Extraction and comparison of cellulose nanocrystals from lemon (Citrus limon) seeds using sulfuric acid hydrolysis and oxidation methods. Carbohydr. Polym., Elsevier **238**, 116180.

92 Wang, W., Du, G., Li, C., Zhang, H., Long, Y. and Ni, Y. (2016) Preparation of cellulose nanocrystals from asparagus (Asparagus officinalis L.) and their applications to palm oil/water Pickering emulsion. Carbohydr. Polym., Elsevier Ltd. **151**, 1–8.

93 Tzoumaki, M. V, Moschakis, T., Kiosseoglou, V. and Biliaderis, C. G. (2011) Food Hydrocolloids Oil-in-water emulsions stabilized by chitin nanocrystal particles. Food Hydrocoll., Elsevier Ltd **25**, 1521–1529.

94 Gao, X., Xu, Z., Liu, G. and Wu, J. (2021) Acta Biomaterialia Polyphenols

as a versatile component in tissue engineering, Elsevier Ltd **119**, 57–74.

95 Zhang, X., Wu, Y., Li, Y., Li, B., Pei, Y. and Liu, S. (2022) Food Hydrocolloids Effects of the interaction between bacterial cellulose and soy protein isolate on the oil-water interface on the digestion of the Pickering emulsions. Food Hydrocoll., Elsevier Ltd **126**, 107480.

96 Sun, C., Gunasekaran, S. and Richards, M. P. (2007) ARTICLE IN PRESS Effect of xanthan gum on physicochemical properties of whey protein isolate stabilized oil-in-water emulsions **21**, 555–564.

CHAPTER 5

PERSONALIZED PHARMACOLOGY THROUGH 3D PRINTING



5.1 Introduction 155
5.2 Experimental section 159
5.2.1 Preparation of the starch-based inks 159
5.2.2 BCNF production 160
5.2.3 3D printing procedure 160
5.2.4 In vitro drug release studies 161
5.3 Results and discussion 162
5.3.1 BCNFs for Ibuprofen loaded NM starch tablets 162
5.3.2 WM starch tablets for GPPE release 179
5.4 Conclusions 187
5.5 References 189

Chapter 5: Personalized pharmacology through 3D printing

5.1 Introduction

In a market where the pharmaceutical industry provides medication in a standardized manner, personalized medicine has emerged as a highly valuable clinical strategy in recent years [1]. In fact, the absorption of drugs is influenced by a multitude of factors, including patient physical characteristics like height/weight as well as biological factors such as individual genetics among others [2, 3]. Given this variability, patients may respond differently to treatments for the same disease, with some of them experiencing positive outcomes while others not [4]. In this regard, considering current diagnostic tools, the ideal approach would involve the design of individualized tablets with dosages and release profiles of specific drugs for each patient [5]. Thus, it is essential to investigate in technologies and materials capable of controlling drug dosage as well as release rates, or hydrophobicity, thereby facilitating customization of treatment regimens for individual patients [6, 7].

In recent years, 3D printing technology has gained significant attention for its numerous benefits and applications in the field of biomedicine and more specifically, pharmacology [8, 9]. This technique enables the creation of drug-stabilized materials using biopolymers, allowing for precise control over drug solubility and bioavailability within the body [10]. This is particularly advantageous for drugs with hydrophobic character, as traditional pharmacology has struggled to adequately regulate their release [11]. The versatility of this technology is noteworthy, as it can produce various types of

structures, ranging from solid drugs to transdermal patches, among others [12, 13]. As a result, 3D printing is considered an appropriate technology for producing personalized medicines that could substitute classic on-demand pharmacology.

The process of 3D printing involves a computer-aided design (CAD) approach, in which the material is deposited in layers one after the other to construct a 3D object [14]. This study employed semi-solid extrusion (SSE), which is also known as direct ink writing (DIW), as 3D printing technology. DIW is a extrusion technique that involves the deposition of semi-solid materials using a syringe-like extrusion system [15]. DIW enables the production of intricate geometries with fine structures and shapes at low printing temperatures without requiring specialized equipment [16, 17]. However, careful characterization of the rheological properties of DIW inks is necessary, as they require appropriate shear-thinning behavior to facilitate extrusion through the nozzle, and sufficient yield stress and recovery capacity to prevent collapse of the printed objects [18, 19].

The most used inks in syringe extrusion 3D printing technology are polymers of natural origin, especially in the biomedicine and the pharmaceutical industries. Natural polymers, such as chitosan, hyaluronic acid, cellulose, starch, collagen, and sodium alginate, are commonly used in 3D printing biomedical applications [20–23]. Starch stands out among all biopolymers due to its low cost, digestibility, non-toxicity, and versatility, making it a popular excipient in various drug delivery formulations [24]. Starch is composed of linear and crystalline amylose and highly branched amylopectin (Figure 5.1), and its functional properties are highly influenced by the percentage of these ramifications, which varies according to the botanical origin [25, 26]. Notably,

the amylopectin branching contributes to the gel-like behavior of hydrated mixtures due to the formation of inter- and intramolecular hydrogen bonds [27, 28]. For this reason, the percentage of amylopectin and the possible presence of other chemical compounds determine factors such as the granule morphology, gelatinization temperature, crystallinity and molecular weight [26, 29–31]. Consequently, 3D-printed pills have shown different drug release profiles depending on the source of the starch [12, 30, 32].

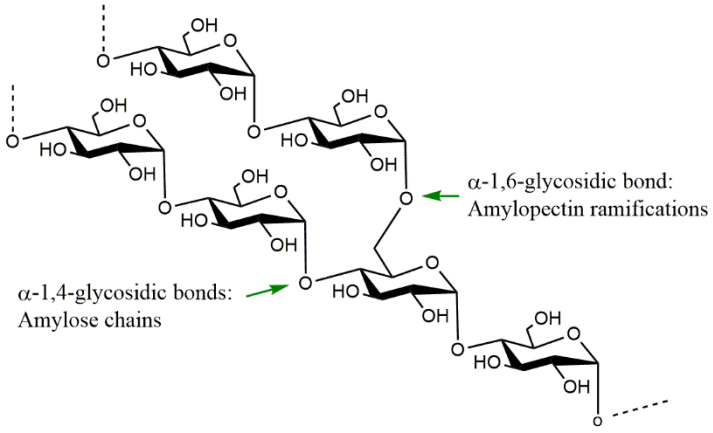

Figure 5.1 *Representation of the molecular structure of starch.*

Besides the main polymer, reinforcing materials are frequently employed to facilitate the shape fidelity of the 3D printed material, and they of course can impact both the rheological behavior and the release kinetics [23, 33]. Among these, cellulose derivatives are highly promising as reinforcing agents in extrusion 3D printing [18, 21, 34]. Particularly, cellulose nanofibers (CNF) possess abundant hydroxyl groups on their surface, which enable them to interact with various materials and be easily incorporated into natural polymeric matrices [33, 35]. As a result, BCNF can serve as rheological modifiers as well as reinforcement agents to enhance the printability of several

natural polymers suitable for biomaterial inks in extrusion-based 3D printing [13, 36].

Furthermore, as BCNFs, polyphenolic plant extracts like GPPE have great potential in 3D printing technology and application. Indeed, due to the strong hydrogen bonds formed between phenolic compounds and polysaccharides, as stated in Chapter 4, polyphenols can greatly contribute to the printability and improve the precision of polysaccharide-based printing products [18, 37, 38]. Additionally, polyphenols could confer antimicrobial, antioxidant or antihypertensive properties, among others, to the final products as it has also been explained previously in Chapter 4 [39–42].

In this chapter, the main aim was to introduce BC and GPPE in 3D printing technology to produce starch-based tablets loaded with hydrophobic and hydrophilic drugs. To that end, this study offered a new approach for personalized medicine development by reutilizing GP agricultural waste. Figure 5.2 shows a schematic representation of the experimental process and objectives of this chapter. On one hand, BCNFs were used as reinforcing agent of the inks, leading to the modulation of their rheological properties and the Ibuprofen release profile. On the other hand, GPPE was employed both as rheological modulator and antioxidant supplement, and its subsequent release kinetics were monitored.

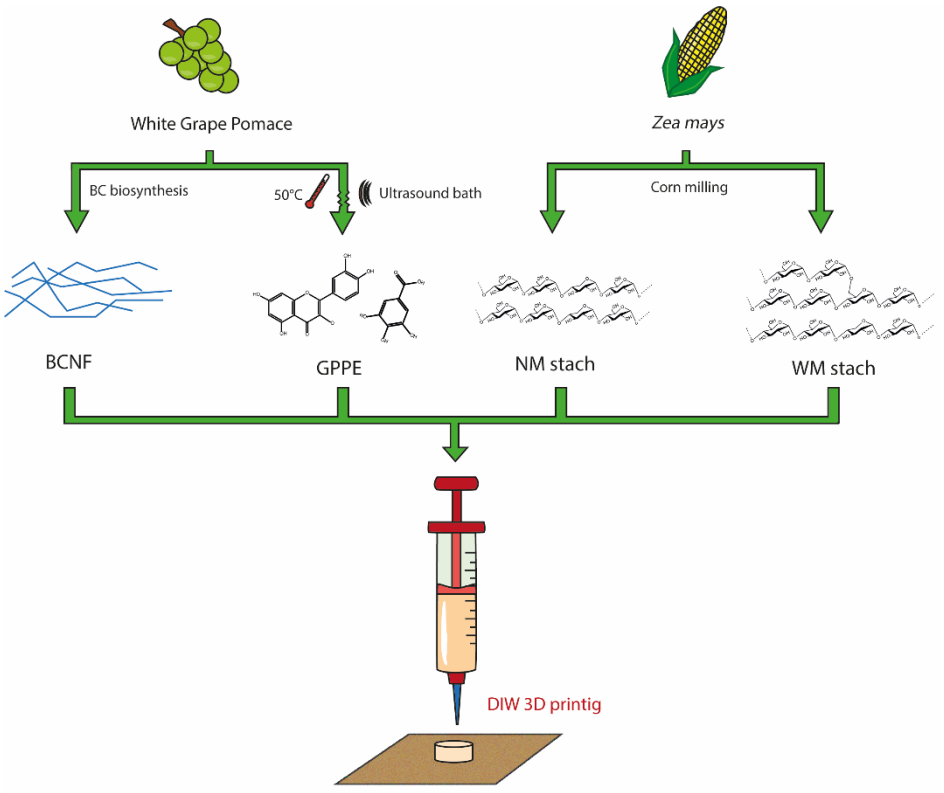

Figure 5.2 *Schematic representation to produce starch inks for 3D printing.*

5.2 Experimental section

5.2.1 Preparation of the starch-based inks

In this work, normal starch (NM) and waxy starch (WM) were chosen based on their previous satisfactory use in achieving controlled release of drugs by this group [12]. The primary difference between NM starch and WM starch lies in their amylose-to-amylopectin ratios. NM starch contains a balanced ratio of both components, while WM starch is predominantly composed of amylopectin, which imparts specific functional properties. Starch inks were prepared by gelatinization of the starch slurries. For that purpose, each starch

was dispersed in deionized distilled water at a concentration of 30 % (w/w) and then heated above its gelatinization temperature while continuously stirring with a magnetic stirrer for 20 minutes. NM and WM starches were gelatinized at 90°C. The NM starch gels were blended with 0.25%, 0.5%, and 1% BCNF (w/w) to yield NM-0.25NF, NM-0.5NF, and NM-1NF samples, respectively. For drug-loaded samples, 5 mg of Ibuprofen was incorporated per gram of gelatinized NM, resulting in IbNM-0.25NF, IbNM-0.5NF, and IbNM-1NF inks. Likewise, WM inks mixed with 1, 2.5, and 5 % (w/w) GPPE were named WM-1PE, WM-2.5PE, and WM-5PE, respectively.

5.2.2 BCNF production

BCNFs were prepared from biosynthesized and washed BC membranes obtained from GP medium as detailed in Chapter 3. In order to disintegrate the nanofibers, firstly the membranes were cut into smaller fragments. Then, a homogenizer was used to further reduce the sample size through homogenization cycles lasting 5 minutes each, at 15000 rpm, for a total of 15 minutes. Finally, the homogeneous paste was ultrasonicated to separate the nanofibers with objective of facilitate their incorporation into the starch ink.

5.2.3 3D printing procedure

The prepared inks were printed using a Voladora 3D printer from Tumaker, S.L. Spain, which was modified for DIW layer-by-layer printing. All samples were printed using a 0.8 mm needle, at a printing speed of 6 mm/s and with 100% infill. Cylinders measuring 10 mm in diameter and 5 mm in height (surface area of 314.2 mm^2, volume of 392.7 mm^3, and aspect ratio of 0.80) were printed. Finally, the printed samples were freeze-dried to stabilize and fix the final forms, as well as to obtain porous final structures to facilitate water absorption

of the final product, which, due to its swelling capacity, could trigger the disintegration of the inks and facilitate the drug release [11].

5.2.4 In vitro drug release studies

Ibuprofen and GPPE were selected as the hydrophobic and hydrophilic drugs, respectively, for in vitro release studies in a simulated intestinal medium (PBS). The ibuprofen-loaded tablets were freeze-dried and then stirred in 50 mL of pH 7.4 PBS solution at 37°C for the release studies. At specific intervals, an aliquot of 1 mL of the solution was taken out and analyzed using UV-vis spectroscopy. The sample was then returned to the beaker. To determine the amount of released ibuprofen, the absorbance signal at 221.5 nm was compared with the standard calibration curve prepared properly.

The ibuprofen cumulative release (ICR) at different time points was calculated in triplicate and using Equation 5.1:

$$ICR\ (\%) = \frac{W_{IB}}{W_t} \cdot 100 \qquad \text{(Equation 5.1)}$$

W_{IB} represents the quantity of ibuprofen that was released at different time points, while W_t indicates the overall quantity of drug that was initially loaded into the printed tablet.

Similarly, the release of GPPE was conducted in 3 mL of release media under the same physiological conditions described above. The amount of GPPE released was also determined by using UV spectrophotometer with the appropriate calibration curve and measuring the absorbance signal at 277 nm. At different stipulated time points, an aliquot of 1 mL was taken to measure its absorbance and then returned to the release medium. To avoid light-induced

oxidation of the extract, the test was performed under semi-dark conditions. The cumulative amount of GPPE released (ECR) at different time points was calculated in triplicate and using the following equation:

$$ECR\ (\%) = \frac{W_E}{W_t} \cdot 100 \qquad \text{(Equation 5.2)}$$

W_E represents the quantity of extract that was released at various time points, while W_t indicates the overall quantity of GPPE that was initially loaded onto the printed tablet.

5.3 Results and discussion

5.3.1 BCNFs for ibuprofen loaded NM starch tablets

5.3.1.1 BCNF and NM ink setup

NM starch has previously been employed by this research group for 3D printing of tablets with specific shapes loading ibuprofen for its subsequent release study [12]. Nonetheless, these NM tablets exhibited rapid disintegration within physiological media, thus impeding release in a controlled manner. In this context, the assessment of BCNF potential to modulate the rheological properties of NM inks and, consequently, the ibuprofen release profile in physiological media was conducted.

First of all, the NM starch granules were analyzed using an optical microscope to confirm the botanical origin of the starch, as each type exhibits a distinct shape [43]. Figure 5.3 shows optical micrographs of NM starch granules.

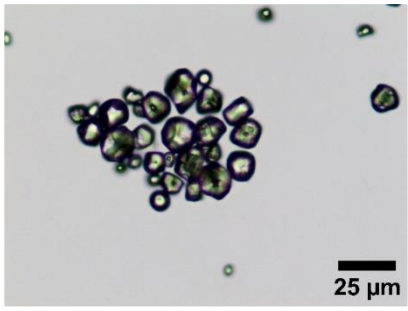

Figure 5.3 *Optical micrograph of the morphology of NM granules.*

As evidenced in Figure 5.1, polygonal granules were observed with maximum lengths of 9.7 ± 2.8 µm. The granules of NM appeared translucent or semitransparent when observed through the optical microscope. Additionally, small concentric rings could be observed in the granule center, which result from the arrangement of the two macromolecules within the internal crystalline structure of the granule. The morphology and size of the NM granules coincided with the previous work reported by this group [12].

Similarly, AFM was used to confirm the mechanical disintegration process of BC and morphologically characterize the BCNFs dispersions. AFM images of BCNF dispersions from GP culture media are represented in Figure 5.4. As shown in AFM images, the nanofibers exhibited lengths of several microns and a mean diameter of 69 ± 18 nm. Additionally, the BNCFs appeared to be well-dispersed due to the previous spin coating process and ultrasonication treatment. When examining Figure 5.4B, nanofibrils exhibited more disruptions, higher diameter variability and were more loosely packed compared to those observed in Chapter 3. This fact was attributed to the mechanical disintegration and ultrasonication processes employed. Nevertheless, BCNF diameter was in agreement with the reported literature

[44], thus the process of obtaining BCNFs and their size and diameter could be considered suitable for their utilization in 3D printing.

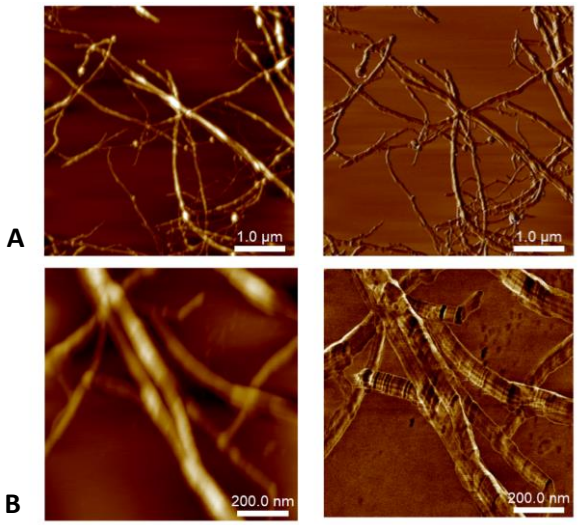

Figure 5.4 *Height and phase AFM images of BCNF dispersions from GP media with 1 µm (**A**) and 200 nm (**B**) scale bars.*

Thereafter, in order to assess the printability and shape fidelity of the prepared inks, rheological characterization was carried out. Indeed, rheological characterization is crucial for predicting how the inks will behave during the 3D printing process. With this aim, flow tests and oscillatory measurements were carried out as detailed in Chapter 2. The data gathered from the flow tests measurements of all NM starch-based inks are depicted in Figure 5.5A and presented in Table 5.1.

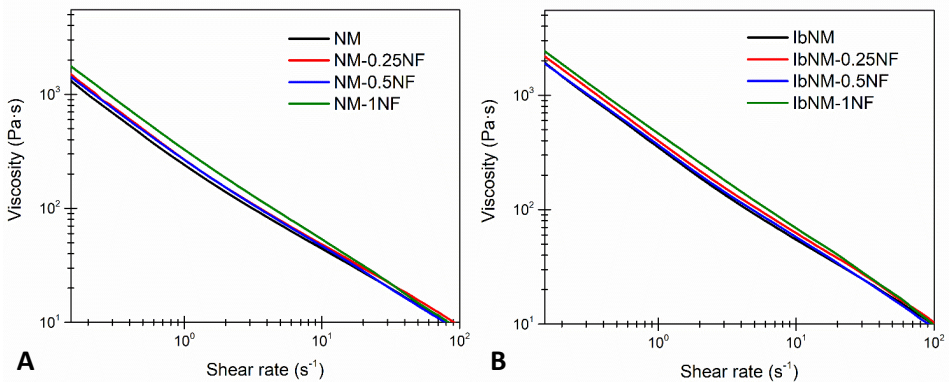

Figure 5.5 *Flow test of NM inks (**A**) and IbNM inks (**B**) reinforced with different concentrations of BCNFs.*

According to the results, all samples exhibited the characteristic shear thinning behavior of non-Newtonian fluids, decreasing their viscosity with the increasing shear rate. This behavior was further analyzed by fitting viscosity data obtained from the flow test to the Power-law model described in Equation 2.5 of Chapter 2 [45]. Consequently, Power-law index (n), consistency coefficient (K), and Pearson correlation coefficient (R^2) could be determined for all NM starch formulations as it is depicted in Table 5.1.

As observed, all NM starch-based inks exhibited a n value less than 1 and an R^2 value close to 1, confirming the non-Newtonian nature of the fluid [46]. Starches with the highest concentration of BCNF exhibited the more pronounced shear thinning behavior compared to bare NM, as evidenced by the decrease in n value. Additionally, the viscosity of the ink increased progressively with the BCNF concentration, particularly notable in the case of NM-1NF, as evidenced by the *K* value.

Table 5.1 *Rheological parameters of unloaded NM reinforced inks: Power-law index (n), consistency coefficient (K), yield stress, flow stress and recovery (%).*

Sample	Flow test			Stress sweep		Recovery test
	n	K	R^2	Yield stress (Pa)	Flow stress (Pa)	Recovery (%)
NM	0.218 ± 0.002	280.44 ± 35.17	0.99	159.0 ± 32.8	219.7 ± 31.0	62.5 ± 8.0
NM-0.25NF	0.208 ± 0.008	317.86 ± 35.75	0.99	218.5 ± 30.5	317.5 ± 59.5	74.3 ± 6.8
NM-0.5NF	0.204 ± 0.001	302.83 ± 4.24	0.99	279.5 ± 106.5	396.5 ± 158.5	68.6 ± 1.3
NM-1NF	0.180 ± 0.005	361.56 ± 23.36	0.99	420.0 ± 81.0	609.0 ± 72.0	65.3 ± 5.0

This relationship between viscosity and the concentration of reinforcing nanofibers has previously been reported with other polymers such as alginate, polyurethane, and silk fibroin/gelatin polymers [13, 47, 48]. The almost identical structure of cellulose and starch would led to numerous strong hydrogen bonding interactions that increased notably the apparent viscosity of the ink, as it has reported elsewhere [49, 50]. This effect was more noticeable at lower shear rates, probably due to the disruption of many of the hydrogen bonds when the material was submitted to the highest shear forces. Therefore, it was deduced that in our case the BCNFs formed strong physical entanglements with the amylose and amylopectin chains, creating a cohesive and structured gel.

Likewise, the rheological behavior of the ibuprofen loaded NM inks was also evaluated, as represented in Figure 5.5B and Table 5.2.

Table 5.2 *Rheological parameters of IbNM reinforced inks: Power-law index (n), consistency coefficient (K), yield stress, flow stress and recovery (%).*

Sample	Flow test			Stress sweep		Recovery test
	n	K	R^2	Yield stress (Pa)	Flow stress (Pa)	Recovery (%)
IbNM	0.192 ± 0.034	471.63 ± 18.16	0.99	360.0 ± 42.0	489.5 ± 22.5	70.0 ± 1.1
IbNM-0.25NF	0.183 ± 0.004	431.06 ± 48.16	0.99	326.1 ± 8.0	426.4 ± 30.6	51.5 ± 5.8
IbNM-0.5NF	0.187 ± 0.014	450.42 ± 39.90	0.99	303.5 ± 51.5	431.6 ± 99.5	51.7 ± 3.5
IbNM-1NF	0.157 ± 0.028	466.30 ± 63.84	0.99	318.0 ± 34.3	503.7 ± 45.7	52.1 ± 2.6

Concerning flow test results, a similar n value was calculated in all cases comparing with their homologous unloaded inks, indicating that the desired shear thinning behavior of the NM samples was not affected by the addition of ibuprofen. In relation to the addition of BCNF, in this case, significant difference was not observed in the values of K and n of the samples.

However, from the observation of the K values in Table 5.2, it can be inferred that the viscosity of ibuprofen loaded inks tended to grow regardless of the BCNF content comparing to that of NM samples. This finding contradicts other previous studies that had reported a plasticizing effect of ibuprofen, resulting in a decrease in ink viscosity [12, 51]. Therefore, we hypothesized that in this instance, the viscosity increase at this specific ibuprofen/starch ratio could be related to hydrophobic interactions between the nonpolar regions of polymer

and drug, in addition to Van der Waals forces. Indeed, various small molecules like ibuprofen can be accommodated and form inclusion complexes with amylose and the longest linear side chains of amylopectin [52]. Indeed, amylose, due to its tendency to minimize its interaction with water, can form inclusion complexes with guest molecules thus influencing starch structure and properties [53–55]. During gelatinization, as the starch granules swell in the presence of heat and water, there is a disruption of the crystalline structure and a reorganization of the amylose molecules. During this process, amylose molecules could adopt a helical conformation as they disperse in the aqueous medium favoring the formation of inclusion complexes with ibuprofen.

In summary, attending to Table 5.1 and 5.2 results, all NM and IbNM inks showed the required shear thinning behavior and viscosity or K values suitable for 3D printing applications [12, 23].

Figures 5.6A and 5.6B display the results of the stress sweep test conducted on both the NM and IbNM inks, respectively. As observed, the findings indicated that G' remained nearly constant and higher than G'' in all cases, indicating solid gel-like behavior of the inks. Overall, the G' values were found to be consistent with the viscosity of the gelatinized starches, with higher values observed in those inks with greater structural complexity, directly associated with increasing BCNF content specially in the case of NM inks. The yield stress (τ_y) was established as the shear stress value at which G' lost the linearity, while the flow stress (τ_f) was calculated from the intersection of G' and G'' (when G'=G'') following previously reported literature (Table 5.1 and 5.2) [56]. Some authors have described τ_f as the minimum force needed for the extrusion of the material through the nozzle [45].

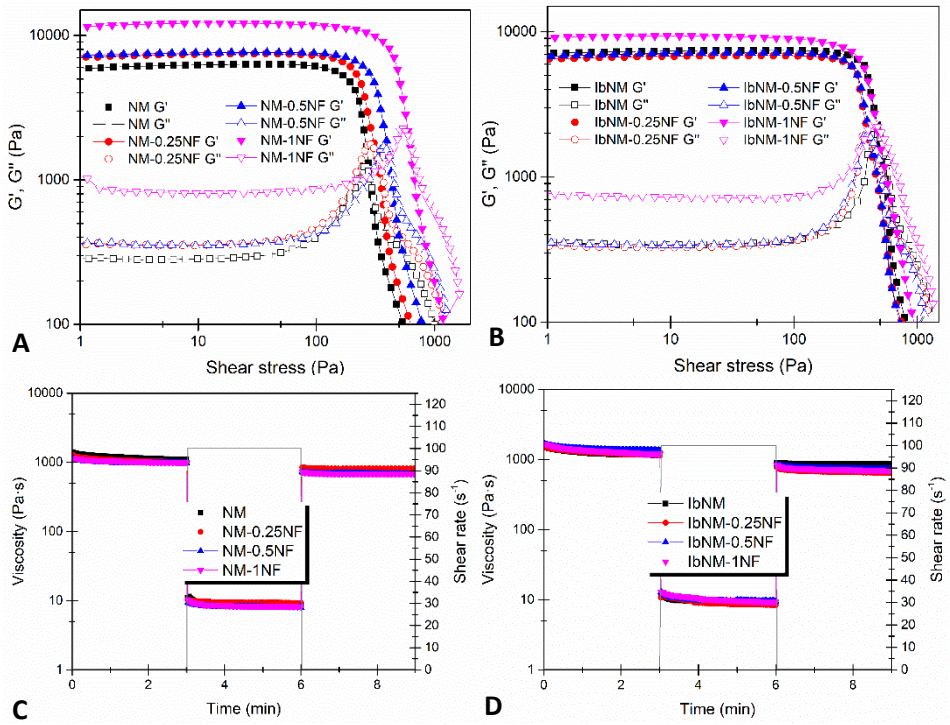

Figure 5.6 *Stress sweep test of NM (**A**) and IbNM (**B**) inks reinforced with different concentrations of BCNFs and recovery test of the same NM (**C**) and IbNM (**D**) inks with BCNFs.*

Based on the results presented in Figure 5.6A and Table 5.1, it can be observed that the incorporation of BCNFs led to a gradual increase in G', τ_y and τ_f in the NM inks. In a similar manner, ibuprofen loaded inks also showed higher G' compared to bare NM inks, thus reflecting the formation of the aforementioned physical entanglement with greater resistance to elastic deformation of the material [19, 57]. Additionally, data in Table 5.2 showed the increase in τ_y and τ_f when ibuprofen was added compared to bare NM ink. Again, as observed in the case of ibuprofen containing inks, the addition of nanofibers had not significant effect on τ_y and τ_f. These results suggested that the interactions and inclusion complexes between starch and ibuprofen might

be simultaneously hindering the interaction of starch with the BCNFs. Nonetheless, the results highlight the role of BCNF and ibuprofen independently in modulating the force required for extruding ink through the nozzle [13, 18, 58].

It should be noted that higher viscosity or higher G' values are not always related to better printability and shape fidelity, since there has to be a balance with the minimum pressure required to make an ink flow through a nozzle of specified length and diameter [59, 60]. Certainly, according to literature, the obtained values suggested that all formulations exhibited adequate τ_y value for good shape fidelity of the inks [18, 61, 62].

To complete the rheological characterization, recovery tests were performed to simulate the real printing conditions. As it can be seen in Figures 5.6C and D, the recovery test consisted of three stages in which the variation of viscosity versus time is measured when the sample is subjected to a certain strain. The recovery percentages are presented in Table 5.1 and 5.2.

The results revealed a recovery percentage of about 70% which was not influenced by the addition of BCNF in the NM formulations. However, attending to the recovery percentages of ibuprofen loaded inks, those containing nanofibers showed a decrease in the recovery capacity, with values around 50%. Again, it seemed that ibuprofen may had prevented the hydrogen bonding between BCNF and starch after the initial structure breakdown. As stated in literature, the addition of cellulose nanofibers did not always have a marked effect on the recovery test, and differences are more easily observable when inks incorporate a fiber percentage higher than 1% (w/w) [11, 13, 62]. Nevertheless, according to Figures 5.6C and D, the viscosity values after

structural recovery were adequate for their application in DIW 3D printing. Consequently, it was observed that all the starch-based formulations exhibited the needed thixotropic behavior, indicating their ability to recover their structural integrity immediately after being subjected to the shear force.

5.3.1.2 3D printing of NM starch-based tablets

After rheological characterization, the inks were used to print starch cylinders using the DIW 3D printing technique. Digital images of the different 3D printed NM tablets are represented in Figure 5.7.

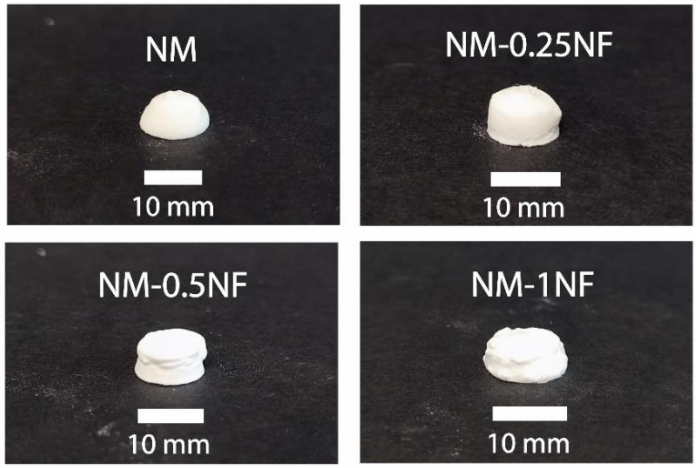

Figure 5.7 *Digital images of 3D printed NM tablets with different concentrations of BCNF after freeze-drying.*

As shown in Figure 5.7, and confirming the results from rheology tests, all formulations could be extruded through the nozzle and those reinforced with BCNF retained the specified cylindrical shape [60]. Although the rheological curves of NM inks were similar to those of their BCNF-reinforced counterparts, cylindrical shape retention was only observed in the cases of inks containing

nanofibers. The results suggested that as the BCNF content increased, the ink better supported the weight of the upper layers presenting more pronounced edges. This effect agreed with the decrease in n values and the increase in τ_f values observed in Table 5.1.

It is worth mentioning that NM-1NF cylinders, despite having an adequate shape fidelity, exhibited a more granular appearance with certain disruptions. Certainly, when the more concentrated inks containing 1% (w/w) BCNF were not adequately homogenized, cases of nozzle obstruction due to BCNF agglomerations could be observed [62]. Prior research has already reported that cellulose nanofibers at concentrations of 1.5% (w/w) tend to form agglomerates and display less dispersion within starch matrices after extrusion compared to lower concentrations of nanofibers. [49].

Correspondingly, the digital images of different 3D printed IbNM inks are displayed in Figure 5.8. It should be noted that all IbNM formulations displayed outstanding shape retention capacity without significant differences among them. This behavior was in line with the proper printability parameters obtained during the rheological characterization (Table 5.2).

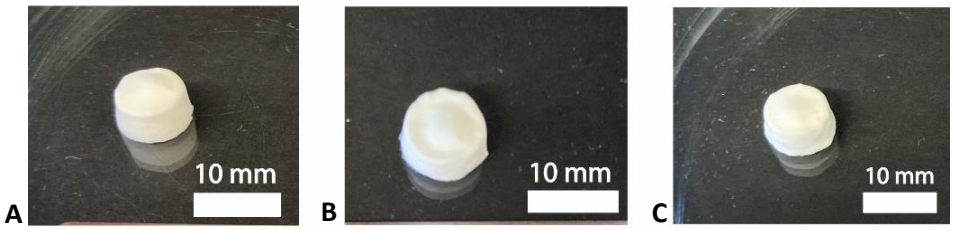

Figure 5.8 *Digital images of 3D printed IbNM tablets with different concentrations of BCNF after freeze-drying: IbNM (A), IbNM-0.5NF (B) and IbNM-1NF (C).*

To sum up, according to the obtained results it was concluded that initial G' values greater than 1000 Pa, or τ_f values higher than 300 Pa could be predictive of successful shape fidelity in agreement with previously published literature [45, 63].

Besides, as described in the rheological study, it was noted that the gradual inclusion of nanofibers led to an increase in the viscosity, G', and τ_f of NM starch inks. However, these differences were not considered substantial enough to significantly impact the shape accuracy of the 3D-printed cylinders. Some authors have suggested that the reinforcing nanofibers may be prone to orient themselves in the direction of extrusion [64]. Indeed, the orientation of cellulose nanofibers during 3D printing of tablets could notably influence the structural integrity, mechanical properties, porosity, shape fidelity, and functionality of the printed structures [35, 65]. Therefore, to analyze the possible nanofiber alignment, XRD component simulation was performed on a NM-1NF tablet as detailed in Chapter 2.

The measured XRD intensities were plotted as an intensity map where the hemisphere-like distribution of scattered intensity was projected on a 2D “pole figure” showing the intensity variation with sample orientation. Figure 5.9A presents the obtained results, where the red tones in the center of the sphere are related to the orientation of the nanofibers towards the normal vector of the NM-1NF tablet. Figure 5.9 illustrates the possible BCNF orientation according to the printing direction in a reinforced NM tablet.

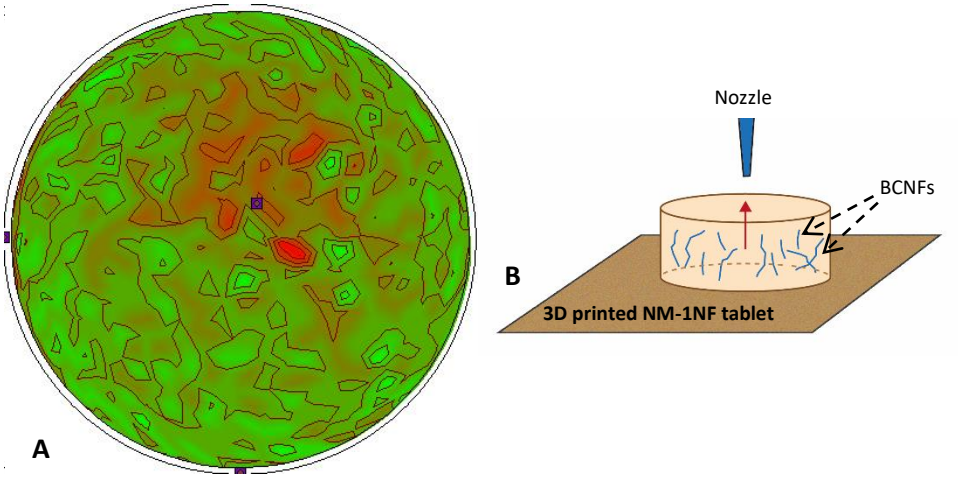

Figure 5.9 *Spherical harmonic model from component simulation in XRD representing BCNF orientation distribution in NM-1NF tablets (**A**). Illustration of BCNF orientation in NM tablets after the 3D printing process (**B**).*

Attending to Figure 5.9A, even it should be considered only as a qualitative approach, considering an orientation dispersion respect to the normal of approximately 30°, it could be observed that BCNFs exhibited a preferential orientation towards the normal, indicating that the extrusion process induced the partial alignment of the nanofibers. Although BCNF orientation exhibited significant dispersion, Huang et al and Yao et al also showed nanofiber orientation influenced by extrusion shear force [47, 66]. It should be noted that by carefully controlling and optimizing the cellulose nanofiber orientation, it is possible to enhance the overall performance and functionality of the printed components [64, 67, 68]. Thus, we hypothesize that this orientation could have contributed to the final shape retention of the 3D printed NM inks.

To conclude with 3D printed NM tablet characterization, the morphology of the tablets obtained from 3D printing was analyzed by SEM as depicted in Figure 5.10. Certainly, it has been reported that an interconnected porous

microstructure is interesting for facilitating polymeric drug transport and delivery [11, 69].

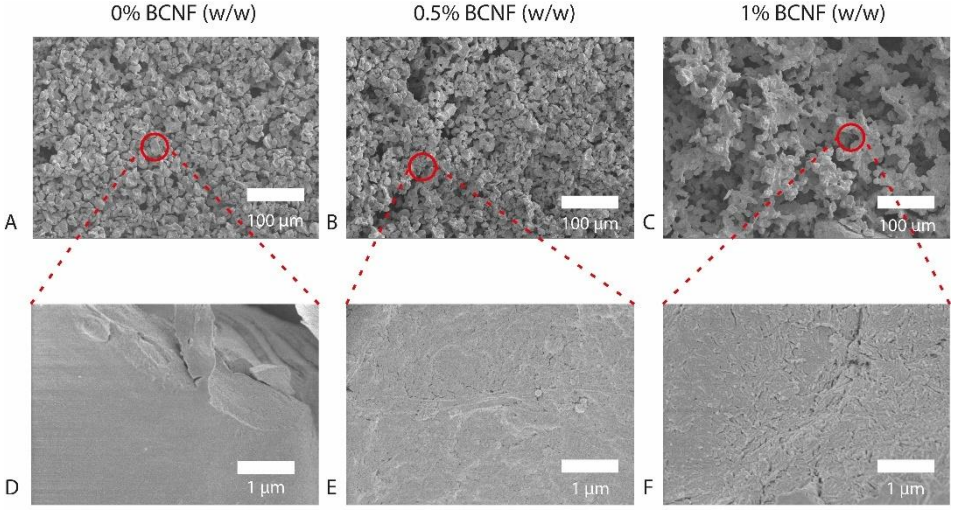

Figure 5.10 *SEM images of the NM tablets loaded with different concentrations of BCNFs (**A**, **B** and **C**), and their respective amplifications (**D**, **E** and **F**).*

Attending to the cross-sectional 5.10A, 5.10B and 5.10C images, a porous and interconnected microstructure could be observed. The less reinforced formulations, NM and NM-0.5NF showed higher homogeneity and compactness, while the sample with 1% (w/w) BCNF revealed more heterogeneity and more porous appearance. This morphology could be related to the formation of small cavities due to the BCNF agglomerations or entanglements mentioned before, that would lead to free spaces after the freeze-drying process (Figure 5.9C). Moreover, the amplified Figures 5.10D, 5.10E and 5.10F showed the presence of nanofibers as the BCNF concentration increased in contrast to the smooth surface of the bare NM samples, confirming their integration into the NM starch matrix.

In the case of the ibuprofen-loaded sample, IbNM-0.5NF, the structure showed the same degree of compactness and homogeneity as its unloaded counterpart (Figure 5.11). These results were in high agreement with those obtained by Gonzalez et al with ibuprofen loaded and unloaded NM samples [12].

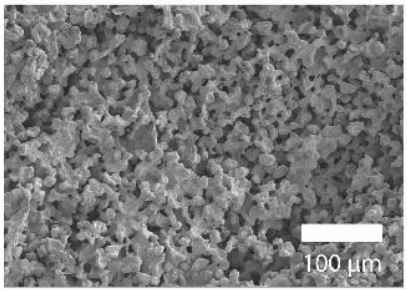

Figure 5.11 *Cross-sectional SEM image of a IbNM-0.5NF tablet.*

Finally, it is worthy to note that SEM images demonstrated that the different layers were properly integrated together in all the samples during the printing process. In fact, the tablets appeared to be a unified structure, indicating consistent material extrusion and accurate deposition and support of the individual layers.

5.3.1.3 Ibuprofen in vitro release

The release kinetics of ibuprofen from the different loaded tablets are shown in Figure 5.12A. The assay was carried out by measuring the ICR (Equation 5.1) released up to 6 hours in PBS at 37 °C. According to the results, the IbNM and IbNM-1NF tablets showed initial similar ibuprofen fast release, in contrast to the IbNM-0.25NF and IbNM-0.5NF, that displayed slower and controlled release kinetics. Indeed, The IbNM and IbNM-1NF tablets exhibited a burst

release effect in the first 45 minutes, eventually reaching an ICR value of 70% and 75% at 360 minutes, respectively.

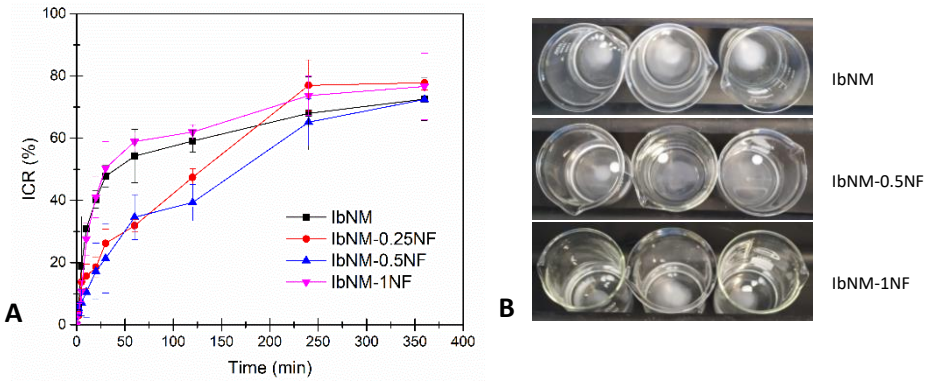

Figure 5.12 *Ibuprofen release in vitro study of the IbNM tablets loaded with different concentrations of BCNF (**A**) and tablet-decomposition study after 45 min ibuprofen release assay of different IbNM tablets in triplicate (**B**).*

The hydrophobic character of ibuprofen determined the release profile to be dependent on the porosity and erosion of the tablets rather than on its solubility in PBS [70]. In this sense, Figure 5.12B shows the disintegration state of loaded tablets after 45 min of release study. As it could be observed, both IbNM and IbNM-1NF cylinders were totally or partially disintegrated at that time (both near 60 % of ICR), respectively. Meanwhile, IbNM-0.5NM tablets maintained their integrity much longer and achieved 35 % of ICR at 45 min. Certainly, as reported by Gonzalez et al, IbNM tablets rapidly lost their structure upon introduction into PBS solutions [12]. In the same way, Hayashi et al. published that under slightly basic pH and 37 °C (simulated intestinal conditions), amylose chains and water increase their interactions [71]. Consequently, PBS could penetrate the matrix more effectively and lead to

rapid tablet disintegration. However, in the presence of nanofibers at concentrations of 0.25% and 0.5% (w/w), this effect was not observed. Hence, it was concluded that nanofibers of IbNM-0.25NF and IbNM-0.5NF tablets helped to preserve the structure by improving the cohesion of the freeze-dried cylinders.

In the case of the IbNM-1NF samples, even if rheology results suggested better preservation of tablet structure and shape fidelity, the samples underwent partial disintegration in the first 45 min. This effect may arise from the agglomerations resulting from the high BCNF content that could increase the number of disruptions and cavities, as shown in the SEM images. At these high concentrations, the nanofibers could contribute to form heterogeneous structures, from where the PBS penetrated the starch matrix more easily.

In this context, the results confirmed that IbNM and IbNM-1NF could be suitable for applications that require burst or flash release. For example, these samples could be used as orally disintegrating tablets, especially for patients with swallowing difficulties, as they can completely disintegrate in the mouth with saliva [72]. On the other hand, IbNM-0.25NF and IbNM-0.5NF would be preferable when a controllable and a higher ICR are intended.

Regarding maximum ICR (%), the obtained values in 6 h are slightly higher than those reported by Parra et al where ibuprofen was released from starch inclusion complexes in a simulated intestinal medium [55]. However, in the present work satisfactory ibuprofen release rates were obtained from a starch matrix without the necessity of any specific treatments in acidic or alkaline environments to favor the inclusion complex formation [52, 73].

5.3.2 WM starch for GPPE release

5.3.2.1 WM and GPPE ink setup

According to literature, WM presents very good printing and shape retention conditions, and due to its high amylopectin content it is an excellent matrix for sustainably releasing drugs in simulated intestinal environment [12]. For this reason, WM was chosen as 3D printed matrix for the release of the water-soluble GPPE. As in the case with NM starch, WM starch granules were first analyzed using an optical microscope as depicted in Figure 5.13.

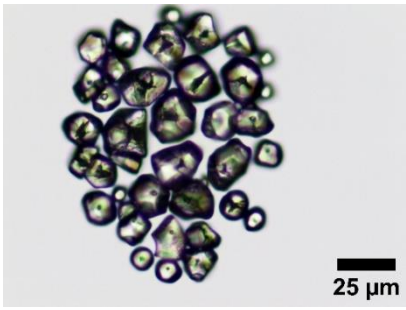

Figure 5.13 *Optical micrograph of the morphology of WM starch granules.*

Attending to the optical micrograph, the length of the starch granules was measured at 14.9 ± 4 µm and showed a polygonal shape with translucent appearance. Again, small concentric rings could be observed in the granule center. These OM results were in agreement with published literature for WM starch granules [12].

Accordingly, a rheological characterization of WM inks was conducted once again to assess their suitability for 3D printing and shape retention when combined with GPPE. GPPE was incorporated into WM gelatinized starch at 1, 2.5 and 5 % (w/w) concentrations. The results of the rheological

characterization performed on the loaded WM inks are shown below in Table 5.3 and Figure 5.14.

Table 5.3 *Rheological parameters of WM inks with GPPE: Power-law index (n), consistency coefficient (K), yield stress, flow stress and recovery (%).*

Sample	Flow test			Stress sweep		Recovery test
	n	K	R^2	Yield stress (Pa)	Flow stress (Pa)	Recovery (%)
WM	0.111 ± 0.024	359.74 ± 7.87	0.99	329.3 ± 19.8	491.7 ± 61.1	29.9 ± 4.4
WM-1PE	0.050 ± 0.002	358.95 ± 58.4	0.99	393.3 ± 21.8	638.0 ± 46.3	34.4 ± 1.4
WM-2.5PE	0.062 ± 0.001	345.14 ± 14.46	0.99	426.5 ± 85.5	626.1 ± 143.0	30.1 ± 2.7
WM-5PE	0.088 ± 0.008	335.09 ± 6.78	0.99	396.0 ± 80.2	666.0 ± 121.5	28.8 ± 7.5

As reflected by the flow test results in Figure 5.14A, all inks showed the desirable shear thinning behavior for DIW 3D printing ($n < 1$). The results obtained were fitted again to the Power law model described previously, and the n and K for the different WM-based inks are shown in Table 5.3. The value of R^2 close to 1 confirmed the non-Newtonian nature of all samples. According to the values of n, the addition of GPPE enhanced the shear thinning behavior compared to the WM sample, fact that was also noticeable in the curves.

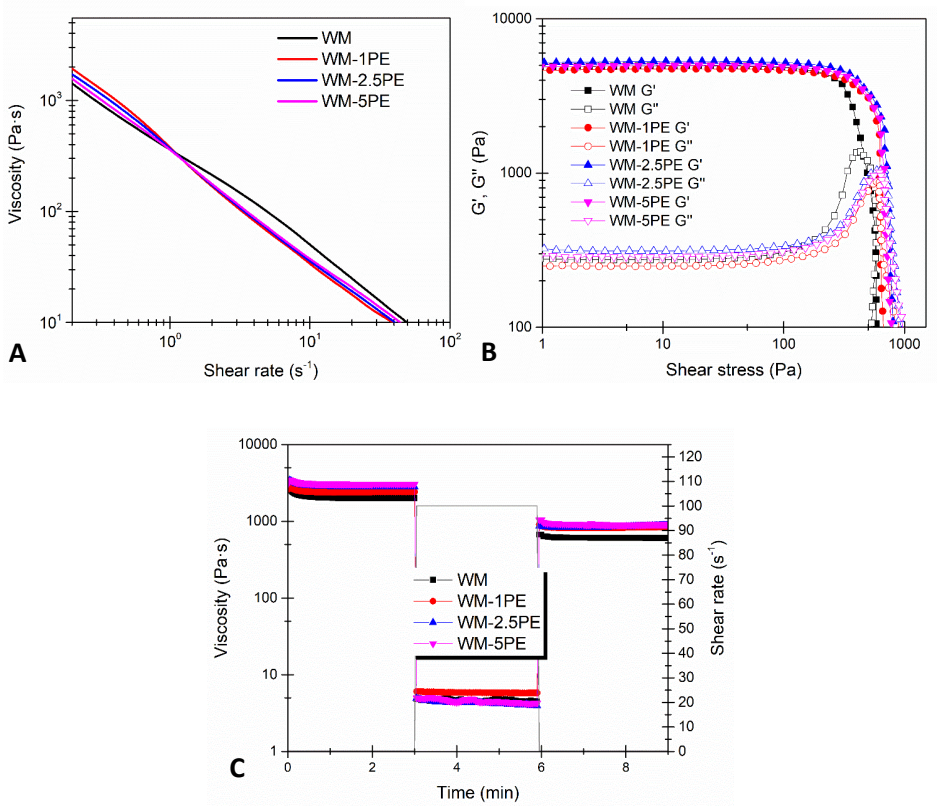

Figure 5.14 *Flow test (**A**), stress sweep test (**B**), and recovery test (**C**) of WM-based inks mixed with different concentrations of GPPE.*

The numerous hydroxyl groups of polyphenols could effectively interact with amylopectin thus modulating the printability and rheological properties of gelatinized starch inks as it has been reported before [23, 37, 74]. The high degree of interaction that might promote polyphenols to be located between the starch chains, reducing their attraction and increasing the separation between them, consequently lowering the viscosity [18, 38, 75]. As for the K values, although major differences were not observed at lower concentrations, a decreasing tendency of viscosity with increasing GPPE concentration was observed.

Additionally, Figure 5.14B shows the stress sweep test of the WM and WM with GPPE inks. As expected, G' remained constant and above G'', with very similar G' values, though a slight increasing tendency was observed with the GPPE content. The τ_y and τ_f values are shown in Table 5.3. Both τ_y and τ_f, showed a slight upward trend with the presence of GPPE, indicating the presence of interactions strong enough to maintain the gel's integrity at higher shear stresses. Indeed, it has been reported that polyphenolic extracts hamper starch retrogradation, thus improving ink extrudability and fidelity [76]. In the case of GPPE, according to the results in Figure 5.14B and Table 5.3, all the WM inks studied showed τ_f parameters compatible with smooth nozzle extrusion and predicted good final strength and shape fidelity [13, 60, 61].

Besides, a recovery test was performed as it is represented in Figure 5.14C. The recovery percentages of each sample are gathered in Table 5.3. The results showed recovery percentages close to 30% for all the inks without significant differences between them. Despite being relatively low values, they showed thixotropic character and capacity to recompose after being subjected to shear stress. Hence, the recovery values obtained here were considered acceptable to continue with the DIY 3D printing process.

Subsequently, the interactions between WM amylopectin and GPPE were analyzed by FTIR in Figure 5.15 [77]. In this regard, significant changes in intensity and slight peak shifts were observed in the -OH stretching band from 3750 to 3000 cm^{-1} when comparing GPPE loaded WM samples and bare WM. These phenomena has been described by numerous authors as an indicative of hydrogen bonding interactions between the two compounds [78–81]. Certainly, Wu et al. also reported –OH bands shift when combining fermented starch with polyphenolic extract from guava leaf [82]. Furthermore, the C-O-C

stretching bands at around 1010 cm^{-1} of WM were progressively shifted to lower wavenumbers with the addition of GPPE (Figure 5.15A), similarly to some earlier reports [80].

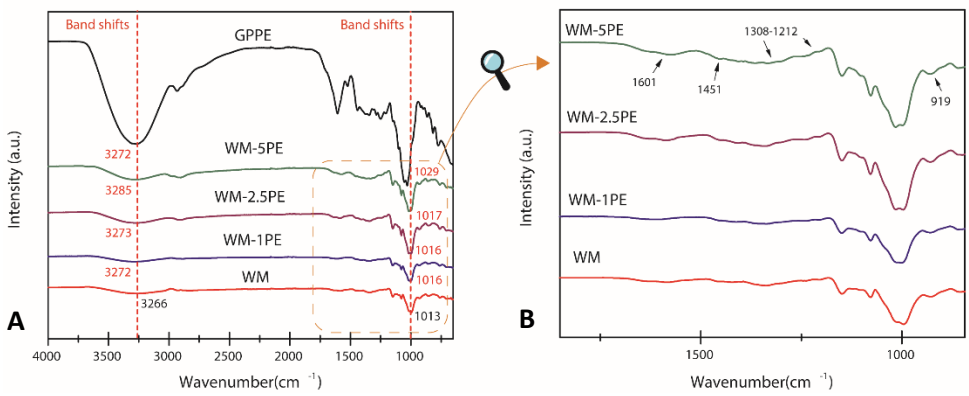

Figure 5.15 *FTIR spectra of WM tablets loaded with GPPE and bare GPPE (**A**), and an amplification of the fingerprint bands of GPPE in 3D printed WM tablets (**B**).*

Attending to Figure 5.15B, WM-GPPE spectra show a gradual increase in the number of characteristic fingerprint bands detailed in Chapter 4 as a result of the physical mixing of both components [80]. The intensity of these bands augmented as the GPPE concentration increased in the WM samples. In summary, based on the results obtained from the FTIR spectra, it can be deduced that the polyphenolic extract was fully integrated into the starch matrix, and most interactions were attributed to hydrogen bonding.

5.3.2.2 3D printing of WM starch-based tablets

WM inks were subjected to the DIW 3D printing process similarly to the NM formulations. In general, they showed smooth extrudability through the nozzle and support capacity for the upper ink layers. Thus, the observed behavior was in accordance with the parameters obtained in the rheological study (Table

5.3). In addition, the internal structure of the printed and freeze-dried tablets was examined through SEM. Figure 5.16 shows the different freeze-dried starch tablets printed with increasing GPPE content and their respective SEM images.

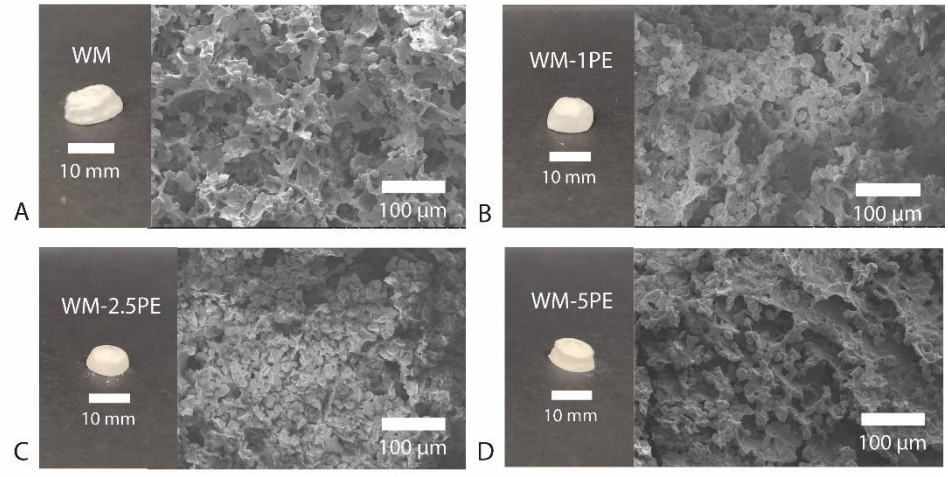

Figure 5.16 *Digital images of 3D printed WM tablets with different concentrations of GPPE with their respective SEM image amplification.*

As observed in the digital images, all pieces respected the cylindrical morphology designed by CAD, being those with higher GPPE concentration smoother and of more homogeneous consistency. Further, SEM images exhibited porous networks that were interconnected. The WM sample displayed a sharper appearance with more distinct edges (Figure 5.16A). Nevertheless, as the concentration of GPPE increased, the samples demonstrated a greater interconnectivity and density. Consequently, the WM-5PE sample seemed to be completely coated with GPPE, resulting in a pasty and less porous appearance (Figure 5.16D). These SEM images are comparable to those published by Wu et al, where the adsorption of guava leaf polyphenolic extract onto starch could be observed, showing a similar effect

[82]. The images also confirmed that polyphenolic extracts could act as modulators in starch 3D printing by also influencing the final internal structure of the printed products after the freeze-drying process. These structural differences after the freeze-drying process could be due to the restriction of starch retrogradation caused by the presence of polyphenols described by Zeng et al [76].

5.3.2.3 GPPE in vitro release

The in vitro release of GPPE from WM starch tablets was measured for 5 h in simulated intestinal medium at 37 °C. Figure 5.17 depicts the GPPE release study as well as WM tablets integrity after 24 h immersion in PBS.

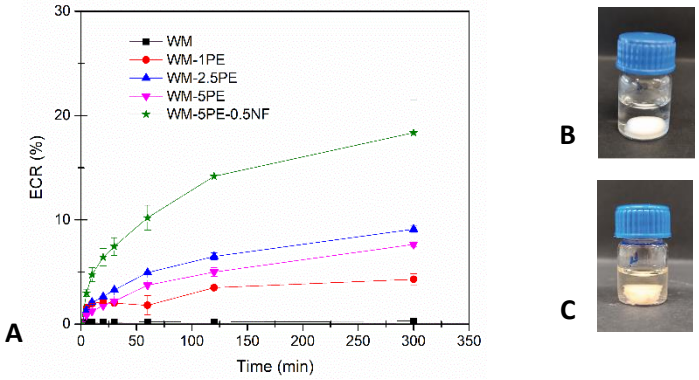

Figure 5.17 *GPPE release in vitro study of the WM and NM tablets loaded with different concentrations of GPPE and BCNF (**A**). Digital images of the WM (**B**) and WM-5PE (**C**) samples after 24 h of being immersed in PBS.*

Firstly, as in the case of the NM tablets, the behavior of the cylinders when introduced into PBS physiological medium was observed (Figures 5.17B and 5.17C). Unlike the NM samples, WM tablets exhibited a more robust matrix and a greater capacity to absorb surrounding fluid while maintaining their

integrity, which may be attributed to their higher degree of amylopectin branching [25, 30]. As shown in Figures 5.17B and 5.17C, all samples retained their cylindrical shape beyond 24 h of testing. This fact is of particular interest when incorporating hydrophilic drugs, in which the disintegration of the tablet is not the main release mechanism.

Attending to GPPE release profiles, all tablets showed a similar pattern, where a sustained release that gradually stabilized at 300 min could be observed. WM-1PE, WM-2.5PE, and WM-5PE samples had release percentages that did not reach 10% after 5 h of testing. These findings suggested that GPPE, due to the strong interactions with starch mentioned previously, were mostly trapped within the WM matrix. The cumulative release increased with the concentration of GPPE in the samples until WM-2.5PE. Thus, it is inferred that in WM-2.5PE and WM-5PE samples, most of the GPPE remained closely associated with the starch regardless of the initial concentration. Therefore, it seems that the same concentration of GPPE could have acted as a release modulator by means of the rheological and structural changes of starch mentioned above.

Moreover, based on the role of BCNFs as release modulators in NM starch-based inks, in order to increase the GPPE release rates, WM-5PE tablet reinforced 0.5 % (w/w) of BCNF (WM-5PE-0.5NF) was prepared. As observed in Figure 5.17, the ECR increased to 20 % in 300 min with the same initial GPPE concentration.

From this perspective, the ability of WM starch to incorporate and retain GPPE even in aqueous media presents an intriguing prospect for food 3D printing [23]. The various matrix configurations that can be achieved, along with the

extract's active functionalities, highlight their potential applications in the biomedical, food, and nutraceutical industries [39, 83]. Additionally, another factor to be considered for starch tablets with GPPE is the color change they undergo due to their oxidation over time, as observed in Figure 5.17C. This reactive sensitivity can be also exploited by using polyphenols as intelligent indicators of specific changes in the environment [84, 85].

5.4 Conclusions

In this chapter, starch tablets were designed using DIW 3D printing technology for personalized drug delivery. Two types of starch inks of different botanical origins, NM and WM, were selected. Given the characteristics of each gelatinized ink, the possibility of adding BCNF and other bioactive compounds to observe their effect on printability and subsequent release was studied.

NM inks presented acceptable rheological characteristics for 3D printing that progressively improved with the addition of nanofibers. Morphological characterization of the 3D printed inks showed how BCNFs contributed to the shape fidelity of final products. However, some structural differences were evident in SEM after the freeze-drying process, which affected the porosity and compactness of the sample. These differences were associated to the dispersion of BCNF into the starch ink and the possible presence of agglomerates during ink homogenization. Thus, when in vitro release tests of ibuprofen were performed, it was observed that the BCNF content modulated the release profile. The NM and NM-1NF formulations produced a burst release effect, while the NM-0.25NF and NM-0.5NF formulations sustained and attenuated ibuprofen release. These results demonstrated the applicability of BCNFs as a rheological and printability reinforcing agents for NM, as well as

modulators of ibuprofen release in a simulated intestinal environment. It should be noted that NM tablets were not able to maintain their structure in physiological media without BCNF reinforcing. Therefore, the combination of NM and BCNF could be a good strategy in the development of tablets for the personalized release of hydrophobic drugs.

In the case of WM inks, it was observed that the rheological properties of the inks were slightly affected by the combination with the polyphenolic extract GPPE. WM presented excellent structural characteristics for DIW 3D printing and GPPE, even at concentrations of 5 % (w/w), did not have a negative impact on ink printability. Morphological and structural characterization confirmed the extrudability and shape fidelity of the inks and the uniform presence of GPPE within the 3D printed cylinders. FTIR analysis also confirmed the integration of the extract into the starch matrix because of the numerous hydrogen bond interactions. GPPE release assays confirmed these interactions between starch and polyphenols, resulting in most phenolic compounds remaining inside the WM tablet. Additionally, the release rate could be accelerated by introducing BCNF to the system. These results demonstrated the potential of BCNF as a mechanism for controlling the release also of functional compounds of natural origin from WM. Furthermore, given the numerous bioactive properties of GPPE, this strategy showed great potential for the development of personalized active tablets and 3D printed edibles for the food, nutraceutical, and biomedical sectors.

5.5 References

1 Hamburg, M. A. and Collins, F. S. (2010) The path to personalized medicine. *N. Engl. J. Med.* **363**, 301–304

2 Horwitz, R. I., Cullen, M. R., Abell, J. and Christian, J. B. (2013) (De)Personalized Medicine. *Science (80-.).* **339**, 1155–1156

3 Raijada, D., Wac, K., Greisen, E., Rantanen, J. and Genina, N. (2021) Integration of personalized drug delivery systems into digital health. *Adv. Drug Deliv. Rev.*, The Author(s) **176**, 113857 https://doi.org/10.1016/j.addr.2021.113857

4 Ilbawi, A. M. and Anderson, B. O. (2015) Cancer in global health: How do prevention and early detection strategies relate? *Sci. Transl. Med.* **7**, 1–5 https://doi.org/10.1126/scitranslmed.3008853

5 Tan, Y. J. N., Yong, W. P., Kochhar, J. S., Khanolkar, J., Yao, X., Sun, Y., et al. (2020) On-demand fully customizable drug tablets via 3D printing technology for personalized medicine. *J. Control. Release*, Elsevier **322**, 42–52 https://doi.org/10.1016/j.jconrel.2020.02.046

6 Kalepu, S. and Nekkanti, V. (2015) Insoluble drug delivery strategies: Review of recent advances and business prospects. *Acta Pharm. Sin. B*, Elsevier **5**, 442–453 https://doi.org/10.1016/j.apsb.2015.07.003

7 Goyanes, A., Wang, J., Buanz, A., Martínez-Pacheco, R., Telford, R., Gaisford, S., et al. (2015) 3D Printing of Medicines: Engineering Novel Oral Devices with Unique Design and Drug Release Characteristics. *Mol. Pharm.* **12**, 4077–4084 https://doi.org/10.1021/acs.molpharmaceut.5b00510

8 Gao, B., Yang, Q., Zhao, X., Jin, G., Ma, Y. and Xu, F. (2016) 4D Bioprinting for Biomedical Applications. *Trends Biotechnol.*, Elsevier Ltd **34**, 746–756 https://doi.org/10.1016/j.tibtech.2016.03.004

9 O'reilly, C. S., Elbadawi, M., Desai, N., Gaisford, S., Basit, A. W. and Orlu, M. (2021) Machine learning and machine vision accelerate 3d printed orodispersible film development. *Pharmaceutics* **13** https://doi.org/10.3390/pharmaceutics13122187

10 Beer, N., Hegger, I., Kaae, S., De Bruin, M. L., Genina, N., Alves, T. L., et

al. (2021) Scenarios for 3D printing of personalized medicines - A case study. *Explor. Res. Clin. Soc. Pharm.* **4**, 100073 https://doi.org/10.1016/j.rcsop.2021.100073

11 Olmos-Juste, R., Guaresti, O., Calvo-Correas, T., Gabilondo, N. and Eceiza, A. (2021) Design of drug-loaded 3D printing biomaterial inks and tailor-made pharmaceutical forms for controlled release. *Int. J. Pharm.*, Elsevier B.V. **609**, 121124 https://doi.org/10.1016/j.ijpharm.2021.121124

12 González, K., Larraza, I., Berra, G., Eceiza, A. and Gabilondo, N. (2022) 3D printing of customized all-starch tablets with combined release kinetics. *Int. J. Pharm.* **622** https://doi.org/10.1016/j.ijpharm.2022.121872

13 Olmos-Juste, R., Alonso-Lerma, B., Pérez-Jiménez, R., Gabilondo, N. and Eceiza, A. (2021) 3D printed alginate-cellulose nanofibers based patches for local curcumin administration. *Carbohydr. Polym.* **264** https://doi.org/10.1016/j.carbpol.2021.118026

14 Pandey, M., Choudhury, H., Fern, J. L. C., Kee, A. T. K., Kou, J., Jing, J. L. J., et al. (2020) 3D printing for oral drug delivery: a new tool to customize drug delivery. *Drug Deliv. Transl. Res.*, Drug Delivery and Translational Research **10**, 986–1001 https://doi.org/10.1007/s13346-020-00737-0

15 Seoane-Viaño, I., Januskaite, P., Alvarez-Lorenzo, C., Basit, A. W. and Goyanes, A. (2021) Semi-solid extrusion 3D printing in drug delivery and biomedicine: Personalised solutions for healthcare challenges. *J. Control. Release* **332**, 367–389 https://doi.org/10.1016/j.jconrel.2021.02.027

16 Placone, J. K. and Engler, A. J. (2018) Recent Advances in Extrusion-Based 3D Printing for Biomedical Applications. *Adv. Healthc. Mater.* **7**, 1–11 https://doi.org/10.1002/adhm.201701161

17 Schwab, A., Levato, R., D'Este, M., Piluso, S., Eglin, D. and Malda, J. (2020) Printability and Shape Fidelity of Bioinks in 3D Bioprinting. *Chem. Rev.* **120**, 11028–11055 https://doi.org/10.1021/acs.chemrev.0c00084

18 Vadillo, J., Larraza, I., Calvo-Correas, T., Gabilondo, N., Derail, C. and Eceiza, A. (2022) Bioactive inks suitable for 3D printing based on

waterborne polyurethane urea, cellulose nanocrystals and Salvia extract. *React. Funct. Polym.*, Elsevier B.V. **175**, 105286 https://doi.org/10.1016/j.reactfunctpolym.2022.105286

19 Liu, Z., Zhang, M., Bhandari, B. and Yang, C. (2018) Impact of rheological properties of mashed potatoes on 3D printing. *J. Food Eng.*, Elsevier Ltd **220**, 76–82 https://doi.org/10.1016/j.jfoodeng.2017.04.017

20 Tappa, K. and Jammalamadaka, U. (2018) Novel biomaterials used in medical 3D printing techniques. *J. Funct. Biomater.* **9** https://doi.org/10.3390/jfb9010017

21 Leppiniemi, J., Lahtinen, P., Paajanen, A., Mahlberg, R., Metsä-Kortelainen, S., Pinomaa, T., et al. (2017) 3D-Printable Bioactivated Nanocellulose-Alginate Hydrogels. *ACS Appl. Mater. Interfaces* **9**, 21959–21970 https://doi.org/10.1021/acsami.7b02756

22 Jose, R. R., Rodriguez, M. J., Dixon, T. A., Omenetto, F. and Kaplan, D. L. (2016) Evolution of Bioinks and Additive Manufacturing Technologies for 3D Bioprinting. *ACS Biomater. Sci. Eng.* **2**, 1662–1678 https://doi.org/10.1021/acsbiomaterials.6b00088

23 Rong, L., Chen, X., Shen, M., Yang, J., Qi, X., Li, Y., et al. (2023) The application of 3D printing technology on starch-based product: A review. *Trends Food Sci. Technol.*, Elsevier Ltd **134**, 149–161 https://doi.org/10.1016/j.tifs.2023.02.015

24 Builders, P. F. and Arhewoh, M. I. (2016) Pharmaceutical applications of native starch in conventional drug delivery. *Starch/Staerke* **68**, 864–873 https://doi.org/10.1002/star.201500337

25 Domene-López, D., García-Quesada, J. C., Martin-Gullon, I. and Montalbán, M. G. (2019) Influence of starch composition and molecular weight on physicochemical properties of biodegradable films. *Polymers (Basel).* **11**, 1–17 https://doi.org/10.3390/polym11071084

26 Singh, N., Singh, J., Kaur, L., Sodhi, N. S. and Gill, B. S. (2003) Morphological, thermal and rheological properties of starches from different botanical sources. *Food Chem.* **81**, 219–231 https://doi.org/10.1016/S0308-8146(02)00416-8

27 González, K., Retegi, A., González, A., Eceiza, A. and Gabilondo, N.

(2015) Starch and cellulose nanocrystals together into thermoplastic starch bionanocomposites. *Carbohydr. Polym.* **117**, 83–90 https://doi.org/10.1016/j.carbpol.2014.09.055

28 Ogunsona, E., Ojogbo, E. and Mekonnen, T. (2018) Advanced material applications of starch and its derivatives. *Eur. Polym. J.*, Elsevier **108**, 570–581 https://doi.org/10.1016/j.eurpolymj.2018.09.039

29 Pérez, S. and Bertoft, E. (2010) The molecular structures of starch components and their contribution to the architecture of starch granules: A comprehensive review. *Starch/Staerke* **62**, 389–420 https://doi.org/10.1002/star.201000013

30 Onofre, F., Wang, Y. J. and Mauromoustakos, A. (2009) Effects of structure and modification on sustained release properties of starches. *Carbohydr. Polym.*, Elsevier Ltd **76**, 541–547 https://doi.org/10.1016/j.carbpol.2008.11.016

31 Karim, A. A., Toon, L. C., Lee, V. P. L., Ong, W. Y., Fazilah, A. and Noda, T. (2007) Effects of phosphorus contents on the gelatinization and retrogradation of potato starch. *J. Food Sci.* **72**, 132–138 https://doi.org/10.1111/j.1750-3841.2006.00251.x

32 Elgaied-Lamouchi, D., Descamps, N., Lefevre, P., Rambur, I., Pierquin, J. Y., Siepmann, F., et al. (2021) Starch-based controlled release matrix tablets: Impact of the type of starch. *J. Drug Deliv. Sci. Technol.*, Elsevier B.V. **61**, 102152 https://doi.org/10.1016/j.jddst.2020.102152

33 Ma, X., Li, R., Zhao, X., Ji, Q., Xing, Y., Sunarso, J., et al. (2017) Biopolymer composite fibres composed of calcium alginate reinforced with nanocrystalline cellulose. *Compos. Part A Appl. Sci. Manuf.*, Elsevier Ltd **96**, 155–163 https://doi.org/10.1016/j.compositesa.2017.02.021

34 Du, H., Liu, W., Zhang, M., Si, C., Zhang, X. and Li, B. (2019) Cellulose nanocrystals and cellulose nanofibrils based hydrogels for biomedical applications. *Carbohydr. Polym.*, Elsevier **209**, 130–144 https://doi.org/10.1016/j.carbpol.2019.01.020

35 Siqueira, G., Kokkinis, D., Libanori, R., Hausmann, M. K., Gladman, A. S., Neels, A., et al. (2017) Cellulose Nanocrystal Inks for 3D Printing of Textured Cellular Architectures. *Adv. Funct. Mater.* **27**

https://doi.org/10.1002/adfm.201604619

36 Sydney Gladman, A., Matsumoto, E. A., Nuzzo, R. G., Mahadevan, L. and Lewis, J. A. (2016) Biomimetic 4D printing. *Nat. Mater.* **15**, 413–418 https://doi.org/10.1038/nmat4544

37 Liu, Y., Yi, S., Sameen, D. E., Hossen, M. A., Dai, J., Li, S., et al. (2021) Designing and utilizing 3D printed chitosan/halloysite nanotubes/tea polyphenol composites to maintain the quality of fresh blueberries. *Innov. Food Sci. Emerg. Technol.*, Elsevier Ltd **74**, 102808 https://doi.org/10.1016/j.ifset.2021.102808

38 Zeng, X., Li, T., Zhu, J., Chen, L. and Zheng, B. (2021) Printability improvement of rice starch gel via catechin and procyanidin in hot extrusion 3D printing. *Food Hydrocoll.*, Elsevier Ltd **121**, 106997 https://doi.org/10.1016/j.foodhyd.2021.106997

39 Vieira, M. V., Oliveira, S. M., Amado, I. R., Fasolin, L. H., Vicente, A. A., Pastrana, L. M., et al. (2020) 3D printed functional cookies fortified with Arthrospira platensis: Evaluation of its antioxidant potential and physical-chemical characterization. *Food Hydrocoll.* **107** https://doi.org/10.1016/j.foodhyd.2020.105893

40 Memar, M. Y., Adibkia, K., Farajnia, S., Kafil, H. S., Yekani, M., Alizadeh, N., et al. (2019) The grape seed extract: A natural antimicrobial agent against different pathogens. *Rev. Res. Med. Microbiol.* **30**, 173–182 https://doi.org/10.1097/MRM.0000000000000174

41 Brezoiu, A. M., Matei, C., Deaconu, M., Stanciuc, A. M., Trifan, A., Gaspar-Pintiliescu, A., et al. (2019) Polyphenols extract from grape pomace. Characterization and valorisation through encapsulation into mesoporous silica-type matrices. *Food Chem. Toxicol.*, Elsevier **133**, 110787 https://doi.org/10.1016/j.fct.2019.110787

42 González-Centeno, M. R., Jourdes, M., Femenia, A., Simal, S., Rosselló, C. and Teissedre, P. L. (2013) Characterization of polyphenols and antioxidant potential of white grape pomace byproducts (Vitis vinifera L.). *J. Agric. Food Chem.* **61**, 11579–11587 https://doi.org/10.1021/jf403168k

43 Schirmer, M., Höchstötter, A., Jekle, M., Arendt, E. and Becker, T. (2013) Physicochemical and morphological characterization of different

starches with variable amylose/amylopectin ratio. *Food Hydrocoll.*, Elsevier Ltd **32**, 52–63 https://doi.org/10.1016/j.foodhyd.2012.11.032

44 Urbina, L., Hernández-Arriaga, A. M., Eceiza, A., Gabilondo, N., Corcuera, M. A., Prieto, M. A., et al. (2017) By-products of the cider production: an alternative source of nutrients to produce bacterial cellulose. *Cellulose* **24**, 2071–2082 https://doi.org/10.1007/s10570-017-1263-4

45 Chen, H., Xie, F., Chen, L. and Zheng, B. (2019) Effect of rheological properties of potato, rice and corn starches on their hot-extrusion 3D printing behaviors. *J. Food Eng.*, Elsevier **244**, 150–158 https://doi.org/10.1016/j.jfoodeng.2018.09.011

46 Li, H., Liu, S. and Li, L. (2016) Rheological study on 3D printability of alginate hydrogel and effect of graphene oxide. *Int. J. Bioprinting* **2**, 54–66 https://doi.org/10.18063/IJB.2016.02.007

47 Huang, L., Du, X., Fan, S., Yang, G., Shao, H., Li, D., et al. (2019) Bacterial cellulose nanofibers promote stress and fidelity of 3D-printed silk based hydrogel scaffold with hierarchical pores. *Carbohydr. Polym.* **221**, 146–156 https://doi.org/10.1016/j.carbpol.2019.05.080

48 Chen, R. De, Huang, C. F. and Hsu, S. hui. (2019) Composites of waterborne polyurethane and cellulose nanofibers for 3D printing and bioapplications. *Carbohydr. Polym.*, Elsevier **212**, 75–88 https://doi.org/10.1016/j.carbpol.2019.02.025

49 Ghanbari, A., Tabarsa, T., Ashori, A., Shakeri, A. and Mashkour, M. (2018) Preparation and characterization of thermoplastic starch and cellulose nanofibers as green nanocomposites: Extrusion processing. *Int. J. Biol. Macromol.*, Elsevier B.V. **112**, 442–447 https://doi.org/10.1016/j.ijbiomac.2018.02.007

50 Alidadi-Shamsabadi, M., Behzad, T., Bagheri, R. and Nari-Nasrabadi, B. (2015) Preparation and characterization of low-density polyethylene/thermoplastic starch composites reinforced by cellulose nanofibers. *Polym. Compos.* **36**, 2309–2316 https://doi.org/10.1002/pc.23144

51 Wiranidchapong, C., Ruangpayungsak, N., Suwattanasuk, P., Shuwisitkul, D. and Tanvichien, S. (2015) Plasticizing effect of ibuprofen

induced an alteration of drug released from Kollidon SR matrices produced by direct compression. *Drug Dev. Ind. Pharm.* **41**, 1037–1046 https://doi.org/10.3109/03639045.2014.925917

52 Shi, L., Zhou, J., Guo, J., Gladden, I. and Kong, L. (2021) Starch inclusion complex for the encapsulation and controlled release of bioactive guest compounds. *Carbohydr. Polym.*, Elsevier Ltd **274**, 118596 https://doi.org/10.1016/j.carbpol.2021.118596

53 Eliasson, A. -C, Carlson, T. L. -. and Larsson, K. (1981) Some Effects of Starch Lipids on the Thermal and Rheological Properties of Wheat Starch. *Starch - Stärke* **33**, 130–134 https://doi.org/10.1002/star.19810330407

54 Heinemann, C., Conde-Petit, B., Nuessli, J. and Escher, F. (2001) Evidence of starch inclusion complexation with lactones. *J. Agric. Food Chem.* **49**, 1370–1376 https://doi.org/10.1021/jf001079u

55 Parra, A. P., Martínez Ramírez, J. A. and Mora Huertas, C. E. (2021) Preparation and characterization of native starch-ibuprofen molecular inclusion complexes. *J. Drug Deliv. Sci. Technol.*, Elsevier B.V. **63**, 102509 https://doi.org/10.1016/j.jddst.2021.102509

56 Cyriac, F., Lugt, P. M. and Bosman, R. (2015) On a New Method to Determine the Yield Stress in Lubricating Grease. *Tribol. Trans.* **58**, 1021–1030 https://doi.org/10.1080/10402004.2015.1035414

57 Balakrishnan, P., Sreekala, M. S., Kunaver, M., Huskić, M. and Thomas, S. (2017) Morphology, transport characteristics and viscoelastic polymer chain confinement in nanocomposites based on thermoplastic potato starch and cellulose nanofibers from pineapple leaf. *Carbohydr. Polym.* https://doi.org/10.1016/j.carbpol.2017.04.017

58 Li, L., Lin, Q., Tang, M., Duncan, A. J. E. and Ke, C. (2019) Advanced Polymer Designs for Direct-Ink-Write 3D Printing. *Chem. - A Eur. J.* **25**, 10768–10781 https://doi.org/10.1002/chem.201900975

59 Pospischil, M., Specht, J., Markus, K., Matthias, H., Mohr, C., Clement, F., et al. (2013) Finger Geometry **4**, 1–6

60 Outrequin, T. C. R., Gamonpilas, C., Siriwatwechakul, W. and Sreearunothai, P. (2023) Extrusion-based 3D printing of food

biopolymers: A highlight on the important rheological parameters to reach printability. *J. Food Eng.* **342** https://doi.org/10.1016/j.jfoodeng.2022.111371

61 Zhang, X., Huo, W., Liu, J., Zhang, Y., Zhang, S. and Yang, J. (2020) 3D printing boehmite gel foams into lightweight porous ceramics with hierarchical pore structure. *J. Eur. Ceram. Soc.*, Elsevier **40**, 930–934 https://doi.org/10.1016/j.jeurceramsoc.2019.10.032

62 Larraza, I., Vadillo, J., Calvo-Correas, T., Tejado, A., Martin, L., Arbelaiz, A., et al. (2022) Effect of Cellulose Nanofibers' Structure and Incorporation Route in Waterborne Polyurethane–Urea Based Nanocomposite Inks. *Polymers (Basel).* **14** https://doi.org/10.3390/polym14214516

63 Bendtsen, S. T., Quinnell, S. P. and Wei, M. (2017) Development of a novel alginate-polyvinyl alcohol-hydroxyapatite hydrogel for 3D bioprinting bone tissue engineered scaffolds. *J. Biomed. Mater. Res. - Part A* **105**, 1457–1468 https://doi.org/10.1002/jbm.a.36036

64 Hausmann, M. K., Siqueira, G., Libanori, R., Kokkinis, D., Neels, A., Zimmermann, T., et al. (2020) Complex-Shaped Cellulose Composites Made by Wet Densification of 3D Printed Scaffolds. *Adv. Funct. Mater.* **30** https://doi.org/10.1002/adfm.201904127

65 Lewicki, J. P., Rodriguez, J. N., Zhu, C., Worsley, M. A., Wu, A. S., Kanarska, Y., et al. (2017) 3D-Printing of Meso-structurally Ordered Carbon Fiber/Polymer Composites with Unprecedented Orthotropic Physical Properties. *Sci. Rep.*, Nature Publishing Group **7**, 1–14 https://doi.org/10.1038/srep43401

66 Yao, J., Chen, S., Chen, Y., Wang, B., Pei, Q. and Wang, H. (2017) Macrofibers with High Mechanical Performance Based on Aligned Bacterial Cellulose Nanofibers. *ACS Appl. Mater. Interfaces* **9**, 20330–20339 https://doi.org/10.1021/acsami.6b14650

67 Ureña-Benavides, E. E. and Kitchens, C. L. (2011) Wide-angle X-ray diffraction of cellulose nanocrystal-alginate nanocomposite fibers. *Macromolecules* **44**, 3478–3484 https://doi.org/10.1021/ma102731m

68 Wang, B., Torres-Rendon, J. G., Yu, J., Zhang, Y. and Walther, A. (2015) Aligned bioinspired cellulose nanocrystal-based nanocomposites with

synergetic mechanical properties and improved hygromechanical performance. *ACS Appl. Mater. Interfaces* **7**, 4595–4607 https://doi.org/10.1021/am507726t

69 Lima-Tenório, M. K., Tenório-Neto, E. T., Garcia, F. P., Nakamura, C. V., Guilherme, M. R., Muniz, E. C., et al. (2015) Hydrogel nanocomposite based on starch and Co-doped zinc ferrite nanoparticles that shows magnetic field-responsive drug release changes. *J. Mol. Liq.*, Elsevier B.V. **210**, 100–105 https://doi.org/10.1016/j.molliq.2014.11.027

70 Abukhadra, M. R., Refay, N. M., Nadeem, A., El-Sherbeeny, A. M. and Ibrahim, K. E. (2020) Insight into the role of integrated carbohydrate polymers (starch, chitosan, and β-cyclodextrin) with mesoporous silica as carriers for ibuprofen drug; equilibrium and pharmacokinetic properties. *Int. J. Biol. Macromol.* https://doi.org/10.1016/j.ijbiomac.2020.04.052

71 Hayashi, A., Kinoshita, K. and Miyake, Y. (1981) The Conformation of Amylose in Solution. I. *Polym. J.* **13**, 537–541 https://doi.org/10.1295/polymj.13.537

72 Comoglu, T. and Unal, B. (2015) Preparation and evaluation of an orally fast disintegrating tablet formulation containing a hydrophobic drug. *Pharm. Dev. Technol.* **20**, 60–64 https://doi.org/10.3109/10837450.2013.862636

73 Zhang, L., Cheng, H., Zheng, C., Dong, F., Man, S., Dai, Y., et al. (2016) Structural and release properties of amylose inclusion complexes with ibuprofen. *J. Drug Deliv. Sci. Technol.*, Elsevier Ltd **31**, 101–107 https://doi.org/10.1016/j.jddst.2015.12.006

74 Xiao, H., Lin, Q., Liu, G. Q., Wu, Y., Wu, W. and Fu, X. (2013) Inhibitory Effects of Green Tea Polyphenols on the Retrogradation of Starches from Different Botanical Sources. *Food Bioprocess Technol.* **6**, 2177–2181 https://doi.org/10.1007/s11947-011-0739-8

75 Sharma, T., Suresh Kumar, G., Chon, B. H. and Sangwai, J. S. (2014) Viscosity of the oil-in-water Pickering emulsion stabilized by surfactant-polymer and nanoparticle-surfactant-polymer system. *Korea Aust. Rheol. J.* **26**, 377–387 https://doi.org/10.1007/s13367-014-0043-z

76 Zeng, X., Zheng, B., Xiao, G. and Chen, L. (2022) Synergistic effect of

extrusion and polyphenol molecular interaction on the short/long-term retrogradation properties of chestnut starch. *Carbohydr. Polym.*, Elsevier Ltd **276**, 118731 https://doi.org/10.1016/j.carbpol.2021.118731

77 Qin, Y., Wang, J., Qiu, C., Hu, Y., Xu, X. and Jin, Z. (2019) Effects of Degree of Polymerization on Size, Crystal Structure, and Digestibility of Debranched Starch Nanoparticles and Their Enhanced Antioxidant and Antibacterial Activities of Curcumin. *ACS Sustain. Chem. Eng.* **7**, 8499–8511 https://doi.org/10.1021/acssuschemeng.9b00290

78 Li, J., Shin, G. H., Lee, I. W., Chen, X. and Park, H. J. (2016) Soluble starch formulated nanocomposite increases water solubility and stability of curcumin. *Food Hydrocoll.*, Elsevier Ltd **56**, 41–49 https://doi.org/10.1016/j.foodhyd.2015.11.024

79 Li, Y., Yang, Y., Zhu, S., Liu, B., Zhong, F. and Huang, D. (2023) Tea polyphenols-OSA starch interaction and its impact on interface properties and oxidative stability of O/W emulsion. *Food Hydrocoll.*, Elsevier Ltd **135**, 108187 https://doi.org/10.1016/j.foodhyd.2022.108187

80 Park, H. R., Rho, S. J. and Kim, Y. R. (2019) Solubility, stability, and bioaccessibility improvement of curcumin encapsulated using 4-α-glucanotransferase-modified rice starch with reversible pH-induced aggregation property. *Food Hydrocoll.*, Elsevier Ltd **95**, 19–32 https://doi.org/10.1016/j.foodhyd.2019.04.012

81 Mohan, P. R. K., Sreelakshmi, G., Muraleedharan, C. V. and Joseph, R. (2012) Water soluble complexes of curcumin with cyclodextrins: Characterization by FT-Raman spectroscopy. *Vib. Spectrosc.*, Elsevier B.V. **62**, 77–84 https://doi.org/10.1016/j.vibspec.2012.05.002

82 Wu, A., Fang, Z., Qin, J., Huang, Z. and Wu, Z. (2023) Characterization and adsorption-release property of fermented porous starch as well as its bioactivity protection for guava leaf polyphenols. *Food Biosci.*, Elsevier Ltd **53**, 102535 https://doi.org/10.1016/j.fbio.2023.102535

83 Oliveira, S. M., Gruppi, A., Vieira, M. V., Matos, G. S., Vicente, A. A., Teixeira, J. A. C., et al. (2021) How additive manufacturing can boost the bioactivity of baked functional foods. *J. Food Eng.* **294**

https://doi.org/10.1016/j.jfoodeng.2020.110394

84 Ghazal, A. F., Zhang, M. and Liu, Z. (2019) Spontaneous Color Change of 3D Printed Healthy Food Product over Time after Printing as a Novel Application for 4D Food Printing. *Food Bioprocess Technol.*, Food and Bioprocess Technology **12**, 1627–1645 https://doi.org/10.1007/s11947-019-02327-6

85 Li, X., Yue, X., Huang, Q. and Zhang, B. (2022) Effects of wet-media milling on multi-scale structures and in vitro digestion of tapioca starch and the structure-digestion relationship. *Carbohydr. Polym.*, Elsevier Ltd **284**, 119176 https://doi.org/10.1016/j.carbpol.2022.119176

86 Lefnaoui, S. and Moulai-Mostefa, N. (2015) Synthesis and evaluation of the structural and physicochemical properties of carboxymethyl pregelatinized starch as a pharmaceutical excipient. *Saudi Pharm. J.*, King Saud University **23**, 698–711 https://doi.org/10.1016/j.jsps.2015.01.021

87 De Brabander, C., Vervaet, C., Görtz, J. P., Remon, J. P. and Berlo, J. A. (2000) Bioavailability of ibuprofen from matrix mini-tablets based on a mixture of starch and microcrystalline wax. *Int. J. Pharm.* **208**, 81–86 https://doi.org/10.1016/S0378-5173(00)00549-4

CHAPTER 6

ADVANCED ANTIMICROBIAL WOUND DRESSING



6.1 Introduction 203

6.2 Experimental section 206

6.2.1 Synthesis of Cs-SH 206

6.2.2 Fluorescent labelling of Cs-SH 207

6.2.3 FITC-Cs-SH and curcumin loaded Cs-SH nanoparticle formation 208

6.2.4 Loading BC by vacuum filtration 209

6.2.5 In vitro FITC-Cs-SH nanoparticle and curcumin delivery 210

6.2.6 Adhesion force tests 212

6.3 Results and discussion

6.3.1 Characterization of Cs-SH nanoparticles 214

6.3.2 Vacuum filtration efficiency 216

6.3.3 In vitro release of FITC-Cs-SH nanoparticles and curcumin 218

6.3.4 Adhesion force tests 222
6.3.5 Antimicrobial tests 225
6.4 Conclusions 226
6.5 References 228

Chapter 6: Advanced antimicrobial wound dressing

6.1 Introduction

The excellent physicochemical properties and biocompatibility of BC make it an outstanding material for biomedicine. Applications related to skin/wound care or tissue engineering are particularly benefited by some of the characteristics of this biopolymer [1]. In this sense, BC and its composites provide cost-effectiveness, infection prevention, painless dressing removal, optimal gas diffusion, thermal management, and elimination of excess exudate [2].

Besides, despite the fact that BC does not naturally possess antimicrobial activity, its entangled nanofiber network structure has supported numerous research efforts to load antimicrobials, antioxidants, anti-inflammatory, and other therapeutic agents for wound-dressing applications [3, 4]. Indeed, BC is an excellent delivery system for transdermal administration, i.e., transmission of active compounds through the skin. Because of its water retention capacity and permeability, it has been used for the treatment of skin disorders for both medical and cosmetic purposes [5–7]. BC does not generate redness, irritation or inflammation and the BC network is penetrated by cellular ingrowth, which creates a new integrated tissue with the biomaterial [8]. Furthermore, BC has proven its suitability for skin, bone, cartilage and blood vessel repair, among others, demonstrating its complete biocompatibility [8–10]. All these reasons make BC an excellent vector for personalized medicine, especially for the controlled release of drugs that are difficult to handle independently in physiological conditions due to their poor solubility or rapid degradation.

The polyphenol 1,7-bis(4-hydroxy-3-methoxyphenyl)-1,6-heptadiene-3,5-dione, also known as curcumin, is extracted from the *curcuma longa* plant. Curcumin displays exceptional pharmacological properties and contains anti-bacterial, antioxidant, anti-Alzheimer, and anti-inflammatory properties [11–13]. Adhesion, migration, invasion, and spreading of malignant cancer cells have all been found to be inhibited by curcumin. In fact, malignant melanoma cells, breast, thyroid, colon, leukemia, prostate, lung, ovarian and pancreatic cancer cells have all been reported to be affected by the apoptosis induced by curcumin [14].

However, curcumin also presents important limitations as its low water solubility, alkaline degradability, quick metabolism, and rapid systemic excretion in bile and urine, leading to very low bioavailability [15]. It has even been reported that it is degraded after 30 minutes at physiological pH [16]. The most notable method for increasing curcumin's availability and solubility is its encapsulation and protection in polymers or nanoparticulate systems [17, 18].

Certainly, nanoparticle-based drug delivery systems have benefits such as drug protection, stability, controlled release, which increases drug specificity, efficacy, and minimize side effects, as well as enhanced cellular uptake, permeability, and retention effects [19]. One of the most often used biopolymers for creating nanoparticles is chitosan (Cs). Deacetylation of chitin yields a cationic biopolymer that is biocompatible, non-toxic, biodegradable, pH-sensitive, antimicrobial, antioxidant, and reasonably priced [20].

Moreover, Cs, which has amine and hydroxyl groups in its chain, can be modified to add additional molecules, ligands, or functional groups to produce a wide range of products. Functionalization with hydrophilic groups such as

thiol is one of the strategies to overcome one of the main disadvantages of Cs, the poor solubility in water and physiological conditions [21, 22].

Thiolated chitosan (Cs-SH) exhibits increased mucoadhesion and permeability as well, in addition to improved solubility, making it particularly effective for drug administration targeting mucus and keratinous biological surfaces [23]. The development of disulfide bridges between thiolated polymers and the cysteine-rich regions of mucins and keratin is associated with the enhanced adhesion of thiomers [21, 23]. The enhanced adherence increases its period in residence in the tissue, which improves the bioavailability of the drug [24]. A high drug concentration at the absorption site can result in a quicker diffusion due to the closer contact with the targeted tissue.

In this regard, taking advantage of the above explained properties of Cs-SH nanoparticles, curcumin and BC, the objective in this chapter was to combine them in a unique hybrid and active biomaterial as illustrated in Figure 6.1. To that end, Cs-SH nanoparticles encapsulating curcumin were firstly synthesized and then loaded into BC membranes by vacuum filtration. The release of these nanoparticles from the membrane was studied in physiological media at different pHs. In addition, morphological characterization of the membranes was performed to confirm the adsorption of the nanoparticles. The adhesion of the Cs-SH nanoparticle-loaded membranes on different tissues was also studied. Finally, the antimicrobial properties of the BC membranes loaded with the nanoparticles were tested.

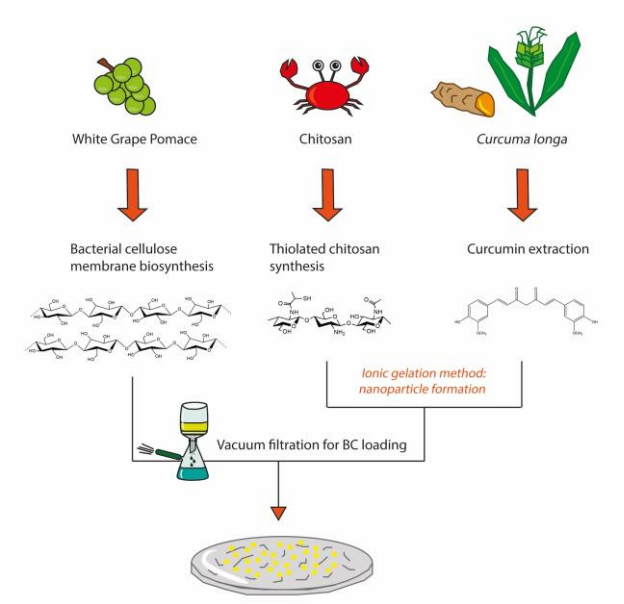

Figure 6.1 *Schematic representation of the research topic and experimental process of Chapter 6.*

6.2 Experimental section

6.2.1 Synthesis of Cs-SH

The functionalization of Cs with thiol groups was completed by amide coupling conjugation with TLA, following previous work developed by this group (Scheme 6.1) [25]. Briefly, Cs was dissolved in 2% (v/v) aqueous HAc until a final concentration of 0.5% (w/v). TLA was activated with EDC and NHS in 1:1 and 1:1.1 M ratios, respectively, while the amine-to-carboxylic acid molar ratio (Cs:TLA) was maintained at 1:1. Then, this second solution was added dropwise to the Cs solution previously alkalinized to pH 5-6 with 1 M NaOH. The mixture was then agitated in the dark at room temperature for 16 hours. Since the pH of the medium affects the thiolate anions concentration [31], the synthesis was carried out at a pH between 5 and 6 to prevent the formation of disulfide

bridges between the polymeric chains. After the reaction time, the resulting products were dialyzed against 5mM HCl solution at 4ºC for 7 days, using Spectra/Por™ 2RC dialysis membranes (molecular weight cut-off 12–14 kDa). Finally, the Cs-SH was lyophilized and collected at 4ºC until further use.

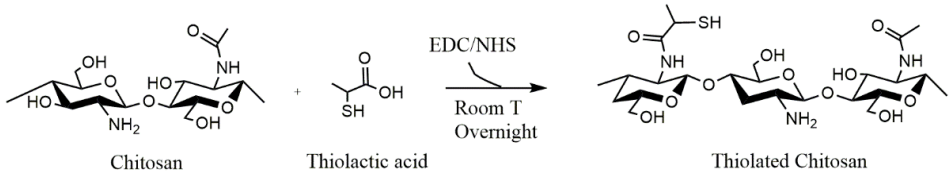

Scheme 6.1 *Schematic diagram of the synthesis of thiolated chitosan (Cs-SH).*

6.2.2 Fluorescent labeling of Cs-SH

The Cs-SH was labeled by the reaction between the main amino group of Cs and the isothiocyanate group of FITC to enable future nanoparticle release monitoring using fluorescent spectroscopy (Scheme 6.2), following the procedure published by Moussa et al with some modifications [26].

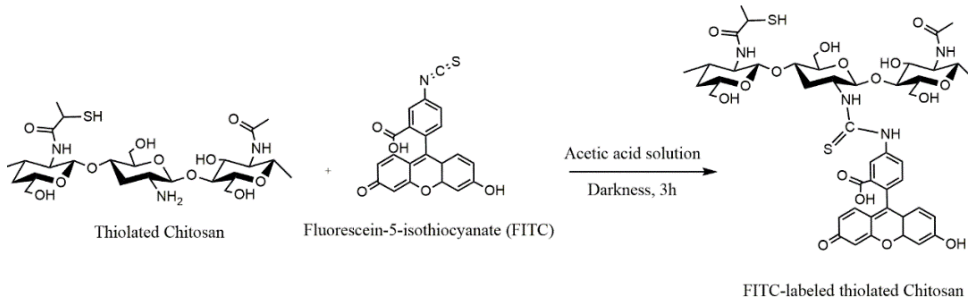

Scheme 6.2 *Schematic diagram of the synthesis of FITC-labeled thiolated chitosan (FITC-Cs-SH).*

In brief, 40 mg of FITC were dissolved in 40 mL dehydrated methanol and it was added to 40 mL of 1% w/v Cs-SH in acetic acid solution. After 3 hours of reaction in the dark and at room temperature, the FITC-labeled Cs-SH (FITC-Cs-

SH) was precipitated by increasing the pH to 10 with 0.5 M NaOH. The unreacted FITC was removed by centrifugation and subsequent rinse with acetone until fluorescence was not visible in the supernatant. As shown in Figure 6.2, successive photographs were taken with a digital camera (Canon PC1564) under ultraviolet light to observe the fluorescence of the supernatants. Finally, the precipitate was resuspended in 40 mL of water, and dialyzed in 4 L of periodically replaced water for 2 days in darkness.

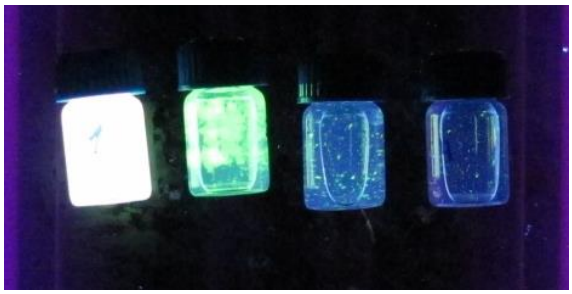

Figure 6.2 *UV photographs of supernatants from successive acetone washes to FITC-labeled Cs-SH.*

6.2.3 FITC-Cs-SH and curcumin loaded Cs-SH nanoparticles formation

The nanoparticles were obtained by ionotropic gelation following the procedure published by Calvo et al with some modifications [27]. First, a FITC-Cs-SH or Cs-SH solution was prepared (0.5 mg/mL) in HAc 2% (w/w) (pH=3). Curcumin loaded nanoparticles were prepared by the addition of curcumin containing ethanol solution (0.2 mg/mL) to the Cs-SH acidic solution to a final Cs:Curcumin 10:1 w/w ratio and stirred for 30 minutes. Then, TPP aqueous solution (0.8 mg/mL) at pH=3 (adjusted with 10 % HAc) was added dropwise to the FITC-Cs-SH or the curcumin containing Cs-SH solutions, leading to a final

Cs:TPP ratio of 1.5:1 w/w. The process was carried out under constant stirring and at room temperature (1h at 1200 rpm). Finally, the Cs-SH, FITC-Cs-SH or curcumin loaded Cs-SH (Cur-Cs-SH) nanoparticles were collected after three cycles of centrifugation (14000 rpm, 1 h) washing with water, and then lyophilized.

The curcumin loading (CL) was determined from the disruption of curcumin-loaded and freeze-dried nanoparticles in ethanol. 2 mg of curcumin loaded nanoparticles were dissolved in 2 mL of ethanol. All tubes were then shaken vigorously for 12 h for complete disruption of the nanocarriers and then the nanoparticles were separated by ultracentrifugation (1h, 14000 rpm). The curcumin content was determined by UV-VIS at 429.5 nm, based on the calibration curve (500-0,1 ppm, R^2=0.9979). All measurements were performed in triplicate. The CL (%) of the nanoparticles was calculated according to the following equation:

$$CL\ (\%) = \frac{W_{Cur}}{W_T} \cdot 100 \qquad \text{(Equation 6.1)}$$

where W_{Cur} is the weight of curcumin into the nanoparticles and W_T is the total weight of the nanocarriers.

6.2.4 Loading BC by vacuum filtration

The nanoparticle dispersions at concentrations of 0.35 mg/mL were forced to pass through the BC membranes by vacuum filtration. Figure 6.3 depicts a schematic representation of the method. Fluorescence of the filtered liquid was measured and correlated it to the retention yield of the membranes using a previously constructed calibration curve of FITC in an aqueous medium.

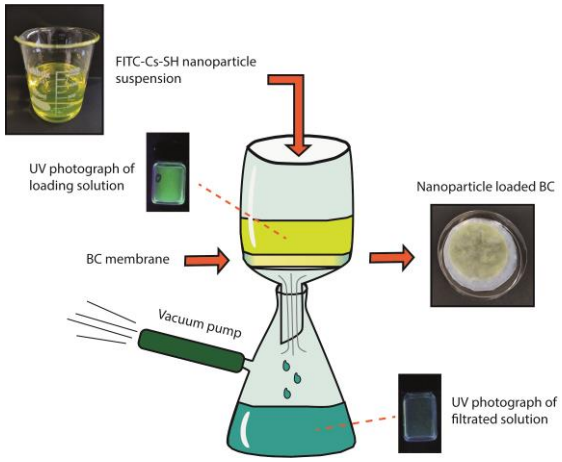

Figure 6.3 *Schematic representation of the vacuum filtration process followed in this chapter for BC loading.*

6.2.5 In vitro FITC-Cs-SH nanoparticle and curcumin delivery

6.2.5.1 FITC-Cs-SH nanoparticle release

Different volumes (30 and 50 mL) of FITC-Cs-SH nanoparticle dispersions of 0.35 mg/mL were used to observe the loading influence on the subsequent release kinetics. The BC samples loaded with 30 mL and 50 mL are referred in this chapter as 30BCnp and 50BCnp, respectively.

First, 12 mm biopsy punches were prepared with the AcuPunch histological tool from 30BCnp and 50BCnp membranes. The release of the FITC-Cs-SH nanoparticles was performed in a thermostat incubator at 50 rpm. The temperature was maintained at 30 ºC and 37 ºC in PBS release media at pH 5.5 and pH 7.4, respectively, with the aim to simulate different physiological conditions of the human body.

In addition, unloaded BC punches were used as controls to discard any residue from the biosynthesis process that could interfere in the fluorescence detection. The number of nanoparticles of each BC punch was estimated from the vacuum filtration yield and BC membrane area. During 2 weeks, 1 mL of the release medium was taken at different times and the fluorescence was measured. All measurements were performed in triplicate and the concentration in the release medium was calculated from calibration curves previously carried out with FITC-Cs-SH nanoparticles in PBS 5.5 and 7.4 (500-0.5 µg/mL, R^2=0.9994 and R^2=0.9986, respectively).

The nanoparticle cumulative release (NCR) (%) was calculated as described in equation 6.2:

$$NCR\ (\%) = \frac{C_{np}}{C_T} \cdot 100 \qquad \text{(Equation 6.2)}$$

where C_{np} is the concentration of FITC-Cs-SH nanoparticles in the release media and C_T is the total concentration of FITC-Cs-SH nanoparticles expected for each biopsy punch.

6.2.5.2 Curcumin release from Cur-Cs-SH nanoparticles

In addition to measure the nanoparticle release from BC membranes, the curcumin release from the nanoparticles was also studied. Briefly, 2 mg of Cur-Cs-SH were suspended separately into 4 mL of PBS buffer at different pH values (5.5 and 7.4) and kept at 37 °C in thermostat incubator with agitation (180 rpm). After certain time intervals, the solutions were centrifuged at 14000 rpm for 1 h and the supernatants were periodically removed from the samples and replaced by fresh buffer. Curcumin was used as UV-Vis standard (500-0.1 ppm, R^2=0.9948) and the amount of released curcumin was quantified by

UV/Vis spectrophotometer at 429.5 nm. All data reported herein were the average of three independent measurements. The curcumin cumulative release (CCR) was calculated as described in equation 6.3:

$$CCR\ (\%) = \frac{Q_{Cur}}{Q_0} \cdot 100 \qquad \text{(Equation 6.3)}$$

Where Q_{Cur} is the quantity of curcumin in the release media and Q_o is the quantity of curcumin calculated for the Cur-Cs-SH nanoparticles.

6.2.6 Adhesion force tests

The adhesion strength of Cur-Cs-SH loaded BC membranes was compared to that of bare BC. As in the drug release study, 30BCnp and 50BCnp samples were chosen to assess their adhesion to different surfaces. The procedure was designed according to some of the guidelines published by Da Silva et al for the mucoadhesion study of polymeric systems [28].

The adhesive properties of the membranes were examined using a TA-XTplusC texture analyzer (Stable Micro Systems, Surrey, UK). 200 mg of mucin from porcine stomach were compressed into disks of 13 mm diameter with a hydraulic press. Compression time and force were 30 seconds and 10 tones, respectively. In addition, porcine skin was acquired from a local butcher for the study of membrane adhesion to keratin-containing tissues, such as human skin [29]. The pig skin was cut into rectangles of 3.0 cm by 2.0 cm, and they were then frozen for further use. Samples with wounds or bruises were discarded. The assays were performed at room temperature and the skin fat was manipulated to maintain a uniform thickness of 3 mm.

After, using double-sided adhesive tape, unloaded and Cur-Cs-SH loaded BC punches of 12 mm were horizontally attached to a cylindrical P/0.5R probe. The mucin disk and skin tissue were hydrated prior to testing by immersion in PBS at pH 7.4 and pH 5.5 for 30 s, respectively. Subsequently, the surface liquid was gently removed and the mucin discs or the porcine skin were placed on the base. The descending speed of the probe was set at 1 mm/s until it reached the surface of the mucin disks/pig skin fragment. The probe stayed for 30 s on the surface of the tissues applying a downward force of 0.03 N. Then, the probe was detached at an ascending speed of 10 mm/s.

The detachment force (F*, N*) and work (W*, N·s*) were calculated with the Exponent Connect 8040 software (Stable Micro Systems, Surrey, UK). The Figure 6.4 summarizes a schematic representation of the adhesion force test. All the measurements were carried out with at least five replicates.

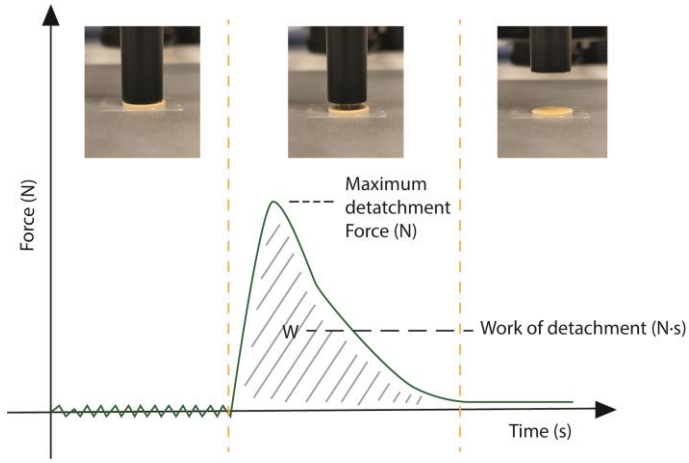

Figure 6.4 *Schematic representation of the mucoadhesive test with nanoparticle-loaded BC and mucin disks.*

6.3 Results and discussion

6.3.1 Characterization of Cs-SH nanoparticles

The synthesis of Cs-SH was conducted by carbodiimide mediated amide coupling between the -NH_2 groups of Cs and the activated carboxylic group of TLA as detailed in Figure 6.1. Cs modification was successfully confirmed by the ninhydrin test with a DS calculated to be 52% (Equation 2.3) [25].

In this chapter, Cs-SH nanoparticles were synthesized using TPP as crosslinker to study their potential application as curcumin encapsulating agents. Hydrodynamic diameter and polydispersity index measurements were conducted by DLS immediately after the preparation of the nanoparticles under acidic conditions (pH=3). The size of nanoparticles is a key factor for their use in the biomedical field, particularly in drug delivery applications. It is known that the limit for passage through the cell membrane via non-energetic endocytosis is 200 nm [22]. The Cs-SH nanoparticles synthesized in this study showed a proper size of 121 ± 2 nm and a low polydispersity index of 0.24, whereas a hydrodynamic diameter of 152 ± 6 nm and polydispersity index of 0.35 were measured for Cur-Cs-SH nanoparticles. These results confirmed the suitability of the method as well as the chosen Cs:TPP ratio. Furthermore, the slightly larger size of the Cur-Cs-SH nanoparticles comparing with Cs-SH nanoparticles, suggested a successful encapsulation of the bioactive polyphenol and was in agreement with previously published diameters of curcumin encapsulating nanoparticles [30, 31]. In fact, the CL (%) of the Cur-Cs-SH nanoparticles was calculated (equation 6.1), and it was found to be 8.40 ± 0.22 %. This value was consistent with reported literature [30, 32, 33].

Cur-Cs-SH nanoparticle dispersion was further analyzed by AFM to observe their morphology and size in the dry state. As observed in Figure 6.5, the sample presented spherical nanoparticles and no aggregates were detected, showing all the particles a diameter of less than 50 nm (27-48 nm).

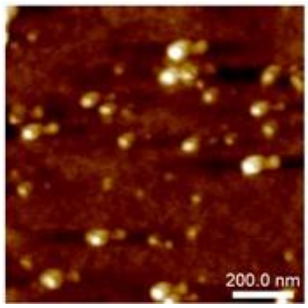

Figure 6.5 *AFM height micrograph of Cur-Cs-SH nanoparticles.*

Finally, the colloidal stability under different conditions is essential for a drug nanocarrier. Thus, the size and Z potential of the prepared Cs-SH and Cur-Cs-SH nanoparticles at different pHs were studied. Figure 6.6 shows the influence of increasing the pH from 3 to 8.5 on the hydrodynamic diameter and the Z potential values of the nanoparticles.

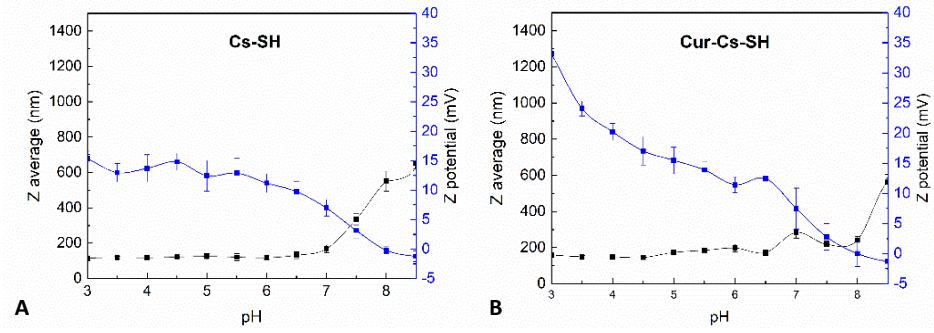

Figure 6.6 *Hydrodynamic diameter (Z average) and Z potential variation with pH for (**A**) Cs-SH and (**B**) Cur-Cs-SH nanoparticles.*

Overall, the results showed similar stable behavior regarding the nanoparticle size. Namely, both Cur-Cs-SH and Cs-SH did not form aggregates or increase in size below pH=7.5. Besides, since the pKa of the amino group of Cs is 6.5, above this pH they should be deprotonated and, consequently, the neat charge of the molecule would be 0. The absence of repulsive forces would provoke the subsequent aggregation and precipitation of the nanoparticles [34].

In this case, the Cs-SH nanoparticles maintained their size up to pH=7, because of the greater stability of the thiolated derivative at higher pHs [21, 35]. Equally, in Cur-Cs-SH dispersions, polymer-polyphenol interactions would further prevent the aggregation of the loaded nanoparticles up to pH=7.5-8. This phenomenon could be related to both hydrophobic and hydrogen bonding interactions between the Cs chains and curcumin [33, 36].

With regards to Z potential value, curcumin loaded nanparticles showed slightly higher Z potential. In both cases, the value decreased as the pH increased, registering the isoelectric point at pH=8. As pH increased, repulsive electrostatic forces decreased, affecting intramolecular and intermolecular interactions and leading to loss of colloidal stability and aggregates [37]. The results confirmed that, these nanoparticles were more stable and showed smaller sizes at acid pH-s as it has been reported before for Cs nanoparticles [38].

6.3.2 Vacuum filtration efficiency

The nanoparticle retention capacity of BC membranes was quantified by measuring the remaining fluorescence of the filtrate at 486 nm excitation and 515 nm emission wavelengths. Concretely, fluorescence of solutions with an

initial concentration of 0.35 mg/mL of FITC-Cs-SH nanoparticles was measured after the vacuum filtration through the BC membrane. According to the obtained values, FITC-Cs-SH concentration decreased to 3.2 ± 1.6 µg/mL after the retention process what corresponded to 99 % nanoparticle retention yield after 45 minutes of vacuum.

The presence of the nanoparticles was confirmed by AFM images in Figure 6.7. Figures 6.7B and 6.7C demonstrate the successful nanoparticle loading in both 30BCnp and 50BCnp membranes, respectively, with the nanofiber network being completely covered by nanoparticles, in contrast to the bare BC membrane shown in Figure 6.7A.

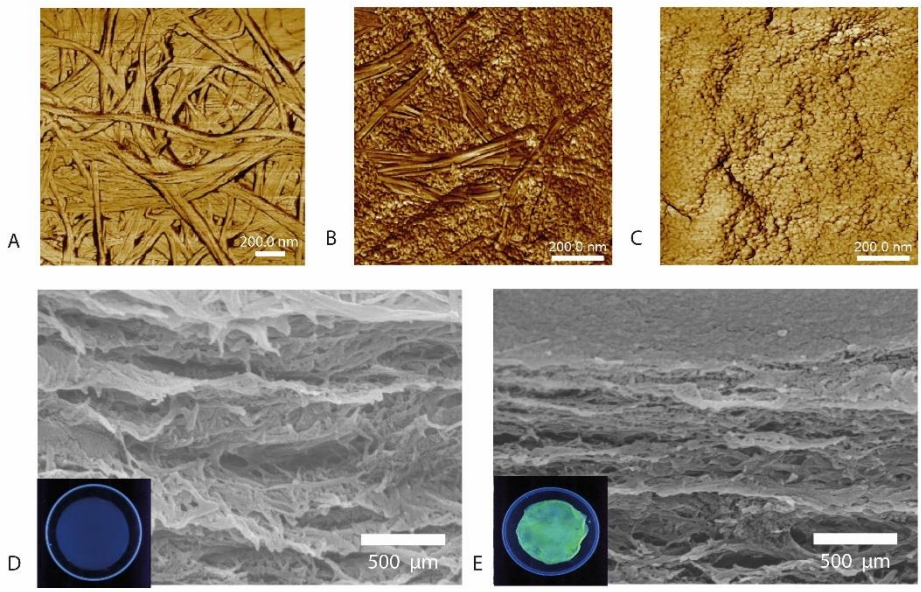

Figure 6.7 *From left to right, AFM phase images of BC, 30BCnp and 50BCnp samples after filtration process (**A**, **B** and **C**). SEM images with miniature UV light photography of unloaded BC and BC loaded with FITC-Cs-SH nanoparticles (**D** and **E**, respectively).*

Due to their finely interconnected porous network, BC membranes demonstrated high efficiency in serving as supports for the filtration and confinement of nanoscale particles, as previously reported [39–41]. Besides, SEM images of the membranes verified the successful distribution of the nanoparticles throughout the membrane in Figures 6.7D and 6.7E. Lastly, the photographs taken under UV light confirmed the homogeneous fluorescence of the BC with FITC-Cs-SH nanoparticles, in contrast to the unloaded BC, as shown in Figure 6.7D and 6.7E.

6.3.3 In vitro release of FITC-Cs-SH nanoparticles and curcumin

6.3.3.1 Release of FITC-Cs-SH nanoparticles

Understanding and controlling release kinetics is especially important when encapsulating drugs that could be cytotoxic above certain concentrations [42–44]. Accordingly, the FITC-Cs-SH loading of BCs was determined based on the CL (%) of the nanoparticles, in order to avoid potential cytotoxic concentrations of curcumin reported in literature [45].

The advantage of using FITC-labeled nanoparticles is that fluorescence can be measured with great sensitivity over wide concentration ranges [46, 47]. It is worth noting that the size of FITC-Cs-SH nanoparticles was very similar to that of Cur-Cs-SH nanoparticles when analyzed by DLS. Namely, they exhibited a Z average of 169 ± 7 nm and a polydispersity index of 0.26.

The release of FITC-Cs-SH nanoparticles from the BC punches at pH 5.5 and pH 7.4 was monitored as depicted in Figure 6.8. Two PBS solutions were used to

simulate different human body conditions, such as, several mucous tissues, or skin wounds (pH=7-8), and skin (pH=4-6), among others [48–51].

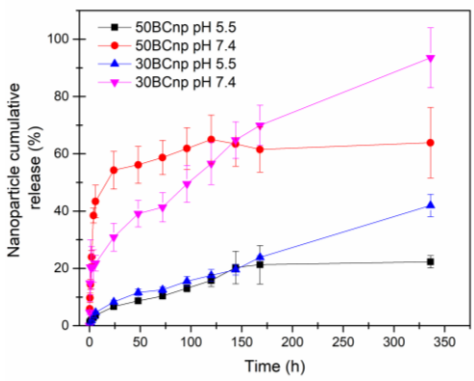

Figure 6.8 *FITC-Cs-SH nanoparticle cumulative release from 30BCnp and 50BCnp samples at pH 5.5 and 7.4 release media.*

Attending to the results in Figure 6.8, it can be observed that the release at pH 7.4 was faster and to a greater extent than that registered at pH 5.5 irrespective of the FITC-Cs-SH loading in the membrane. This could be related to the stability and electric charge of the nanoparticles measured by DLS at different pHs. As detailed before, at pH 5.5 the Cs-SH nanoparticles possessed some charge and stable size that could favor the interaction with cellulose and thus better penetrate the nanofiber network. These interactions between glucan chains, coming from the similarity of polysaccharide structures of Cs and BC, would favor retention in the membrane and delay its release to the medium [52]. Hence, at pH 5.5 a slower sustained release of FITC-Cs-SH was observed during the two weeks, reaching NCR values of 42 % and 22 % for the 30BCnp and 50BCnp, respectively. Additionally, the results showed that a smaller volume of nanoparticle loading solution increased the FITC-Cs-SH long-

term release. Whereas higher loading volumes reached the maximum value of NCR approximately at the end of the first week (168 h).

In this way, the liberation curves indicated that the higher nanoparticle initial concentration in the BC, the greater the final amount of FITC-Cs-SH retained in the membrane. Therefore, the release profile of nanoparticles could be controlled at pH 5.5 by adjusting the volume of the initial loading solution. This finding was also observed by Li et al and Wu et al when they studied the sustained release of silver nanoparticles from the BC [43, 44].

On the other hand, the FITC-Cs-SH release profile at pH 7.4 showed relevant different behavior than that at pH 5.5. Indeed, burst release was noticed when the loaded punches were submerged in PBS in this case, which could be associated to the release of nanoparticles placed on the surface and to the loosen of the immersed membrane after the packing effect of the vacuum filtration process [14, 53, 54]. This loosen phenomenon also occurred at pH 5.5, but as previously mentioned, the stability of the nanoparticles decreased above pH 7 thus provoking the easier release to the medium. From this point, the BC punches with different initial loads followed distinct release rates at same pH. It is worth noting that the release rate from 50BCnp samples after 6 h did not increase considerably, reaching a maximum NCR value of 57% in two weeks. These results are consistent with those published by Numata et al that registered maximum delivery rates of 60 % in 6 hours with retinol-loaded PEO-b-PCL nanoparticles nanoparticle released from BC [55]. The release kinetics observed in our study were comparable to the hyperbolic curves of doxorubicin release from $CaCO_3$ microparticles-BC published by Cacicedo et al, in which the drug release was highly influenced by the pH and the chemical stability of the $CaCO_3$ crystals [53].

On the contrary, after the first 5 h of burst release, 30BCnp samples released nanoparticles in a sustained manner until the 93% of NCR in two weeks (Figure 6.8). Hence, as in the case of PBS 5.5, BC punches with lower initial FITC-Cs-SH concentration showed sustained release until the end of the 2-week study period. Then, results in Figure 6.8 suggested that a higher initial charge of nanoparticles decreased the final NCR, as observed for pH 5.5. In this context, it was concluded that the influence of membrane loading would be a topic of future research, where an approach should be adopted considering its subsequent release of curcumin.

6.3.3.2 Curcumin release from Cur-Cs-SH nanoparticles

The release profile of curcumin from nanoparticles was investigated over a period of 240 h in PBS pH 7.4 and PBS pH 5.5 solutions, as represented in Figure 6.9.

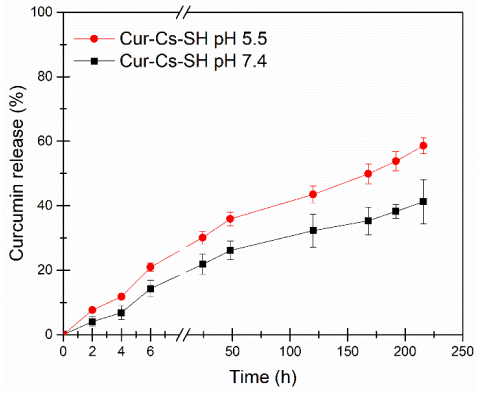

Figure 6.9 *In vitro curcumin cumulative release profile of Cur-Cs-SH nanoparticles at pH 5.5 and pH 7.4.*

In general, a sustained release profile was observed, characterized by a slow and lineal increase of curcumin concentration. This sustained release probably

resulted from the diffusion of the drug through the nanoparticle and the slow degradation of the carrier matrix [56]. This liberation model of Cs-based nanoparticles has been previously reported for various drugs, including curcumin [13, 32]. The limited and gradual release has been related to the poor solubility of curcumin in aqueous media, thus hindering its transport from the nanoparticles [21, 32]. For this reason, the increased hydrophilic nature of Cs-SH was beneficial, it facilitated the medium to penetrate and free the drug [63].

Regarding the pH of release media, the achieved CCR after 240 h was lower at pH 7.4 than at pH 5.5, 60 % and 40 % respectively, in accordance with reported literature [30]. Besides, these CCR values were higher than the previously reported drug release percentages for BC films directly loaded with curcumin, demonstrating the effectiveness of its encapsulation [14, 17], and similar to those published by other authors with different drugs released from Cs-SH derivative [57, 58]. Indeed, as explained before, at lower pH the protonation of amino groups (NH_2) results in higher electrostatic repulsion, facilitating the curcumin release.

6.3.4 Adhesion force tests

The adhesive properties of a matrix designed for drug release have noteworthy influence on improving accurate delivery to cells and accelerating the recovery of damaged tissues [59, 60]. Mucin disks and porcine skin were selected as target tissues to mimic mucosal tissues (pH 7.4) and human skin (pH 5.5) surfaces, respectively. In fact, compared to other animals, pigs have a higher degree of anatomical, physiological, metabolic, and histological similarities [61, 62].

As already explained in Figure 6.4, the detachment work (W), defined as the area under force vs time curve, and the maximum detachment force (F) of loaded BC and unloaded BC membranes were calculated. The obtained results are represented in Figure 6.10.

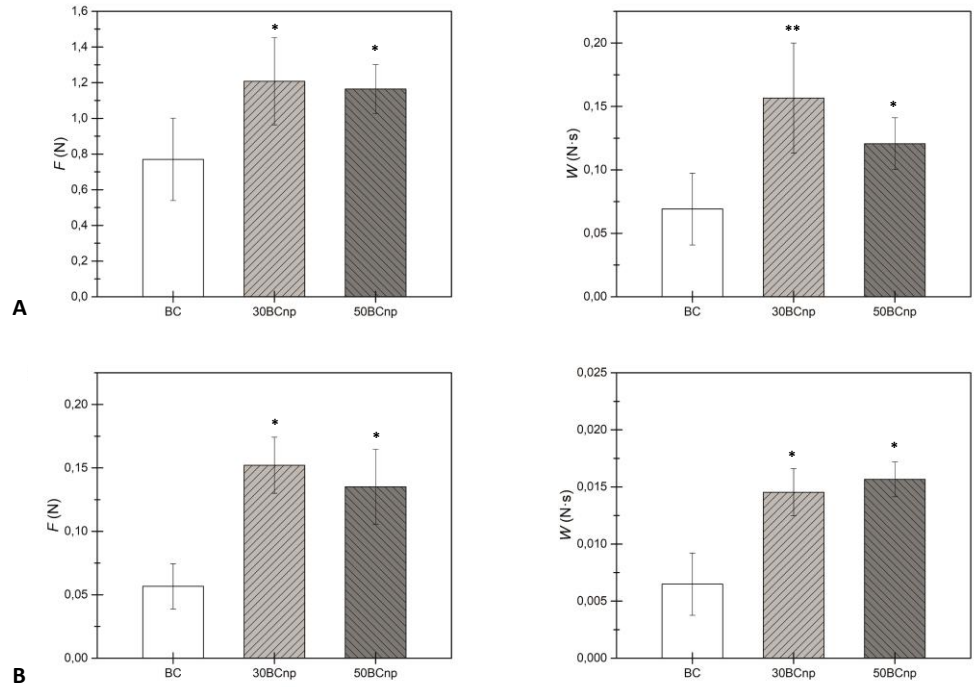

Figure 6.10 *The adhesion-force test carried out with BC, 30BCnp and 50BCnp samples on mucin disks (**A**) and porcine skin (**B**) at pH 7.4 and pH 5.5, respectively. (*) Refers to the statistically significant difference with the BC punch without nanoparticles. (**) Refers to the statistically significant difference between the two nanoparticle-loaded BCs.*

In the case of mucoadhesion tests (Figure 6.10A), the samples loaded with nanoparticles showed significantly higher F and W values in both cases in comparison to unloaded BC punches. The mucoadhesiveness enhancement was attributable to the disulfide bond formation between the thiol groups of

the Cs-SH and the cysteine residues of mucin glycoproteins [18, 23, 63, 64]. Moreover, the presence of curcumin may play an additional role in adhesion improvement via H-bonding and π-π interaction with mucus glycoproteins as suggested by some authors [65].

As observed with the concentration of Cur-Cs-SH nanoparticles, the detachment W values of the 30BCnp values were significantly higher than those obtained for the 50BCnp. The higher W could be related to the better dispersion and absence of aggregates within the BC of the less loaded samples. Barthelmes et al. studied the mucoadhesiveness of Cs-SH micro and nanoparticles and showed that, due to the increased surface area of the nanoparticles, mucin contact and adhesiveness were enhanced [66]. Considering that the test was carried out at pH 7.4 and in line with the in vitro nanoparticle release results, the possible presence of larger aggregates would decrease the surface area of the nanoparticles and, consequently, diminish their effective interactions with glycoproteins.

With regards to skin adhesion capacity, several authors had reported adhesion enhancement of chitosan by the incorporation of thiol moieties [24, 60]. According to the results in Figure 6.10B, the Cur-Cs-SH-loaded BC punches showed significantly higher F and W adhesion values to porcine skin than the unloaded BC suggesting again the formation of disulfide bridges between the Cs-SH and skin keratinocytes [67].

In this context, the F and W absolute values were lower than in the mucoadhesion tests, probably due to the reduced amount of accessible cysteine residues in porcine skin in comparison to mucin disks. In this assay, no differences were observed in the adhesion of BCs with different nanoparticle

loadings. It is worthy to note that in this case the porcine skin surfaces were immersed in pH 5.5 to model skin conditions, preventing the formation of Cur-Cs-SH aggregates that would decrease the surface area [68, 69].

Regarding the absolute values of F and W obtained in the study, it is difficult to compare them with other previous works due to the lack of standardization of the mucoadhesion tests [28]. However, in this work the loading of Cur-Cs-SH nanoparticles significantly increased the adhesion of BC membranes to simulated mucosal and dermal surfaces. These thiolated nanoparticles prolonged the residence time, led to higher drug concentration at the mucosal surface and thus the bioavailability.

6.3.5 Antimicrobial tests

The presence of opportunistic microbes has the potential to hinder the reparative and regenerative phases in healing processes, preventing the restoration of the anatomical and physiological integrity and resulting in chronic nonhealing wounds [70, 71]. Therefore, the antimicrobial activity of Cur-Cs-SH-loaded BC membranes was studied using an agar diffusion test against *S. aureus* and *E. coli*, as observed in Figure 6.11.

Figures 6.11A and 6.11B show ≈1 cm^2 30BCnp films with a clear halo of *S. aureus* and *E. coli* growth inhibition after 24 hours of incubation, respectively. This antimicrobial capacity may be attributed to the combined activity of Cs-SH and the curcumin diffused into the agar during the 24-hour study period.

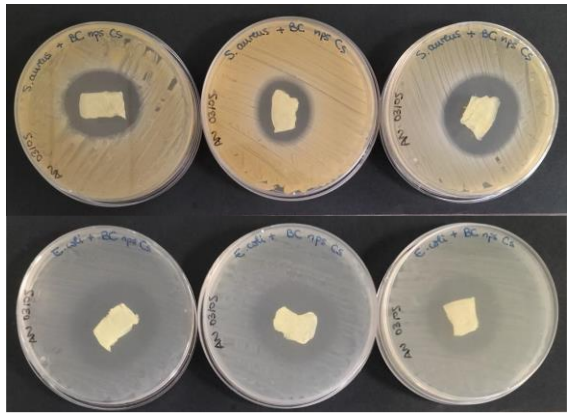

Figure 6.11 *Antimicrobial agar diffusion assay results for 30BCnp samples against S. aureus (**A**) and E. coli (**B**) at 24 h in triplicate.*

Attending to the results, it was hypothesized that Cs-SH nanoparticles enhance the effectiveness of the encapsulated polyphenol in such assays due to the difficulty of curcumin to diffuse through the agar medium [14, 72]. In fact, as mentioned in the introduction section, curcumin is a widely recognized bioactive compound. Given its lipophilic and amphiphilic molecular structure, curcumin binds to the bacterial cell wall, affecting its permeability and ultimately leading to cell lysis [73].

Additionally, as observed in Figure 6.11, it can be asserted that Cur-Cs-SH nanoparticles not only possess antimicrobial properties but also prevent bacterial adhesion and subsequent biofilm formation on BC [14, 74]. Certainly, it has been reported that Cs-SH can act as both gram-positive and gram-negative bacterial growth inhibitor, sometimes more effectively than Cs itself [75, 76]. Therefore, given the biocompatibility of BC, this type of combined antimicrobial strategy is promising for applications such as wound dressings or tumor treatment.

6.4 Conclusions

BC membranes, as exceptional biopolymers, have displayed promising potential in wound healing and tissue engineering owing to their remarkable biocompatibility across various tissues and physiological conditions. Nonetheless, their complete application in biomedicine is limited by two key challenges. Firstly, the hydrophilic nature of BC hinders the handling and delivery of lipophilic drugs. Secondly, the inherent adhesion capacity of BC could require modifications to enhance its adherence to target tissues.

This study involved the synthesis and characterization of Cur-Cs-SH nanoparticles integrated into BC membranes using vacuum-assisted filtration. Analytical techniques such as ninhydrin test confirmed the successful modification of 52% of Cs amines with thiol groups. The addition of thiol groups not only endowed Cs with supplementary adhesive properties but also increased its solubility in aqueous media. Furthermore, the encapsulation of the lipophilic drug curcumin, known for its antioxidant, antimicrobial, and anticancer attributes, during the nanoparticle synthesis process, was also achieved.

The results from DLS revealed the suitability of the ionic gelation method and the chosen Cs:TPP ratio. Cs-SH nanoparticles exhibited a size of 121 ± 2 nm, while Cur-Cs-SH nanoparticles were slightly larger at 152 ± 6 nm. Stability studies demonstrated the formation of stable nanoparticles within a wider pH range due to the presence of thiol groups and encapsulated curcumin, preventing aggregation or changes in hydrodynamic diameter until a pH above 7.5.

The effectiveness of BC as a matrix for nanoparticle retention was confirmed by the vacuum-assisted filtration process, achieving a close to 99% nanoparticle absorption rate within 45 minutes. In vitro release studies exhibited a pH and initial loading-dependent release profile, with the release kinetics controllable through the initial charge of FITC-Cs-SH in the BC. Both 30BCnp and 50BCnp samples demonstrated significantly higher adhesion values than the control BC on mucin disks and porcine skin, indicating the potential of Cs-SH nanoparticles to enhance the performance of BC in human mucous membranes and skin tissues.

The antimicrobial nature of the BC30np membranes was confirmed through agar diffusion tests, showcasing clear antibacterial activity against *S. aureus* and *E. coli*. Overall, the successful encapsulation of curcumin into Cs-SH nanoparticles and their integration into BC membranes resulted in a sustained release of curcumin, which can be crucial in controlling cytotoxic concentrations and delivering curcumin to specific human cells effectively.

In this chapter, the bioavailability of curcumin was increased by encapsulating it in Cur-Cs-SH nanoparticles, which in turn provided antimicrobial properties and enhanced adhesion of BC membranes, thereby expanding their applications in biomedicine.

6.5 References

1 Blanco Parte, F. G., Santoso, S. P., Chou, C. C., Verma, V., Wang, H. T., Ismadji, S., et al. (2020) Current progress on the production, modification, and applications of bacterial cellulose. *Crit. Rev. Biotechnol.*, Taylor & Francis **40**, 397–414 https://doi.org/10.1080/07388551.2020.1713721

2 Sulaeva, I., Henniges, U., Rosenau, T. and Potthast, A. (2015) Bacterial

cellulose as a material for wound treatment: Properties and modifications: A review. *Biotechnol. Adv.*, Elsevier Inc. **33**, 1547–1571 https://doi.org/10.1016/j.biotechadv.2015.07.009

3 Barja, F. (2021) Bacterial nanocellulose production and biomedical applications. *J. Biomed. Res.* **35**, 310–317 https://doi.org/10.7555/JBR.35.20210036

4 Zmejkoski, D., Spasojević, D., Orlovska, I., Kozyrovska, N., Soković, M., Glamočlija, J., et al. (2018) Bacterial cellulose-lignin composite hydrogel as a promising agent in chronic wound healing. *Int. J. Biol. Macromol.* **118**, 494–503 https://doi.org/10.1016/j.ijbiomac.2018.06.067

5 Fernandes, I. de A. A., Maciel, G. M., Ribeiro, V. R., Rossetto, R., Pedro, A. C. and Haminiuk, C. W. I. (2021) The role of bacterial cellulose loaded with plant phenolics in prevention of UV-induced skin damage. *Carbohydr. Polym. Technol. Appl.* **2**, 100122 https://doi.org/10.1016/j.carpta.2021.100122

6 Perugini, P., Bleve, M., Cortinovis, F. and Colpani, A. (2018) Biocellulose masks as delivery systems: A novel methodological approach to assure quality and safety. *Cosmetics* **5** https://doi.org/10.3390/cosmetics5040066

7 Morais, E. S., Silva, N. H. C. S., Sintra, T. E., Santos, S. A. O., Neves, B. M., Almeida, I. F., et al. (2019) Anti-inflammatory and antioxidant nanostructured cellulose membranes loaded with phenolic-based ionic liquids for cutaneous application. *Carbohydr. Polym.*, Elsevier **206**, 187–197 https://doi.org/10.1016/j.carbpol.2018.10.051

8 Scherner, M., Reutter, S., Klemm, D., Sterner-Kock, A., Guschlbauer, M., Richter, T., et al. (2014) In vivo application of tissue-engineered blood vessels of bacterial cellulose as small arterial substitutes: Proof of concept? *J. Surg. Res.*, Elsevier Inc **189**, 340–347 https://doi.org/10.1016/j.jss.2014.02.011

9 Pang, M., Huang, Y., Meng, F., Zhuang, Y., Liu, H., Du, M., et al. (2020) Application of bacterial cellulose in skin and bone tissue engineering. *Eur. Polym. J.*, Elsevier **122**, 109365 https://doi.org/10.1016/j.eurpolymj.2019.109365

10 Svensson, A., Nicklasson, E., Harrah, T., Panilaitis, B., Kaplan, D. L.,

Brittberg, M., et al. (2005) Bacterial cellulose as a potential scaffold for tissue engineering of cartilage. *Biomaterials* **26**, 419–431 https://doi.org/10.1016/j.biomaterials.2004.02.049

11 Portes, E., Gardrat, C., Castellan, A. and Coma, V. (2009) Environmentally friendly films based on chitosan and tetrahydrocurcuminoid derivatives exhibiting antibacterial and antioxidative properties. *Carbohydr. Polym.*, Elsevier Ltd **76**, 578–584 https://doi.org/10.1016/j.carbpol.2008.11.031

12 Peng, S., Li, Z., Zou, L., Liu, W., Liu, C. and McClements, D. J. (2018) Enhancement of Curcumin Bioavailability by Encapsulation in Sophorolipid-Coated Nanoparticles: An in Vitro and in Vivo Study. *J. Agric. Food Chem.* **66**, 1488–1497 https://doi.org/10.1021/acs.jafc.7b05478

13 Nasab, N. A., Kumleh, H. H., Beygzadeh, M., Teimourian, S. and Kazemzad, M. (2018) Delivery of curcumin by a pH-responsive chitosan mesoporous silica nanoparticles for cancer treatment. *Artif. Cells, Nanomedicine Biotechnol.*, Informa UK Limited, trading as Taylor & Francis Group **46**, 75–81 https://doi.org/10.1080/21691401.2017.1290648

14 Subtaweesin, C., Woraharn, W., Taokaew, S., Chiaoprakobkij, N., Sereemaspun, A. and Phisalaphong, M. (2018) Characteristics of curcumin-loaded bacterial cellulose films and anticancer properties against malignant melanoma skin cancer cells. *Appl. Sci.* **8** https://doi.org/10.3390/app8071188

15 Shoba, G., Joy, D., Joseph, T., Majeed, M., Rajendran, R. and Srinivas, P. S. S. R. (1998) Influence of piperine on the pharmacokinetics of curcumin in animals and human volunteers. *Planta Med.* **64**, 353–356 https://doi.org/10.1055/s-2006-957450

16 Goel, A., Kunnumakkara, A. B. and Aggarwal, B. B. (2008) Curcumin as "Curecumin": From kitchen to clinic. *Biochem. Pharmacol.* **75**, 787–809 https://doi.org/10.1016/j.bcp.2007.08.016

17 Chiaoprakobkij, N., Suwanmajo, T., Sanchavanakit, N. and Phisalaphong, M. (2020) Curcumin-Loaded Bacterial Cellulose/Alginate/Gelatin as A Multifunctional Biopolymer Composite Film. *Molecules* **25**, 1–18

https://doi.org/10.3390/molecules25173800

18 Raja, M. A., Zeenat, S., Arif, M. and Liu, C. (2016) Self-assembled nanoparticles based on amphiphilic chitosan derivative and arginine for oral curcumin delivery. *Int. J. Nanomedicine* **11**, 4397–4412 https://doi.org/10.2147/IJN.S106116

19 Cao, S., Deng, Y., Zhang, L. and Aleahmad, M. (2022) Chitosan nanoparticles, as biological macromolecule-based drug delivery systems to improve the healing potential of artificial neural guidance channels: A review. *Int. J. Biol. Macromol.*, Elsevier B.V. **201**, 569–579 https://doi.org/10.1016/j.ijbiomac.2022.01.017

20 Gao, Y. and Wu, Y. (2022) Recent advances of chitosan-based nanoparticles for biomedical and biotechnological applications. *Int. J. Biol. Macromol.*, Elsevier B.V. **203**, 379–388 https://doi.org/10.1016/j.ijbiomac.2022.01.162

21 Maria, S., Sarwar, H. S., Sohail, M. F., Imran, M., Salman Qureshi, O., Raza, A., et al. (2020) Synthesis and characterization of pre-activated thiolated chitosan nanoparticles for oral delivery of octreotide. *J. Drug Deliv. Sci. Technol.* **58** https://doi.org/10.1016/j.jddst.2020.101807

22 Esquivel, R., Juárez, J., Almada, M., Ibarra, J. and Valdez, M. A. (2015) Synthesis and characterization of new thiolated chitosan nanoparticles obtained by ionic gelation method. *Int. J. Polym. Sci.* **2015** https://doi.org/10.1155/2015/502058

23 Federer, C., Kurpiers, M. and Bernkop-Schnürch, A. (2021) Thiolated Chitosans: A Multi-talented Class of Polymers for Various Applications. *Biomacromolecules* **22**, 24–56 https://doi.org/10.1021/acs.biomac.0c00663

24 Huang, L., Zhu, Z., Wu, D., Gan, W., Zhu, S., Li, W., et al. (2019) Antibacterial poly (ethylene glycol) diacrylate/chitosan hydrogels enhance mechanical adhesiveness and promote skin regeneration. *Carbohydr. Polym.* **225** https://doi.org/10.1016/j.carbpol.2019.115110

25 Guaresti, O., Basasoro, S., González, K., Eceiza, A. and Gabilondo, N. (2019) In situ cross–linked chitosan hydrogels via Michael addition reaction based on water–soluble thiol–maleimide precursors. *Eur. Polym. J.*, Elsevier **119**, 376–384

https://doi.org/10.1016/j.eurpolymj.2019.08.009

26 Moussa, S. H., Tayel, A. A. and Al-Turki, A. I. (2013) Evaluation of fungal chitosan as a biocontrol and antibacterial agent using fluorescence-labeling. *Int. J. Biol. Macromol.*, Elsevier B.V. **54**, 204–208 https://doi.org/10.1016/j.ijbiomac.2012.12.029

27 Alonso, M. J., Calvo, P., Remuñán-López, C. and Vila-Jato, J. L. (1997) Novel Hydrophilic Chitosan – Polyethylene Oxide Nanoparticles as Protein Carriers. *J. Appl. Polym. Sci.* **63**, 125–132

28 da Silva, J. B., Ferreira, S. B. de S., Reis, A. V., Cook, M. T. and Bruschi, M. L. (2018) Assessing mucoadhesion in polymer gels: The effect of method type and instrument variables. *Polymers (Basel).* **10**, 1–19 https://doi.org/10.3390/polym10030254

29 Kim, S., Kang, J. Y., Balance, W. C., Sutton, B. P., Shin, D. H., Jang, K. H., et al. (2021) Fabrication of cell penetrating peptide-conjugated bacterial cellulose nanofibrils with remarkable skin adhesion and water retention performance. *Int. J. Pharm.*, Elsevier B.V. **600**, 120476 https://doi.org/10.1016/j.ijpharm.2021.120476

30 Anitha, A., Deepa, N., Chennazhi, K. P., Lakshmanan, V. K. and Jayakumar, R. (2014) Combinatorial anticancer effects of curcumin and 5-fluorouracil loaded thiolated chitosan nanoparticles towards colon cancer treatment. *Biochim. Biophys. Acta - Gen. Subj.*, Elsevier B.V. **1840**, 2730–2743 https://doi.org/10.1016/j.bbagen.2014.06.004

31 Lee, W. H., Loo, C. Y., Young, P. M., Rohanizadeh, R. and Traini, D. (2016) Curcumin Nanoparticles Attenuate Production of Pro-inflammatory Markers in Lipopolysaccharide-Induced Macrophages. *Pharm. Res.* **33**, 315–327 https://doi.org/10.1007/s11095-015-1789-9

32 Omer, A. M., Ziora, Z. M., Tamer, T. M., Khalifa, R. E., Hassan, M. A., Mohy-Eldin, M. S., et al. (2021) Formulation of quaternized aminated chitosan nanoparticles for efficient encapsulation and slow release of curcumin. *Molecules* **26**, 1–14 https://doi.org/10.3390/molecules26020449

33 Nguyen, M. H., Yu, H., Kiew, T. Y. and Hadinoto, K. (2015) Cost-effective alternative to nano-encapsulation: Amorphous curcumin-chitosan nanoparticle complex exhibiting high payload and supersaturation

generation. *Eur. J. Pharm. Biopharm.*, Elsevier B.V. **96**, 1–10 https://doi.org/10.1016/j.ejpb.2015.07.007

34 López-León, T., Carvalho, E. L. S., Seijo, B., Ortega-Vinuesa, J. L. and Bastos-González, D. (2005) Physicochemical characterization of chitosan nanoparticles: Electrokinetic and stability behavior. *J. Colloid Interface Sci.* **283**, 344–351 https://doi.org/10.1016/j.jcis.2004.08.186

35 Maculotti, K., Genta, I., Perugini, P., Imam, M., Bernkop-Schnürch, A. and Pavanetto, F. (2005) Preparation and in vitro evaluation of thiolated chitosan microparticles. *J. Microencapsul.* **22**, 459–470 https://doi.org/10.1080/02652040500162220

36 Yu, H., Tran, T. T., Teo, J. and Hadinoto, K. (2016) Dry powder aerosols of curcumin-chitosan nanoparticle complex prepared by spray freeze drying and their antimicrobial efficacy against common respiratory bacterial pathogens. *Colloids Surfaces A Physicochem. Eng. Asp.* https://doi.org/10.1016/j.colsurfa.2016.05.053

37 Hejjaji, E. M. A., Smith, A. M. and Morris, G. A. (2018) Evaluation of the mucoadhesive properties of chitosan nanoparticles prepared using different chitosan to tripolyphosphate (CS:TPP) ratios. *Int. J. Biol. Macromol.*, Elsevier B.V. **120**, 1610–1617 https://doi.org/10.1016/j.ijbiomac.2018.09.185

38 Athavale, R., Sapre, N., Rale, V., Tongaonkar, S., Manna, G., Kulkarni, A., et al. (2022) Tuning the surface charge properties of chitosan nanoparticles. *Mater. Lett.*, Elsevier B.V. **308**, 131114 https://doi.org/10.1016/j.matlet.2021.131114

39 Wu, A., Hu, X., Ao, H., Chen, Z., Chu, Z., Jiang, T., et al. (2022) Rational design of bacterial cellulose-based air filter with antibacterial activity for highly efficient particulate matters removal. *Nano Sel.* **3**, 201–211 https://doi.org/10.1002/nano.202100086

40 Mautner, A. and Bismarck, A. (2021) Bacterial nanocellulose papers with high porosity for optimized permeance and rejection of nm-sized pollutants. *Carbohydr. Polym.*, Elsevier Ltd **251**, 117130 https://doi.org/10.1016/j.carbpol.2020.117130

41 Chen, M., Kang, H., Gong, Y., Guo, J., Zhang, H. and Liu, R. (2015) Bacterial Cellulose Supported Gold Nanoparticles with Excellent

Catalytic Properties. *ACS Appl. Mater. Interfaces* **7**, 21717–21726 https://doi.org/10.1021/acsami.5b07150

42 Almasi, H., Jafarzadeh, P. and Mehryar, L. (2018) Fabrication of novel nanohybrids by impregnation of CuO nanoparticles into bacterial cellulose and chitosan nanofibers: Characterization, antimicrobial and release properties. *Carbohydr. Polym.* https://doi.org/10.1016/j.carbpol.2018.01.067

43 Wu, J., Zheng, Y., Song, W., Luan, J., Wen, X., Wu, Z., et al. (2014) In situ synthesis of silver-nanoparticles/bacterial cellulose composites for slow-released antimicrobial wound dressing. *Carbohydr. Polym.*, Elsevier Ltd. **102**, 762–771 https://doi.org/10.1016/j.carbpol.2013.10.093

44 Li, Z., Wang, L., Chen, S., Feng, C., Chen, S., Yin, N., et al. (2015) Facilely green synthesis of silver nanoparticles into bacterial cellulose. *Cellulose* **22**, 373–383 https://doi.org/10.1007/s10570-014-0487-9

45 Copetti, P. M., Bissacotti, B. F., da Silva Gündel, S., Bottari, N. B., Sagrillo, M. R., Machado, A. K., et al. (2022) Pharmacokinetic profiles, cytotoxicity, and redox metabolism of free and nanoencapsulated curcumin. *J. Drug Deliv. Sci. Technol.*, Elsevier B.V. **72**, 103352 https://doi.org/10.1016/j.jddst.2022.103352

46 Li, M. G., Lu, W. L., Wang, J. C., Zhang, X., Wang, X. Q., Zheng, A. P., et al. (2007) Distribution, transition, adhesion and release of insulin loaded nanoparticles in the gut of rats. *Int. J. Pharm.* **329**, 182–191 https://doi.org/10.1016/j.ijpharm.2006.08.040

47 Amini, Y., Amel Jamehdar, S., Sadri, K., Zare, S., Musavi, D. and Tafaghodi, M. (2017) Different methods to determine the encapsulation efficiency of protein in PLGA nanoparticles. *Biomed. Mater. Eng.* **28**, 613–620 https://doi.org/10.3233/BME-171705

48 Liu, L., Yao, W. D., Rao, Y. F., Lu, X. Y. and Gao, J. Q. (2017) pH-responsive carriers for oral drug delivery: Challenges and opportunities of current platforms. *Drug Deliv.* **24**, 569–581 https://doi.org/10.1080/10717544.2017.1279238

49 Finnegan, M., Duffy, E. and Morrin, A. (2022) The determination of skin surface pH via the skin volatile emission using wearable colorimetric

sensors. *Sens. Bio-Sensing Res.*, Elsevier B.V. **35**, 100473 https://doi.org/10.1016/j.sbsr.2022.100473

50 Pandey, M., Choudhury, H., Abdul-Aziz, A., Bhattamisra, S. K., Gorain, B., Carine, T., et al. (2021) Promising drug delivery approaches to treat microbial infections in the vagina: A recent update. *Polymers (Basel).* **23**, 1–65 https://doi.org/10.3390/polym13010026

51 Bennison, L., Miller, C., Summers, R., Minnis, A., Sussman, G. and McGuiness, W. (2017) Bennison **25**, 63–69

52 Ju, S., Zhang, F., Duan, J. and Jiang, J. (2020) Characterization of bacterial cellulose composite films incorporated with bulk chitosan and chitosan nanoparticles: A comparative study. *Carbohydr. Polym.*, Elsevier **237**, 116167 https://doi.org/10.1016/j.carbpol.2020.116167

53 Cacicedo, M. L., Cesca, K., Bosio, V. E., Porto, L. M. and Castro, G. R. (2015) Self-assembly of carrageenin-CaCO3 hybrid microparticles on bacterial cellulose films for doxorubicin sustained delivery. *J. Appl. Biomed.*, Korea Institute of Oriental Medicine **13**, 239–248 https://doi.org/10.1016/j.jab.2015.03.004

54 Taokaew, S., Nunkaew, N., Siripong, P. and Phisalaphong, M. (2014) Characteristics and anticancer properties of bacterial cellulose films containing ethanolic extract of mangosteen peel. *J. Biomater. Sci. Polym. Ed.*, Taylor & Francis **25**, 907–922 https://doi.org/10.1080/09205063.2014.913464

55 Numata, Y., Mazzarino, L. and Borsali, R. (2015) A slow-release system of bacterial cellulose gel and nanoparticles for hydrophobic active ingredients. *Int. J. Pharm.*, Elsevier B.V. **486**, 217–225 https://doi.org/10.1016/j.ijpharm.2015.03.068

56 Hasan, M., Ben Messaoud, G., Michaux, F., Tamayol, A., Kahn, C. J. F., Belhaj, N., et al. (2016) Chitosan-coated liposomes encapsulating curcumin: Study of lipid-polysaccharide interactions and nanovesicle behavior. *RSC Adv.*, Royal Society of Chemistry **6**, 45290–45304 https://doi.org/10.1039/c6ra05574e

57 Sudhakar, S., Chandran, S. V., Selvamurugan, N. and Nazeer, R. A. (2020) Biodistribution and pharmacokinetics of thiolated chitosan nanoparticles for oral delivery of insulin in vivo. *Int. J. Biol. Macromol.*,

Elsevier B.V. **150**, 281–288 https://doi.org/10.1016/j.ijbiomac.2020.02.079

58 Ali, K. A., El-Naa, M. M., Bakr, A. F., Mahmoud, M. Y., Abdelgawad, E. M. and Matoock, M. Y. (2022) The dual gastro- and neuroprotective effects of curcumin loaded chitosan nanoparticles against cold restraint stress in rats. *Biomed. Pharmacother.*, Elsevier Masson SAS **148**, 112778 https://doi.org/10.1016/j.biopha.2022.112778

59 Makhlof, A., Werle, M., Tozuka, Y. and Takeuchi, H. (2010) Nanoparticles of glycol chitosan and its thiolated derivative significantly improved the pulmonary delivery of calcitonin. *Int. J. Pharm.*, Elsevier B.V. **397**, 92–95 https://doi.org/10.1016/j.ijpharm.2010.07.001

60 Lin, Z., Li, R., Liu, Y., Zhao, Y., Ao, N., Wang, J., et al. (2020) Histatin1-modified thiolated chitosan hydrogels enhance wound healing by accelerating cell adhesion, migration and angiogenesis. *Carbohydr. Polym.*, Elsevier **230**, 115710 https://doi.org/10.1016/j.carbpol.2019.115710

61 Varum, F. J. O., Veiga, F., Sousa, J. S. and Basit, A. W. (2011) Mucoadhesive platforms for targeted delivery to the colon. *Int. J. Pharm.*, Elsevier B.V. **420**, 11–19 https://doi.org/10.1016/j.ijpharm.2011.08.006

62 Aka-Any-Grah, A., Bouchemal, K., Koffi, A., Agnely, F., Zhang, M., Djabourov, M., et al. (2010) Formulation of mucoadhesive vaginal hydrogels insensitive to dilution with vaginal fluids. *Eur. J. Pharm. Biopharm.*, Elsevier B.V. **76**, 296–303 https://doi.org/10.1016/j.ejpb.2010.07.004

63 Leitner, V. M., Walker, G. F. and Bernkop-Schnürch, A. (2003) Thiolated polymers: Evidence for the formation of disulphide bonds with mucus glycoproteins. *Eur. J. Pharm. Biopharm.* **56**, 207–214 https://doi.org/10.1016/S0939-6411(03)00061-4

64 Cesari, A., Fabiano, A., Piras, A. M., Zambito, Y., Uccello-Barretta, G. and Balzano, F. (2020) Binding and mucoadhesion of sulfurated derivatives of quaternary ammonium-chitosans and their nanoaggregates: An NMR investigation. *J. Pharm. Biomed. Anal.*, Elsevier B.V. **177**, 112852 https://doi.org/10.1016/j.jpba.2019.112852

65 Chuah, L. H., Billa, N., Roberts, C. J., Burley, J. C. and Manickam, S. (2013) Curcumin-containing chitosan nanoparticles as a potential mucoadhesive delivery system to the colon. *Pharm. Dev. Technol.* **18**, 591–599 https://doi.org/10.3109/10837450.2011.640688

66 Barthelmes, J., Dünnhaupt, S., Unterhofer, S., Perera, G., Schlocker, W. and Bernkop-Schnürch, A. (2013) Thiolated particles as effective intravesical drug delivery systems for treatment of bladder-related diseases. *Nanomedicine* **8**, 65–75 https://doi.org/10.2217/nnm.12.76

67 Vasconcelos, A., Freddi, G. and Cavaco-Paulo, A. (2008) Biodegradable materials based on silk fibroin and keratin. *Biomacromolecules* **9**, 1299–1305 https://doi.org/10.1021/bm7012789

68 Mueller, C., Verroken, A., Iqbal, J. and Bernkop-Schnuerch, A. (2012) Thiolated chitosans: In vitro comparison of mucoadhesive properties. *J. Appl. Polym. Sci.* https://doi.org/10.1002/app.35622

69 Laffleur, F. (2017) Evaluation of chemical modified hydrogel formulation for topical suitability. *Int. J. Biol. Macromol.*, Elsevier B.V. **105**, 1310–1314 https://doi.org/10.1016/j.ijbiomac.2017.07.152

70 Nagoba, B. and Davane, M. (2019) Studies on wound healing potential of topical herbal formulations- do we need to strengthen study protocol? *J. Ayurveda Integr. Med.*, Elsevier Ltd **10**, 316–318 https://doi.org/10.1016/j.jaim.2019.09.002

71 Williams, H., Campbell, L., Crompton, R. A., Singh, G., McHugh, B. J., Davidson, D. J., et al. (2018) Microbial Host Interactions and Impaired Wound Healing in Mice and Humans: Defining a Role for BD14 and NOD2. *J. Invest. Dermatol.*, The Authors **138**, 2264–2274 https://doi.org/10.1016/j.jid.2018.04.014

72 Kumari, M. and Nanda, D. K. (2022) Potential of Curcumin nanoemulsion as antimicrobial and wound healing agent in burn wound infection. *Burns*, Elsevier 1–14 https://doi.org/10.1016/j.burns.2022.10.008

73 Tyagi, P., Singh, M., Kumari, H., Kumari, A. and Mukhopadhyay, K. (2015) Bactericidal activity of curcumin I is associated with damaging of bacterial membrane. *PLoS One* **10**, 1–15 https://doi.org/10.1371/journal.pone.0121313

74 Hogt, A. H., Dankert, J. and Feijen, J. (1986) Adhesion of coagulase-negative staphylococci to methacrylate polymers and copolymers. *J. Biomed. Mater. Res.* **20**, 533–545 https://doi.org/10.1002/jbm.820200409

75 Geisberger, G., Gyenge, E. B., Hinger, D., Käch, A., Maake, C. and Patzke, G. R. (2013) Chitosan-thioglycolic acid as a versatile antimicrobial agent. *Biomacromolecules* **14**, 1010–1017 https://doi.org/10.1021/bm3018593

76 Croce, M., Conti, S., Maake, C. and Patzke, G. R. (2016) Synthesis and screening of N-acyl thiolated chitosans for antibacterial applications. *Carbohydr. Polym.*, Elsevier Ltd. **151**, 1184–1192 https://doi.org/10.1016/j.carbpol.2016.06.014

CHAPTER 7

GENERAL CONCLUSIONS, FUTURE WORK AND LIST OF PUBLICATIONS

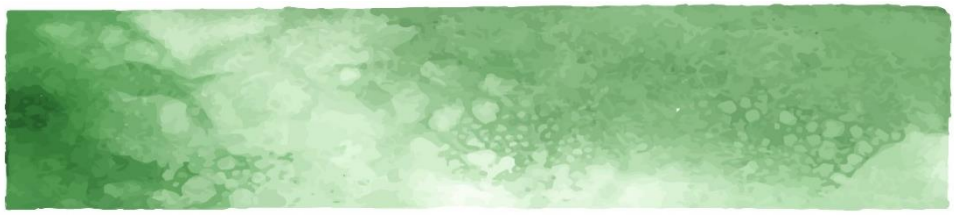

7.1	**General conclusions**	241
7.2	**Future work**	244
7.3	**List of publications**	246

Chapter 7: General conclusions, future work and list of publications

7.1 General conclusions

Circular economy presents itself as a sustainable alternative for proper socio-economic development of the community. Precisely, the biorefinery of industrial waste, understood from a biotechnological perspective, offers an approach towards valorization that can be addressed from different angles. In this context, as described throughout the thesis, GP agricultural waste, represents an opportunity to develop high-value products due to its richness in nutrients and active compounds. Thus, comprehensive strategies have been proposed in this work to minimize the impact of a waste with negative implications, both globally and locally in the Basque Country.

Initially, the roots of this work were established by developing a culture medium using GP for the biosynthesis of BC. Sugar analysis confirmed the suitability of GP as a carbon source for the growth of the acidophilic strain *Komagataeibacter medellinensis* ID13488. Additionally, ultrasound-assisted sugar extraction methods and water thermal treatments proved to be effective in enhancing the availability of reduced sugars. In fact, one of the advantages of GP as an agro-industrial waste is the possibility of developing effective culture media without extensive pre-treatments or with minimal raw material treatments.

Static cultures and agitated cultures were compared, successfully producing BC in the form of membranes and spheres, respectively. In this regard, gentle agitation proved to be the most effective in obtaining BC spheres with

competitive production yields compared to static cultures. Unlike other reported residues in the literature, a small concentration of GP was sufficient for bacterial proliferation. Furthermore, it was confirmed that the intrinsic crystallinity and purity of BC were not affected by the GP culture medium or the agitated cultivation conditions. In terms of applicability, BC spheres exhibited superabsorbent capacity due to their porous structure and increased surface area. Thus, they absorbed significant amount of the natural fertilizer urea, retained it, and rapidly released it under aqueous conditions. Certainly, the aim was to confer practical utility to BC within the agricultural sector.

BC produced from GP media was also used to obtain BCNCs. Enzymatic hydrolysis was explored as an alternative to common acid hydrolysis, considering the less sustainable nature of the latter. Characterization results of BCNCs showed similar size distribution, thermal resistance, and crystallinity values in both hydrolysis treatments. In parallel, phenolic compounds were extracted from GP using an ultrasound-assisted hydroalcoholic treatment. This more environmentally friendly alternative extraction of polyphenols proved to be effective, as a wide variety of phenolic compounds were identified, and antioxidant capacity was demonstrated through different mechanisms of action.

With the aim of achieving an integral valorization of GP, as suggested by the current trend of agricultural waste biorefinery, BCNCs and GPPE were combined in a synergistic complex. The BCNC-GPPE complex demonstrated a protective effect on the polyphenols, resulting in a prolonged antioxidant capacity. Moreover, the polyphenols played a role in modulating the surface charge of the BCNCs, enhancing their hydrophobic characteristics and improving their colloidal properties. As a result, the complex exhibited an

increased ability to stabilize Pickering emulsions with lipid-protective antioxidant activity. Moreover, the biocompatibility of GPPE enhanced the value-added condition of the product and expanded its applicability in the cosmetic, nutraceutical, and pharmaceutical sectors.

BCNFs are recognized nanoreinforcements for enhancing the mechanical properties of numerous polymeric matrices. With this aim, BC was mechanically disintegrated to obtain BCNFs and combine them with starch inks for 3D DIW printing. The addition of BCNFs significantly influenced the printability and ibuprofen release profiles in NM formulations, indicating the potential of BCNFs as effective reinforcing agents and release modulators. Moreover, the successful integration of GPPE into WM inks demonstrated the minimal impact on printability and emphasized again the potential of BCNFs in controlling the subsequent release of the polyphenols on physiological media. These results suggested a promising pathway for the development of personalized active tablets and 3D printed edibles for various sectors, including food, nutraceutical, and biomedical applications.

Lastly, Cs-SH nanoparticles were created with enhanced water solubility and mucoadhesive properties. These nanoparticles were employed to encapsulate curcumin and were successfully integrated into BC membranes via vacuum filtration, demonstrating high nanoparticle-retention efficiency. Release assays of FITC-Cs-SH nanoparticles indicated a pH-dependent release profile in physiological conditions, influenced by the initial sample concentration. The presence of nanoparticles led to improved adhesion on BC, suggesting the potential of Cs-SH nanoparticles in enhancing drug release in human mucous membranes and skin tissues. Additionally, the agar diffusion test results confirmed the antimicrobial activity of the nanoparticle-loaded membranes,

displaying significant antibacterial effects against *S. aureus* and *E. coli*. These findings highlighted the effective role of BC as a robust matrix for the retention of Cs-SH nanoparticles, thereby enhancing their biomedical application, notably in the efficient encapsulation and delivery of curcumin.

7.2 Future work

The work developed in this thesis opens up numerous topics for further research and more sustainable methodological approaches. Firstly, the extraction processes during the project have focused on ultrasound-assisted methods and the use of hydroalcoholic media to avoid excessive use of harmful solvents. However, considering the promising results obtained, an interesting line of further investigation would be the validation of these treatments and their in-depth comparison with the existing literature. Likewise, enzymatic hydrolysis promises to be a method worthy of future focus. Therefore, validation studies aimed at enhancing its performance and achieving precision in the production of BCNCs could be highly advantageous in diverse fields.

One of the main discoveries of this work has been the excellent bioactive properties of GPPE. Therefore, the main focus of future research would be to explore all possible properties of GPPE and its application in novel utilities.

Certainly, during the international stay carried out at the University of Strasbourg, under the supervision of Dr. Lydie Ploux and Dr. Corinne Nardin, various antimicrobial and biocompatibility assays were conducted. The objective in this case was to develop antimicrobial BC membranes against the opportunistic pathogen *Streptococcus Epidermidis*. The results showed that GPPE exhibited antimicrobial activity against *S. epidermidis*, but only when in

suspension. The interaction through physical absorption of GPPE with BC seemed to affect negatively its bacterial antibiofilm capacity. These findings were supported by confocal microscopy and colony-forming unit counting. The same results were observed with the antimicrobial peptides POM1 and POM2, highly effective experimental peptides that lost their activity when introduced into BC membranes.

For this reason, considering the results from Chapter 6, a highly promising research topic would be to utilize Cs-SH nanoparticles to encapsulate GPPE or antimicrobial peptides and introduce them into BC membranes through vacuum filtration. The drug release would be dependent on the release of the nanoparticles from the BC membrane, and their mucoadhesion would enhance biodisponibility. This approach could potentially address the issue of the observed loss of antibacterial effectiveness during the international stay.

Moreover, the antimicrobial activity of GPPE can be explored against other strains, and given the versatility of BC, it could be employed in various applications. For instance, in the case of Pickering emulsions from Chapter 4, the bactericidal activity against *S. epidermidis* could be studied to develop creams to eradicate infections caused by this opportunistic pathogen.

On the other hand, the combination of GPPE and starch can be examined in the development of controlled-release antioxidant supplements. In this case, 3D printing and the utilization of BCNFs could also facilitate customization of the printed shape and release of the active compound.

7.3 List of publications and communications

7.3.1 List of publications

Authors	Julen Diaz-Ramirez, Leire Urbina, Arantxa Eceiza, Aloña Retegi, Nagore Gabilondo.
Title	Superabsorbent bacterial cellulose spheres biosynthesized from winery by-products as natural carriers for fertilizers.
Journal	International Journal of Biological Macromolecules
Year	2021
Impact factor	8.025 (JCR 2021)
Rank	47/297 Biochemistry & Molecular Biology (JCR 2021) 8/73 Chemistry, Applied (JCR 2021) 6/90 Polymer science (JCR 2021)

Authors	Julen Diaz-Ramirez, Senda Basasoro, Kizkitza González, Arantxa Eceiza, Aloña Retegi, Nagore Gabilondo.
Title	Integral Valorization of Grape Pomace for Antioxidant Pickering Emulsions.
Journal	Antioxidants (Special Issue: Antioxidant Properties of Bioactive Compounds in Fruit and Vegetable Waste).
Year	2023
Impact factor	7.0 (JCR 2022)
Rank	46/285 Biochemistry & Molecular Biology (JCR 2022) 6/60 Chemistry, Medicinal (JCR 2022) 12/142 Food Science & Technology (JCR 2022)

Authors	Julen Diaz-Ramirez, Senda Basasoro, Stefano Torresi, Arantxa Eceiza, Aloña Retegi, Nagore Gabilondo.
Title	Bacterial cellulose/thiolated chitosan nanoparticles hybrid antimicrobial dressing for curcumin delivery.
Journal	International Journal of Biological Macromolecules. (Under review)
Year	2023
Impact factor	8.2 (JCR 2022)
Rank	35/285 Biochemistry & Molecular Biology (JCR 2022) 7/73 Chemistry, Applied (JCR 2022) 5/86 Polymer science (JCR 2022)

Authors	Julen Diaz-Ramirez, Irene Méndez, Kizkitza Gonzalez, Arantxa Eceiza, Aloña Retegi, Nagore Gabilondo.
Title	Bacterial cellulose nanofibers and polyphenolic extract from grape pomace integration in 3D printing for personalized pharmacology.
Journal	In preparation
Year	2024

7.3.2 List of communications

Authors	Julen Diaz-Ramirez, Arantxa Eceiza, Aloña Retegi, Nagore Gabilondo.
Title	Bacterial Cellulose nanocrystals and polyphenolic extract from grape pomace for Pickering emulsions.
Congress	5th International Symposium on Bacterial Cellulose.
Year	2022

Participation	Oral presentation
Place	Jena, Germany

Authors	Julen Diaz-Ramirez, Leire Urbina, Arantxa Eceiza, Aloña Retegi, Nagore Gabilondo.
Title	Txakolin ekoizpenaren hondakinetatik abiatuz balio erantsidun nanozelulosa bakterianoaren sintesi eta karakterizazioa.
Congress	Materialen Zientzia eta Teknologia V. Kongresua.
Year	2021
Participation	Poster
Place	Bilbao, Spain

Authors	**G**abriel Arner, Olatz Guaresti, Leire Urbina, Julen Diaz-Ramirez, Arantxa Eceiza, Aloña Retegi, Nagore Gabilondo.
Title	Novel chitosan-coated bacterial cellulose hydrogels for controlled delivery systems.
Congress	4th International Symposium on Bacterial Cellulose.
Year	2019
Participation	Poster
Place	Porto, Portugal

ANNEXES



List of Abbreviations 251
List of Figures 255
List of Schemes 263
List of Tables 263
Supplementary material 265

List of abbreviations

3D	Three–dimensional
ABTS	2,2'-azinobis(3-ethylbenzothiazoline-6-sulfonic acid) diammonium salt
AFM	Atomic force microscopy
AH	Acid hydrolysis
BC	Bacterial cellulose
BCNC	Bacterial cellulose nanocrystals
BCNF	Bacterial cellulose nanofibres
CAD	Computer-aided design
CCR	Curcumin cumulative release
CD	Conjugated dienes
CI	Crystallinity index
CL	Curcumin loading
CNC	Cellulose nanocrystal
Cs	Chitosan
Cs-SH	Thiol–functionalized chitosan
Cur-Cs-SH	Curcumin loaded thiolated chitosan
CUR	Cumulative urea release
DAc	Degree of acetylation
DCM	Dichloromethane
DD	Deacetylation degree
DIW	Direct ink writing

DLS	Dynamic light scattering
DMAB	4-dimethylamino benzaldehyde
DMEM	Dulbecco´s mofied Eagle´s medium
DMSO	Dimethyl sulfoxide
DPPH	2,2-diphenyl-1-picrylhydrazyl
DS	Degree of substitution
DSC	Differential scanning calorimetry
dTG	Derivative thermogravimetric curve
EA	Elemental analysis
ECR	Extract cumulative release
EDC	N–(3–dimethylaminopropyl)– N´ethylcarbodiimide hydrochloride
EDTA	Ethylenediaminetetraacetic acid
EH	Enzymatic hydrolysis
ER	Emulsion ration
ESI	Electro-spray ionization
FBS	Fetal Bovine Serum
FITC	Fluorescein-5-isothiocyanate
FITC-CS-SH	FITC labeled thiolated Cs
FTIR	Fourier transformed infrared spectroscopy
G1P	Glucose-1-phosphate
G6P	Glucose-6-phosphate
GC	Gas chromatography

GA	Gallic acid
GP	Grape pomace
GPPE	Grape pomace polyphenolic extract
GRAS	Generally Recognized as Safe
HAc	Acetic acid
HPAEC-PAD	High Performance Anion-Exchange Chromatography with Pulsed Amperometric Detection
HS	Hestrin and Schramm
ICR	Ibuprofen cumulative release
LVR	Linear viscoelastic region
MS	Mass Spectrometry
MTT	3-(4,5-dimethylthiazol-2-yl)-2,5-diphenyltetrazolium bromide
NCR	Nanoparticle cumulative release
NHS	N–hydroxysuccinimide
NM	Normal maize
O/W	Oil-in-water
PBS	Phosphate buffer solution
QTOF	Quadrupole time-of-flight
ROS	Reactive Oxygen Species
SEM	Scanning electron microscopy
SSE	Semi-solid extrusion
TE	Trolox equivalent

TEM	Transmission electron microscopy
TGA	Thermogravimetric analysis
TLA	Thiolactic acid
TPC	Total phenolic content
TPP	Sodium tripolyphosphate pentabasic
UDPG	Uridine diphosphate glucose
UL	Urea loading
UHPLC	Ultra High Performance Liquid Chromatography
UTP	Uridine triphosphate
UV	Ultraviolet
UV–vis	Ultraviolet–visible
WCA	Water contact angle
WHC	Water holding capacity
WM	Waxy maize
W/O	Water-in-oil
XRD	X–ray diffraction

List of Figures

Chapter 1

Figure 1.1. Graphical representation of the white wine production process with the waste generated at each step. 5

Figure 1.2. Representation of the main compounds that can be found in each component of GP. 6

Figure 1.3. Schematic representation of the main phenolic compounds present in white GP. The dashed lines refer to the condensation process of phenolic acids/polyphenols in the formation of tannins. 9

Figure 1.4. GP applications classified according to the type of treatment required and the main products obtained. 11

Figure 1.5. Molecular structure of cellulose and distribution of its crystalline and amorphous regions. 15

Figure 1.6. Graphical representation of the biosynthesis process of BC by K. medellinensis. G6P=Glucose-6-phosphate, GK=Glucokinase, G1P=Glucose-1-phosphate UTP=Uridine triphosphate, PGM=Phosphoglucomutase, UDPG=Uridyl di-phosphate glucose, UDPGP= UDPG phosphorylase, CSC=Cellulose synthase complex. 17

Figure 1.7. Graphical representation of the different valorization strategies explored in this work. 29

Chapter 3

Figure 3.1. Graphic representation of the biosynthesis processes of BC from GP under static and agitated growth conditions. 78

Figure 3.2. Graphical representation of the urea loading process onto BC spheres for UL calculation, followed by its subsequent release and spectrophotometric detection. 79

Figure 3.3. Variation of glucose and fructose contents in static (A) and agitated (B) GP culture media at 5% (w/v). 86

Figure 3.4. FTIR spectra of BC samples in static and agitated conditions from HS and GP culture media. 88

Figure 3.5. X-ray diffraction patterns of BC in static and agitated conditions from HS and GP culture media. 90

Figure 3.6. BC samples produced in agitated GP cultures at rotation speeds of (A) 120 rpm, (B) 130 rpm and (C) 150 rpm. 92

Figure 3.7. Height (left) and phase (right) AFM images of BC samples from agitated GP and static GP culture media are represented in (A) and (B), respectively. 93

Figure 3.8. SEM images of BC surfaces produced in static (A) and agitated (B) GP cultures 94

Figure 3.9. DSC curves of urea, urea-loaded BC sphere, and BC sphere after the release study. 96

Chapter 4

Figure 4.1. Graphical representation of the interactions between BC and phenolic compounds characteristic of GP through hydrogen bonding (red dashed lines). 110

Figure 4.2. Schematic representation of the used enzymatic hydrolysis process. 113

Figure 4.3. Schematic representation of the used acid hydrolysis process. 114

Figure 4.4. Digital images of a BCNC-stabilized Pickering emulsion (top) and the study of the creamy phase under an optical microscope (bottom). 117

Figure 4.5. AFM images and size distribution of BCNC EH (A) and BCNC AH (B), respectively. 119

Figure 4.6. X-ray diffractograms (A) and FTIR spectra (B) of BC, BCNC EH and BCNC AH samples. 120

Figure 4.7. TGA (A) and dTG (B) curves of BC, BCNC EH and BCNC AH samples. 121

Figure 4.8. FTIR spectrum of GPPE. 123

Figure 4.9. WCA values of the different BC films immersed in solutions with increasing concentrations of GPPE (0-10 mg/mL). 125

Figure 4.10. Z potential value evolution of BCNC EH and BCNC EH-GPPE (A) and BCNC AH and BCNC AH-GPPE (B) dispersions. 126

Figure 4.11. Viability of 3T3 cells exposed to different GPPE concentration media for 24 hours. BC refers to media without GPPE and ns indicates a statistically non-significant difference with the negative control. 128

Figure 4.12. BCNC, BCNC-GPPE complex- and TW20-stabilized olive oil-in-water emulsion's oxidative stability measured through CD increase (A). Illustration of the stabilization of an oil-in-water emulsion with the BCNC-GPPE complex (B). 131

Figure 4.13. ER and emulsion drop D [4,3] of hexadecane-in-water Pickering emulsions stabilized by neat BCNC AH and BCNC AH-GPPE complex (A), and neat BCNC EH and BCNC EH-GPPE complex (B). 133

Figure 4.14. Optical microscope images of hexadecane-in-water Pickering emulsions stabilized by different concentrations of BCNC AH, BCNC AH-GPPE complex, BCNC EH and BCNC EH-GPPE complex dispersions. GPPE concentration remained constant against increasing concentrations of BCNCs. 135

Figure 4.15. Flow test measurements of hexadecane-in-water BCNC and BCNC-GPPE Pickering emulsions. 137

Figure 4.16. Dynamic oscillatory strain test (A) and frequency sweep tests (B) of hexadecane-in-water BCNC and BCNC-GPPE Pickering emulsions. Storage modulus (filled symbols) and loss modulus (empty symbols). 137

Chapter 5

Figure 5.1. Representation of the molecular structure of starch. 157

Figure 5.2. Schematic representation of the followed procedure to produce starch inks for 3D printing. 159

Figure 5.3. Optical micrograph of the morphology of NM granules. 163

Figure 5.4. Height and phase AFM images of BCNF dispersions from GP media with 1 µm (A) and 200 nm (B) scale bars 162

Figure 5.5. Flow test of NM inks (A) and IbNM inks (B) reinforced with different concentrations of BCNFs. 165

Figure 5.6. Stress sweep test of NM (A) and IbNM (B) inks reinforced with different concentrations of BCNFs and recovery test of the same NM (C) and IbNM (D) inks with BCNFs. 169

Figure 5.7. Digital images of 3D printed NM tablets with different concentrations of BCNF after freeze-drying. 171

Figure 5.8. Digital images of 3D printed IbNM tablets with different concentrations of BCNF after freeze-drying: IbNM (A), IbNM-0.5NF (B) and IbNM-1NF (C). 172

Figure 5.9. Spherical harmonic model from component simulation in XRD representing BCNF orientation distribution in NM-1NF tablets (A). Illustration of BCNF orientation in NM tablets after the 3D printing process (B). 174

Figure 5.10. SEM images of the NM tablets loaded with different concentrations of BCNFs (A, B and C), and their respective amplifications (D, E and F). 175

Figure 5.11. Cross-sectional SEM image of a IbNM-0.5NF tablet. 176

Figure 5.12. Ibuprofen release in vitro study of the IbNM tablets loaded with different concentrations of BCNF (A) and tablet-decomposition study after 45 min ibuprofen release assay of different IbNM tablets in triplicate (B). 177

Figure 5.13. Optical micrograph of the morphology of WM starch granules. 179

Figure 5.14. Flow test (A), stress sweep test (B), and recovery test (C) of WM-based inks mixed with different concentrations of GPPE. 181

Figure 5.15. FTIR spectra of WM tablets loaded with GPPE and bare GPPE (A), and an amplification of the fingerprint bands of GPPE in 3D printed WM tablets (B). 183

Figure 5.16. Digital images of 3D printed WM tablets with different concentrations of GPPE with their respective SEM image amplification. 185

Figure 5.17. GPPE release in vitro study of the WM and NM tablets loaded with different concentrations of GPPE and BCNF (A). Digital images of the WM (B) and WM-5PE (C) samples after 24 h of being immersed in PBS. 185

Chapter 6

Figure 6.1. Schematic representation of the research topic and experimental process of Chapter 6. 206

Figure 6.2. UV photographs of supernatants from successive acetone washes to FITC-labeled Cs-SH. 208

Figure 6.3. Schematic representation of the vacuum filtration process followed in this chapter for BC loading. 210

Figure 6.4. Schematic representation of the mucoadhesive test with nanoparticle-loaded BC and mucin disks. 213

Figure 6.5. AFM height micrographs of CS-SH and Cur-Cs-SH nanoparticles. 215

Figure 6.6. Hydrodynamic diameter (Z average) and Z potential variation with pH for (A) Cs-SH and (B) Cur-Cs-SH nanoparticles. 215

Figure 6.7. From left to right, AFM phase images of BC, 30BCnp and 50BCnp samples after filtration process (A, B and C). SEM images with miniature UV light photography of unloaded BC and BC loaded with FITC-Cs-SH nanoparticles (D and E, respectively). 217

Figure 6.8. FITC-Cs-SH nanoparticle cumulative release from 30BCnp and 50BCnp samples at pH 5.5 and 7.4 release media. 219

Figure 6.9. In vitro curcumin cumulative release profile of Cur-Cs-SH nanoparticles at pH 5.5 and pH 7.4. 221

Figure 6.10. The adhesion-force test carried out with BC, 30BCnp and 50BCnp samples on mucin disks (A) and porcine skin (B) at pH 7.4 and pH 5.5. (*) Refers to the statistically significant difference with the BC punch without nanoparticles. (**) Refers to the statistically significant difference between the two nanoparticle-loaded BCs. 223

Figure 6.12. Antimicrobial agar diffusion assay results for 30BCnp samples against *S. aureus* (A) and *E. coli* (B) at 24 h in triplicate. 226

List of Schemes

Chapter 6

Scheme 6.1. Schematic diagram of the chemical synthesis of thiolated chitosan (Cs-SH). 207

Scheme 6.2. Schematic diagram of the chemical synthesis of FITC-labeled thiolated chitosan (FITC-Cs-SH). 207

List of Tables

Chapter 3

Table 3.1. GP concentration, supplementation with nitrogen sources, BC production and glucose + fructose content of the different culture media tested under static conditions. Culture media with additional nitrogen source was labelled with *pp* in reference to peptone. 81

Table 3.2. GP concentration, supplementation with nitrogen sources, BC production and glucose + fructose content of the different culture media tested under agitated conditions. *Us*, *H* and *Us + H* refer to the application of ultrasound treatment, hot water treatment and the combination of both treatments, respectively. Culture media with yeast extract were labelled with *ex*. 83

Table 3.3. I_β percentage and CI values of the different culture media in static and agitated conditions. 89

Table 3.4. Nanofiber diameter and WHC of BC from GP cultures in static and agitated conditions. 94

Chapter 4

Table 4.1. The half-life of DPPH assay was measured for bare GPPE and the BCNC AH-GPPE and BCBN EH-GPPE complexes under various light and temperature conditions. 130

Chapter 5

Table 5.1. Rheological parameters of NM reinforced inks: Power-law index (n), consistency coefficient (K), yield stress, flow stress and recovery (%). 166

Table 5.2. Rheological parameters of IbNM reinforced inks: Power-law index (n), consistency coefficient (K), yield stress, flow stress and recovery (%). 167

Table 5.3. Rheological parameters of WM inks with GPPE: Power-law index (n), consistency coefficient (K), yield stress, flow stress and recovery (%). 180

Supplementary material

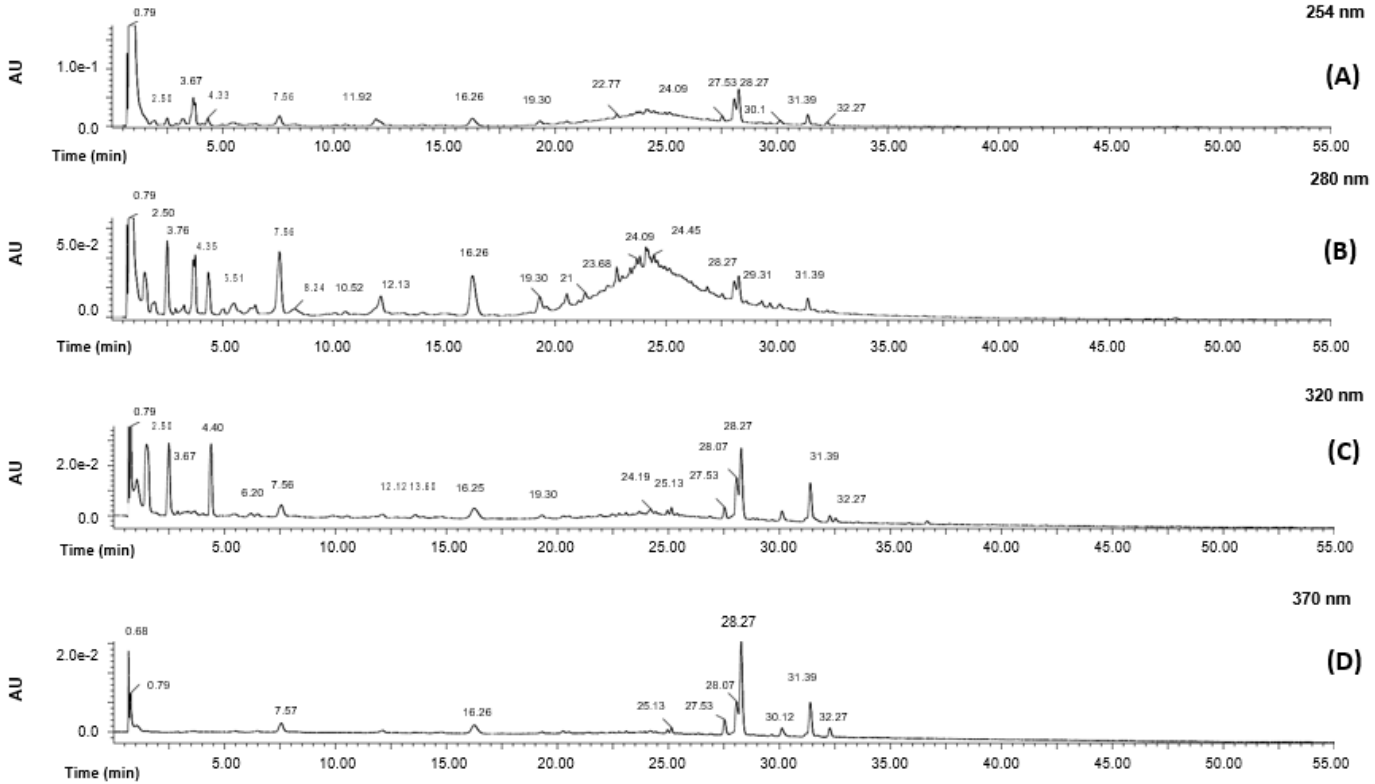

Figure S1. Diode array detector (DAD) chromatogram of GPPE at; 254 nm (A); 280 nm (B); 320 nm (C); and, at 370 nm (D).

Table S1. Characterization of polyphenols from GPPE determined by UHPLC-Q-TOF-MS/MS analysis. Abbreviations: *Cat* (Catechin), *Epi* (Epicatechin), *Gal* (Galic acid), *gal* (galactose, galactosil, galactoside), *glc* (glucose, glycosyl, glycoside), *glcr* (glucuronic acid, glucuronide), *hex* (hexose, hexosyl, hexoside), *Iso* (Isorhamnetin), *Kaem* (Kaempferol), *PB* (Procyanidin), *((Epi)Cat)) 3* (Procyanidin trimer), *Que* (Quercetin) and *pCoum* (p-Coumaric acid, p-coumaroyl).

Com.No	Tentative identification	LC tR (min)	DAD UV Bands (nm)	ESI(+)-Q-ToF **Exp. Acc. Mass $[M+H]^+$ Error (mDa)**	**Formula for the detected $[M+H]^+$**	**Adducts and Fragment ions of $[M+H]^+$**	ESI(-)-Q-ToF **Exp. Acc. Mass $[M-H]^-$ Error (mDa)**	**Formula for the detected $[M-H]^-$**	**Adducts and Fragmentions of $[M-H]^-$**
Flavanols									
1	((Epi)cat)3 (1)	3.30283		867.2136 -0.2	C45H39O18	715.1639 [U(1,3A)MD]+ 579.1514 [MD]+ 427.1038 [U(1,3A)D]+ 409.0928 [M(1,3A-H2O)D]+ 291.0873 [U]+ 289.0716 [D]+ 247.0620 [U-C2H2O]+ 139.0394 [D(1,3A)]+ 127.0396 [D(1,4A+2H)]+ 123.0446 [D(1,2B)]+	865.1980 1.8	C45H37O18	713.1509 [U(1,3A)MD]- 577.1340 [MD]- 425.0869 [U(1,3A)D]+ 407.0772 [M(1,3A-H2O)D]- 289.00705 [D]- 287.0551[U]- 245.0446 [U-C2H2O]+ 125.0231 [D(1,4A+2H)]-
2	PBI	5.52280		579.1508 0.5	C30H27O12	427.1032 [U(1,3A)D]+ 409.0925 [U(1,3A-H2O)D]+ 291.0872 [D]+ 289.0707 [U]+ 287.0553[U(1,3A)D(1,2A-H2O)]+	577.1351 0.5	C30H25O12	425.0874 [U(1,3A)D]- 407.0773 [U(1,3A-H2O)D]- 289.0714 [D]- 245.0815 [U-C2H2O]+ 125.0239 [D(1,4A+2H)]-

					247.0606 [U-C2H2O]+ 139.0393 [D(1,3A)]+ 127.0393 [D(1,4A+2H)]+ 123.0444 [D(1,2B)]+			
3	((Epi)cat)3 (2)	5.84283	867.2133 -0.3	C45H39O18	715.1653[U(1,3A)MD]+ 579.1497 [MD]+ 427.1021 [U(1,3A)D]+ 409.0907 [M(1,3A-H2O)D]+ 291.0858 [D]+ 289.0703 [U]+ 247.0593 [U-C2H2O]+ 139.0389 [D(1,3A)]+ 127.0386 [D(1,4A+2H)]+ 123.0438 [D(1,2B)]+	865.1988 0.8	C45H37O18	713.1503 [U(1,3A)MD]- 577.1327 [MD]- 425.0864 [U(1,3A)D]- 407.0763 [M(1,3A-H2O)D]- 289.0697 [D]- 287.0549 [U]- 125.0234 [D(1,4A+2H)]-
4	PBII	6.51280	579.1496 -0.7	C30H27O12	427.1029 [U(1,3A)D]+ 409.0921 [U(1,3-H2O)D]+ 291.0865 [D]+ 289.0704 [U]+ 287.0557 [U(1,3A)D(1,2A-H2O)]+ 247.0600 [U-C2H2O]+ 139.0388 [D(1,3A)]+ 127.0389 [U(1,4A+2H)D]+	577.1358 1.2	C30H25O12	425.0867 [U(1,3A)D]- 407.0761 [U(1,3A-H2O)D]- 289.0707 [D]- 245.0810 [U-C2H2O]+ 125.0234 [D(1,4A+2H)]-

						123.0441 [D(1,2B)]+			
5	Cat	7.59	278	291.0873	C15H15O6	207.0659[Rup(A)]+	289.0717	C15H13O6	205.0502 [Rup(A)]-
				0.4		147.0447 [0,4B-2H2O]+	0.5		137.0235 [1,3A]-
						139.0394 [1,3A]+			123.0235 [1,3B-CO]-
						123.0446 [1,2B]+			109.0284 [1,3A-CO]-
						289.0712 [U]+			287.0561 [U]-
						247.0603 [U-C2H2O]+			245.0461 [U-C2H2O]+
						139.0396 [D(1,3A)]+			125.0229 [D(1,4A+2H)]-
						127.0391 [D(1,4A+2H)]+			
						123.0446 [D(1,2B)]+			
9	((Epi)cat)3 (5)	9.80	283	867.2099	C45H39O18	715.1680 [U(1,3A)MD]+	865.1988	C45H37O18	713.1501 [U(1,3A)MD]-
				-3.7		579.1483 [MD]+	0.8		577.1353 [MD]-
						427.1022 [U(1,3A)D]+			425.0852 [U(1,3A)D]-
						409.0907 [M(1,3A-H2O)D]+			407.0757 [M(1,3A-H2O)D]-
						291.0872 [D]+			289.0707 [U]-
						289.0711 [U]+			287.0555 [D]-
						247.0605 [U-C2H2O]+			125.0229 [D(1,4A+2H)]-
						139.0392 [D(1,3A)]+			
						127.0394 [D(1,4A+2H)]+			
						123.0438 [D(1,2B)]+			
10	PB IV	12.19	280	579.1500	C30H27O12	427.1014 [U(1,3A)D]+	577.1349	C30H25O12	425.0867 [U(1,3A)D]-
				-0.3		409.0914 [U(1,3-H2O)D]+	0.3		407.0765 [U(1,3A-H2O)D]-

					291.0860 [D]+			289.0711 [D]-
					289.0701 [U]+			245.0811 [U-C2H2O]+
					287.0550 [U(1,3A)D(1,2A-H2O)]+			125.0237 [D(1,4A+2H)]-
					247.0597 [U-C2H2O]+			
					139.0388 [D(1,3A)]+			
					127.0389 [U(1,4A+2H)D]+			
					123.0441 [D(1,2B)]+			
11	((Epi)cat)3 (6)	13.20 283	867.2144	C45H39O18	715.1669[U(1,3A)MD]+	865.1988	C45H37O18	713.1475 [U(1,3A)MD]-
			0.8		579.1511 [MD]+	0.8		577.1346 [MD]-
					409.0907 [M(1,3A-H2O)D]+			425.0858 [U(1,3A)D]-
					427.1017 [U(1,3A)D]+			407.0772 [M(1,3A-H2O)D]-
					409.0919 [M(1,3A-H2O)D]+			289.0705 [U]-
					291.0868 [D]+			287.0553 [D]-
					289.0701 [U]+			125.0236 [D(1,4A+2H)]-
					247.017 [U-C2H2O]+			
					139.0388 [D(1,3A)]+			
					127.0393 [D(1,4A+2H)]+			
					123.0442 [D(1,2B)]+			
12	PB-gallate-1	14.05 280	731.1599	C37H31O16	579.1152 [PB+H-Gallic acid]+	729.1398	C37H29O16	577.1331 [PB-H-Gallic acid]+
			-1.3			-5.8		425.0861 [U(1,3A)D]-

					409.0924 [U(1,3-H2O)D]+			407.0756 [U(1,3A-H2O)D]-
					291.0868 [D]+			289.0707 [D]-
					287.0546 [U(1,3A)D(1,2A-H2O)]+			245.0457 [U-C2H2O]+
					247.0604 [U-C2H2O]+			125.0235 [D(1,4A+2H)]-
					139.0393 [D(1,3A)]+			
					123.0446 [D(1,2B)]+			
13	PB-gallate-2	15.14	280	731.1599	C37H31O16	579.1125[PB+H-Gallic acid]+	729.1398	C37H29O16	577.1013 [PB-H-Gallic acid]+
				-1.3		427.1024 [U(1,3A)D]+	-5.8		425.0869 [U(1,3A)D]-
						409.0923 [U(1,3-H2O)D]+			407.0763 [U(1,3A-H2O)D]-
						289.0714 [U]+			289.0705 [D]-
						287.0555 [U(1,3A)D(1,2A-H2O)]+			245.0455 [U-C2H2O]+
						247.0611 [U-C2H2O]+			125.0234 [D(1,4A+2H)]-
						139.0393 [D(1,3A)]+ 127.0389 [U(1,4A+2H)D]+			
						123.0446 [D(1,2B)]+			
14	Epi	16.31	278	291.0869	C15H15O6	207.0655 [Rup(A)]+	289.0719	C15H13O6	205.0499 [Rup(A)]-
				0.0		147.0443 [0,4B-2H2O]+	0.7		137.0237 [1,3A]-
						139.0391 [1,3A]+			123.0443 [1,3B-CO]-
						123.0444 [1,2B]+			109.0286 [1,3A-CO]-
						119.0494 [0,4B-2H2O-CO]+			

15	((Epi)cat)3 (7)	17.25 283	867.2144	C45H39O18	715.1636 [U(1,3A)MD]+	865.1988	C45H37O18	713.1501 [U(1,3A)MD]-
			0.8		579.1479 [MD]+	0.8		577.1334 [MD]-
					409.0903[M(1,3A-H2O)D]+			425.0869 [U(1,3A)D]-
					427.1001 [U(1,3A)D]+			407.0769 [M(1,3A-H2O)D]-
					409.0903 [M(1,3A-H2O)D]+			289.0706 [U]-
					291.0859 [D]+			287.0557 [D]-
					289.0701 [U]+			245.0437 [U-C2H2O]+
					247.0596 [U-C2H2O]+			125.0236 [D(1,4A+2H)]-
					139.0387 [D(1,3A)]+			
					127.0391 [D(1,4A+2H)]+			
					123.0442 [D(1,2B)]+			
16	PB-gallate-3	19.33 280	731.1599	C37H31O16	579.1143 [PB+H-Gallic acid]+	729.1398	C37H29O16	577.1335 [PB-H-Gallic acid]+
			-1.3		427.1016 [U(1,3A)D]+	-5.8		425.0869 [U(1,3A)D]-
					409.0914 [U(1,3-H2O)D]+			407.0764 [U(1,3A-H2O)D]-
					289.0705 [U]+			289.0710 [D]-
					287.0551 [U(1,3A)D(1,2A-H2O)]+			245.0447 [U-C2H2O]+
					247.0596 [U-C2H2O]+			125.0233 [D(1,4A+2H)]-
					139.0387 [D(1,3A)]+			
					127.0389 [U(1,4A+2H)D]+			
					123.0440 [D(1,2B)]+			

17	PB V	20.37 280	579.1500	C30H27O12	427.1017 [U(1,3A)D]+	577.1349	C30H25O12	425.0868 [U(1,3A)D]-
			-0.3		409.0924 [U(1,3-H2O)D]+	0.3		407.0765 [U(1,3A-H2O)D]-
					291.0858 [D]+			289.0706 [D]-
					289.0701 [U]+			245.0808 [U-C2H2O]+
					287.0548 [U(1,3A)D(1,2A-H2O)]+			125.0234 [D(1,4A+2H)]-
					247.0597 [U-C2H2O]+			
					139.0390 [D(1,3A)]+			
					127.0388 [U(1,4A+2H)D]+			
					123.0443 [D(1,2B)]+			
18	((Epi)cat)3 (8)	20.55 283	867.2144	C45H39O18	715.1688 [U(1,3A)MD]+	865.1988	C45H37O18	713.1500 [U(1,3A)MD]-
			0.8		579.1496 [MD]+	0.8		577.1340 [MD]-
					409.0920 [M(1,3A-H2O)D]+			425.0862 [U(1,3A)D]-
					427.1017 [U(1,3A)D]+			407.0761 [M(1,3A-H2O)D]-
					409.0920 [M(1,3A-H2O)D]+			289.0705 [U]-
					291.0869 [D]+			287.0551 [D]-
					289.0712 [U]+			245.0436 [U-C2H2O]+
					247.0603 [U-C2H2O]+			125.0231 [D(1,4A+2H)]-
					139.0394 [D(1,3A)]+			
					127.0393 [D(1,4A+2H)]+			
					123.0441 [D(1,2B)]+			

19	PB VI	26.17	280	579.1509	C30H27O12	427.1044 [U(1,3A)D]+	577.1349	C30H25O12	425.0864 [U(1,3A)D]-
				0.6		409.0916 [U(1,3-H2O)D]+	0.3		407.0749 [U(1,3A-H2O)D]-
						289.0712 [U]+			289.0701 [D]-
						289.0712 [U]+			245.0805 [U-C2H2O]+
						287.0560 [U(1,3A)D(1,2A-H2O)]+			125.0235 [D(1,4A+2H)]-
						247.0612 [U-C2H2O]+			
						139.0392 [D(1,3A)]+			
						127.0397 [U(1,4A+2H)D]+			
						123.0443 [D(1,2B)]+			
20	PB-gallate-4	29.38	280	731.1599	C37H31O16	579.1165 [PB+H-Gallic acid]+	729.1398	C37H29O16	577.1031 [PB-H-Gallic acid]+
				-1.3		427.1029 [U(1,3A)D]+	-5.8		425.0853 [U(1,3A)D]-
						409.0916 [U(1,3-H2O)D]+			407.0756[U(1,3A-H2O)D]-
						289.0713 [U]+			289.0704 [D]-
						287.0558 [U(1,3A)D(1,2A-H2O)]+			245.0444 [U-C2H2O]+
						247.0597 [U-C2H2O]+			125.0234 [D(1,4A+2H)]-
						139.0387 [D(1,3A)]+			
						127.0389 [U(1,4A+2H)D]+			
						123.0446 [D(1,2B)]+			
Flavonols									
21	Que-hex-hex-1	20.28	264, 344	627.1572	C27H31O17	465.1021 [Y1]+	625.137	C27H29O17	463.0862 [Y1]-
				1.1		303.0500 [Y0]+	-3.5		301.0342 [Y0]-

22	Que-hex-hex-2	24.47	264, 344	627.1562 0.1	C27H31O17	465.1035 [Y1]+ 303.0496 [Y0]+	625.1401 -0.4	C27H29O17	463.0878 [Y1]- 301.0352 [Y0]-
23	Que-hex-hex-3	25.18	264, 344	627.1562 0.1	C27H31O17	465.1048 [Y1]+ 303.0511 [Y0]+	625.1401 -0.4	C27H29O17	463.0873 [Y1]- 301.0343 [Y0]-
24	Que-3-O-gal	27.57	255, 353	n.d.	C21H21O12	487.0854 [M+Na]+ 303.0511 [Y0]+	463.0824 -5.3	C21H19O12	
25	Que-3-O-glucoronide	28.11	255, 352	479.0824 -0.2	C21H19O13	303.0506 [Y0]+ 257.0452 [Y0-CHO-OH]+ 229.0494 [Y0-CHO-OH-CO]+ 153.0182 [1,3A]+	477.0667 -0.2	C21H17O13	301.0347 [Y0]- 151.0029 [1,3A]-
26	Que-3-O-glc	28.33	255, 352	n.d.	C21H21O12	487.0849 [M+Na]+ 303.0491 [Y0]+	463.0918 4.1	C21H19O12	301.0328 [Y0]- 271.0233 [Y0-CHO-H]- 255.0289 [Y0-CHO-OH]- 151.0027 [1,3A]-
27	Kaem-3-O-gal	30.15	265, 345	449.1081 -0.3	C21H21O11	n.d. [M+Na]+ 287.0553 [Y0]+	447.0929 0.2	C21H19O11	285.0378 [Y0]- 151.0025 [1,3A]-
28	Kaem-3-O-Glucoronide	31.25	265, 345	463.0878 0.1	C21H19O12	n.d. [M+Na]+ 287.0557 [Y0]+ 153.0183 [1,3A]+	461.0701 -1.9	C21H17O12	285.0390 [Y0]- 151.0027 [1,3A]-
29	Kaem-3-O-glc	31.43	265, 348	449.1080	C21H21O11	n.d. [M+Na]+	447.0934	C21H19O11	285.0377 [Y0]-

				-0.4	287.0558[Y0]+		0.7		151.0027 [1,3A]-
30	Iso-3-O-gal	31.77	254, 352	479.1192	C22H23O12	317.0663 [Y0]+	477.1033	C22H21O12	477.1033 [M-H]-
				0.2			0.0		315.0447 [Y0]-
31	Iso-3-O-glc	32.32	254, 352	479.1188	C22H23O12	317.0663 [Y0]+	477.1042	C22H21O12	477.1033 [M-H]-
				-0.2			0.9		315.0447 [Y0]-
Hydroxycinnamic acids									
32	pCumhex	10.58	313	n.d.			325.0925	C15H17O8	163.0392 [Y0]-
						0.2		119.0491 [Y0-CO2]-	
Hydroxybenzoic acid									
33	Gal acid	1.92	271	171.0301			169.0107	C7H5O5	125.0232 [M-H-CO2]-
							-3.0		107.0132 [M-H-H2O-CO2]-
									79.0178 [M+H-CO2-H2O-CO]-
34	Galloyl Derivative	3.60	279	Unknown	153.0199 [Y0-H2O]+		Unknown	169.0154 [Y0]-	
					125.0236 [Y0-H2O-CO]+			79.0181 [Y0-CO2-H2O-CO]-	
					109.0290 [Y0-H2O-CO2]+				
					107.0136 [Y0-2H2O-CO]+				
					81.0345 [Y0-CO2-H2O-CO]+				